THESIS

MODELING AND DESIGN OF A POWER BOOSTED TURBO-COMPRESSION COOLING SYSTEM

Submitted by

Nickolas Richard Roberts

Department of Mechanical Engineering

In partial fulfillment of the requirements

For the Degree of Master of Science

Colorado State University

Fort Collins, Colorado

Summer 2021

Master's Committee:

Advisor: Todd M. Bandhauer

Jason C. Quinn
James Cale

ABSTRACT

MODELING AND DESIGN OF A POWER BOOSTED TURBO-COMPRESSION COOLING SYSTEM

Waste heat recovery technologies have the potential to reduce fuel consumption and address increased electricity and cooling demands in shipboard applications. Existing thermally driven power and cooling technologies are simply too large to be installed on ships where space for new equipment is extremely limited. This study addresses major shipboard challenges through the modeling and design of a volume optimized turbo-compression cooling system (TCCS). The TCCS is driven by low-grade waste heat in the shipboard diesel generator set jacket water and lubrication oil and was designed to be a drop-in replacement of electric chiller systems. A case study of a marine diesel generator set and electric chiller is presented, including annual engine loading and seawater temperature profiles. Three TCCS integration options and five working fluids (R134a, R1234ze(E), R1234yf, R245fa, R515a) were evaluated over the range of case study conditions using a fixed heat exchanger effectiveness thermodynamic model. The hybrid thermally and electricity driven "power boosted" TCCS reduced electricity consumption for cooling by over 100 kW_e. Plate and frame heat exchanger models were used to size and optimize the system to fit within the volume of a commercial centrifugal chiller of equal cooling capacity. The system used R134a, provided 200-tons of cooling, and had an electric coefficient of performance (COP) of 9.84 at the design conditions. Optimized heat exchanger and pipe geometries were fixed, and the model was run over the range of case study conditions to determine annual fuel savings of 92.1 mt yr^{-1} and a weighted average generator set power density improvement of 11.0%. Heat exchangers,

turbomachinery, and piping were solid modeled to demonstrate that the system fits within the required footprint (40.6 ft^2) and volume (267 ft^3). The designed system was estimated to cost $295,036 in equipment and $442,554 in total installed costs. The resulting payback period was 5.77 years while operating for only 3,954 hours per year. Over a 15-year period, the net present value and internal rate of return were $176,734 and 16%, respectively.

ACKNOWLEDGEMENTS

There are so many amazing people in my life that have led me to where I am today. First and foremost, I would like to thank Dr. Todd Bandhauer for everything he has provided me with the past 2+ years. I was fortunate enough my Junior year as an undergraduate to have Dr. Bandhauer as my professor for heat and mass transfer. His passion and pride in his lab and research led me to joining his team, REACH CoLab, for my Senior project and ultimately continuing into graduate school. Dr. Bandhauer has always treated myself and others as equals and it has been a pleasure to work beside him on countless projects and proposals.

Of course, the completion of this work would not have been possible without the support and contribution of others in the REACH CoLab. I cannot thank Derek Young, Alex Grauberger, and John Simon enough as they have been incredibly important in my development as an engineer and contributor in the lab. Since day 1 they have provided a tremendous amount of time and support. I'd also like to thank Sam Colosimo and Shane Garland for helping to read, review and further my work.

I would like to thank my friends and family for all of their love and support. I would have never been able to move from Massachusetts to Colorado for school if not for the support of my grandparents – both of whom attended CSU. My parents and sisters have been huge parts of my life and have helped shaped me into the person I am today. And lastly, thank you Erin for being with me and supporting me every step of the way. Moving 2,000 miles west for 4+ years definitely presented its challenges, but thank you for your unwavering patience, I love you!

TABLE OF CONTENTS

LIST OF TABLES

LIST OF FIGURES

NOMENCLATURE

Variable	Description	Units
A	Area	m^2
ASHRAE	American Society of Heating, Refrigeration and Air-Conditioning Engineers	-
BNI	Barber Nichols Inc.	-
Bo	Boiling Number	-
$CaCl_2$	Calcium Chloride	-
CAT	Caterpillar	-
CCHP	Combined Cooling Heating and Power	-
CEPCI	Chemical Engineering Plant Cost Index	-
CFC	Chlorofluorocarbon	-
Cost	Cost	$
COTS	Commercial-off-the-Shelf	-
C	Heat Capacity Rate	$kW\ K^{-1}$
c_p	Specific Heat Capacity	$kJ\ kg^{-1}\ K^{-1}$
CSU	Colorado State University	-
COP	Coefficient of Performance	-
D	Diameter	m
Depth	Depth	m
D_h	Hydraulic Diameter	m
DOD	Department of Defense	-
DOE	Department of Energy	-
E	Enhancement Factor	-
$\dot{E}$	Energy Rate	kW
EDC	Electrically Driven Chiller	-
EES	Engineering Equation Solver	-
EIA	Energy Information Administration	-
EL	Engine Load	%
EPA	Environmental Protection Agency	-
f	Friction Factor	-
F	Factor	-
g	Gravitational Acceleration	$m\ s^{-2}$
G	Mass Flux	$kg\ m^{-2}$
GWP	Global Warming Potential	-
h	Heat Transfer Coefficient	$kW\ K^{-1}\ m^{-2}$
HCFC	Hydrochlorofluorocarbon	-
HFC	Hydrofluorocarbon	-

HFO	Hydrofluoro-olefin	-
HX	Heat Exchanger	-
i	Enthalpy	kJ kg^{-1}
IRR	Internal Rate of Return	%
K	Thermal Conductivity	kW K^{-1} m^{-1}
L	Length	m
LHV	Lower Heating Value	kJ kg^{-1}
LiBr	Lithium Bromide	-
LMTD	Log Mean Temperature Difference	K
M	Molecular Weight	kg $kmol^{-1}$
m	Mass	kg
$\dot{m}$	Mass Flow Rate	kg s^{-1}
N	Number of Plates or Fittings	-
NPSH	Net Positive Suction Head	ft
NPV	Net Present Value	$
ODP	Ozone Depletion Potential	-
ORC	Organic Rankine Cycle	-
ORVC	Organic Rankine Vapor Compression	-
P	Perimeter	m
P_c	Critical Pressure	kPa
PFD	Process Flow Diagram	-
PFE	Plate Frame Heat Exchanger	-
Pr	Prandtl Number	-
P_r	Pressure Ratio	-
Ps	Plate Spacing	m
Pt	Plate Thickness	m
q	Heat Flux	kW m^{-2}
$\dot{Q}$	Heat Transfer Rate	kW
R	Thermal Resistance	K kW^{-1}
R_t	Net Cash Flow	$
ROI	Return on Investment	-
RPM	Revolutions per Minute	rev min^{-1}
S	Suppression Factor	-
SC	Subcooled	-
SH	Superheated	-
SLHX	Suction Line Heat Exchanger	-
SOA	State-of-the-Art	-
t	Number of Time Periods	-
T	Temperature	℃
TCCS	Turbo-Compression Cooling System	-
TDC	Thermally Driven Chiller	-

TP	Two-Phase	-
u	Velocity	$m\ s^{-1}$
U	Overall Heat Transfer Coefficient	$kW\ K^{-1}\ m^{-2}$
UA	Overall Heat Transfer Conductance	$kW\ K^{-1}$
US	United States	-
v	Specific Volume	$m^3\ kg^{-1}$
V	Volume	m^3
VCC	Vapor-Compression Cycle or Chiller	-
W	Width	m
$\dot{W}$	Work	kW
WHR	Waste Heat Recovery	-
x	Vapor Quality	-
X_{tt}	Martinelli Parameter	-
y	Discount Rate	%
Greek Symbols		
β	Chevron Angle	radians
Δ	Difference	
ε	Heat Exchanger Effectiveness	
η	Efficiency	%
μ	Dynamic Viscosity	$kg\ m^{-1}\ s^{-1}$
ρ	Density	$kg\ m^{-3}$
Subscripts		
a	Acceleration	
abs	Absorption Chiller	
actual	Actual	
b	boiler	
c	Cold Side	
cc	Cooling Cycle	
ccc	Cooling Cycle Condenser	
ch	Chiller or Cooling Cycle Evaporator	
channel	Heat Exchanger Channel	
chill	Chilled Water or Chiller	
comp	Compressor	
cond	Condenser	
conv	Convective	
cs	Cross-Sectional	
ec	Economizer	
elec	Electric	
engine	Engine	
eq	Equivalent	
ext	External	

f	Friction	
fg	Vaporization	
fuel	Fuel (MGO)	
g	Gravitational	
gen	Generator	
h	Hot Side	
heat	Heat	
HX	Heat Exchanger	
i	Inlet	
in	Input	
install	Installation	
JW	Jacket Water	
l	Liquid	
m	Mean	
man	Manifold	
max	Maximum	
mech	Mechanical	
min	Minimum	
new	New	
o	Outlet	
oil	Lubrication Oil	
orig	Original	
pc	Power Cycle	
pcc	Power Cycle Condenser	
pipe	Pipe	
plate	Plate	
ports	Ports	
pump	Pump	
r	Refrigerant	
re	Recuperator	
region	Fluid Phase Region	
s	Isentropic	
sc	Subcooled	
sf	Surface	
sh	Superheated	
sl	Suction Line	
TCCS	Turbo-compression Cooling System	
thermal	Thermal	
tp	Two-Phase	
turb	Turbine	
v	Vapor	
vcc	Vapor Compression Chiller	

CHAPTER 1 Introduction

1.1 Motivation

By 2050 the world's population is expected to increase from 7.8 billion to 9.8 billion [1] and energy usage is projected to increase by nearly 50% [2], most of which is from developing countries. Increased energy consumption has obvious environmental impacts such as long-term issues related to global warming. Temperatures are expected to rise between 2.5°F to 10°F over the next century [3], which has serious implications on shorelines and severe weather, including extreme temperatures in already arid climates. Adding to these issues is the inefficiencies of our energy generation and consumption. Lawrence Livermore National Laboratory creates annual energy flow diagrams for U.S. energy consumption [4], shown in Figure 1-1. The diagram starts with the energy consumption of various sources (e.g. coal, natural gas, solar, etc.) and follows it to its end use where it is either used for energy services or is rejected energy, typically in the form of heat. It is seen that approximately 67% of our energy consumption ends up as rejected energy. Using renewable resources is key to reducing this number but will take a significant amount of time to achieve a large reduction in wasted energy.

One industry unlikely to experience a rapid shift to cleaner and more efficient forms of energy generation is the marine sector. Marine ships rely on large diesel engines for propulsion and auxiliary power generation. These marine diesel engines are typically less than 50% efficient, meaning over half of the fuel energy is wasted in the form of heat. Marine shipping is an integral part of the world's economy, with over 90% of the world's trade carried by sea. As a result, shipping is responsible for emitting an average of 1,015 million tons of CO_2 per year, which is

3.1% of global CO_2 emissions [5]. Companies are unlikely to make efforts to reduce carbon emissions unless there is a significant financial backing or savings [6]. Since fuel costs account for more than 50% of operational costs [7-10], finding ways to reduce fuel consumption with low upfront capital cost could incentivize companies to decrease their carbon emissions while also producing financial savings.

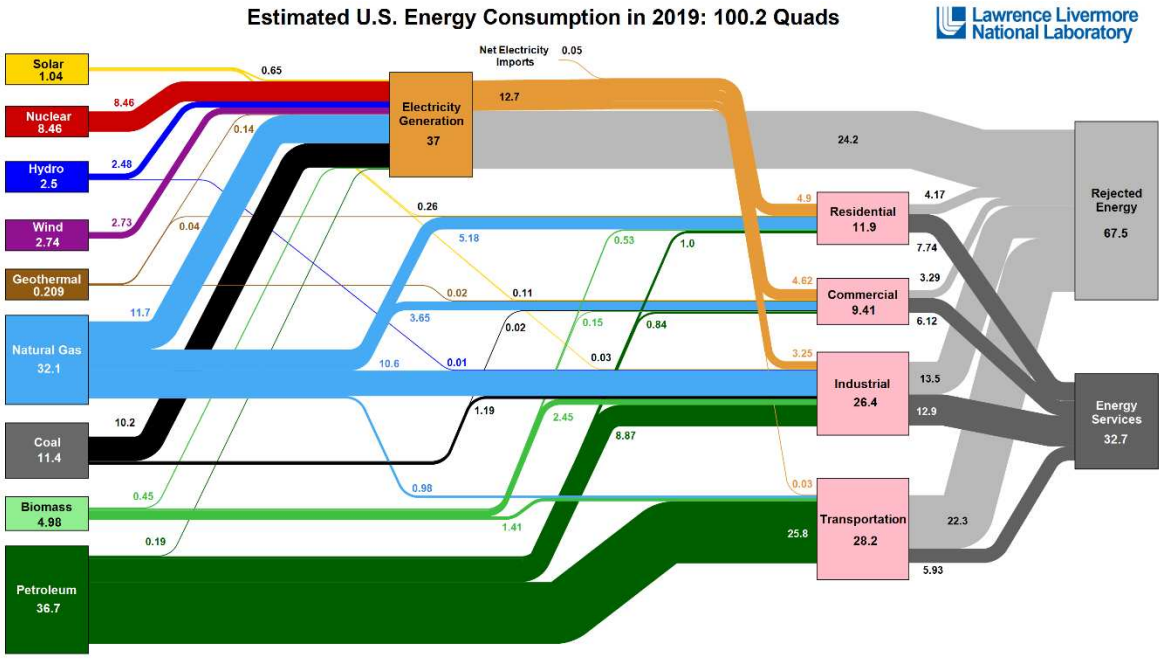

Figure 1-1: Lawrence Livermore National Laboratory national energy flow diagram for 2019 [4]

There is a need to improve the power density and fuel efficiency of propulsion and power generation prime movers as electrical energy on ships increase. New energy intensive technologies and rising temperatures result in an increased demand for cooling capacity, which further increases the electrical demand on ships. Financially, fuel prices continue to rise and therefore there is a desire to cut fuel costs by improving the fuel efficiency of prime movers. An additional benefit of increased fuel efficiency is a ship can spend more time at sea between refueling. Technology developed for the marine sector can also address a larger land-based commercial market and impact the fuel consumption and emissions of global power generation systems.

1.2 Methods for Improvement

There are several simple energy savings measures that can be taken to reduce the fuel consumption of large marine ships over longer periods of time. An energy management survey taken in 2015 found the most popular energy saving measures that were actively implemented or planned [6]. The most popular energy saving methods are hull and propeller cleaning, slow steaming, and hull coating. There are also many optimization techniques such as voyage planning optimization, advanced weather routing, and engine performance optimization. Periodic hull cleaning is estimated to improve efficiency by up to 9%, but hull cleaning can only occur at discrete points in time and the journey must be planned around when and where hull cleaning will occur [11]. Additionally, the hull will foul and reduce savings over long journeys. Slow steaming is a common practice and is simply the reduction of speed which leads to significant decreases in fuel consumption and carbon emissions. A 2012 study found that a 10% reduction in speed results in a 19% decrease in CO_2 emissions, even after considering the decreased capacity [12]. Slow steaming's profitability is market dependent and the drawback is reduced delivery speeds. If the demand for shipped goods increases, the optimal speed rate of the vessels will increase [13]. The energy savings measures addressed in Figure 1-2 are relatively inexpensive methods for reducing the energy consumption of shipping fleets. However, they do not directly address the wasted energy from the shipboard diesel engines and depend on careful operational planning, which may not be possible in some scenarios.

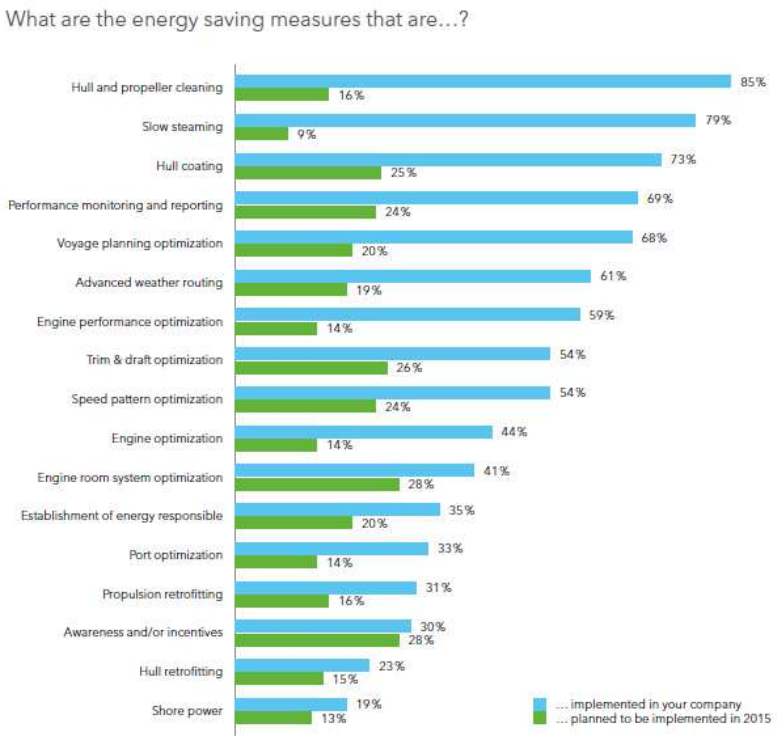

Figure 1-2: Energy saving measures that are implemented by shipping fleets, survey [6]

An additional method to reduce fuel consumption is to utilize waste heat from the on-board engines to produce useful heating, cooling, or electricity. As previously mentioned, marine diesel engines used to propel large ships or generate electricity are typically less than 50% efficient, meaning over half of the fuel energy is wasted in the form of heat. Waste heat capture and utilization has an increased upfront capital costs compared to previously discussed strategies but can have consistent long-term savings without altering the operation of the ship.

1.3 Waste Heat Availability

There are four main waste heat streams in large marine diesel engines that can be used for waste heat recovery (WHR) applications: exhaust gas, jacket water, lubrication oil, and aftercooler air [14,15]. An energy flow diagram for a CAT 280-8 marine diesel engine [16] at full engine load is shown in Figure 1-3.

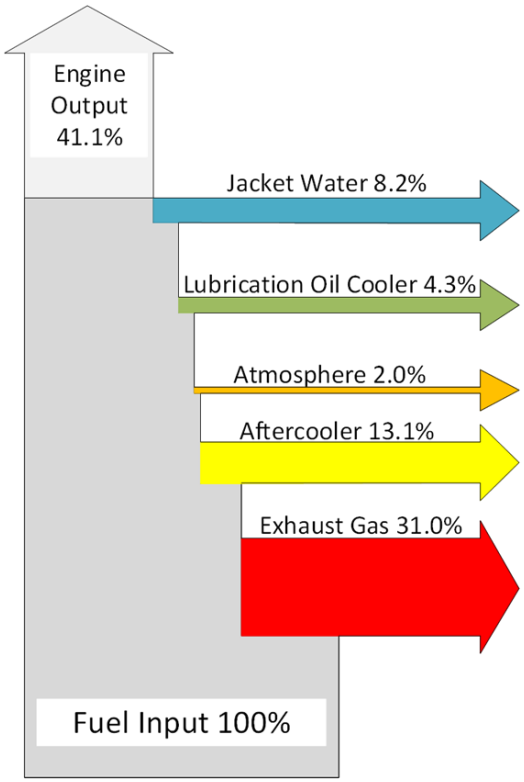

Figure 1-3: CAT 280-8 marine diesel engine energy flow diagram [16]

The CAT C280-8 has a thermal efficiency of 41.1%, meaning that 58.9% of the fuel's energy is rejected as heat. Exhaust gas WHR is most commonly studied due to its high percentage of energy (31.0%) and its high temperatures (>400°C), but there are major challenges with recovering this heat. Due to highly variant operation of marine diesel generators, the exhaust gas flows and temperatures are also highly transient and can cause thermal fatigue in the WHR equipment, resulting in the formation of macroscopic cracks and equipment failure [17]. As a result, the exhaust gas recovery heat exchangers must be made of special, high temperature materials which are expensive and difficult to manufacture [18,19]. The addition of a heat exchanger to recover exhaust gas also increases the engine back-pressure, which can reduce engine performance and increase engine emissions [20,21]. The issues discussed here do not prevent exhaust gas WHR from being possible, but they do increase the complexity and cost of the system. Aftercooler heat rejection is the second largest percentage of energy loss in a marine diesel engine

(13.1%). The aftercooler is used to cool air at the inlet of the combustion chamber, after it has passed through the turbocharger. The aftercooler heat rejection is ambient dependent, meaning as the air to turbo temperature goes up, the heat rejection must also increase to maintain a constant temperature. However, the aftercooler water is maintained at 32°C, which is too low of a temperature to be of significant use in a WHR system. Heat recovery from the lubrication oil (~90°C) and jacket water (~95°C) present an alternative strategy to exhaust gas WHR. While the lower temperatures result in lower WHR system performance, they are still hot enough to be of use, require less expensive and complex equipment, and account for a combined 12.5% of the fuel's energy.

1.4 Waste Heat Recovery Systems

There are several methods of utilizing low-grade waste heat (<100°C), including providing useful heating, cooling, or electricity. Using waste heat for space heating or water heating is often the simplest and least expensive option of WHR and may be the most economically favorable depending on the application and location. On marine ships heating is typically provided using fuel driven hot water boilers and are a relatively minor consumer of energy, especially on commercial container ships [22]. Using WHR for heating would have a direct reduction in fuel use on the ship but would have no impact on the electrical end-use of the diesel generators. Electrical generation systems, such as an organic Rankine cycle (ORC), are commonly used to convert heat to electrical energy. In ORCs, waste heat vaporizes a pressurized organic, carbon-based fluid which subsequently expands in a turbine to produce electricity through a generator. Low-grade waste heat ORCs are typically <15% efficient [23], resulting in a relatively small improvement in power density or fuel savings. In addition, the installation of ORCs on ships requires considerable space without the benefit of removing redundant equipment such as a hot water boiler or chiller.

A third WHR method is to use the waste heat to drive a thermally driven chiller (TDC) which provides cooling to be used in space conditioning or refrigeration. The use of TDCs offsets the electricity consumption of traditional electrically driven chillers (EDCs). Ships often have several redundant chillers and the use of TDCs presents an opportunity to replace this existing equipment. There are four primary types of TDCs: absorption, adsorption, ejector, and organic-Rankine vapor compression (ORVC). Single-effect absorption chillers are the most common low-grade TDC for land-based applications but have several challenges that make them difficult to employ in marine applications. Adsorption chillers are less complex than absorption, and can operate with very low heat source temperatures, but suffer from very low performances. Ejector chillers are less commonly studied due to operational difficulties and low performances but have no moving parts and low-maintenance requirements. ORVCs offer similar performance to absorption chillers but depend heavily on the efficiency of turbomachinery components. The present study will focus exclusively on the use of low-grade heat sources from marine diesel engines to power a TDC. The literature review will examine the working principle and pros and cons of each type of TDC, as well as research done specifically within the marine sector.

1.5 Research Objectives

While there have been numerous studies investigating the use of waste heat recovery to produce heating, electricity, or cooling in marine environments, research does not address practical challenges related to implementation. These challenges include meeting strict volume and weight requirements while also providing a significant performance boost and favorable economics. The current study will present a TDC known as the turbo-compression cooling system (TCCS) coupled to a marine diesel generator set. This study furthers past research in TDCs and TCCS development by presenting a case study of a diesel generator set coupled to an electric chiller using engine data,

an annual engine operational load profile, and an annual seawater temperature profile. Three TCCS configuration options and five working fluids are presented and thermodynamically modeled over the range of engine load and seawater conditions. A singular configuration and working fluid were selected and detailed plate and frame heat exchanger models were coupled to the thermodynamic model. Heat exchangers were optimized for performance while fitting in a pre-defined volume. A final performance model was created by fixing the optimized heat exchanger and piping geometries and the model was run over the range of conditions to determine annual power density improvement and fuel savings. Finally, an economic model is presented and the TCCS is compared to SOA absorption technology.

1.6 Thesis Organization

The followings chapters present the design methodology and performance modeling of a low-grade waste heat driven turbo-compression cooling system used to provide chilling on a large marine ship. Chapter 2 provides a literature review of existing thermally driven chillers, including their working principles, performance, economics, and challenges. Research applied specifically to the marine sector will be given additional focus. Chapter 3 describes the modeling approach for all steps of the design, including an overview of the case study and details of the thermodynamic, heat exchanger, and economic models. Chapter 4 provides results from the thermodynamic study and presents the solid model and performance of the optimized design that meets shipboard requirements. Chapter 5 presents conclusions and recommendations for future work. Chapter 6 lists citations used throughout the presented study. Finally, the Appendix shows step-by-step calculations for the thermodynamic model and heat exchanger sizing model at design conditions with R134a, as well as details for system costing.

CHAPTER 2 Literature Review

Thermally driven chillers absorb heat from external sources to provide a cooling effect that can used for comfort cooling or refrigeration. TDCs share similar components to electrically driven chillers which are traditionally used for cooling due to their simplicity and low costs. The following section will begin with a discussion of electrically driven chillers and metrics that can aid in the comparison of the performance and cost of TDCs and EDCs. After this introduction, the four main types of TDCs will be discussed: absorption, adsorption, ejector, and organic Rankine vapor compression. TDCs operate using a variety of heat sources (e.g. boiler exhaust heat, engine coolant, solar-driven, etc.) and can be used for different applications (e.g. land-based, maritime, comfort cooling, refrigeration). The technology discussions will begin with a broad overview of the TDCs, not limited by their heat source or application, followed by a detailed description of research done specifically in the maritime sector. Maritime studies are unique in that space and resources onboard ships are very limited, operating conditions are highly variable, and there are special restrictions in place such as limiting the use of toxic or flammable fluids. After the overview of state-of-the-art (SOA) TDCs, the turbo-compression cooling system will be introduced, and past research discussed. Finally, remaining gaps in research will be identified and the specific aims of this study will be presented.

2.1. Overview of Cooling Technology

Electrically driven chillers are widely used to provide either chilled water for comfort cooling or low temperature ammonia in refrigeration applications. EDCs operate using a vapor-compression cycle (VCC) and consist of a working fluid and four primary components: a compressor, condenser, expansion valve, and evaporator. The working fluid is the fluid contained

within the system and does not come in direct contact with any external fluid streams or components other than those shown in Figure 2-1. An external stream is used to transfer heat to or from the cycle but is not used in every component. External streams are typically water, water-glycol mixture, or ammonia depending on the application. At the first state point in Figure 2-1, the working fluid is a low-pressure, low-temperature, two-phase mixture. A cooling effect is generated in the evaporator (1-2) by absorbing heat from a warmer external stream, thus cooling the external stream and evaporating the working fluid. Heat transfer is maximized by having the working fluid enter the evaporator in a two-phase or saturated liquid phase because the working fluid temperature does not increase, and the temperature of the two fluid streams will not converge as quickly. The evaporated fluid at state point 2 is then compressed to a higher-pressure state by an electrically driven compressor (2-3). The higher-pressure vapor at state point 3 is then condensed to a saturated liquid state in the condenser (3-4), in which the working fluid rejects heat to a colder external stream. The external stream is typically water or a water-glycol mixture, but air-cooled condensers may also be used. If water or water-glycol is used, a cooling tower may be required to reject heat to the ambient. Maritime applications can use seawater as a coolant, which negates the need for a cooling tower. After being liquified in the condenser, the working fluid is throttled to a low-pressure state in an expansion valve (4-1) and the cycle is then repeated. Rather than reject heat to the ambient through an air-cooled condenser or cooling tower, some integrated systems reject heat to hot water streams to reduce the natural gas consumption of hot water boilers. These systems are termed heat pumps or heat recovery chillers and are sized to provide a certain heat load rather than the cooling load. However, the cooling performance of these systems is lower because of the higher external stream temperatures.

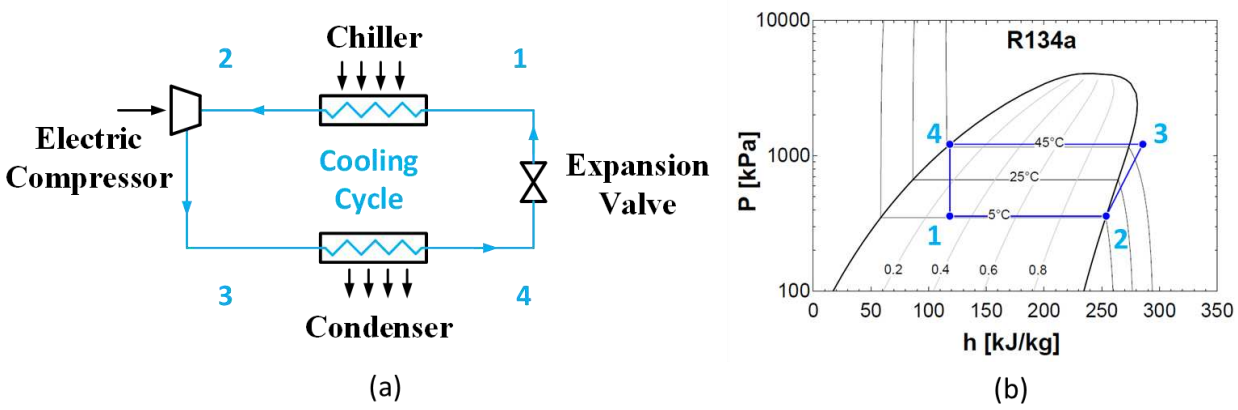

Figure 2-1: (a) Simplified process flow diagram of a standard electrically driven vapor compression chiller and (b) a pressure-enthalpy diagram depicting the state points of a VCC using R134a as a working fluid.

TDCs also include an evaporator to cool an external fluid stream and a condenser to reject heat to the ambient. However, many of the components and working principles differ from EDCs. Some TDCs still require relatively small amounts of electricity to power components such as working fluid pumps. To compare the performance of different systems and studies, common performance metrics must be used. The coefficient of performance (COP) is often used to describe the performance of EDCs and TDCs. This study will use three versions of the COP to describe system performance where appropriate: overall COP, electrical COP, and thermal COP. The overall COP is the ratio of the amount of cooling, $\dot{Q}_{chill}$, to the useful energy input, $\dot{E}_{in}$. For EDCs, the useful energy input is the amount of electricity consumed by the compressor. For TDCs, the useful energy input is the amount of heat input to the system plus the amount of electricity consumed.

$$\mathrm{COP} = \frac{\dot{Q}_{chill}}{\dot{E}_{in}} \tag{2.1}$$

In certain scenarios within this study, it is desirable to compare the amount of cooling per unit of electricity consumed. The electrical COP is defined in Equation (2.2):

$$\mathrm{COP_{elec}} = \frac{\dot{Q}_{chill}}{\dot{E}_{elec,in}} \tag{2.2}$$

where $\dot{E}_{elec,in}$ is the electricity consumed by the system. Lastly, it is common to neglect any electricity consumption in TDCs, as the electricity draw is usually relatively small compared to the heat input. Therefore, the thermal COP is given by Equation (2.3):

$$\mathrm{COP_{thermal}} = \frac{\dot{Q}_{chill}}{\dot{Q}_{heat}} \tag{2.3}$$

where $\dot{Q}_{heat}$ is the useful heat input to the system. Equations (2.1) through (2.3) are useful in comparing different systems with the same operational conditions or one system with different operating conditions, but can be misleading. In general, the overall COP of electrically driven systems should not be compared to thermally driven systems as the type of energy inputs are not alike. Additionally, comparative systems may have different external fluid temperatures which impacts performance but is not obvious by comparing COPs. In general, higher heat source temperatures result in higher COPs and care should be taken to report external fluid temperatures when comparing specific studies.

As mentioned in Chapter 1, companies are unlikely to invest in a new technology unless there is a significant financial backing or savings. Therefore, it is important to compare economic metrics in addition to performance metrics. The main economic metric used to compare different systems in this paper is specific cost, as defined in Equation (2.4).

$$\text{Specific Cost} = \frac{\text{System Cost}}{\dot{Q}_{chill}} \tag{2.4}$$

Specific cost can be used to compare different electrically and thermally driven chiller technologies at different scales. A higher specific cost indicates that the system is more expensive per unit of cooling. Specific cost will be the sole economic metric used in the literature review, but

other metrics such as payback period and net present value will be introduced in the subsequent chapters.

2.2. State-of-the-Art Thermally Driven Cooling Systems

There are four main types of state-of-the-art thermally driven cooling systems: absorption, adsorption, ejector, and organic Rankine vapor compression. In the following section, an overview of each type of TDC will be presented. The working principle, performance and economic metrics, advantages and disadvantages, and innovative research on the technology will be discussed. A summary will then be provided for research conducted specifically on using the technology in the marine sector. Following this section will be an introduction to the turbo-compression cooling system (TCCS) and a review of past research. Lastly, marine sector research needs for TDCs and the TCCS will be presented and the specific aims of the study defined.

2.2.1. Absorption Systems

Absorption chillers are the most prevalent thermally driven chillers worldwide and are sold by major commercial chiller manufacturers such as Trane [24], Carrier [25], and York [26]. A simplified process flow diagram (PFD) of a single-effect absorption chiller is shown in Figure 2-2. The working principle of a single-effect absorption chiller is not significantly different from a vapor compression chiller. As seen in the PFD of a vapor compression chiller, Figure 2-1, and a single-effect absorption chiller, Figure 2-2, each contains a condenser, expansion valve, and an evaporator. They differ in that a vapor compression chiller uses an electric compressor to provide compression of the working fluid, whereas an absorption chiller uses a “thermal compressor”, consisting of a secondary fluid, an absorber, a pump, a generator, an expansion valve, and sometimes a solution heat exchanger (HX). The benefit of an absorption chiller is that the

compression is done with very little electrical energy, but it comes at the cost of a more complex, larger, and more expensive system.

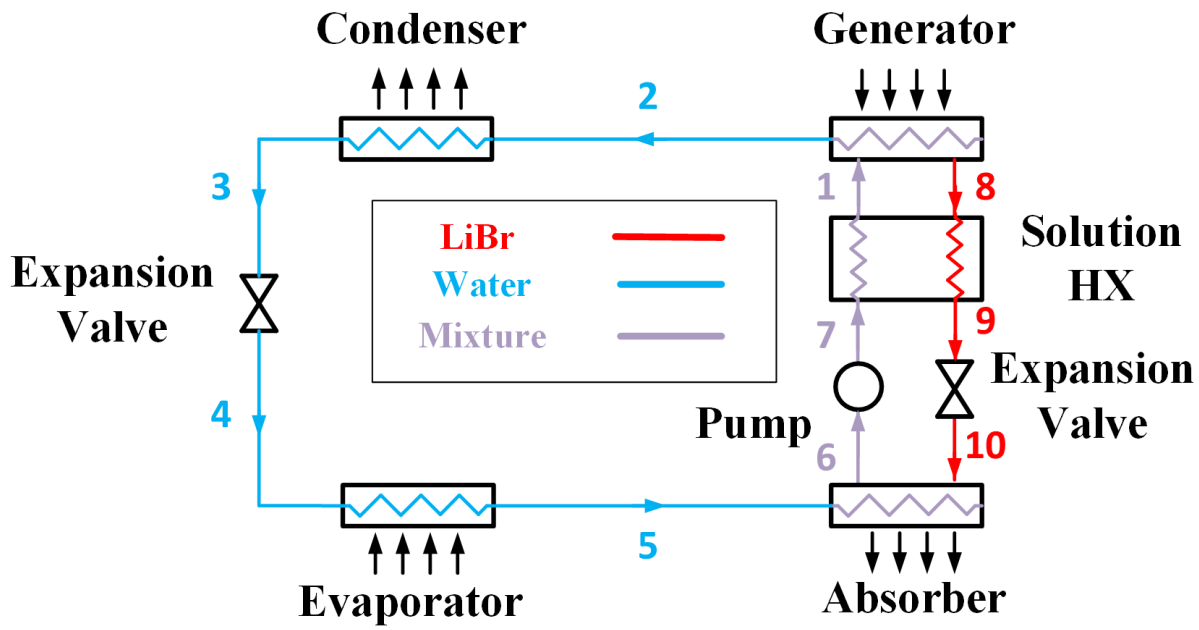

Figure 2-2: Single effect absorption chiller process flow diagram

Absorption chillers operate using a working fluid pair, commonly water and lithium bromide (LiBr) for space cooling needs or ammonia and water for refrigeration. Figure 2-2 and the following discussion are based on an LiBr-water single-effect absorption chiller. Beginning at state point 1 in Figure 2-2, the working fluid is a mixture of water and LiBr. The more volatile fluid (water in a water-LiBr system) is vaporized in the generator by absorbing heat from the heat source (e.g. engine coolant). Once the water is separated from the LiBr, it is liquified in the condenser (2-3) by an external stream. Then, the water is throttled to a low-pressure, low-temperature state in an expansion valve (3-4). The water is then evaporated in the evaporator (4-5) to provide a cooling effect to an external stream. Meanwhile, heat from the separated LiBr exiting the generator at state point 8 is used to preheat the LiBr-water mixture entering the generator in the solution HX (8-9) and is then throttled to a low-pressure state in an expansion

valve (9-10). The low-pressure water (state point 5) and low-pressure LiBr (state point 10) are then bonded in the absorber. This absorption process is exothermic, and the heat generated must be rejected to the ambient. The mixture is then pumped to the generator pressure using a relatively small amount of electricity in a solution pump (6-7) and preheated in the solution HX (7-1) before re-entering the generator.

The working principle shown in Figure 2-2 is that of a single-effect absorption chiller. Single-effect absorption chillers are most prevalent in low-grade heat applications (~100°C) and typically have COPs of 0.6-0.7 [27,28]. However, more complex and higher efficient absorption chillers exist. Double effect chillers utilize high-pressure and intermediate-pressure generators to maximize the use of higher-temperature heat sources, such as high-pressure steam or exhaust gas. Double effect absorption chillers typically have COPs of 1.2-1.4 [29,30] because of the more efficient cycle and higher-grade heat sources. Many commercial manufacturers also sell double-effect absorption chillers. Even higher-effect absorption chillers have been studied, such as a triple-effect absorption chiller [31] which can reach COPs exceeding 1.7 [32]. These systems are not commercially available, likely due to a decreasing benefit of adding additional effects, especially when considering the increased complexity and costs.

There are several possible working fluid combinations for absorption chillers. Water-LiBr or ammonia-water are the most commonly used because of favorable performance and environmental properties. When designing an absorption chiller, the working fluid pair should meet criteria that includes: absence of solid phase, favorable volatility ratio and affinity, moderate pressures, high chemical stability, non-corrosive, non-toxic and non-flammable, and high latent heat [33]. Water-LiBr meets a number of these criteria and is suitable for low-grade heat sources of 75°C-125°C. Water-LiBr absorption chillers are desirable due to the combination of non-toxic,

environmentally friendly fluids but have some inherent challenges with operation. LiBr is a salt, and at high LiBr concentrations or low solution temperatures crystals of LiBr may form which block piping or the passages in the solution heat exchanger and can cause a system shutdown [33]. Another cause for crystallization is the use of extremely cold water in the condenser or absorber, which is avoidable in some land-based applications that use a controllable cooling tower, but is more difficult to control in a maritime application where seawater is used as the coolant. Additionally, since the refrigerant is water, the absorber and evaporator must operate at vacuum pressures to provide cooling at standard chilled water temperatures. As a result, the system requires larger volume equipment to avoid pressure drop and it must be sealed properly to prevent air leaks which can cause crystallization. Lastly, the use of salt within the system results in serious corrosion attacks on the heat exchangers and piping [34], which can reduce the lifetime of the system and requires specialized materials such as titanium or copper nickel alloys to prevent. These challenges make operating LiBr-water systems more complicated, increases maintenance time, and increases the size and cost of the system. Ammonia-water systems operate with higher source temperatures of 125°C-170°C and are more suitable for refrigeration applications which require cooling below 0°C. Ammonia-water systems do not have the same crystallization challenges as water-LiBr systems, but ammonia is highly toxic and pose signification health risks at high concentrations [35]. As a result, ammonia-water absorption chillers are unlikely to be used for maritime applications. An alternative to LiBr and ammonia absorption systems is the use of ionic liquids [36]. Ionic liquids are melting salts that remain in the liquid phase over a range of temperatures including room-temperature. They have favorable properties for absorption chillers such as being non-flammable and non-toxic and having good thermal stability and solubility. However, these

combinations are not commercially available and still use water as the refrigerant in the working pair, meaning that low-pressures and large volume equipment are still required.

In the US, the absorption chiller market has struggled to take off. Despite seeing relatively high sales in the 50's and 60's, absorption chillers experienced a sharp decline in sales in the mid-1970s [37]. A major reason for the decline was a rise in natural gas prices and fuel availability, as well as governmental policies. While sales have recovered slightly since the 90's, absorption chiller sales in the US are still far behind global values. Absorption chillers accounted for less than 4% of the total North American chiller market's sales in 2008. Most of these sales are for smaller, single-effect absorption chillers as opposed to larger, double-effect absorption chillers. However, globally, it is estimated that over 45% of all large chillers sold are absorption chillers. Most of these units are sold in Japan, South Korea, and China [38]. Overall, absorption chillers are 5.7% of the global chiller revenue as of 2014 [39]. Failure to adopt absorption more frequently, especially in the US, is due to technical issues and social stigmas around the technology and the high initial costs required to install absorption chillers. Absorption chillers are significantly larger, heavier, and more expensive than their main competitor: electric chillers. For absorption chillers to be profitable there must be favorable utility costs, namely high costs of electricity and low costs of gas for direct fired chillers or combined cooling, heating, and power (CCHP) installations. This is necessary because the cost of commercial electric chillers [40] are significantly cheaper than absorption chillers [41], shown in Table 2-1. Water-cooled commercial centrifugal chiller costs are typical values based on a range of products available on the market in 2017. The specific cost of equipment for a similarly sized LiBr-water chiller is over twice that of a commercial centrifugal electric chiller ($425 ton^{-1} vs. $930 ton^{-1} at the ~400-ton scale). Installation costs are also significantly higher for absorption chillers, likely due to heat recovery, complex controls, and

significantly larger footprints and volumes. The installation factor is defined by Equation (2.5). An install factor over 1 indicates that the construction and installation costs are greater than the equipment costs.

$$\text{Installation Factor} = \frac{\text{Construction and Installation Cost}}{\text{Equipment Cost}} \tag{2.5}$$

When factoring in the construction and installation costs, it is clear that absorption chillers are prohibitively very expensive, especially at smaller scales (<400-tons).

Table 2-1: Cost and performance of commercial water-cooled centrifugal chillers and LiBr-water single-stage absorption chillers [40] [41]

System	**1**	**2**	**3**	**4**
Design	**Centrifugal Chiller**	**LiBr-Water Single Stage Absorption Chiller**		
Energy Source	**Electricity**	**Hot Water**	**Hot Water**	**Steam (Low Pressure)**
Nominal Cooling Capacity (tons)	400	50	440	1,320
Full-Load COP	6.6	0.70	0.74	0.79
Equipment Cost ($/ton)	$425	$2,010	$930	$820
Construction and Installation Costs ($/ton)	$50	$3,990	$1,370	$980
Installation Factor	0.12	1.99	1.47	1.20
Total Installed Cost ($/ton)	$475	$6,000	$2,300	$1,800

As expected, the specific cost of the system increases when "stages" or "effects" are added to the system, as seen in Table 2-2. At the 330 to 440-ton range, a hot water single stage chiller costs \$930 ton^{-1} in equipment costs, compared to \$1,190 ton^{-1} for a steam (high-pressure) two stage chiller and \$1,330 ton^{-1} for an exhaust fired two stage chiller. A similar trend can be observed when comparing systems at the >1,000-ton capacity scale.

Table 2-2: Cost and performance of LiBr-water two-stage absorption chillers [41]

System	1	2	3	4
Design	**LiBr-Water Two Stage Absorption Chiller**			
Energy Source	**Steam (High Pressure)**		**Exhaust Fired**	
Nominal Cooling Capacity (tons)	330	1,320	330	1,000
Full-Load COP	1.42	1.42	1.35	1.38
Equipment Cost ($/ton)	$1,190	$1,000	$1,330	$930
Construction and Installation Costs ($/ton)	$1,810	$1,200	$1,970	$1,070
Installation Factor	1.52	1.20	1.48	1.15
Total Installed Cost ($/ton)	$3,000	$2,200	$3,300	$2,000

2.2.1.1. Review of Maritime Research

Absorption chillers have previously been installed and are operated on commercial vessels, most commonly on cruise ships [42], but their use in the maritime sector is rare. As previously discussed, absorption chillers require high investment costs and large space compared to vapor compression chillers. Volume constraints are especially of concern on ships and in retrofit scenarios where the space simply does not exist for absorption chillers. In addition, the ship's movements can cause issues for absorption chillers, such as refrigerant overflow and mixing. To account for these issues, some companies offer absorption chillers for marine vessel conditions by adding anti-rolling and pitching constructions [43] [44]. Lastly, marine engines have highly variable operation and waste heat duties are not constant. Therefore, a back-up electrical chiller is needed for cases when the absorption chiller is unable to meet cooling demand due to low waste heat availability [45].

Despite challenges with using absorption for marine vessels, multiple shipboard absorption studies exist. The following discussion will be on studies that have specifically focused on using absorption chillers for maritime applications. Of specific interest are papers that examine off-design performance, such as variable seawater or engine operation conditions, and studies that include practical design considerations. A summary of the papers selected for discussion in this literature review are provided in Table 2-3.

Figure 2-3: Maritime absorption chiller by Heinen & Hopman [43]

Ouadha et. al. [46] presented a general thermodynamic study on the impacts of varying condenser, generator, and chiller temperatures on the performance of an absorption chiller operating with a marine diesel engine. The study concluded that there is sufficient heat in marine diesel engines for proper absorption operation, but noted that there were theoretical limits on the lower end of generator temperatures (<70°C) in which the cycle was considered impractical and would not function. The study also displayed trends associated with changing fluid temperatures and found that increasing the generator and evaporator temperatures or decreasing the condenser and absorber temperatures led to higher system performance. This study presents the base for a

thermodynamic study but does not discuss any practical challenges such as pressure drop, equipment size, fluid concerns, or system capacity.

Table 2-3: Summary of studies for absorption chillers in maritime applications

Authors	Working Fluid Pair	Generator Temp.	Condenser Temp.	Chiller Temp.	Cooling Duty	COP
		°C	°C	°C	kW	-
Ammar et. al. [47]	LiBr-Water	85 to 95	20 to 40	5 to 25	250	0.76 to 0.86
Cao et. al. [48]	LiBr-Water	-	-	6.7	-	0.64
Cao et. al. [22]	LiBr-Water	-	-	6.7	-	0.59
Liang et. al. [49]	Ammonia-Water	50 to 90	15	0	7,000 to 18,000	0.79
Liang et. al. [50]	Ammonia-Water	90 to 120	20	5	400 to 2400	0.1
Ouadha et. al. [46]	Ammonia-Water	60 to 120	20 to 45	-10 to 10	-	0.5 to 0.75
Salmi et. al. [51]	LiBr-Water and Ammonia-Water	50 to 120	30 or 40	-20 to 10	150 to 350	0.3 to 0.85

Ammar et. al. [47] furthers this work by applying a simple single-effect LiBr-water absorption refrigeration unit to a case study of a high speed passenger vessel operating in the Red Sea area. This ship operated between ports in Saudi Arabia and Egypt 300 times a year, with cruise times of 8 hours per trip. The ship has (4) 7,200 kW main engines and requires 250 kW of air conditioning. The authors compared extracting heat from the exhaust gas using an intermediate water loop at 95°C-85°C and the engine's jacket water directly at 85°C-75°C; however, since both heat streams could supply the absorption unit with sufficient heat (344 kW), it was found that the jacket water system was more economically favorable due to lower install costs and maintenance. While the study includes the impacts of varying condenser, evaporator, and generator temperatures, it is not clear if these varying temperatures were used in the economic results, as

there is no mention of an ambient temperature or engine operation profiles. The final results of the study were that the absorption refrigeration unit could save 156 tons of fuel per year (a 23% reduction), and the total 18 year life cycle costs would be $336,230 for the jacket water system and $355,683 for the exhaust driven system. The resulting payback was estimated to be 6 years when using an installation factor of 0.12, discount rate of 10%, and annual fuel inflation of 2%. While the study is an improvement over past work by including economic considerations and a case study, there is no discussion of operational profiles, space constraints, or other practical design considerations such as crystallization.

An additional case study was performed by Salmi et. al. [51] on using a single effect absorption system on a B.Delta37 bulk carrier with LiBr-water and ammonia-water working pairs. The study compared using exhaust gas, jacket water, and scavenge air over a range of engine loads from 25% to 74% with condenser temperatures at 30°C under ISO climate conditions and 40°C under tropical conditions. It was found that there was enough waste heat in the exhaust gas and jacket water of the main engine to provide the required cooling duty of the ship (150 kW_{th}) over the range of engine loads at ISO conditions, but the scavenge air does not provide enough heat at lower engine loads. However, when using jacket water as the heat source the system operates close to the low evaporator temperature limit and the system malfunctions. The system is also unable to operate at all at higher condenser temperatures (40°C) for evaporator temperatures between 2°C and 10°C. The study concluded with presenting a theoretical potential savings of 70% electricity used for air conditioning in ISO conditions and 61% in tropical conditions, equating to 47 to 95 tons of fuel saved annually, respectively. The authors do note that there is a potential issue with the motion of the ship reducing performance of absorption chillers, but claim that even with a 40% reduction in performance there is enough waste heat to provide the required cooling in this case

study. Overall, the study found that absorption could provide sufficient cooling over a range of engine loads, so long as the condenser temperatures do not rise significantly above 30°C. The study did not consider space restraints, variable ambient profiles, or economic considerations.

Cao et. al. [48] also investigated the use of a single effect LiBr-water absorption chiller for cooling on a cargo ship. A transient model was developed which included detailed modeling of the interior cabins and auxiliary systems such as chilled water pumps and thermostat set points. The exhaust gas driven absorption chiller was seawater cooled and chilled water was delivered to individual cabins using parallel pumps. The hot water leaving the generator was used for hot water needs before being pumped back to the exhaust gas heat exchanger. Results indicated that the waste heat driven system had an electrical COP of 9.4, including the auxiliary power usage, compared to 3.6 for the baseline case. As a result, the fuel consumption and CO_2 emissions were reduced by 62% in a case study performed for Miami's climate. Results were also compared to Baltimore and Abu Dhabi's climates, which indicated that greater fuel savings are possible in hotter climates. The authors address challenges from crystallization, swaying and vibration of the ship, and corrosion. The study does not go into detail on the amount of waste heat available or the cooling duty in kW_{th}, and does not provide seawater or engine operational profiles, or any economic considerations. The authors note that the cargo ship modeled only has 16 cabins, which represents limited fuel savings potential, compared to 2,000 cabins on a cruise ship. Therefore, air conditioning only represents 0.11% of fuel consumption on cargo ships, compared to >13% on a cruise ship. A follow up study by Cao et. al. [22] addressed this challenge by using a cascaded absorption-compression configuration which provided chilled water for comfort cooling in cabins and to cool the air used in the condensers of the electrically driven VCC reefers, which provide refrigeration for containers. By cooling the air used in the condensers of the VCC reefers, the

performance of these systems increases, thus reducing electricity consumption for refrigeration of containers. This study also built upon the prior publication by the same authors by including models for sea route weather, VCC reefers, and the main engine. Two sea routes were used: one from South Korea to Pakistan that lasted 1000 hours, and one that is from Japan to San Francisco that is 300 hours. Performance results indicated that the new cascaded system reduces the diesel generator's fuel consumption by 38% for the South Korea to Pakistan route, and improved VCC reefer COP by 75%. The study also included an economic analysis which compared the capital, maintenance, and operational costs of the baseline and proposed system. Operational costs were found by using simulated values that lasted from June 8th to July 20th and the route was repeated 6 times a year. The capital costs were estimated to be $480,504 for the baseline system and $540,317 for the proposed system. Using a fuel cost of $360 ton^{-1}, lifetime of 25 years, and a discount rate of 10%, it was found that the proposed system had a NPV that was 88% of the baseline case despite having a higher capital cost, and the payback period was approximately 4 years.

Studies performed by Liang et. al. [49] also investigated the use of a cascade waste heat driven system for marine ships, but coupled the use of an ammonia-water absorption system with a steam Rankine power generation cycle instead of the hot water and VCC reefer system presented by Cao et. al. [22]. The first study used exhaust gas from a 51,480 kW marine engine to directly vaporize and superheat steam in the Rankine cycle. The condenser of the Rankine cycle also acted as the generator of the absorption system, which was seawater cooled and directly cooled air in the evaporator. The main parameter studied was the condensing temperature of the Rankine cycle, which is also the generator temperature of the absorption system. It was found that increasing the condensing temperature decreased the Rankine cycle power generation and the absorption chiller cooling capacity, indicating that a lower condenser temperature results in the highest potential

savings. The study also investigated the exergy efficiency of using only a steam Rankine cycle compared to the proposed cascade system and found that with a condensing temperature of 50°C and a steam superheat amount of 100°C, the exergy efficiency of the proposed system was increased by 84% over the Rankine system only. A second study by Liang et. al. [50] made further improvements to the cascaded system by including an additional expander in the absorption cycle and improved utilization of available heat. The steam Rankine system remained unchanged from the previous study. The absorption system utilizes a turbine to produce electricity and drop the pressure from the generator pressure to the evaporator pressure instead of an expansion valve. In addition, the condenser acts as a preheater and the exhaust gas leaving the evaporator of the Rankine cycle enters the generator of the absorption system. The reason for these changes is that it was found that the amount of cooling produced in the previous study was in excess of what ships required. At its optimal operation point, the system produced an equivalent electricity output of 5,223 kW_e, which is a 7.6% improvement to the power density of the marine engine. Unfortunately, these studies by Liang et. al. focus only on thermodynamic performance and do not consider any implementation challenges such as design, volume, or cost.

In summary, there are multiple paper studies focused on the performance of absorption chiller use on marine vessels. COPs varied based on operating conditions but were generally between 0.5 and 0.8. However, only a few studies presented a specific case study or provided an economic analysis of the absorption system compared to other systems. Additionally, no studied provided design considerations such as the size of the system. This is important as many marine vessels have extremely limited space. While the proposed system by Liang et. al. [49,50] is innovative in its ability to produce both electricity and cooling, it is unlikely to be implemented on

a ship due to the expected large footprint and high capital costs, which is a common theme for absorption chillers for both land-based and shipboard applications.

2.2.2. Adsorption Systems

Adsorption chiller systems are significantly less common than absorption chillers, but commercial options are still available [52]. Like absorption, adsorption chillers require a working pair of substances but utilize a solid adsorbent bed and a working fluid as opposed to two fluids. The adsorbent bed is a material which contains highly porous bodies with large internal surface area and have strong adsorption properties to a specific gas [53]. When only one bed is used, adsorption chillers can only run in batch mode, meaning that they cannot provide continuous cooling. This is due to the adsorbent bed having two purposes: desorption and adsorption. Multiple beds can be used to provide continuous cooling, but this increases the complexity of the system. A process flow diagram is shown in Figure 2-4. Most of the components remain the same as a vapor-compression cycle, namely the condenser, expansion valve, and evaporator. However, there are multiple discrete steps required to provide cooling in an adsorption chiller. First, valves 1 and 2 are closed and a heat source (e.g. hot water) is used to heat the adsorbent bed. The adsorbent bed is typically mounted against a metal surface to allow for heat transfer to occur between the fluid (hot water) and the adsorbent bed. Since the valves are closed, the adsorbent bed acts as a closed system and the refrigerant vapor pressure and temperature inside the bed increases. Once the vapor pressure matches the condenser pressure, valve 1 is opened and the desorption process begins. Heat is continued to be supplied to the adsorbent bed which results in some of the refrigerant leaving the solid surface. The desorbed vapor then flows to the condenser (2-3) where cooling water liquifies the refrigerant. Valve 1 is closed when the minimum concentration level is met in the adsorber. With both valves closed, the heat source in the adsorbent bed is replaced by cooling

water to pre-cool the adsorbent bed and reduce the vapor pressure to the evaporator pressure. The final step is to open valve 2 which allows the refrigerant to flow from the condenser through the expansion valve (3-4), which reduces the pressure and thus temperature of the refrigerant. In the evaporator, the refrigerant is evaporated (4-5) to provide a cooling effect to an external stream, typically chilled water. The evaporated fluid is then re-adsorbed into the adsorption bed (5-6) and the process repeats.

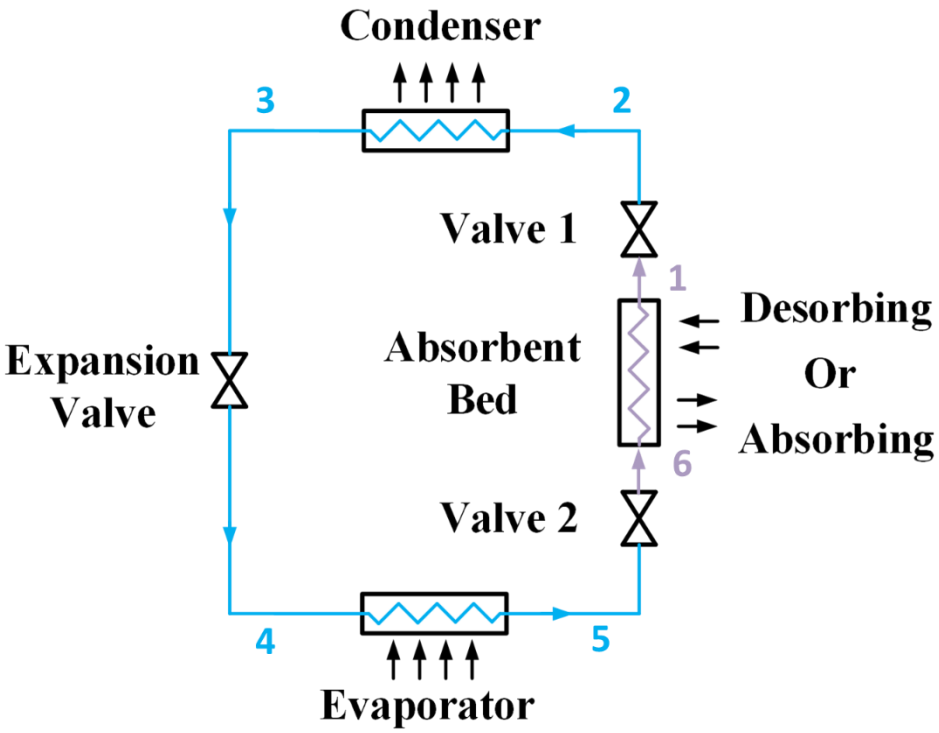

Figure 2-4: Single bed adsorption chiller process flow diagram

There are several advantages to utilizing an adsorption chiller over a vapor-compression chiller or absorption chiller. The first is that adsorption chillers do not require a pump or other rotating equipment. The removal of these components improves reliability and reduces maintenance cost and time, and results in quieter, vibration free operation. With no oil-cooled components, maintenance is not required to change filters or conduct oil changes. Pumps and compressors also represent a source of inefficiencies and eliminating these components should

result in higher utilization of energy. Another advantage is the ability to operate over a wide range of heat sources, including as low as 50°C [54]. This enables a broader range of applications and avoids challenges associated with utilizing low-temperature sources such as engine jacket water. As mentioned in [51], absorption chillers using jacket water as the heat source operate very close to their boundary limit, in which the system would malfunction if reached.

Figure 2-5: Commercial double bed adsorption chiller by Bry-Air [52]

The largest drawback of adsorption chillers is that they typically suffer from relatively low COPs of ~0.2-0.4 [55-57]. This is partially attributed to the use of ultra-low waste heat temperatures but is also due to poor heat and mass transfer properties of the adsorbent bed [58]. For this reason, the adsorbent-refrigerant pair selection has a significant impact on performance. The most common pairs are silica gel/water, zeolite/water, activated carbon/methanol, activated carbon/ammonia, calcium chloride/ammonia and composite adsorbent/ammonia [53]. Further, adsorbent-refrigerant pairs can be divided into three primary categories: physical, chemical, or composite.

Physical adsorbent-refrigerant pairs rely on Van der Waals forces amongst molecules in the adsorption process and are the most common adsorption chiller type. Silica gel-water is used in low-temperature heat source applications and is known to have higher COPs than its alternatives. The downside of this pair is that it is limited exclusively to low-temperature sources as the silica-gel will break down at higher temperatures (>120°C). Zeolite-water is an alternative to silica-gel and is very stable at higher heat source temperatures which makes it suitable for exhaust gas waste heat recovery. However, zeolite has less favorable heat transfer properties leading to lower COPs than silica-gel at similar operating conditions. Additionally, using water a refrigerant is challenging due to freezing concerns and the required low pressures (vacuum), leading to leakage issues and larger volume equipment. Activated carbon-ammonia systems avoid this issue by having reasonable working pressures (>1000 kPa) and are suitable for high-temperature heat sources. Activated carbon also has relatively low adsorption heat, which means that the system is more efficient at using heat in the desorption processes, thus increasing COPs. The obvious drawback to activated carbon-ammonia systems is that ammonia is toxic [35] and is unsuitable for some applications. Activated carbon-methanol systems are more suitable than ammonia systems for low-temperature heat sources but face similar challenges to silica-gel systems in that they cannot be used above a certain temperature and require vacuum operating pressures.

Chemical adsorbent-refrigerant working pairs use strong chemical bonds between the adsorbent and refrigerant, meaning that new types of molecules are formed in the process. Chemical pairs have more favorable mass transfer properties because they are not limited by the surface area of the solid material [53]. In general, chemical working pairs are suitable for very low-temperature operation. The biggest drawback of these systems is that they have lower stability

due to agglomeration and salt swelling, and thus the performance and COP is reduced [59]. Therefore, chemical adsorbent-refrigerant working pairs are less common than physical pairs.

More recently, composite adsorbent-refrigerant pairs have been developed to synthetically improve physical and chemical pairs and remove challenges typically associated with each. For chemical adsorbents, composite materials aim to improve the heat and mass transfer properties and limit swelling characteristics, while for physical adsorbents they aim to increase the adsorption quantity. The issue commonly faced with composite adsorbents is that there is a tradeoff between improving mass transfer properties and improving heat transfer properties, and it is difficult to find a balance between the two [60].

Since adsorption chillers are far less prevalent than absorption chillers, there is very limited cost and market data available. Three studies were found which clearly identified a capacity and cost for adsorption systems and are summarized in Table 2-4. Henninger et. al. [61] presented a study which focused on the cost of thermally driven heat pumps at the sub 50 kW_{th} cooling scale. The authors note that the difficulty in estimating commercial adsorption costs is due to limited data and a lack of specifications of what is included in provided costs (e.g. controls, machine only, installation, etc.). With these difficulties in mind, the authors estimated that adsorption equipment costs ranged from 1,199 to 1,446 Euro per kW_{th}, or $3,540 to $4,270 per ton in present day USD. These equipment costs are a significant increase over absorption chillers, which cost approximately $2,010 per ton at the 50-ton scale [41]. A US Department of Defense (DOD) funded effort by Southern Research Institute [62] investigated the design and installation of a solar-driven adsorption chiller at a DOD facility in South Carolina. The system selected for the project was a Power Partners Eco-Max silica-gel adsorption chiller rated at 80-tons of cooling. The cost of this unit was $191,000, or $2,388 per ton of cooling. This is considerably less than the cost estimated

by Henninger et. al., likely due to differing scales which have large impacts on specific costs as the equipment gets smaller. However, it still represents an increase in specific costs compared to absorption chillers. The total project installation costs were $772,672, or $9,658 per tons of cooling, and includes various equipment purchases such as pumps, piping, solar panels, storage tanks, and subcontractor costs. Lastly, a recent study by Alahmer et. al. [63] included an economic analysis of a solar-driven adsorption chiller operating in Perth, Australia. The modeled system provided a peak cooling duty of approximately 11.5 kW_{th}. The economic calculations assumed a specific cost of $2,100 per kW_{th}, or $7,386 per ton, and found that a payback period of approximately 11 years was possible for a residential building application.

Table 2-4: Cost of adsorption systems

Study	[61]	[62]	[63]
Cooling Capacity (tons)	< 14.2	80	3.3
Cooling Capacity (kW_{th})	< 50	281	11.5
Equipment Cost ($/ton)	$3,540 to $4,270	$2,388	$7,386
Equipment Cost ($/$kW_{th}$)	$1,006 to $1,214	$679	$2,100
Total Installed Cost ($/ton)	-	$9,658	-
Total Installed Cost ($/$kW_{th}$)	-	$2,746	-

2.2.2.1. Review of Maritime Research

Due to the lower performance, higher specific costs, and similarly large volumes as absorption chillers, there are no commercial options for marine adsorption chillers. In addition, there are a limited number of studies focused specifically on using adsorption chillers on marine vessels, summarized in Table 2-5, all of which are for use on fishing vessels at the sub 20 kW_{th} cooling scale.

Table 2-5: Summary of studies for adsorption chillers in maritime applications

Authors	Adsorbent – Refrigerant Pair	Heat Source Temp	Condenser Temp.	Chiller Temp.	Cooling Duty	COP
		°C	°C	°C	kW	-
Wang et. al. [64]	Activated carbon/$CaCl_2$ and ammonia	47 to 130	-	-15	17.1 to 17.8	-
Wang et. al. [65]	Expanded graphite/$CaCl_2$ and ammonia	550	25	-15.6	5.1	0.38
Zisheng et. al. [66]	-	245	28	-18	6.6	0.29
Palomba et. al. [67]	Activated carbon and ethanol	80		0	10	0.07

As addressed by Wang et. al. [64], there are two main issues with using adsorption chillers for marine applications: (1) there is limited space on fishing vessels so the cooling systems must be compact and, (2) there is an incompatibility issue between ammonia refrigerant, steel, seawater, and copper. The authors address the first issue by utilizing a compound adsorbent of activated carbon and $CaCl_2$ with ammonia as a refrigerant. This compound bed improves the gas permeability, thermal conductivity, and dimensional stability compared to standard chemical adsorbent options, and has a high refrigerant holding capacity and sorption rate. The second issue is addressed through the use of a heat pipe type adsorber. Ammonia systems typically use steel materials, and seawater cooled systems require copper alloys to avoid corrosion, but ammonia is not compatible with copper. The proposed system avoids this issue by using a heat pipe which includes a steel section for heating of the adsorbent bed using exhaust gas directly, and a copper section that uses seawater to cool the adsorbent bed. The working fluid within the heat pipe is water. The study experimentally tested the heat pipe performance at a sub-6 kW_{th} cooling scale and predicted that the system could provide 17.8 kW_{th} of refrigeration at -15°C by using two adsorbent beds which each include 64 heat pipes. While this study includes an innovative strategy

to make adsorption refrigeration more viable on marine vessels, it does not address issues with the toxicity of ammonia, the physical size of the full-scale system, or economic considerations.

A double heat pump design was introduced by Wang et. al. [65] which improved upon past work by reducing the number of valves used within the system and further improved the heat transfer performance of the adsorber. The working principle of the system is slightly different from a traditional two-bed adsorption chiller. The system is broken down into two sections: a thermal compressor and the ammonia refrigerator. The thermal compressor includes a shell and tube exhaust gas heat exchanger, a shell and tube condenser, and two different heat pipes used in the adsorbers. One heat pipe is a two-phase closed thermosyphon type and is used for cooling, and the other is a split type used for heating. This double heat pipe design still allows for separation of ammonia and copper material. The adsorbent material was an expanded graphite-$CaCl_2$ compound. The refrigeration section includes two shell and tube condensers and evaporators which have a fluid management valve connecting them. Simulation results indicated that the proposed system could provide 5.1 kW_{th} of chilled water at -15.6°C when the seawater temperature was 25°C and 13.4 kW_{th} of exhaust gas heat was available at 550°C.

Another option to avoid material issues associated with ammonia and seawater is to use intermediate loops to avoid the direct contact of seawater in the absorber, as studied by Zishen et. al. [66]. In this study, the authors compare a simple two-bed adsorption system that is directly seawater cooled and exhaust gas heated to one that is indirectly cooled and heated. The system that was directly heated has a COP of 0.29 when using 245°C exhaust gas, 28°C seawater, and the evaporator temperature is -18°C. The benefit to this style system is the simple structure allows for a more compact system and allows for the use of a simpler control program, but the system is also likely to have corrosion issues. The indirect cooling and heating system had better heat and

pressure recovery and a higher COP, although the authors do not discuss in detail how much the indirect system improved performance. While the indirect system avoids some corrosion issues in the adsorber, the system requires more complicated controls and results in lower refrigeration capacity per unit volume. Detail is not provided in this study on the specific materials and fluids used within the system.

While the previously mentioned studies generally focus on the use of adsorption chillers for ice making applications, Palomba et. al. [67] provides a case study of the use of an adsorption chiller for food preservation on an Italian fishing vessel. One important practical design consideration for this application is that non-toxic refrigerants are necessary to avoid contaminating the fish. For this reason, the authors selected an activated carbon and ethanol adsorption system. The case study was performed on a vessel representative of an Italian fishing fleet with an engine power of 195 kW and a gross registered tonnage (GRT) of 20. The baseline system was a R422a screw-type refrigeration system used to keep fish frozen at an assumed temperature of 0°C. The waste heat recovery system and cold room were dynamically modeled as inputs to the adsorption performance model and two case scenarios were compared: (1) introduction of 100 kg of fish every 4 hours into the cold room and (2) constant introduction of 25 kg of fish every hour from 3 a.m. to 8 p.m.. The adsorption performance model was calibrated using data from a 300 W prototype. The resulting simulation indicated that between 570 and 1480 kg yr^{-1} of fuel could be saved depending on the operational scenario, compared to 1200 and 1599 kg yr^{-1} for an exhaust driven absorption chiller. The authors acknowledge that no economic analysis is performed because there are no commercial adsorption units for fishing vessels and the proposed technology is only in the prototype phase, indicating that the cost uncertainty would be too large. In addition, the authors discuss that in order for adsorption and absorption chillers to be

successfully implemented in the marine field, two aspects play a critical role: the availability of reasonably sized equipment and the design and integration into a devoted waste heat recovery system.

The marine-based adsorption studies discussed here are very limited in scope to small-scale refrigeration applications, either for ice making or frozen fish storage. It is clear that the technology has not progressed to commercial scales and several operational and practical barriers exist which prevent adsorption chillers from being successful in providing standard chilled water temperatures on larger ships including cost, size, weight, performance, and material-based issues.

2.2.3. Ejector and Organic Rankine-Vapor Compression Systems

Ejector and organic Rankine-vapor compression (ORVC) systems are two other types of TDCs which have similar working principles in that they consist of a power and cooling cycle. Neither system is commercially available, but there has been continued research and development to improve the performance and viability of the two systems. A PFD of a simple ORVC system is provided in Figure 2-6. Unlike absorption and adsorption chillers, ORVC and ejector systems can use a single working fluid. The working fluid in the power cycle first enters the waste heat boiler as a high pressure, subcooled fluid and is vaporized by absorbing heat from an external source (5-1). The superheated vapor is then expanded in a turbine (1-2) to produce mechanical work. This mechanical work can either directly power a compressor by utilizing a turbo-compressor, as shown in Figure 2-6, or electricity can be produced in a generator and then converted back to mechanical work in the compressor. The latter has increased energy losses, resulting in lower overall performance, but has improved flexibility through the ability to produce electricity for other purposes. In Figure 2-6, the power and cooling cycle share a common condenser to reduce the number of components and expensive heat exchangers, but separate sub cycle condensers can also

be used. If two condensers are used, separate optimized fluids can be used for each sub cycle to improve performance. After expanding in the turbine, the refrigerant is combined with the compressor discharge (2-3) and then liquified in the condenser (3-4) by an external stream. A portion of the total refrigerant flow is pumped back to the boiler pressure (4-5) to be re-vaporized and produce more power. The rest of the refrigerant flow is throttled to a lower pressure in an expansion valve (8-9). The refrigerant at this point is at a low-pressure, low-temperature state and typically in the two-phase region. The refrigerant is then vaporized (9-6) in the cooling cycle evaporator, thus providing a cooling effect to an external stream. Finally, the vaporized refrigerant is then compressed in the compressor and the cycle is repeated.

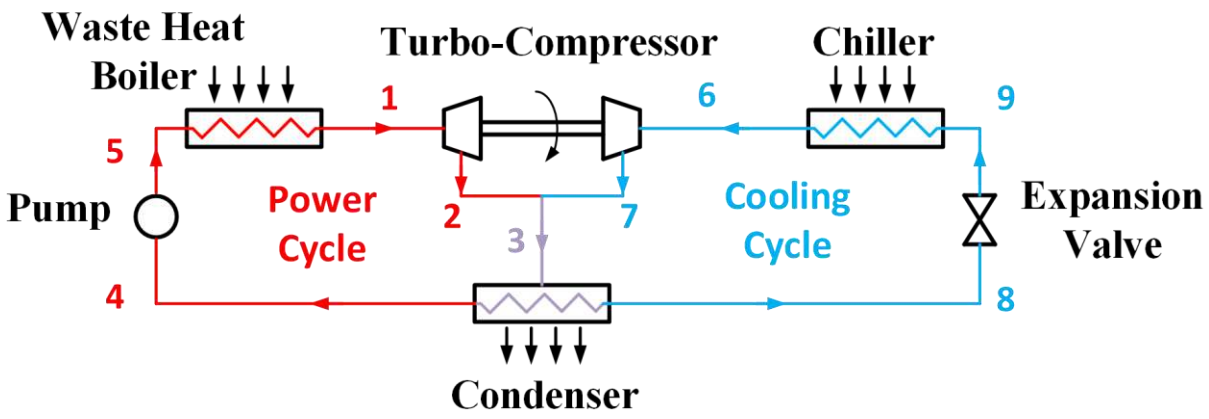

Figure 2-6: Organic Rankine-vapor compression process flow diagram

The major advantage of ORVC systems over absorption and adsorption technologies is the flexibility in working fluid selection. Commercial absorption and adsorption systems typically use either water or ammonia as the working fluid, which either results in freezing and vacuum pressure issues or the use of a toxic fluid. ORVCs can use refrigerants and equipment that are used in commercial electrically driven vapor-compression chillers, including those that are medium-pressure, non-toxic, non-flammable, and environmentally favorable. The system performance can be optimized depending on the application and desired operating conditions. The use of medium-

pressure refrigerants also enables to use of compact heat exchanger devices. A more detailed discussion of possible working fluids is provided in Chapter 3. The performance of ORVC systems generally fall between adsorption and single-effect absorption chillers with COPs around 0.5-0.6 [68,69]. The drawback of ORVCs is that they have multiple complicated turbomachinery components, including a refrigerant pump, turbine, and compressor. These moving components are more likely to breakdown and increase down time and maintenance costs. Additionally, the isentropic efficiencies of these components will have significant impacts on the system performance. Lastly, there are concerns regarding the durability, reliability, and ability to scale down the turbo-compressor [70].

Since ORVC cooling systems are not commercially available their costs are not well established. However, the cost of an ORVC can be estimated by assuming two commercially available subsystems are used: an organic Rankine cycle (ORC) and a vapor-compression cycle (VCC). A cost breakdown of three different scaled ORVCs is provided in Table 2-6. The type of VCC technology, and thus cost and performance, is dependent on the scale. Small-scale ORCs (<50 kW_e) are more suitable to drive a scroll chiller which are typically air-cooled and have lower efficiencies and higher specific costs compared to water-cooled centrifugal chillers, which are more commonly used for chillers greater than 200-tons [40]. Small scale (20-50 kW_e) ORC system costs were estimated by Smith et. al. [71], and were based on the detailed design of a 50 kW air cooled system that utilized waste heat at 100°C. A larger scale estimate was based on a UTC Power ZeNOx 200 kW_e ORC [72]. Compared to absorption costs in Table 2-1, the installed specific costs of an ORVC at the ~50 tons and ~400 tons scales are less than 50% of the costs of a single-effect LiBr absorption chiller. If improvements can be made to performance, reliability, and flexibility, ORVCs have the potential to overcome commercial absorption chillers.

Table 2-6: Cost and performance of ORVC systems using distinct sub cycle installations

ORC Output (kW_e)	20	50	200
ORC Specific Cost ($/$kW_e$)	$2,000	$1,500	$1,000
Installed ORC Cost	$40,000	$75,000	$200,000
VCC Type	Scroll (Air-Cooled)		Centrifugal (Water-Cooled)
VCC COP	3.0	3.0	6.6
Cooling Capacity (kW_{th})	60	150	1320
Cooling Capacity (tons)	17.1	42.6	375
VCC Specific Cost ($/ton)	$1125	$1025	$475
Installed VCC Cost	$19,192	$43,716	$178,277
Total Installed ORVC Cost	$59,192	$118,716	$378,277
ORVC Specific Cost ($/ton)	$3,470	$2,784	$1,008

Ejector systems overcome challenges with durability, reliability, and scalability of the turbo-compressor by replacing the turbine and compressor with an ejector nozzle, shown in Figure 2-7. The high-temperature, high-pressure vapor leaving the waste heat boiler (state point 1 in Figure 2-6) enters the nozzle in the primary flow section on the left end of the nozzle. The primary flow is then expanded, which decreases the pressure and increases the velocity to supersonic speeds and creates a vacuum in the mixing section. The low-pressure vapor leaving the cooling cycle evaporator (state point 6 in Figure 2-6) is drawn into this space through the secondary flow entrance at the bottom of the nozzle and mixes with the primary flow. The mixture is then diffused in the diffuser section to reduce the velocity and achieve the desired pressure of the condenser. The ejector acts as a compressor but does not have any moving parts, thus reducing complexity and maintenance. As a result, the system is less complex and the only moving part is the power cycle pump.

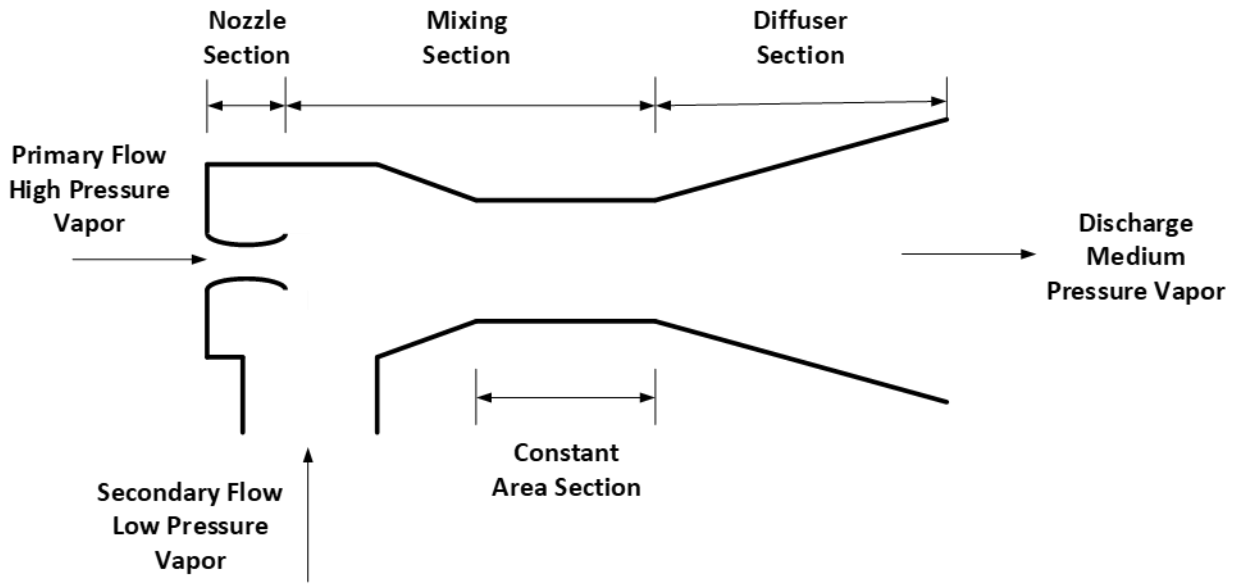

Figure 2-7: Ejector nozzle working principle

Ejector cooling systems are far less studied compared to the previous discussed TDCs, and the internal flow mechanics within the nozzle are difficult to model and are not well understood [70]. This makes optimization of the nozzle difficult, and ejector systems experience relatively low COPs of ~0.2-0.4 [73,74]. Another drawback is the lack of flexibility during operation compared to an ORVC, which can have various speeds and operate over a wider range of conditions. Korres et. al. [75] performed an experimental study which compares the performance of two different ejector nozzles with different geometries under various inlet and outlet pressures. It was seen that the performance of the ejector decreased significantly as the reverse compression ratio (suction pressure divided by the condenser pressure) approached 1.

Ejector systems are limited to laboratory settings and there is no published information on their costs. It can be assumed that ejector systems would be slightly less expensive than ORVCs as the only difference is the replacement of a complicated turbo-compressor with a simpler ejector nozzle.

2.2.3.1. Review of Maritime Research

There has been limited research on ORVC and ejector cooling systems for shipboard applications, summarized in Table 2-7.

Table 2-7: Summary of studies for ORVC and ejector chillers in maritime applications

Authors	System Description	Refrigerant	Heat Source Temp	Condenser Temp.	Chiller Temp.	COP
			°C	°C	°C	-
Bounefour et. al. [76]	ORVC	R134a, R290, R600, R600a, R1270	70 to 100	40	5	0.25 to 0.55
Bounefour et. al. [77]	Simple and serial cascade ORVCs	R134a, R290, R600, R600a, R1270	70 to 100	40	5	0.15 to 0.6
Bounefour et. al. [78]	Simple, recuperative, and serial cascade ORVCs	R134a, R600, R600a	70 to 100	30 to 50	-15 to 15	0.1 to 0.6
Bu et. al. [79]	ORVC	R134a, R290, R600, R600a, R123, R245fa	80 to 160	30 to 40	-5	0.18 to 0.46
Ezgi et. al. [80]	Steam ejector refrigeration system	Water	315 to 380	-2 to 32	4	0.11 to 0.29

Bounefour et. al. conducted multiple studies on using waste heat from marine diesel engines to power an ORVC system. The first study [76] was a thermodynamic and exergenic analysis of five different working fluids: propane (R290), butane (R600), isobutane (R600a), propylene (R1270), and R134a. Unfortunately, all these fluids, with the exception of R134a, are natural fluids with A3 ASHRAE classification, meaning they are highly flammable. While in later papers the authors recognize this concern and mention the need for additional safety protocols, they do not study any additional fluids. In the ORVC studied, the turbine mechanical work directly powers the cooling cycle compressor and the two cycles share a common condenser and working fluid. The working fluid mass flow rate was set at 1 kg s^{-1}, the evaporation temperature was 5°C,

the condenser temperature was 40°C, and the turbomachinery isentropic efficiencies were set at 75% to 80%. The only parameter that was varied was the boiler exit temperature which ranged from 60°C to 90°C, representing a waste heat temperature of 70°C to 100°C. As expected, increasing the boiler temperature increased the system performance, although the authors did not mention if the waste heat duty was constant or if it also increased. COP and cooling duty were provided over the range of boiler temperatures. The exergy study revealed that the highest exergy losses were in the evaporator, condenser, boiler, and then the expander. A follow up study [77] proposed an improvement to the standard ORVC by using a cascade boiler. Two boilers were used instead of one, theoretically drawing out more of the waste heat and producing more superheating. However, this strategy requires an additional large heat exchanger and pump, as well as more complicated piping and control systems. The study was performed using the same fluids and methodology as the previous study, but the waste heat hot water stream mass flow rate was set at 1.46 kg s^{-1} instead of the ORC working fluid mass flow rate. The cascade system had significantly higher ORC net power output, but the COP appears to be similar to the standard ORVC. A third study [78] included a recuperative ORC and more variable operating conditions. In this study, only R600, R600a, and R134a were considered. Additional parameters, such as the compressor pressure ratio and expander volume ratio were considered as design parameters. The condenser between the ORC and VCC was no longer shared, and two separate condensers were used. The waste heat flow rate was once again set, this time at 1.3 kg s^{-1}. The boiler exit temperature varied from 60°C to 90°C, the evaporator temperature -15°C to 15°C, and the condenser temperature 30°C to 50°C. No mention was made of the temperatures of the external streams or heat exchanger effectiveness values. The results showed that the cascade ORC had the highest power output. As expected, due to the additional components, the cascade ORC had the highest exergy loss, followed by the

standard ORC and then the recuperative ORC. The COPs for the different systems ranged from approximately 0.1 to 0.6 over the studied conditions. The recuperative ORC and cascade ORC had COP improvements of 0.52% and 2.4% over the standard ORC, respectively. These are mild improvements and likely do not justify the additional components and complexity of the system. The results also showed the effect of varying the boiler, evaporator, and condenser temperatures on system performance. It was shown that condenser saturation temperature had the highest impact due to it effecting the performance of the ORC and the VCC. Lastly, through these three studies, it was shown the R600 and R600a had the optimal performance over other natural refrigerants and R134a, even when two fluids could be used. The studies performed by Bounefour et. al. introduced three proposed ORVC systems for shipboard cooling applications and performed a thermodynamic and exergy analysis over a range of saturation temperatures. The issues with these studies are a lack of variable waste heat duties, heat exchanger information, and non-flammable refrigerants studied. In addition, no consideration was made for economics or design issues such as volume and material constraints.

Bu et. al. [79] have also studied ORVC systems for shipboard applications, but specifically studied ice making for fishing boats to preserve fish. This application is characterized by the reduced evaporator temperature of approximately -5°C. Six working fluids were studied: R123, R134a, R245fa, R600, R600a, and R290. The system had a coupled turbine and compressor and a common condenser which was seawater cooled. Two heat streams were used: exhaust gas and jacket water. The jacket water heated the refrigerant first, followed by the exhaust gas. The temperature of the hot water ranged from 80°C to 160°C and the condenser temperature from 30°C to 40°C. The evaporator temperature was set at -5°C and the waste heat total was set at 200 kW between the two streams. The isentropic efficiencies were also set between 80% to 90%. The

results indicated ORC efficiencies between 6% and 12%, with R290 and R134a having the highest efficiencies. The authors do note, however, that these fluids also have higher operating pressures and therefore would have higher investments. On the cooling cycle, COPs range from 3.24 to 5.25, with R123 having the maximum COP and R134a having the lowest. The authors also introduce a parameter called the CRPR which is the ratio of the COP to the pressure ratio in the compressor. The authors claim that a higher CRPR is indicative of better refrigeration performance, and R600a and R600 have the highest CRPR. However, R600 is under vacuum pressures at the compressor inlet. Since R600 is highly flammable, an air leak could cause an explosion. R600a has a higher pressure above ambient at the compressor inlet, making it a safer option. Due to this reason, as well as modest performance and favorable environmental properties, the authors suggest that R600a is the most suitable fluid for a shipboard ORVC. A major drawback of this study is a lack of information regarding the waste heat streams, including the division of waste heat between the exhaust gas and jacket water. Also, the waste heat amount is fixed, and the temperature is varied. In actual operation, the waste heat will vary in the jacket water, and the temperature is more likely to be fixed.

Only one study, performed by Ezgi et. al. [80], was found that focused on an ejector refrigeration system for a shipboard application. The study specifically focused on a cooling system for a naval surface ship. A seawater cooled steam ejector refrigeration system and a steam ejector heat pump were considered and compared to a water-LiBr absorption heat pump and a vapor-compression heat pump. Design and off-design conditions were considered, and exhaust gas was used as the waste heat source. The case study included two 3000 kW diesel engines and the engine load was varied between 50% and 100% load. The ship was also said to require 144 kW_{th} of heating and 116 kW_{th} of cooling, although the studied system exceeded these amounts

significantly. The ejector system heated hot water to 40°C-45°C, cooled chilled water from 12°C to 7°C, and used seawater that ranged from -2°C-32°C. The working fluid of the system was water, and seawater and exhaust fouling were considered. At design conditions, the cooling COP ranged from 0.3-0.4 depending on the boiler pressure, and 300 kW_{th} to 800 kW_{th} of cooling was provided. At off design conditions the COP dropped as low as 0.1, emphasizing the issue with ejector refrigeration systems performance. The system performance was compared to a VCC with a COP ranging from 2 to 4. The results showed that for 1000 operating hours, the ejector system would save 33,712 L -120,447 L of fuel in heating mode ($33,621-$120,122) and 7,581 L - 27,139 L of fuel in cooling mode ($7,561-$27,065).

ORVC and ejector systems design-based research is very limited. All the ORVC studies discussed focused solely on thermodynamic performance of varying fluids and configurations and lacked discussion on practical considerations such as size and cost. In addition, only one ejector cooling system study was found for shipboard cooling and was the only study to include a specific case study and presented fuel savings and costs. However, even this study failed to include an estimated cost of the system.

2.3. Turbo-Compression Cooling System

A recently studied and tested ORVC variant is the Turbo-Compression Cooling System (TCCS), which has been in development at Colorado State University (CSU). The TCCS includes an ORC coupled to a VCC using a common shaft in a high efficiency centrifugal turbo-compressor. The TCCS was first studied by Bandhauer and Garland as part of an ARPA-e ARID program to reduce water consumption of a 565 MW natural gas combined cycle power plant [81]. In this study, a recuperative ORC and a supercritical ORC were investigated to power the turbo-compressor and reduce the heat exchanger area required for dry air cooling and used dry-air

condensers within the TCCS. Flue gas at 106°C was used to power the turbo-compressor and cool circulating water from 27°C to 16°C which is used to cool the bottoming cycle of the power plant. Unique to this study was the use of a magnetically coupled turbo-compressor which hermetically sealed the two cycles from one another and allowed for separate fluids to be used, thus optimizing each cycle. In this study, the subcritical ORC used RC318, the supercritical ORC used R218, and the cooling cycle used R152a. These fluids were selected to achieve optimal turbine and compressor sizes and speeds while maintaining high efficiencies (>80%), which were verified using Ns-Ds Cordier diagrams. The supercritical TCCS was able to reduce the required dry-air cooling heat exchanger thermal conductance (UA) by 26% (from 150.7 to 111.5 MW K^{-1}). The impact of varying condenser temperatures from 20°C to 35°C and exhaust outlet temperatures from 45°C to 90°C on the system COP and UA was also included in this study.

A follow up study by Garland et. al. modeled a scaled down 250 kW_{th} TCCS over a range of ambient conditions, from 15°C to 30°C, to supply chilled water at 7°C [82] to allow for more direct comparison to traditional TDCs. Only the recuperative TCCS was included in this study and used HFE7000 as the working fluid in the ORC and R152a in the VCC. An off-design modeling methodology was used in this study which including turbine and compressor performance maps generated by Barber Nichols Inc. (BNI) to predict turbomachinery efficiency. The transfer efficiency of the magnetic coupling was assumed to be a constant 93%. Heat exchanger UAs were calculated at the design condition (15°C ambient) and were fixed at off-design conditions to simulate a fixed heat exchanger size. Results from the model indicated that increasing the ambient temperature resulted in decreasing mass flow rates. Above 30.6°C the compressor entered the stall region on the compressor map and was unable to operate. It is important to note that the turbo-compressor used in this study was designed for a lower compressor lift scenario, and that

increasing the evaporator pressure would increase flow rate which would avoid stall. A turbo-compressor optimized for the proper operating conditions should avoid this issue. Overall, the COP of the TCCS ranged from 1.29 to 0.49 at ambient conditions of 15°C and 30.6°C, respectively. There was also a sharp decrease in cooling duty at higher ambient conditions (a 70% reduction) due to the turbine power reducing from 13.9 kW to 8.0 kW.

The scaled down, 250 kW_{th} TCCS was then designed, built, and experimentally tested at off-design conditions at CSU [83]. As shown in Figure 2-8, the test facility included the power and cooling cycles which used a magnetically coupled turbo-compressor, an exhaust gas simulation loop, a chilled water simulation loop, and four dry air cooling towers. The turbo-compressor was designed and fabricated by BNI to provide 12.4 kW of turbine power and 11.6 kW of compressor power at 30,000 RPM. Heat exchangers were custom fabricated by Modine Manufacturing and are aluminum brazed heat exchangers. Working fluids were HFE7000 and R134a in the power and cooling cycle, respectively. Tests were performed at an ambient temperature of 27.5°C and exhaust gas flow rate, temperature, and cooling tower air side mass flow rates were held constant. Tests were performed by varying the power cycle pump speed and the cooling cycle expansion valve position to adjust the flow rates of each sub cycle. The power cycle mass flow rate varied from 0.3 to 0.5 kg s^{-1} and was limited by compressor surge at the lower limit and lack of superheat at the outlet of the boiler at the upper limit. The cooling cycle flow varied from 0.5 to 0.8 kg s^{-1} and was limited by the geometry of the expansion valve. It was found that the highest COP was 1.84 and occurred with a power cycle mass flow rate of 0.39 kg s^{-1}, a cooling cycle mass flow rate of 0.74 kg s^{-1}, and a chiller saturation temperature of 31.8°C.

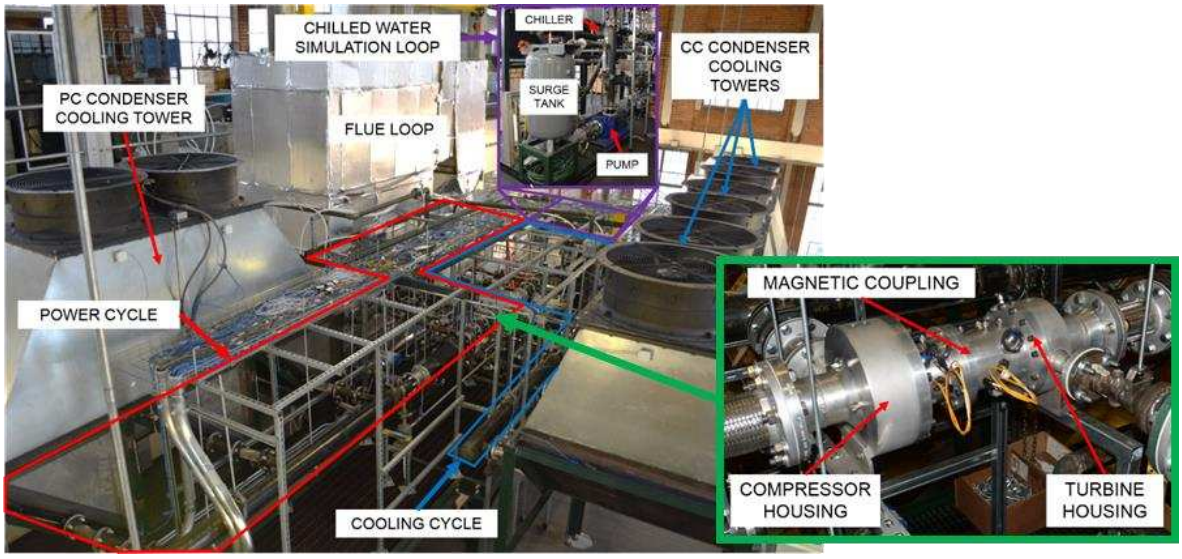

Figure 2-8: Overview of the TCCS test facility

From the experimental data, Garland et. al. developed a validated scaling method to predict heat exchanger and turbomachinery performance at off-design conditions [84]. The scaling methodology included a UA scaling method for the heat exchangers, in which original temperature assumptions for the baseline case were replaced with UAs. The UAs were then scaled based on the heat transfer coefficient, heat duty, and heat exchanger area. Additionally, the turbo-compressor was scaled using performance maps for the turbine and compressor. Using a maldistribution factor for the exhaust flow rate resulted in good connection between the off-design model and experimental data over a range of power and cooling cycle flow rates, with the COP predicted within +/-2.0% by the modeling approach. The issue with this modeling approach is that there was some discrepancy between the saturation temperatures in the model and experimental data, and a wide range of flow rates was studied but ambient conditions were not. Varying condenser water temperatures and waste heat flow rates is an essential part of this study and will be further studied using new methods.

Additional studies were performed for the TCCS driven by low-grade waste heat from marine diesel engines. Unlike the previous work discussed, these studies did not include a

recuperator in the ORC, a magnetically coupled turbo-compressor, or custom heat exchangers. Gibson et. al. [85] performed a technoeconomic optimization study of a TCCS driven by 2 MW_{th} of engine coolant waste heat at 88°C. The system used R134a as the working fluid and delivered chilled water at 7°C with a seawater temperature of 32.2°C. A thermodynamic model was first created which assumed constant turbomachinery efficiencies of 80% and used fixed heat exchanger effectiveness values to calculate the system performance. The thermodynamic model was then coupled to detailed plate frame heat exchanger (PHE) sizing models. All heat exchangers had the same set plate length, width, thickness, and distance between plates. Using heat transfer and pressure drop correlations from literature, the model predicted the number of plates needed based on the set effectiveness value. The authors note that the use of PHEs enable a more compact design and are easy to use and clean. They also allow for different materials to be used depending on the application (e.g. titanium for seawater contact). An economic model was also included to predict the cost of the heat exchangers, turbo-compressor, power cycle pump, pipes, and refrigerant charge. Fuel savings were found by assuming the system was operating for 85% of the year, the engine thermal efficiency was 35%, and the baseline electric chillers COP was 4. The heat exchangers were optimized by altering the set effectiveness values, thus changing the size of the heat exchangers, to reduce the payback period of the system. The optimized system had a COP of 0.312, cost $338,623, and saved $135,668 in fuel per year, resulting in a payback period of 2 years and 6 months. It was also found that the heat exchangers accounted for 84% of the total system equipment costs and that payback period was most sensitive to changes in the two-phase regions of the condensers.

Another study by Young et. al. [86] furthered marine TCCS research by investigating 5 different fluids: R134a, R245fa, R1234ze(E), R152a, and R600a. The study used the same

modeling approach which coupled a thermodynamic model to a heat exchanger sizing model and economic model to determine system performance and economic returns. The model was again used to optimize heat exchanger sizes to minimize payback period. Results indicated that a system using R152a as the working fluid could be optimized to have a payback period of 1.46 years with an initial capital cost of $181,846. However, the minimized payback period was not indicative of the optimal return on investment (ROI). A system utilizing R1234ze(E) had the largest ROI over a ten-year lifetime of $1,399,666. This system had a higher payback period of 1.87 years but had the largest COP of the five fluids at 0.415. The authors also demonstrated that a higher COP system does not necessarily result in higher economic returns. For example, increasing the COP from 0.384 to 0.528 increased annual fuel savings by $61,931 for a system operating with R134a, but the investment costs of the system increased by 4.4 times, with the largest increase being in refrigerant charge costs. If operated for 10 years, the payback optimized system would have a ROI that is $610,320 more than the higher performing system. This study laid the groundwork for coupling thermodynamic, heat exchanger, and economic models and utilized the TCCS for shipboard applications but did not investigate off-design conditions or recuperative heat exchanger strategies.

2.4. Research Needs for Shipboard Thermally Driven Cooling Systems

The provided literature review introduced the four major thermally driven chiller technologies: absorption, adsorption, ORVC, and ejector. An overview of the working principles, pros and cons, market availability, and cost were all discussed. In addition, the status of each technology in the maritime sector was discussed. Only absorption chillers are available commercially for shipboard applications, but their use is rare and is mostly limited to cruise ships. Their rare use is most likely due to large system volumes, high specific costs, and the common use

of ammonia which has a high toxicity. Adsorption, ejector, and ORVC research for maritime use is very limited and typically fail to address the challenges with maritime applications, such as:

- There is very limited space in mechanical rooms on ships. Commercial TDCs are often significantly larger than electrically driven chillers. There is a need for more compact designs, which is difficult with absorption and adsorption technologies as they often use water as a working fluid and operate with vacuum pressures.
- Thermally driven chillers often require backup electric chillers for when there is insufficient waste heat availability or if the engine is not operating. This further increases the footprint required to install a TDC.
- There are numerous concerns with capturing exhaust gas from diesel engines, including thermal fatigue and failure of the heat recovery heat exchangers. However, there are limited studies that focus on only the capture of low-grade waste heat sources.
- Fluids used on ships should be non-toxic and non-flammable. Many studies included fluids that were either toxic (e.g. ammonia) or flammable (e.g. R600a). These fluids are non-starters for certain applications.
- Marine engine and generator set loads are highly variable, as is the operating environment. The thermally driven chillers must operate over a wide range of waste heat availability and cooling water temperatures. However, there are limited case studies that take this into account.

ORVCs are a promising technology for this application because they are not limited by fluid or material types, meaning that they can use a non-toxic, non-flammable, medium pressure fluid that is appropriate for shipboard use. Therefore, the system can be designed to use compact heat exchanger technologies to reduce the footprint of the system. They can also operate with low-

temperature heat sources (<90°C) and have relatively simple operating principles. An ORVC variant, the TCCS, has been studied for use on ships with compact plate frame heat exchangers, but work was limited to a simple cycle, one operating condition, and the system was optimized based on economic considerations. The following are remaining research needs for ORVC/TCCS systems for shipboard applications:

- Provide a complete case study, including engine data, engine operation profile, seawater temperature, and cooling requirements for a representative ship.
- Study fluids over the case study data that would be acceptable for shipboard use, meaning that they have favorable thermal and environmental properties, but are also non-flammable, non-toxic, and are commercially available.
- Optimize equipment sizes based on volume instead of economic returns. While economics are an important driver for implementation, systems that are too large are non-starters for certain applications and retrofit projects.
- Improve system performance through either heat recuperation strategies or alternative integration plans.
- Study off-design engine and seawater temperature conditions using detailed heat exchanger models with fixed geometries and compare to simpler off-design methodologies.

2.5. Specific Aims for this Study

The current study aims to address main challenges associated with using thermally driven chillers for maritime applications. It was seen through the literature review that existing TDC technologies are unsuitable for shipboard use, either due to their prohibitive sizes, use of inappropriate fluids or materials, required operating conditions, or their unfavorable economics.

The current work aims to address these challenges and further TCCS research through the following specific aims:

- Present a case study of a ship operating with variable engine loads and seawater temperatures to use as inputs to the TCCS performance and sizing models.
- Evaluate fluid and system configurations based on system performance over the case study range of conditions.
- Optimize the TCCS heat exchangers based on an allowed volume while maximizing performance. Provide a solid model visualization demonstrating that the system can fit within the allowed dimensions.
- Study the final designed system over the initial range of conditions using a fixed geometry approach. Compare performance, size, and economic results to SOA technologies.

The overall goal of the work is to provide a detailed case study and design methodology that results in a TDC that could implemented on a space constrained ship. The design must meet strict performance and size goals while being economically attractive. The overall modeling approach is applicable to other systems and applications for design case sizing of equipment and off-design performance modeling.

CHAPTER 3 Modeling Approach

The present study builds upon past turbo-compression cooling system and thermally driven chiller research by providing a case study of a ship and a design methodology that addresses major challenges with implementing TDCs on ships. While commercial absorption chillers exist for marine applications, their use is extremely rare due to high costs, volume, and unreliable operation. Studies exist on other types of TDCs for shipboard use, but often fail to address the challenges that have limited the adoption of absorption chillers. In this work, a detailed case study is first presented which is representative of a large ship. Data from this case study is used to determine the performance of the TCCS. Three different TCCS operational configurations are presented and five different working fluids are thermodynamically modeled and compared based on performance over a range of conditions. The shipboard TCCS was then designed using heat exchanger models and optimized to fit within the dimensions of a commercial electrically driven chiller. The designed system is then again studied over the range of case study conditions with fixed equipment sizes to determine yearly savings. The costs of individual components are estimated and used to perform economic calculations and results are compared to state-of-the-art technologies.

This chapter will first present the case study used in this work, including engine selection and data, engine operational profile, and a seawater temperature profile. The TCCS configurations considered and an example calculation will then be provided, followed by an overview of the modeling approach. Next, details of the TCCS thermodynamic model, including working fluid selection, inputs, and equations will be presented. Heat exchanger models used to predict the size and performance of the designed system will then be described. Lastly, the fixed geometry performance modeling methodology and economic modeling will be provided in detail.

3.1. Case Study

A case study of a large shipboard diesel generator set and an electric seawater cooled chiller is presented in this section. In actual operation, multiple engines and chillers are used at part loads to provide the required amount of grid electricity and cooling. However, focus will be placed on a single engine and a single chiller to provide variable amounts of electricity and constant cooling demands, as shown in Figure 3-1.

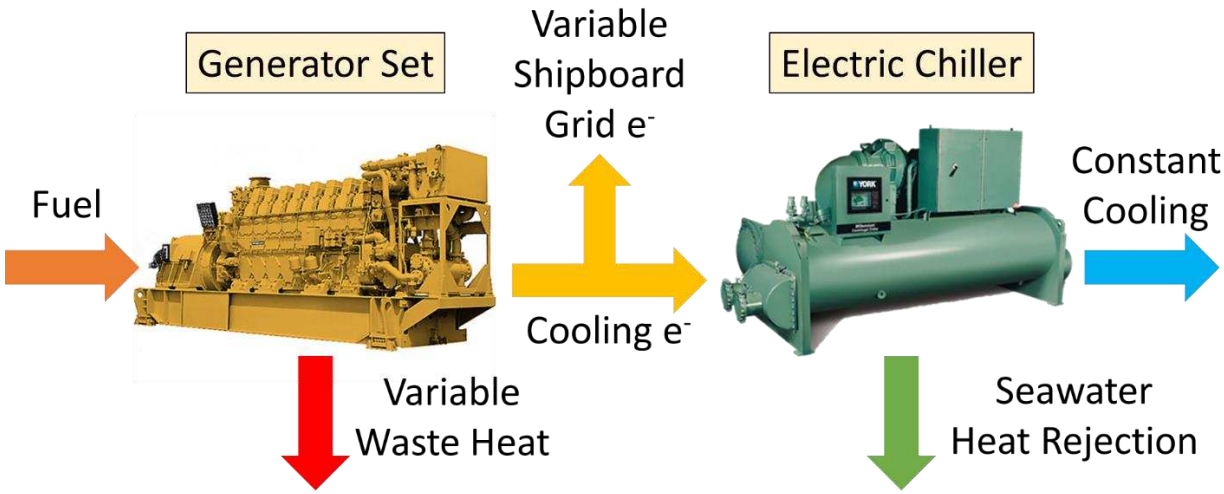

Figure 3-1: Baseline electrical and cooling system

As a part of prior shipboard TCCS efforts [85,86], the US Navy provided typical engine operation data for T-AKE Lewis and Clark class ships, shown in Table 3-1. These ships are used to deliver cargo to other ships at sea, including ammunition, food, repair parts, and small quantities of fuel. The total annual operating hours of a single engine is 3,954 hours and the average load condition is 41.7%.

Table 3-1: Representative annual operational profile of the baseline engine

% Engine Loading	25%	50%	75%	85%	100%
Annual Hours at Each Loading Condition (per engine)	2,056	1,283	313	302	0

Likewise, an annual seawater temperature profile was also provided by the US Navy for T-AKE class ships, shown in Table 3-2. Seawater is used to directly cool important equipment, such as the engines and chillers. This capability is unique to maritime applications as it completely removes the need for a cooling tower or air-cooled condensers.

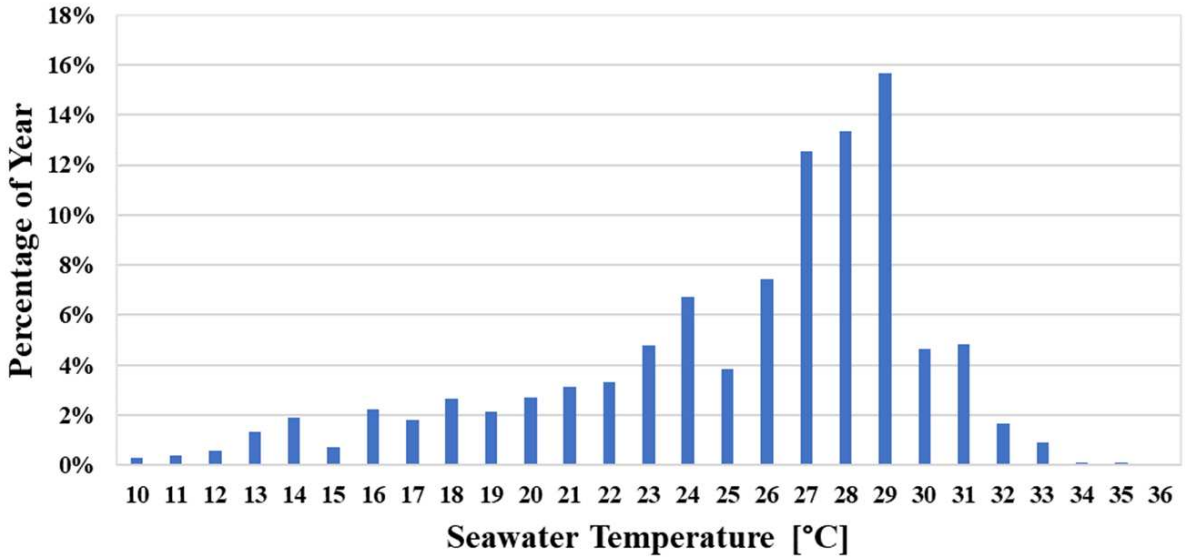

Figure 3-2: Representative annual seawater temperature profile

The representative annual engine load and seawater temperature profile allow for system performance to be calculated at a variety of operational conditions. It was assumed that the generator set was a Caterpillar (CAT) C280-8s [16]. This engine provides 2,710 kW of mechanical power, or 2,600 kW_e assuming a generator efficiency of 96%. A summary of engine specifications is provided in Table 3-2.

Of particular interest is the amount of waste heat available in the jacket water and lubrication oil, which will be used to drive the TCCS. The jacket water enters the engine at 90°C and was assumed to leave at 95°C, while the lubrication oil enters the engine at 85°C and leaves at 90°C. These temperatures are fixed regardless of engine load, but the flow rates and waste heat

availability decrease with decreasing engine load. Curve fits of the jacket water and lubrication oil heat rejection as a function of engine load are shown in Figure 3-3 and are described by Equation (3.1) and Equation (3.2):

$$\dot{Q}_{JW} = 3.9545 * EL + 145.06 \quad (3.1)$$

$$\dot{Q}_{oil} = 1.3297 * EL + 152.39 \quad (3.2)$$

where $\dot{Q}_{JW}$ is the heat rejection in the jacket water, $\dot{Q}_{oil}$ is the heat rejection in the lubrication oil, and EL is the engine load as a percentage of full load.

Table 3-2: CAT 280-8 engine specifications

Type	**C280-8**
Configuration	In-Line 8, 4-Stroke-Cycle-Diesel
Engine speed, RPM	1000
Engine output, kW	2710
Cylinder bore, mm	280
Stroke, mm	300
Displacement, L	148
Compression ratio	13:1
Fuel consumption (100% load), g/kW-hr	199.5
Engine efficiency (100% load), %	42.4%

It was also necessary to model the baseline shipboard chiller to calculate fuel savings from using the TCCS. Simulations were performed using the modeling approach discussed in Section 3.4. It was assumed that the baseline chiller had a weighted average COP of 4.19. Cooling equipment in commercial buildings typically account for approximately 15% of the facility's electricity consumption. Based on the data provided by the US Navy for the total engine plant, the average engine loading condition with multiple engines online is 86.7% of a single engine's capacity, or 2,254 kW_e when applied to the representative engine used in this study. Assuming a

chiller COP of 4.19 and that 15% of the 2,254 kW_e is consumed by the chillers, the average cooling duty on the representative ship is approximately 400-tons. Since the focus of this study is on a single chiller and engine, it can be safely assumed that 200-tons of continuous cooling is required by the ship over the 3,954 operational hours.

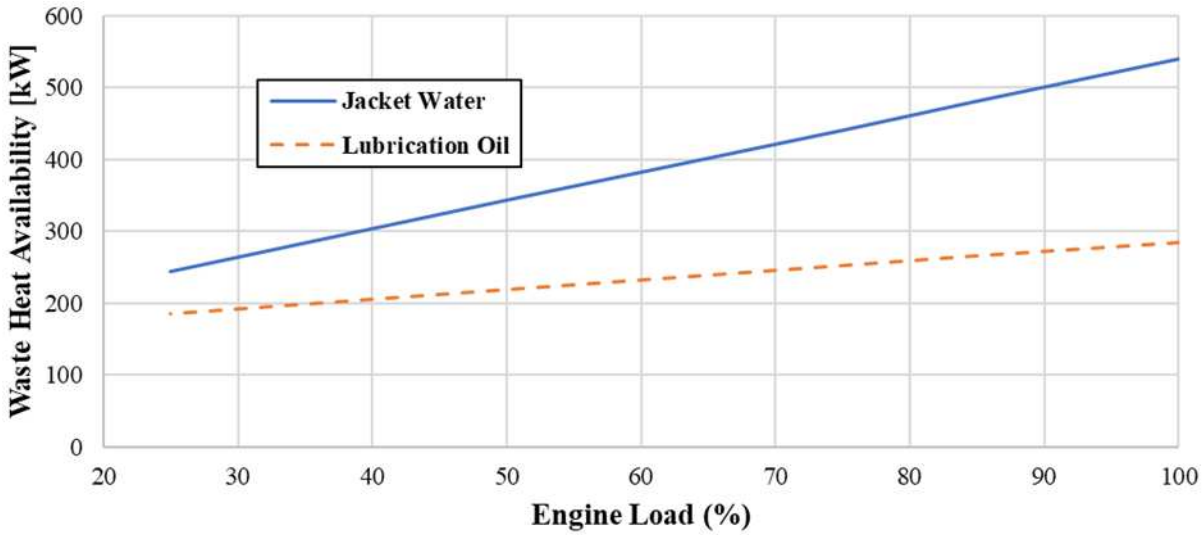

Figure 3-3: Heat rejection of the jacket water and lubrication oil in a C280-8 engine [16]

3.2. Turbo-Compression Cooling System

The turbo-compression cooling system consists of two thermodynamic cycles: a power cycle (ORC) and a cooling cycle (VCC), as shown in Figure 3-4. Starting with the power cycle, the waste heat source (e.g. jacket water and lubrication oil) vaporizes a refrigerant in the waste heat boiler. The superheated vapor is then expanded in the centrifugal turbine of the turbo-compressor. The power produced in the turbine is directly transferred to the compressor in the cooling cycle by using a shared shaft. A recuperator recovers some of the heat of the turbine discharge to preheat the refrigerant entering the boiler. After the recuperator, the refrigerant is condensed in the seawater condenser and pumped back to the boiler pressure. In the cooling cycle, the superheated vapor leaving the evaporator is further heated in the suction line heat exchanger (SLHX) by the condenser discharge. The SLHX serves two main purposes. The first is that

superheating the vapor ensures that liquid droplets do not enter the compressor, which could erode the compressor impeller. The second purpose is to subcool the refrigerant leaving the condenser, which decreases the evaporator inlet enthalpy and improves the cooling cycle performance. The drawback to incorporating a SLHX is that it increases the specific work of the compressor and increases the temperature of the compressor discharge. These drawbacks are countered by the addition of a cross-cycle economizer, where the hot vapor at the compressor discharge preheats the fluid entering the waste heat boiler. The cooling cycle vapor leaving the economizer is then condensed in the seawater condenser and SLHX before being throttled to a low pressure by the expansion valve. The low-pressure, low-temperature refrigerant is then vaporized in the evaporator and provides a cooling effect to an external flow.

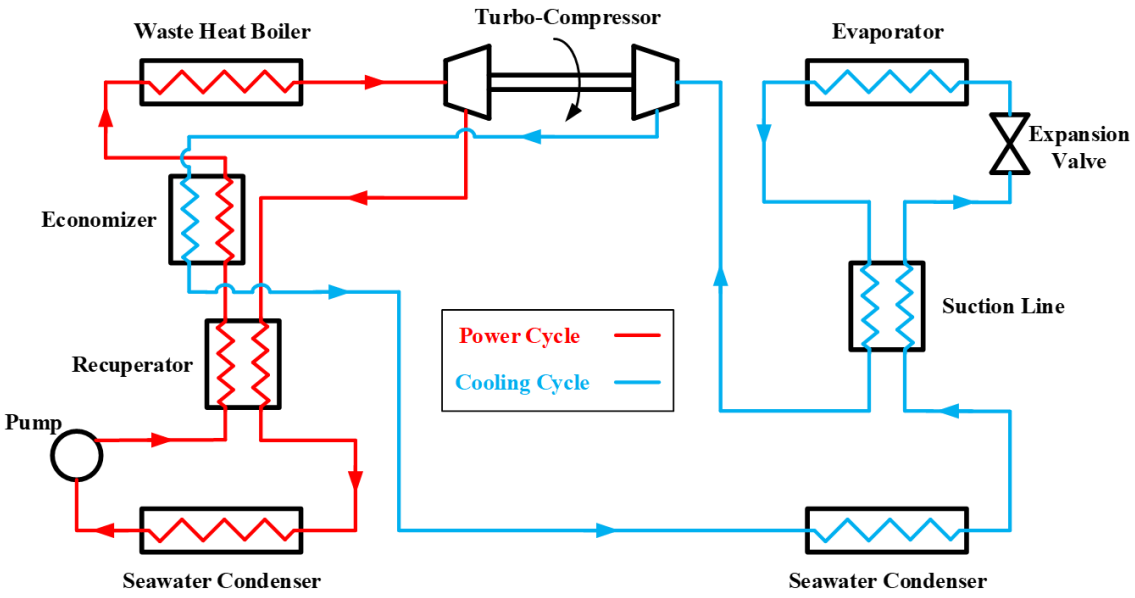

Figure 3-4: Recuperative TCCS process flow diagram

Three system integration strategies are modeled in this study, displayed in Figure 3-5, to determine the optimal configuration for maximizing power savings. Option 1 is to provide supplemental chilled water to reduce the cooling load on the baseline shipboard electric vapor compression chiller. The TCCS operates in parallel with the baseline system to reduce the chilled

water flow rate cooled by the electric chiller. The reduction in cooling load reduces the compressor power required in the electric vapor compression chiller. In Option 2, the TCCS pre-cools the condenser seawater used in the baseline chiller to boost performance. The baseline COP is increased by reducing the condenser saturation pressure, thus reducing the compressor lift and power required for the same cooling load. Option 3, termed the power boosted TCCS, adds an electric compressor in series with the turbo-compressor. This strategy allows the TCCS to meet cooling requirements over a range of waste heat availabilities while completely replacing the baseline electric chiller. The addition of an electric compressor also increases the heat transfer in the cross-cycle economizer and improves the power cycle performance. Due to the high efficiency turbo-compressor, heat recuperation strategies, and high effectiveness heat exchangers, the cooling cycle in the TCCS is more efficient than traditional chiller systems, and thus additional electricity savings are realized by producing all the cooling with the power boosted TCCS.

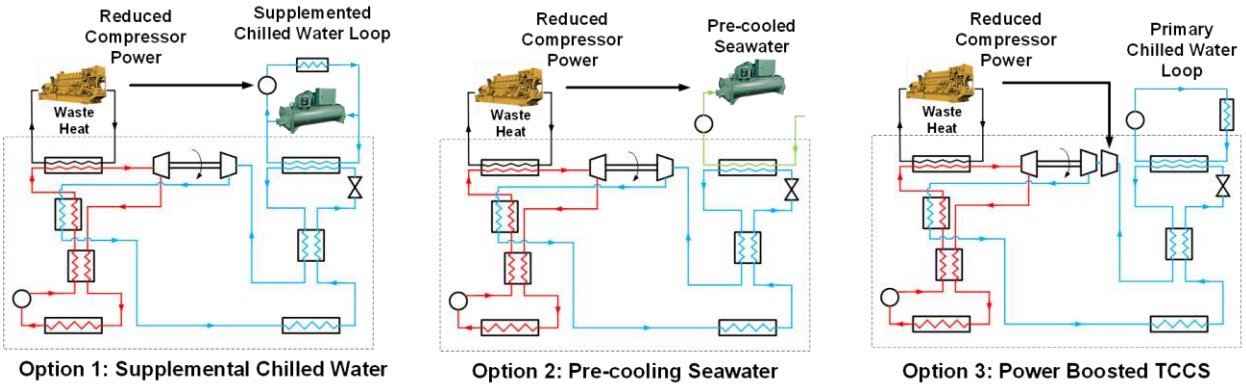

Figure 3-5: Three TCCS configurations are used in this study

3.3. Overview of Modeling Approach

The purpose of the modeling methodology introduced in this study is to allow for quick investigation into multiple configurations, fluids, and operating conditions followed by a more detailed design of a system to meet strict volume requirements. An overview of the modeling steps

is shown in Figure 3-6. The case study presented is of a marine diesel generator set co-located with an electric chiller for shipboard cooling, and includes engine performance and heat availability, a yearly operating profile, a seawater temperature profile, and a baseline electrical chiller model. A survey of possible refrigerants was conducted to select five working fluids appropriate for this case study. Using fundamental thermodynamic equations, the performance of the TCCS is predicated over the range of conditions from the case study. A single configuration and fluid are then selected to be designed. Once a design point is chosen, detailed plate and frame heat exchanger models are used to size heat exchangers based on commercial-off-the-shelf (COTS) devices. Heat exchanger sizes are optimized to remain below a defined core volume while maximizing performance. Pipes are also sized, and a solid model is created to provide a visual representation of the system and ensure that the system fits in the allowed volume. After sizing the equipment, heat exchanger and pipe geometries are fixed, and the performance model is run for all seawater and engine loading conditions. This is repeated twice: once to determine power density improvement (engine load is fixed) and once to determine fuel savings (engine load decreases based on offset electricity). Next, an economic model is applied to predict the cost of individual components and installation, and annual savings are calculated. Finally, the performance, design, and economic results are compared to SOA absorption technologies.

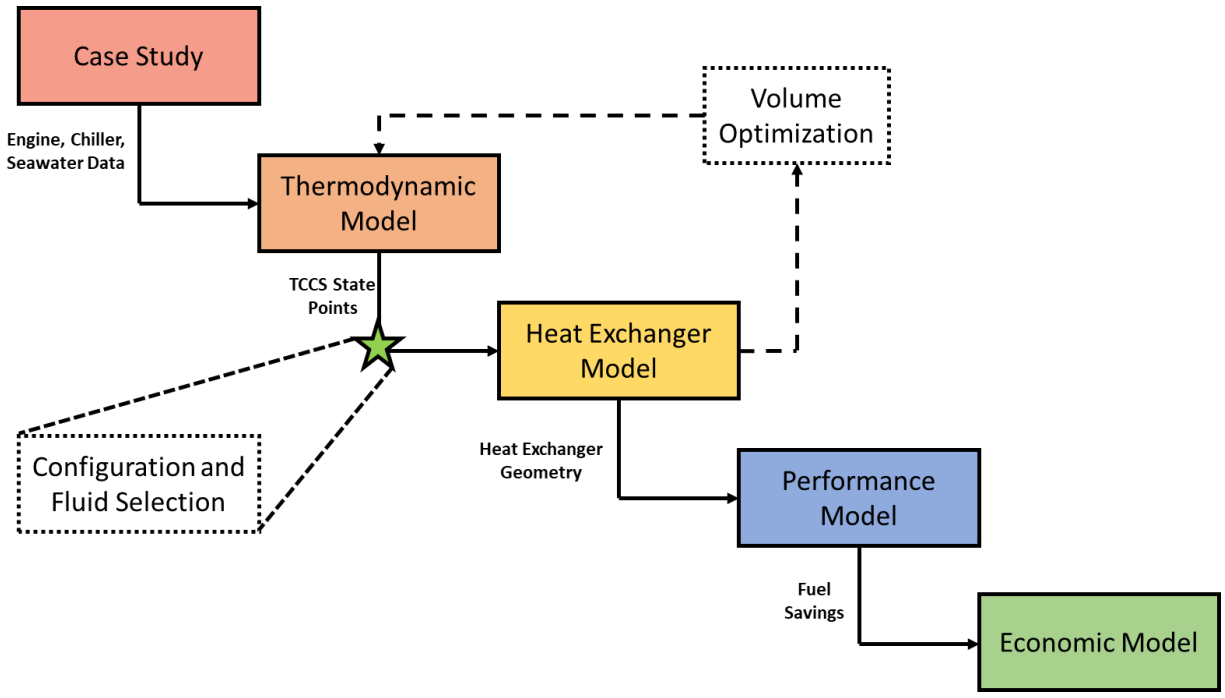

Figure 3-6: High level block diagram of the modeling approach

3.4. Thermodynamic Modeling

This section outlines the steps, equations, and general methodology used to create a TCCS thermodynamic performance model. The thermodynamic model uses several inputs to calculate the TCCS state points, as shown in Figure 3-7. In Section 3.4.1 the state points of the TCCS will be defined and a representative T-s diagram discussed. Section 3.4.2 will discuss the working fluid selection process and the final working fluids chosen. Working fluids were compared for performance, but only one was selected for the system design. Section 3.4.3 presents the equations used to model the TCCS and the baseline chiller and metrics used to compare system configurations.

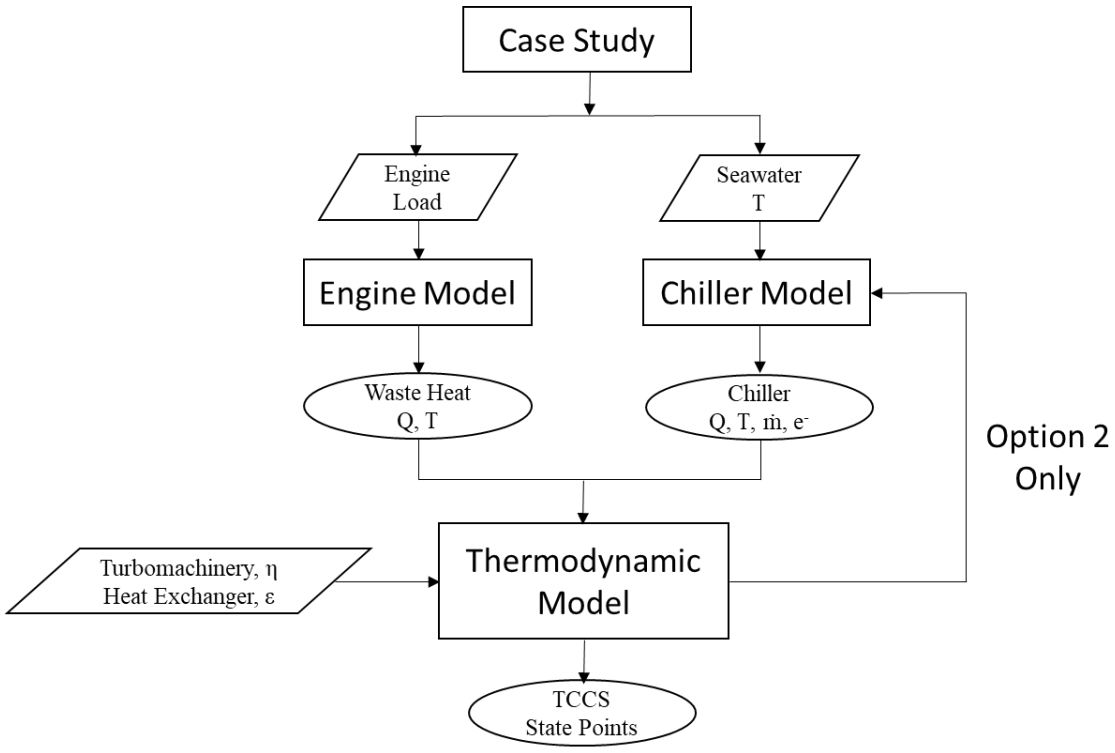

Figure 3-7: Thermodynamic model block diagram

3.4.1. System Model State Points

This section is a high-level overview of the thermodynamic performance modeling method. Figure 3-8 displays the complete system diagram with a simplified TCCS (no heat recuperation or electric compressor). Waste heat in the C280-8 jacket water and lubrication oil are used to heat an intermediate loop, which then vaporizes the refrigerant in the TCCS power cycle. Electricity is also used to power the power cycle pump and electric compressor in Option 3. The condensers are cooled by seawater in split separate streams so that the temperature and saturation pressures are as low as possible. The fluid flow in the cooling cycle evaporator is either chilled water or seawater used in the baseline VCC.

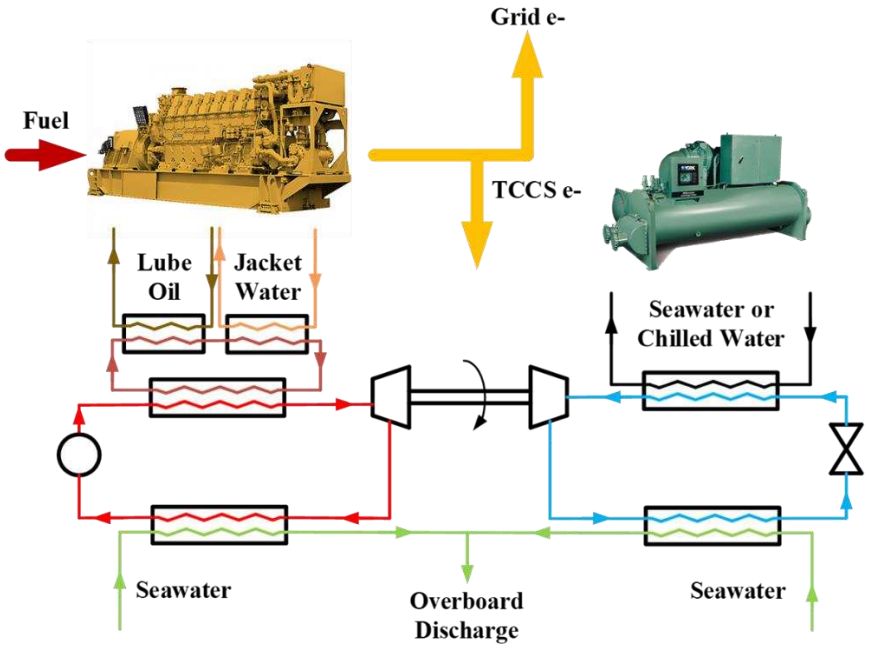

Figure 3-8: Full system model

The TCCS is modeled by defining several state points at the inlet and outlets of components. Heat exchangers where the working fluid undergoes a phase change (condensers, boiler, and evaporator) are split into multiple sections depending on the fluid phase. The seawater condensers and waste heat boiler contain three regions (subcooled liquid, two-phase, and superheated vapor), while the evaporator only contains two-phase and superheated regions. The fluids in the recuperative heat exchangers do not undergo phase change and therefore only contain one section. Figure 3-9 displays the TCCS flow diagram with split heat exchangers and all state points labeled. Option 3, which adds an electric compressor, would have an additional two state points between the two compressors. Figure 3-10 lists state point thermodynamic values and displays a T-s and P-h diagram for a representative TCCS system with 70% effective heat exchangers. The calculations are for a system driven by 748 kW_{th} of waste heat at 94.3°C and cooled by 29°C seawater to produce 393 kW_{th} of cooling, equating to a thermal COP of 0.53. The working fluid in both sub cycles is R134a.

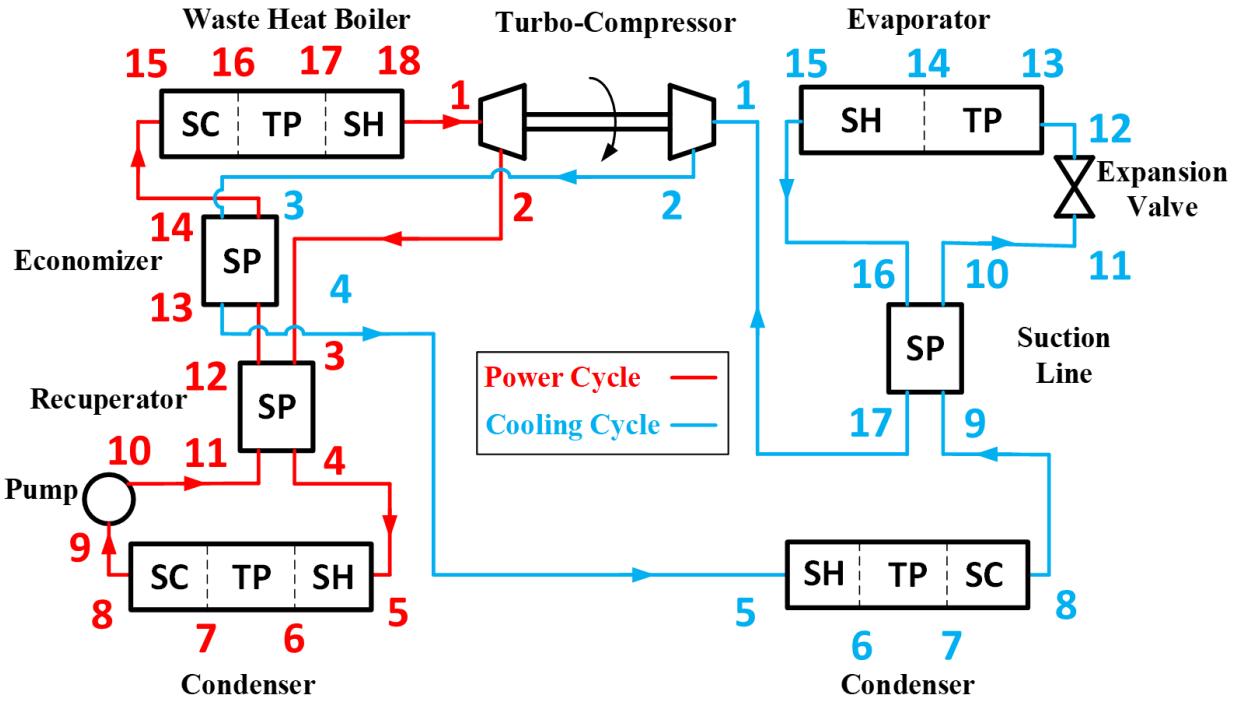

Figure 3-9: Process flow diagram for a seawater cooled TCCS with multiple heat recuperation heat exchangers and labeled state points

At state point 1 in the power cycle (shown in red), a high pressure superheated vapor enters the turbine of the turbo-compressor. The refrigerant is expanded in the turbine (1-2), which has an isentropic efficiency of 80% to produce 68.6 kW of mechanical work. This process increases the entropy and decreases the pressure from 2465 kPa to 951 kPa. The medium pressure superheated vapor then transfers 37 kW_{th} of heat (3-4) in the power cycle recuperator to preheat the refrigerant entering the boiler (11-12). The refrigerant is then cooled down to a saturated vapor state (5-6), condensed (6-7), and subcooled (7-8), by rejecting 734 kW_{th} to seawater. The subcooled refrigerant is then pumped from 940 kPa to 2480 kPa (9-10) in the power cycle pump, which has an isentropic efficiency of 35% and consumes 16 kW_e. As mentioned, some heat is recovered in the recuperator (11-12), before an additional 39 kW_{th} of heat is added through the cross-cycle economizer (13-14). Overall, the two recuperative heat exchangers increase the refrigerant temperature from 39°C to 51°C. Lastly, 748 kW_{th} of waste heat from the jacket water and lubrication oil is used to bring the

high-pressure refrigerant to a saturated liquid phase (15-16), vaporize it (16-17), and provide an additional 12°C of superheating (17-18). The cycle is then repeated starting at the turbine inlet (1).

In the cooling cycle, low-pressure refrigerant at 342 kPa is compressed to 939 kPa in the compressor (1-2). The compressor either consists of only the turbo-compressor, or a turbo-compressor and electric compressor in series. If the latter is used, an additional state point is created to observe the performance of each compressor individually. The hot compressor discharge then transfers 39 kW_{th} to the power cycle (3-4) in the cross-cycle economizer, cooling the vapor from 68°C to 51°C. Like the power cycle, the refrigerant is brought to a saturated vapor state (5-6), condensed (6-7), and subcooled (7-8) by rejecting 421 kW_{th} of heat in the seawater cooled condenser. The subcooled refrigerant then transfers 45 kW_{th} of heat (9-10) to the evaporator outlet (16-17), further subcooling the refrigerant from 36°C to 22°C and increasing cooling cycle performance by reducing the enthalpy of the fluid entering the evaporator. The subcooled, medium-pressure refrigerant is expanded from 924 kPa to 352 kPa in an isenthalpic expansion valve (11-12), meaning that the enthalpy remains unchanged across the component. After the expansion valve, the refrigerant is at 5°C and has a vapor quality of 0.122. The refrigerant is then fully vaporized (13-14) and superheated (14-15) by an external chilled water stream, thus cooling 393 kW_{th} of chilled water from 10.4°C to 6.7°C. The refrigerant is further superheated by the suction line heat exchanger (16-17) and piped back to the compressors where the cycle is then repeated. In summary, the power cycle has a waste heat to power efficiency of 7.0% when accounting for the power draw of the refrigerant pump, and the cooling cycle has a COP of 5.84. The overall COP is 0.514, and the electric COP is 24.6.

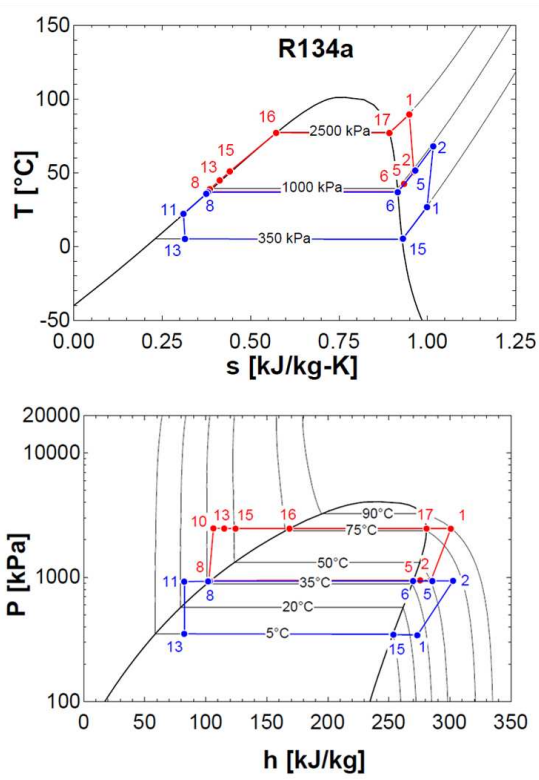

	Power Cycle	P [kPa]	T [C]	h [kJ/kg]	s [kJ/kg-K]
1	Turbine Inlet	2465	89	301	0.949
2	Turbine Outlet	951	51	285	0.962
3	Recuperator Inlet (Hot)	950	51	285	0.962
4	Recuperator Outlet (Hot)	947	42	276	0.934
5	Condenser Inlet	946	42	276	0.934
6	Condenser Sat. Vap.	945	37	270	0.916
7	Condenser Sat. Liq.	942	37	104	0.382
8	Condenser Outlet	941	36	103	0.377
9	Pump Inlet	940	36	103	0.377
10	Pump Outlet	2480	39	106	0.385
11	Recuperator Inlet (Cold)	2479	39	106	0.385
12	Recuperator Outlet (Cold)	2476	45	115	0.413
13	Economizer Inlet (Cold)	2475	45	115	0.413
14	Economizer Outlet (Cold)	2472	51	124	0.441
15	Boiler Inlet	2471	51	124	0.441
16	Boiler Sat. Liq.	2470	77	169	0.572
17	Boiler Sat. Vap.	2467	77	281	0.893
18	Boiler Outlet	2466	89	301	0.949
	Cooling Cycle	**P [kPa]**	**T [C]**	**h [kJ/kg]**	**s [kJ/kg-K]**
1	Compressor Inlet	342	27	273	1.000
2	Compressor Outlet	939	68	303	1.017
3	Economizer Inlet (Hot)	938	68	303	1.017
4	Economizer Outlet (Hot)	935	51	286	0.966
5	Condenser Inlet	934	51	286	0.966
6	Condenser Sat. Vap.	933	37	270	0.917
7	Condenser Sat. Liq.	930	37	103	0.379
8	Condenser Outlet	929	36	102	0.375
9	Suction Line Inlet (Hot)	928	36	102	0.375
10	Suction Line Outlet (Hot)	925	22	82	0.310
11	Expansion Valve Inlet	924	22	82	0.310
12	Expansion Valve Outlet	352	5	82	0.314
13	Evaporator Inlet	351	5	82	0.314
14	Evaporator Sat. Vap.	348	5	253	0.929
15	Evaporator Outlet	347	5	254	0.931
16	Suction Line Inlet (Cold)	346	5	254	0.931
17	Suction Line Outlet (Cold)	343	27	273	0.999

Power cycle mass flow: 4.2 kg s^{-1} Cooling cycle mass flow: 2.3 kg s^{-1}

Figure 3-10: Representative state points and T-s, P-h diagrams for a TCCS with R134a

3.4.2. Working Fluid Selection

One advantage of ORVC systems is that they are not limited by the working fluids of the two cycles. There have been numerous studies that focused on determining environmentally friendly refrigerants that maintain high cycle performance [76,86]. Environmental impacts of refrigerants are normally represented by the global warming potential (GWP) and the ozone depletion potential (ODP). Chlorofluorocarbons (CFCs) and hydrochlorofluorocarbons (HCFCs) are known to have medium to high GWP and ODP and are either banned or being phased out in many countries. Currently hydrofluorocarbons (HFCs), such as R134a, are commonly used in refrigeration systems. HFCs are characterized by having zero ODP but still having medium to high GWP. This has led to the recent development of hydrofluoro-olefins (HFOs), which have zero ODP and very low GWP. Natural refrigerants such as isobutane (R600a) are very environmentally

friendly and have been shown in previous studies to have favorable thermodynamic qualities for ORVC systems but are highly flammable.

ASHRAE has developed designation and safety classifications for the flammability and toxicity of refrigerants, shown in Figure 3-11 [87]. Class A refrigerants have lower toxicity levels, and only pose a risk at very high concentrations of greater than 400 ppm. The number following the class indicates the flammability of the refrigerants. A1 refrigerants have no flame propagation at the tested air temperature of 140°F and an atmospheric pressure of 14.7 psia, while A3 refrigerants experience flame propagation at 140°F and at concentrations less than 0.1 kg-m^{-3} with a heat of combustion greater than 19,000 kJ-kg^{-1}.

Another important characteristic of refrigerants that must be considered is the slope of the saturated vapor curve on a temperature-entropy (T-s) diagram. There are three categories of fluids: dry, isentropic, and wet. Dry fluids are characterized by a positive saturated vapor slope. This is preferred in ORC systems because it ensures that liquid droplets won't form in the turbine during expansion, which could seriously damage the turbine blades. Isentropic fluids have a slope of infinity and can be used in ORC systems if there is sufficient superheating prior to expansion. R134a is an example of an isentropic fluid, and its T-s diagram was presented in Figure 3-10. Wet fluids have a negative slope and should be avoided in ORC systems as there is a high chance that the fluid will enter the two-phase region during expansion.

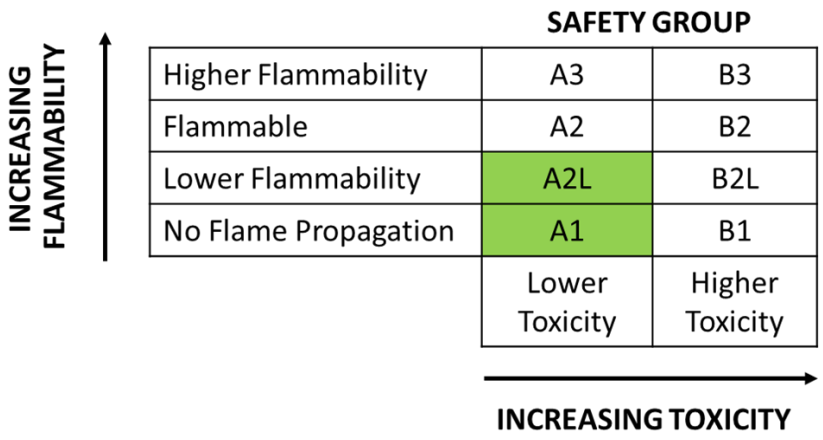

Figure 3-11: ASHRAE designations for the flammability and toxicity of refrigerants [87]

A fluid search was performed to find refrigerants that are considered acceptable for use on a shipboard chiller. The baseline fluid is R134a as it is an industry standard for use in vapor compression chillers. US Environmental Protection Agency (EPA) guidance indicates that R134a will not be allowed in new equipment as of January 1, 2024 except for a narrow list of exceptions, such as for military marine vessels [88]. Therefore, a focus should be placed on finding environmentally friendly alternatives. Fluids selected for this study have zero ODP and a GWP less than that of R134a. Fluids were also limited to being isentropic or dry fluids and must have A1 or A2L ASHRAE classifications.

Five fluids were chosen to be included in this performance study: R134a, R1234ze(E), R1234yf, R245fa, and R515a, whose characteristics are shown in Table 3-3. R1234ze(E) is a common candidate for replacing R134a in chillers as it has similar thermodynamic performance and a very low GWP. R1234yf is commonly used in the automotive sector for mobile air conditioning systems. R245fa is commonly found in ORC systems but will also be banned in 2024 along with R134a. R515a is an azeotropic blend of 88% R1234ze(E) and 12% R227ea and has been shown to have similar performance to R134a [89].

Table 3-3: Summary of working fluids selected for this study

Fluid	Class	GWP (100yr)	ODP	Type	Flammability (ASHRAE)	Toxic	Critical Temperature (°C)	Critical Pressure (kPa)
R134a	HFC	1430	0	Isentropic	A1	No	101	4059
R1234ze(E)	HFO	6	0	Isentropic	A2L	No	109.4	3632
R1234yf	HFO	<1	0	Isentropic	A2L	No	94.7	3382
R245fa	HFC	1030	0	Dry	A1	No	154	3651
R515a	Azeotropic Blend	402	0	Isentropic	A1	No	108.7	3566

3.4.3. Thermodynamic System Modeling

This section discusses any assumptions, inputs, and equations used to model the thermodynamic performance of the TCCS over the range of case study conditions. The methodology described here was used for the comparison of working fluids and configurations. Additional detail was added to the model as the design progressed, as will be discussed in subsequent sections. However, many of the operating parameters and equations introduced in this section will be used in the more detailed model versions. In addition, the fundamental equations discussed in this section were used to model the baseline shipboard electrically driven chiller. Table 3-4 lists the primary fixed inputs used in the TCCS thermodynamic model. Lubrication oil and jacket water outlet temperatures, 85°C and 90°C respectively, are nominal temperatures of the fluids entering the engines [16]. The temperature rise in the engine for both fluids was assumed to be 5°C, which is below the listed alarm temperatures, which are 92°C and 103°C for the lubrication oil and jacket water, respectively. Chilled water temperatures were assumed to be 10.39°C (50.7°F) return and 6.67°C (44°F) supply. Note that in Option 2, the TCCS precools seawater for baseline equipment instead of chilled water. Waste heat availability and condenser water temperature ranges are representative of the case study engine and ship operation, as discussed in Section 3.1. The remaining values in Table 3-4 are realistic assumptions based on past TCCS

research [83,84]. Turbine and compressor isentropic efficiencies of approximately 80% have been demonstrated in a lab environment. The pump isentropic efficiency of 35% is conservative estimate of a side channel pump [90]. While other pump options have higher efficiency values, side channel pumps can operate in low Net Positive Suction Head (NPSH) conditions to prevent cavitation, and thus offer superior operational flexibility. Pressure drops in heat exchangers and pipes were modeled in detailed once equipment was sized but were assumed to be between 1 and 3 kPa per section for the thermodynamic comparison of system options and fluids.

Table 3-4: Fixed TCCS thermodynamic inputs

Fixed Inputs	Value
Inlet/outlet lubrication oil temperature	90°C/85°C
Inlet/outlet jacket water temperature	95°C/90°C
Inlet condenser water temperature	10°C-36°C
Inlet/Outlet chilled water temperature (Options 1 and 3)	10.39°C/6.67°C
Lubrication oil waste heat	186 kW - 265 kW
Jacket water waste heat	244 kW – 481 kW
Turbine isentropic efficiency	80%
Compressor isentropic efficiency	80%
Pump isentropic efficiency	35%
Mechanical transfer isentropic efficiency	98%
Pipe pressure drop	1 kPa
Subcooled/Superheat pressure drop	1 kPa
Two-phase pressure drop	3 kPa
Recuperative heat exchanger pressure drop	3 kPa
Condenser Subcooling	1°C
Condenser Seawater Temperature Rise	6°C

As discussed in Section 3.4.1, heat exchangers are split into multiple sections to enable the modeling of every fluid phase of the working fluid. Each heat exchanger section has an associated heat exchanger effectiveness, ε, as defined by Equation (3.3):

$$\varepsilon = \frac{\dot{Q}_{actual}}{\dot{Q}_{max}} \tag{3.3}$$

where $\dot{Q}_{actual}$ is the heat duty of the heat exchanger section and $\dot{Q}_{max}$ is the theoretical maximum heat transfer value, and is based on fluid properties, flow rates, and temperatures. The heat exchanger effectiveness was fixed for a select number of heat exchanger regions and are listed in Table 3-5. Not all heat exchanger effectiveness values can be fixed or the model would be over constrained due to values set in Table 3-4. The condenser subcooled regions were defined by a subcooling amount, and a condenser seawater temperature rise was used instead of the superheat region effectiveness. The waste heat boiler two-phase region was not fixed because the heat duty and hot water inlet and outlet temperatures were defined based on case study data. The chosen values in Table 3-5 are arbitrary values and are realistic/moderate estimates. These values were set constant over the entire range of studied engine and seawater conditions for all studied fluids.

A set of thermodynamic and heat transfer equations were simultaneously solved in EES to study the performance of the three TCCS configurations operating with variable conditions. An electric vapor compression chiller was also modeled as the baseline case for improvement comparison and to determine the performance of the integrated system in Option 2. Values listed in Table 3-4 and Table 3-5 were held constant over the studied conditions for the TCCS. To simplify the analysis, it was assumed that the systems were operating under steady state conditions, heat loss from all components and piping was negligible, and the cooling cycle expansion valve was isenthalpic. All auxiliary work and component performance, such as pumping power for external fluids, were neglected in this study. To calculate these values, more information is needed about the ship design, which is outside the scope of this study. The seawater was modeled as a water and salt mixture with a salinity of 3.5%. The lubrication oil was modeled using 10W engine

oil and the intermediate loop was a 30% propylene glycol-water mixture. Lastly, the chilled water and jacket water were simply modeled as water.

Table 3-5: Heat exchanger effectiveness fixed values

Heat Exchanger	Region	Value
Boiler	Subcooled	0.7
	Superheat	0.7
Condensers	Two-Phase	0.7
Evaporator	Two-Phase	0.7
	Superheated	0.1
Recuperator	-	0.7
Economizer	-	0.7
Suction Line	-	0.7
Intermediate Loop	-	0.9

Heat exchangers were modeled by solving an energy balance in each fluid section. Equation (3.4) is an energy balance on the external stream, either seawater, intermediate hot water loop, or chilled water. $\dot{Q}$ is the heat transfer from the external stream to the working fluid, $\dot{m}_{ext}$ is the mass flow rate of the external fluid stream, c_p is the specific heat capacity of the fluid which is assumed to be constant in each region, and $T_{ext,i}$ and $T_{ext,o}$ are the fluid temperatures at the inlet and outlet, respectively.

$$\dot{Q} = \dot{m}_{ext} * c_p * (T_{ext,i} - T_{ext,o}) \quad (3.4)$$

Similarly, Equation (3.5) is an energy balance on the refrigerant side, where $\dot{m}_r$ is the mass flow rate of the refrigerant and $i_{r,i}$ and $i_{r,o}$ are the enthalpies at the inlet and outlet, respectively.

$$\dot{Q} = \dot{m}_r * (i_{r,i} - i_{r,o}) \quad (3.5)$$

Equation (3.6) represents the efficiency of the heat transfer process. The heat exchanger effectiveness, ε, is the ratio of the heat transferred to the maximum possible heat transfer, as shown in Equation (3.3). A higher effectiveness value is indicative of a larger or more efficient heat exchanger. C_{min} is the minimum heat capacity rate between the refrigerant and external stream. The heat capacity rate is simply the product of the mass flow rate and specific heat capacity. $T_{h,i}$ and $T_{c,i}$ are the inlet temperatures of the hot side and cold side fluid, respectively. For example, in the condenser the refrigerant is the hot side fluid, and the seawater is the cold side fluid.

$$\dot{Q} = \varepsilon * C_{min} * (T_{h,i} - T_{c,i}) \tag{3.6}$$

Equations (3.4) through (3.6) are used for each heat exchanger section to model system performance with varying external fluid temperatures and flow rates.

Similarly, the performance of turbomachinery was modeled using energy balances and isentropic efficiencies. The isentropic efficiency of the turbine, η_{turb}, is given in Equation (3.7), where $i_{r,o,s}$ is the isentropic enthalpy at the outlet of the turbine. If the inlet conditions and outlet pressure of the turbine are known, Equation (3.7) was used to calculate the actual enthalpy at the outlet of the turbine. Equation (3.8) was then used to determine the outlet turbine power, $\dot{W}_{turb}$.

$$\eta_{turb} = \frac{i_{r,i} - i_{r,o}}{i_{r,i} - i_{r,o,s}} \tag{3.7}$$

$$\dot{W}_{turb} = \dot{m}_r * (i_{r,i} - i_{r,o}) \tag{3.8}$$

Turbine power is directly transferred to the cooling cycle compressor by using a common shaft in the turbo-compressor. However, there are small mechanical losses which are accounted for in Equation (3.9), where η_{mech} is the mechanical shaft efficiency and $\dot{W}_{comp}$ is the compressor work. Equations (3.10) and (3.11) were then used to model both the pump and the compressor.

$$\dot{W}_{comp} = \dot{W}_{turb} * \eta_{mech} \tag{3.9}$$

$$\dot{W} = \dot{m}_r * (i_{r,o} - i_{r,i}) \tag{3.10}$$

$$\eta = \frac{i_{r,o,s} - i_{r,i}}{i_{r,o} - i_{r,i}} \tag{3.11}$$

By simultaneously solving Equations (3.4) through (3.11) with the case study data and fixed inputs from Table 3-4 and Table 3-5, the performance of the system was calculated. As discussed in Section 2.1, performance metrics are typically the ratio of the desired output to the desired input. In this study, the electric power draw of the pump was significant and therefore included in the efficiency calculations. In the power cycle, the pump work, $\dot{W}_{pump}$, is subtracted from the turbine work to better represent the power cycle performance, η_{pc}, as seen in Equation (3.12).

$$\eta_{pc} = \frac{\dot{W}_{turb} - \dot{W}_{pump}}{\dot{Q}_{boiler}} \tag{3.12}$$

The COP of the cooling cycle, COP_{cc} is given by Equation (3.13), where $\dot{W}_{comp,total}$ is the sum of the mechanical compressor work in the turbo-compressor and any additional work provided by an electrical compressor.

$$COP_{cc} = \frac{\dot{Q}_{chill}}{\dot{W}_{comp,total}} \tag{3.13}$$

The objective of the modeling process was to compare the potential energy savings that could be provided by the three different TCCS integration options and five different working fluids. As discussed in Section 3.1, it was assumed that the ship required a continuous 200 tons of cooling over the studied range of conditions. In Option 1, providing waste heat driven supplemental cooling, 200 tons of cooling was set as the maximum cooling that can be provided by the TCCS. When the maximum cooling duty was met, which occurred at colder seawater temperatures, the jacket water mass flow rate was reduced, thus reducing the waste heat duty and

maintaining the maximum cooling duty. The amount of cooling provided and electricity consumed by the TCCS was calculated over the range of operating conditions. Two metrics were used to compare the different fluids: thermal COP and power reduction versus the baseline system. The thermal COP was previously defined in Equation (2.3). Power reduction is defined as the amount of electricity that is offset by the TCCS, as seen in Equation (3.14). COP_{VCC} is the COP of the baseline shipboard chiller.

$$\text{Power Reduction Option 1} = \frac{\dot{Q}_{chill}}{COP_{VCC}} - \dot{W}_{pump} \tag{3.14}$$

In Option 2, the TCCS thermodynamic model was integrated the VCC baseline model. The condenser seawater mass flow rate was calculated at varying seawater temperatures in the baseline model. The cooling duty of the baseline chiller was set at 200 tons over the range of conditions. The condenser seawater mass flow rate from this chiller was set as the external stream mass flow rate in the evaporator of the TCCS model and the outlet seawater temperature over the range of conditions was calculated. The outlet seawater temperature was then set as the inlet condenser seawater temperature in the VCC model. The different TCCS working fluids were compared based on seawater temperature reduction and the power reduction versus the baseline system. For this option, power reduction is calculated by Equation (3.15).

$$\text{Power Reduction Option 2} = \dot{W}_{comp,VCC,orig} - \dot{W}_{comp,VCC,new} - \dot{W}_{pump} \tag{3.15}$$

Option 3 utilized an electric compressor with the turbo-compressor to provide a continuous 200 tons of cooling, eliminating the need for the separate baseline chiller. The electric compressor was modeled in series with the turbo-compressor and had the same isentropic efficiency. With the cooling load set, the model calculated the required compressor work for the cooling cycle. The difference between the required compressor work and the turbo-compressor work was the electric

compressor work. If the turbo-compressor could provide all the required work, the electric compressor work was set to 0 kW and the jacket water mass flow rate was reduced so that the turbo-compressor power equaled the required compressor power. Different fluids were compared in Option 3 by their electrical COPs, defined in Equation (2.2), and the power reduction versus the baseline system, defined in Equation (3.16).

$$\text{Power Reduction Option 3} = \dot{W}_{comp,VCC,orig} - (\dot{W}_{pump} + \dot{W}_{comp,elec}) \quad (3.16)$$

3.4.3.1 Baseline Chiller Model

The baseline chiller was modeled using the same equations as the TCCS thermodynamic model, but only contained four components: an electric compressor, condenser, evaporator, and expansion valve. The model was set up using the fixed inputs listed in Table 3-6. From the model, the chiller condenser flow rate and compressor power draw could be calculated at design conditions. The chiller cooling duty was then set at 200-tons and the condenser flow rate was set to be constant while the inlet condenser water was varied over the range of seawater temperatures studied. The initial values were calibrated to achieve a weighted average COP of 4.19.

Table 3-6: Baseline shipboard chiller fixed model inputs

Fixed Inputs	Value
Cooling Duty	200-tons
Chilled Water Inlet/Outlet Temperatures	10.39°C/6.67°C
Condenser Water Temperature Rise	6°C
Compressor Efficiency	0.75
Condenser Two-Phase Effectiveness	0.35
Condenser Subcool Effectiveness	0.01
Evaporator Two-Phase Effectiveness	0.40
Evaporator Superheat Effectiveness	0.01

Higher COP chillers may be available for land-based applications. For example, an Airdale TurboChill TTWC12L water cooled chiller has a nominal capacity of 200-tons and a design COP of 5.05 [91]. However, this chiller is also 31% larger than the baseline chiller used in this study.

In general, larger volume heat exchangers should achieve higher effectiveness values and system COPs. For space-constrained and shipboard applications, smaller heat exchangers will result in lower system COPs.

3.5. Plate and Frame Heat Exchangers

Heat exchanger selection is crucial to the design of any thermal system because they can take up a considerable volume and account for more than 80% of total system cost [85]. Traditional electrically driven chillers use shell and tube type heat exchangers, which are relatively easy to build and maintain and can be used for a variety of applications. However, shell and tube heat exchangers are prohibitively large. Plate heat exchangers (PHEs), shown in Figure 3-12, are a more compact and lighter alternative to shell and tube heat exchangers but are more limited in their operational temperature and pressure ranges and have higher pressure drops due to the smaller flow channels.

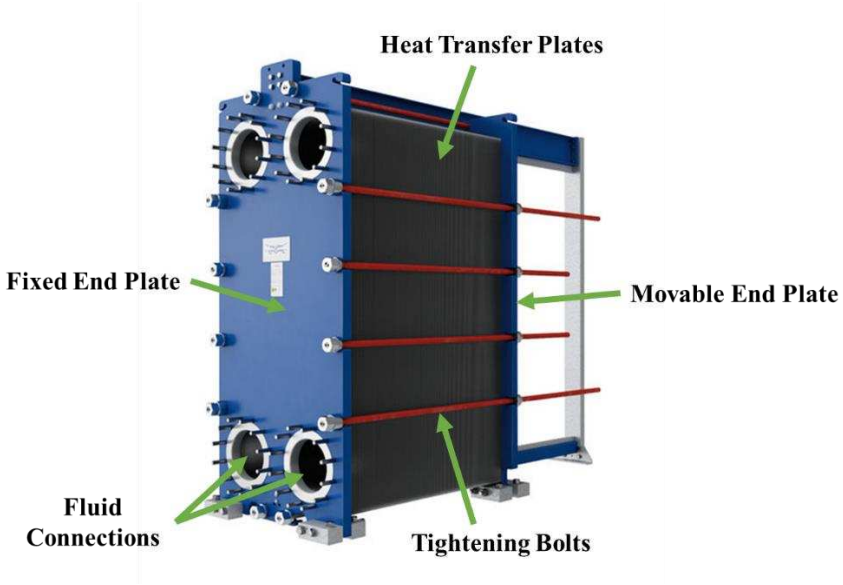

Figure 3-12: Plate and frame heat exchanger structure [92]

As shown in Figure 3-12, PHEs include a fixed end plate, multiple heat transfer plates, and a movable end plate. The fixed end plate has inlet and outlet fluid connection ports for both fluids. Fluids may enter on opposite ends of the plate in a counter flow arrangement, or on the same end in a parallel flow arrangement. The heat transfer plates are typically separated using a rubber gasket, which forms a channel for the fluid to flow between plates. The working principle of a counter flow gasketed PHE is shown in Figure 3-13. The two fluids alternate channels to indirectly exchange heat. The corrugated heat transfer plates are available in a variety of patterns and materials for specific applications. The use of gaskets allows for plates to be easily taken off for cleaning or replacement and allows for adjustments to the number of plates based on desired performance. Tightening bolts are used to apply pressure to the gaskets forming a tight seal to prevent leakage. For higher pressure or temperature applications, or for a more compact design, plates can be either welded or brazed together to create a permanent seal.

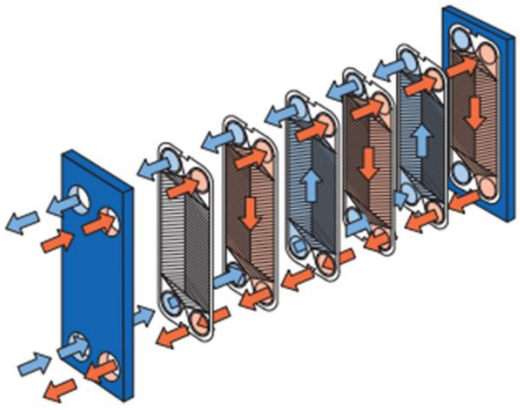

Figure 3-13: Working principle of plate heat exchangers [92]

Plate heat exchangers are an ideal option for a shipboard TCCS because they are compact, flexible in size and materials, and are commercially available. The goal of this study is to present a preliminary design of a system that can fit within the volume of a commercial chiller of the same

cooling capacity while maximizing COTS components and performance. To meet this goal, compact PHEs must be used in replace of traditional shell and tube heat exchangers. Commercial Alfa Laval gasketed and brazed heat exchanger models were selected and sized based on individual operating conditions and size constraints. The number of plates were then be optimized to maximize performance while remaining within an allowed volume. After optimizing heat exchanger and pipe sizes, a solid model was created to demonstrate that the system fits within the allowed space. R134a was used as the working fluid because it is the industry standard for vapor compression chillers. There are also numerous heat transfer coefficient correlations available in literature for R134a, increasing the confidence of detailed heat exchanger sizing and performance calculations. In addition, an evaporative plate frame heat exchanger sizing model was created and validated for TCCS operating conditions and the outcomes of the study will be leveraged in this work [93]. The specific modeling approach and fundamental equations will be defined in the following section.

3.5.1. Heat Exchanger Modeling

The heat exchanger models presented in this study serve two purposes: predict the heat transfer surface area and number of plates required to meet performance goals defined in the thermodynamic model and predict thermodynamic performance with fixed heat transfer surface area. An overview of the modeling approach is shown in Figure 3-14. The model was first developed as a sizing model and was integrated into the thermodynamic model described in Section 3.4. The heat exchanger model uses fluid temperatures, mass flow rates, heat exchanger effectiveness, and heat duty as inputs. Plate geometry, such as plate length, width, thickness, material, and spacing were also set constant based on commercial heat exchanger models. Outputs of the sizing model were required number of heat transfer plates and refrigerant pressure drop. The

optimized number of plates were then fixed, and the model was used to predict performance and will be discussed in Section 3.6.

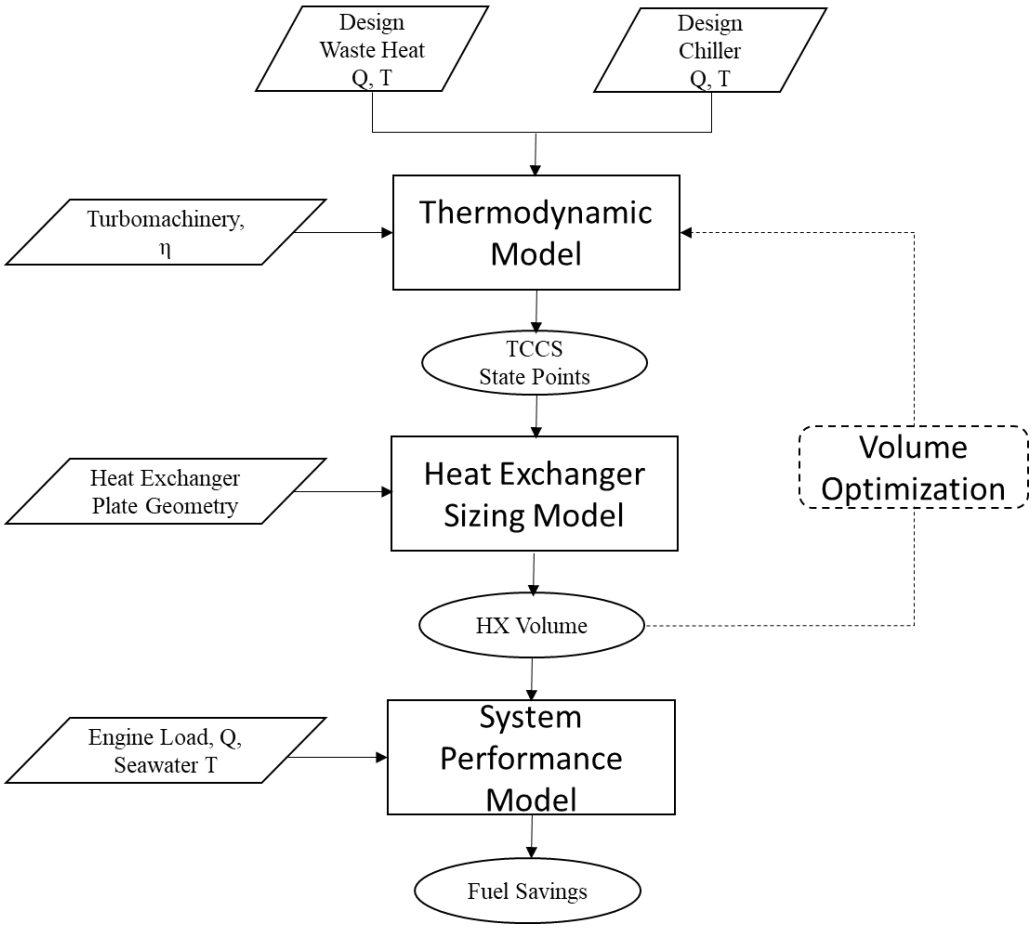

Figure 3-14: Heat exchanger sizing and performance model block diagram

Figure 3-15 displays an overview of the heat exchanger geometry and variables used in the heat exchanger models, as well as the flow path and sections of the power cycle boiler. In Figure 3-15, L_{sc}, L_{tp}, and L_{sh} are the lengths associated with the subcooled, two-phase, and superheated regions, respectively. L_{ports} is the distance between the inlet and outlet ports which was assumed to be the distance traveled by the refrigerant and W_{plate} is the width of the plate. L_{total} is the total heat exchanger length and is used in total heat exchanger volume calculations. Lastly, Pt and Ps are plate thickness and plate spacing, respectively. The plate thickness was 0.5 mm and the plate

spacing was 2.574 mm for all heat exchangers. The refrigerant enters the power cycle boiler at the bottom port and exits at the top, while the intermediate hot water loop fluid enters at the top and exits at the bottom of the end plate.

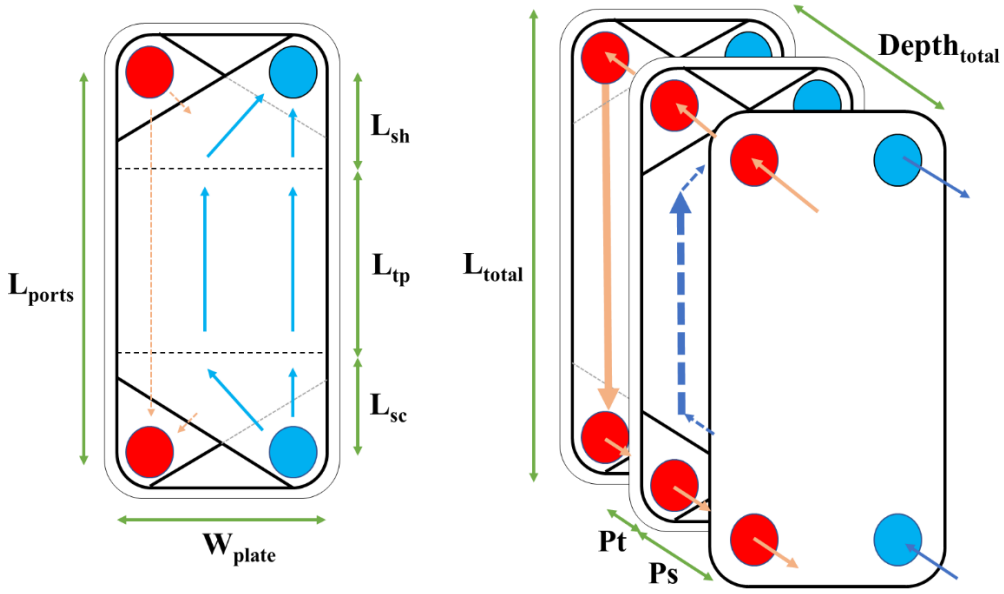

Figure 3-15: Power cycle boiler heat exchanger flow path and geometry

As seen in Figure 3-15, there are three distinct subsections in the boiler, one for each fluid phase. The validated evaporative model developed by Simon III [93] included 20 total sections: 5 for the subcooled region, 12 for the two-phase region, and 3 for the superheated region. The models developed by Gibson et. al. [85] and Young et. al. [86] only included 3 heat exchanger sections. It was found during this work that the 3-section model produces very similar results compared to dividing the model into 20 sections, and therefore was used to reduce computational complexity. The condenser model also has three heat exchanger sections, but the refrigerant flows in the downwards direction while the seawater flows upwards. The cooling cycle evaporator follows the same fluid path as the power cycle boiler, but only contains a two-phase region and a superheated region. The recuperative heat exchangers each only have one fluid section as no phase change occurs. Flow directions were not considered in these heat exchangers since the fluid flow is

dependent on equipment placement and piping routes. Therefore, while the fluids operate in a counter flow arrangement, it was assumed that both flows had gravitational pressure losses as a conservative estimate.

Since the heat exchanger model was integrated with an already developed thermodynamic model, all necessary fluid conditions, such as inlet and outlet temperatures and flow rates, were already known. However, the heat exchanger equations introduced below were performed for individual heat transfer channels. This means that the fluid mass flow rate used was the global mass flow rate divided by the number of fluid channels in the heat exchanger. For each fluid stream, the number of channels was estimated to be the number of plates divided by 2. Equation (3.17) was then used to find the heat transfer rate for a single channel. The number of plates were iterated using the following design approach.

$$\dot{Q}_{channel} = \frac{\dot{m}_r}{0.5 * N_{plates}} * (i_{r,i} - i_{r,o}) \tag{3.17}$$

With all fluid conditions known, a UA-LMTD design approach was used for sizing the heat exchangers. This approach relates the heat duty of the region to the overall heat transfer coefficient, the heat transfer surface area, and the inlet and outlet temperatures of both fluids. Equation (3.18) provides this relationship and was the primary link between the thermodynamic model and the heat exchanger model:

$$\dot{Q}_{channel} = UA_{channel} * LMTD \tag{3.18}$$

where $\dot{Q}_{channel}$ is the heat transfer rate of the region, U is the overall heat transfer coefficient, A is the heat transfer surface area, and LMTD is the log mean temperature difference between the fluids. The log mean temperature difference is defined by Equation (3.19).

$$\mathrm{LMTD} = \frac{\Delta T_2 - \Delta T_1}{\ln\left(\frac{\Delta T_2}{\Delta T_1}\right)} \tag{3.19}$$

Subscripts 1 and 2 are related to either endpoint of the heat exchanger region. Since all heat exchangers used in this study were counter flow, ΔT_1 and ΔT_2 are defined by Equations (3.20) and (3.21), respectively.

$$\Delta T_1 = T_{h,i} - T_{c,o} \tag{3.20}$$

$$\Delta T_2 = T_{h,o} - T_{c,i} \tag{3.21}$$

With all fluid temperatures and the heat transfer rates known, Equations (3.18) through (3.21) were used to calculate the product of the overall heat transfer coefficient and heat transfer area, UA, for each region. The UA is further defined by using a thermal resistance network, as shown in Equation (3.22):

$$UA_{channel} = \left(R_h + R_{plate} + R_c\right)^{-1} \tag{3.22}$$

where R_h and R_c are the thermal convective resistances of the hot side and cold side fluids, respectively, and R_{plate} is the thermal conductive resistance of the heat transfer plate. The convective resistances were calculated using Equation (3.23):

$$R_{conv} = (h * A_{sf})^{-1} \tag{3.23}$$

where A_{sf} is the heat transfer surface area and h is the heat transfer coefficient, which is determined using correlations introduced in the following section. The wall thermal resistance is defined by Equation (3.24):

$$R_{plate} = \frac{Pt}{K_{plate} * A_{sf}} \tag{3.24}$$

where Pt is the plate thickness and K_{plate} is the thermal conductivity of the plate material. The heat transfer surface area was calculated for each region and is given in Equation (3.25).

$$A_{sf} = L_{region} * W_{plate} \quad (3.25)$$

L_{region} is either L_{sc}, L_{tp}, or L_{sh} in Figure 3-15 for phase change heat exchangers, or L_{port} in recuperative heat exchangers. For heat exchangers with multiple sections, the sum of the region lengths must equal the total port-to-port length. For heat exchangers with three sections, this is shown in Equation (3.26).

$$L_{port} = L_{sc} + L_{tp} + L_{sc} \quad (3.26)$$

Equations (3.17) through (3.26) were solved iteratively to determine the number of plates required, and thus the total heat exchanger size. The heat exchanger depth and total volume are given by Equation (3.27) and (3.28), respectively.

$$Depth_{total} = N_{plates} * (Pt + Ps) \quad (3.27)$$

$$Volume_{total} = Depth_{total} * L_{total} * W_{plate} \quad (3.28)$$

3.5.2. Correlations for Heat Transfer Coefficients

To calculate the heat transfer coefficient for each fluid region, a number of empirical correlations from literature must be used. Separate correlations exist depending on the fluid, heat exchanger geometry, flow conditions, and fluid phase. A summary of heat transfer correlations used for each heat transfer section is provided in Table 3-7. Correlation selection was influenced by past work by Simon III [93] and Young [94]. It is important to note that heat transfer coefficients were calculated for individual heat exchanger channels, as discussed in Section 3.5.1. Therefore, all mass flow rates and heat duties were calculated based on the number of channels and is an iterative process when using the model to size heat exchangers.

Hsieh and Lin developed a correlation for evaporation heat transfer of R410a in a PHE [95], shown in Equation (3.29), and is used for the two-phase region of the waste heat boiler and cooling cycle evaporator.

$$h_r = E * h_l + S * h_{pool} \tag{3.29}$$

This correlation combines heat transfer correlations developed by Dittus-Boelter [96] for h_l and Cooper [97] for h_{pool}, given in Equations (3.30) and (3.31), respectively.

$$h_l = 0.023 * Re_l^{0.8} * Pr^n * \frac{k_l}{D_h} \tag{3.30}$$

$$h_{pool} = 55 * P_r^{0.12} * M^{-0.5} * q^{0.67} \tag{3.31}$$

In Equation (3.30), Re_l is the liquid phase Reynolds number, Pr is the Prandtl number, k_l is the fluid conductivity, D_h is the hydraulic diameter, and n is equal to 0.4 if the fluid is being heated, or 0.3 if the fluid is being cooled. In Equation (3.31), P_r is the ratio of the fluid pressure to its critical pressure, M is the molecular weight of the refrigerant, and q is the imposed heat flux. Relevant equations for these parameters are provided in Equations (3.32) through (3.35):

$$Re_l = \frac{G * D_h}{\mu_l} = \frac{4 * \dot{m}_r}{P * \mu_l} \tag{3.32}$$

$$Pr = \frac{\mu_l * c_p}{k_l} \tag{3.33}$$

$$D_h = \frac{4 * A_{cs}}{P} \tag{3.34}$$

$$q = \frac{\dot{Q}_{channel}}{L_{region} * W_{plate}} \tag{3.35}$$

where G is the refrigerant mass flux, μ is the refrigerant viscosity, P is the fluid channel wetted perimeter, and A_{cs} is the fluid channel cross-sectional area. In Equation (3.35), the use of the region length adds computational complexity and instability to the model because it requires numerous iterations to solve. To avoid this issue, the length term used in the heat flux equation was assumed constant. For the waste heat boiler and both condensers it was assumed that the two-phase region was half of the total port-to-port length, while in the evaporator it was assumed that the two-phase region was 80% of the total length. Hsieh and Lin [95] modified the Dittus-Boelter and Cooper

correlations by adding an enhancement factor, E, and suppression factor, S, given by Equations (3.36) and (3.37), respectively.

$$E = 1 + 24000 * Bo^{1.16} + 1.37 * (X_{tt})^{-0.86} \quad (3.36)$$

$$S = \left(1 + 1.15 * 10^{-6} * E^2 * Re_l^{1.17}\right)^{-1} \quad (3.37)$$

Bo is the boiling number and X_{tt} is the Martinelli parameter, as given in Equations (3.38) and (3.39):

$$Bo = \frac{q}{G * i_{fg}} \quad (3.38)$$

$$X_{tt} = \left(\frac{1 - x_m}{x_m}\right)^{0.9} * \left(\frac{\rho_v}{\rho_l}\right)^{0.5} * \left(\frac{\mu_l}{\mu_v}\right)^{0.1} \quad (3.39)$$

where i_{fg} is the enthalpy of vaporization, ρ is the fluid density, and x_m is the mean vapor quality, which is assumed to be 0.5 for the boiler and condensers because there is only one heat exchanger section for the two-phase region. For the evaporator, the mean vapor quality was the average of the inlet vapor quality and the saturated vapor quality, 1.

Table 3-7: Summary of heat transfer correlations used

Heat Exchanger	Fluid	Heat Exchanger Section		
		Subcooled	**Two-Phase**	**Superheat**
Waste Heat Boiler	Refrigerant	Thonon et. al. [98]	Hsieh and Lin [95]	Thonon et. al.
	30% PG/Water Mixture	Muley [99]		
Condensers (PC+CC)	Refrigerant	Thonon et. al.	Yan et. al. [100]	Thonon et. al.
	Seawater	Muley		
Evaporator	Refrigerant	-	Hsieh and Lin	Thonon et. al.
	Water	-	Muley	
Recuperative Heat Exchangers	Refrigerant	-	-	Thonon et. al.

Yan et. al. developed a condensation heat transfer correlation for R134a in a PHE [100], shown in Equation (3.40):

$$h_r = 4.118 * Re_{eq}^{0.4} * Pr^{1/3} * \frac{k_l}{D_h} \tag{3.40}$$

where Re_{eq} is the equivalent Reynolds number and uses an equivalent refrigerant mass flux, as given by Equations (3.41) and (3.42). The mean vapor quality, x_m, is again assumed to be 0.5.

$$Re_{eq} = \frac{G_{eq} * D_h}{\mu_l} \tag{3.41}$$

$$G_{eq} = G * \left[1 - x_m + x_m * \left(\frac{\rho_l}{\rho_v}\right)^{0.5}\right] \tag{3.42}$$

Thonon et. al. correlation [98], which was developed for water with Reynolds numbers between 50 and 15,000, was used for all single phase refrigerant regions. This correlation, shown in Equation (3.43), is dependent on the chevron angle of the heat exchanger plate, measured from vertical. For this study it was assumed that the chevron angle was 60 degrees.

$$h_r = 0.2267 * Re^{0.631} * Pr^{1/3} * \frac{k}{D_h} \tag{3.43}$$

All external fluids (seawater, glycol, chilled water) generally experienced lower Reynolds numbers and were modeled using a correlation by Muley [99], given in Equation (3.44):

$$h_g = 0.44 * \left(\frac{6\beta}{\pi}\right)^{0.38} * Re^{0.5} * Pr^{1/3} * \frac{k}{D_h} \tag{3.44}$$

where β is the chevron angle of the heat exchanger plate, which was again assumed to be 60 degrees. The correlations presented in this section allow for the calculation of required heat transfer area, but critical to heat exchanger design optimization is pressure drop, which will be presented next.

3.5.3. Pressure Drop in Heat Exchangers

Pressure drop correlations are an essential component of heat exchanger models. There are multiple sources of pressure loss in heat exchangers, including frictional pressure drop, ΔP_f,

manifolds and ports pressure drop, ΔP_{man}, gravitational pressure drop, ΔP_g, and pressure drop from the acceleration or deceleration from evaporating or condensing the refrigerant, ΔP_a.

$$\Delta P_{total} = \Delta P_f + \Delta P_{man} + \Delta P_g + \Delta P_a \tag{3.45}$$

The acceleration/deceleration pressure drop, as well as the gravitational pressure drop, are direction dependent. A refrigerant flowing downwards will experience gravitational and deceleration pressure rises and have a negative value in Equation (3.45). In addition, the manifold pressure drop is relatively small and ranges from 1% to 3% of the total pressure drop [95]. Therefore, the manifold geometry and pressure loss was neglected in this study to further simplify the heat exchanger model.

The gravitational pressure drop in the single phase region is a simple fundamental equation shown in Equation (3.46):

$$\Delta P_g = \rho * g * L_{region} \tag{3.46}$$

where g is the acceleration due to gravity. For the two-phase region, an equivalent density is used, as defined by Equation (3.47).

$$\rho_{eq} = x_m * \rho_v + (1 - x_m) * \rho_l \tag{3.47}$$

Likewise, the pressure drop due to acceleration or deceleration from evaporating or condensing is given in Equation (3.48).

$$\Delta P_a = G^2 * \left(\rho_v^{-1} - \rho_l^{-1}\right) * \Delta x \tag{3.48}$$

The frictional pressure drop in the two-phase region of the heat exchanger channels, shown in Equation (3.49), is dependent on a empirically obtained friction factor, f_{tp}.

$$\Delta P_f = \frac{2 * f_{tp} * G^2 * L_{region}}{\rho_{eq} * D_h} \tag{3.49}$$

For the waste heat boiler and cooling cycle evaporator, Hsieh and Lin [95] recommend using Equation (3.50):

$$f_{tp} = 23820 * \left(Re_{eq}\right)^{-1.12} \tag{3.50}$$

where the equivalent Reynolds number, Re_{eq}, is calculated from Equation (3.41). Likewise, Yan et. al. [100] recommend Equation (3.51) for the friction factor in condensing heat exchangers:

$$f_{tp} = 94.75 * \left(Re_{eq}\right)^{-0.0467} * Re^{-0.4} * Bo^{0.5} * \left(\frac{P}{P_c}\right)^{0.8} \tag{3.51}$$

where the P is the inlet fluid pressure, P_c is the refrigerants critical pressure, and Bo is the boiling number as calculated in Equation (3.38). The frictional pressure drop in the single phase regions of the heat exchangers was modeled using Equation (3.52):

$$\Delta P_f = \frac{2 * f_{thonon} * \rho * u_{channel}^2 * L_{region}}{D_h} \tag{3.52}$$

where $u_{channel}$ is the velocity of the refrigerant at the inlet of the channel region, and f_{thonon} is the Thonon friction factor. The Thonon friction factor is given by Equation (3.53).

$$f_{thonon} = 0.6857 * Re^{-0.172} \tag{3.53}$$

To determine the total pressure drop of the heat exchanger, the frictional, gravitational, and acceleration or deceleration pressure drops from each region are summed. For the condensing heat exchangers, the refrigerant flow is downwards, and the gravitational and deceleration pressure drops are subtracted from the frictional pressure drop to determine the overall pressure loss across the heat exchanger. The pressure drop for each region is integrated with the thermodynamic model, and the two models are iterated during sizing.

3.5.4. Heat Exchanger Optimization

Proper heat exchanger selection and sizing are necessary for implementing a thermally driven chiller on space-limited ships. As discussed in Chapter 2, existing technologies are unable to be used in this market due to their extremely large volumes. In this study, the TCCS heat exchangers were optimized to maximize performance while being no larger than an existing commercial chiller of the same cooling capacity. For this comparison, a 200-ton Daikin WMC dual centrifugal compressor water cooled chiller was used for comparison. The details of this chiller are shown in Figure 3-16.

Company	Daikin
Model	WMC 036D-SN
Length	134.7 in (3.42 m)
Width	43.4 in (1.10 m)
Height	79 in (2.00 m)
Footprint	40.6 ft^2 (3.77 m^2)
Volume	267 ft^3 (7.57 m^3)

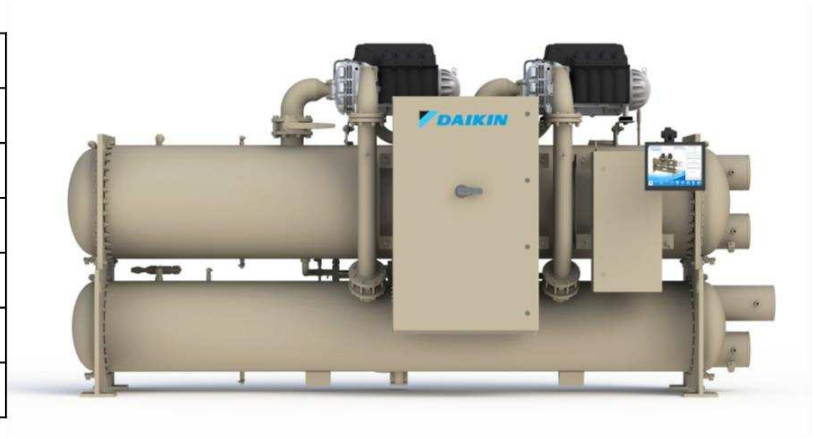

Figure 3-16: Daikin WMC chiller used for dimension constraints [101]

The goal of the TCCS modeling and optimization was to design a system that does not exceed the length, width, or height of the Daikin chiller. A block diagram of the heat exchanger sizing and optimization process is provided in Figure 3-17. The process included four distinct steps: model selection, maximum sizing, and two parametric sweeps. Heat exchanger models were selected based on Alfa Laval commercially available gasketed and brazed heat exchangers [92].

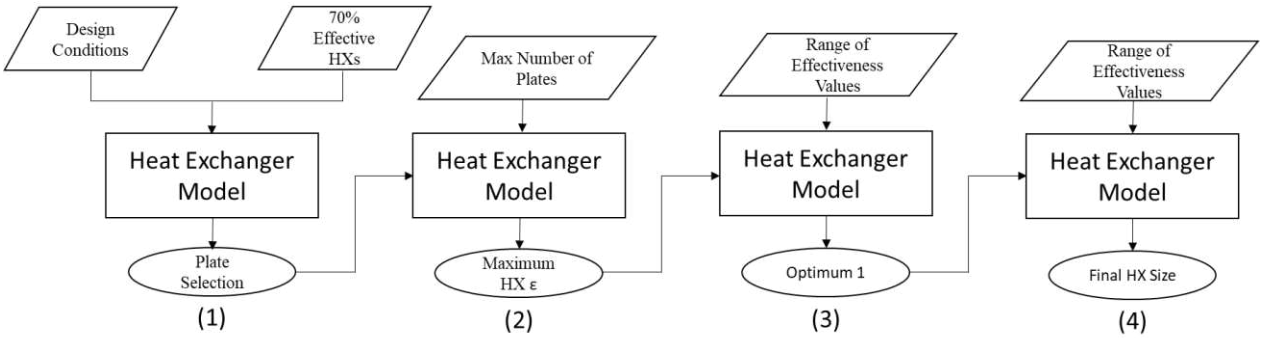

Figure 3-17: Heat exchanger optimization block diagram

The first optimization step was to size the heat exchangers using the design conditions listed in Table 3-8 and heat exchanger effectiveness values of 70%. One heat exchanger section effectiveness was used as the primary variable for heat exchanger. For the power cycle boiler, the superheat region effectiveness was variable, while the two-phase region of the condensers and cooling cycle evaporator were varied. The recuperative heat exchangers only had one section and therefore one effectiveness value, which was varied. Different heat exchanger models were selected and modeled until reasonable pressure drops were observed (e.g. <20 kPa) and reasonable plate amounts were calculated (e.g. <500 plates). In addition, models selected could be no taller than 79 inches or wider than 43 inches. Once models were selected using heat exchanger effectiveness values of 70%, the effectiveness of each heat exchanger was increased until the plate count matched the maximum number of plates of that model. Maximum number of plates were determined through data sheets. The selected models, their geometry, and the associated maximum effectiveness are listed in Table 3-9.

Table 3-8: Heat exchanger sizing design conditions

Fixed Inputs	Value
Inlet/outlet hot water loop temperature	94.3°C/84.4°C
Inlet/outlet condenser water temperature	29°C/35°C
Inlet/outlet chilled water temperature	10.39°C/5.56°C
Boiler heat duty	748 kW
Chiller heat duty	703 kW
Turbine isentropic efficiency	80%
Compressor isentropic efficiency	80%
Pump isentropic efficiency	35%
Mechanical transfer isentropic efficiency	98%
Condenser subcooling	1°C
Pipe pressure drop	1 kPa

The sum of the heat exchanger cores for the maximum effectiveness system was 3.61 m^3, which is almost half of the allowed total volume (7.57 m^3). Based on prior design work it was determined that plate and frame heat exchanger cores fill approximately 32% of the total system volume, indicating that the maximum effectiveness heat exchanger system would be too large. Therefore, heat exchangers were optimized using a parametric table of heat exchanger effectiveness values to determine the combination of heat exchanger sizes that fit within 2.42 m^3. The allowed heat exchanger core volume (32%) is dependent on several factors, such as heat exchanger type, number of piping routes, and amount of other equipment, and can be adjusted as necessary in future work. Two parametric sweeps were used to determine the final system heat exchanger sizes. Details of each sweep will be provided in Chapter 4.

Table 3-9: Heat exchanger selected models and maximum sizes

Heat Exchanger:	Boiler	PC Condenser	Evaporator	CC Condenser	Recuperator	Economizer	Suction Line
Model	M10 (semi-welded)	AQ4L (gasketed)	AC500DQ (brazed, 2 cores)	AQ4L (gasketed)	AC500DQ (brazed)	AC500DQ (brazed)	AC500DQ (brazed)
L_{port}	0.718 m	1.338 m	0.632 m	1.338 m	0.632 m	0.632 m	0.632 m
L_{total}	1.084 m	1.981 m	0.739 m	1.981 m	0.739 m	0.739 m	0.739 m
W_{plate}	0.438 m	0.448 m	0.322 m	0.448 m	0.322 m	0.322 m	0.322 m
Max N_{plates}	300	400	540	400	270	270	270
Depth	0.922 m	1.230 m	1.660 m	1.230 m	0.830 m	0.830 m	0.830 m
Volume	0.438 m^3	1.092 m^3	0.395 m^3	1.092 m^3	0.198 m^3	0.198 m^3	0.198 m^3
Effectiveness	0.75	0.82	0.82	0.80	0.75	0.78	0.77

3.5.5. Pipe Sizing and Pressure Drop

After heat exchangers were sized and optimized, piping routes were sized based on pressure drop. It was assumed that a 1.5-meter piping route was required to connect each component. Design conditions remained the same as from heat exchanger sizing, shown in Table 3-8. Pressure drop calculations were very similar to single phase heat exchanger calculations and were calculated using Equation (3.54).

$$\Delta P_{pipe} = f_{pipe} * \frac{L_{pipe}}{D_{pipe}} * \frac{\rho * u^2}{2} \tag{3.54}$$

Fluid properties used to calculate the velocity, u, were assumed to be the average of inlet and outlet pipe conditions. The Reynolds numbers in each piping route were very large (>10^5), indicating turbulent flow throughout the system. Therefore, Equation (3.55) was used to determine the pipe friction factor, f_{pipe} [102].

$$f_{pipe} = 0.0032 + \frac{0.221}{Re^{0.237}} \tag{3.55}$$

The Reynolds number was calculated using Equation (3.32). The fluid between the expansion valve and the evaporator was in the two-phase region, so the equivalent Reynolds number, equivalent mass flux, and equivalent density, provided in Equations (3.41), (3.42), and (3.47), were used to calculate the pressure drop in this pipe. Pipe diameters were selected in ½ inch increments to achieve pressure drops of approximately 1 kPa or less. Selected pipe sizes and their pressure drops at design conditions are listed in Table 3-10.

Table 3-10: Pipe sizes and pressure drops

Power Cycle				Cooling Cycle			
Pipe Number	**Description**	**Diameter**	**Pressure Drop [Pa]**	**Pipe Number**	**Description**	**Diameter**	**Pressure Drop [Pa]**
Pipe 1	Turbine to Recuperator	3.5″	901	**Pipe 1**	Compressor to Economizer	3.5″	876
Pipe 2	Recuperator to Condenser	3.5″	875	**Pipe 2**	Economizer to Condenser	3.5″	788
Pipe 3	Condenser to Pump	2″	784	**Pipe 3**	Condenser to Suction Line	2″	640
Pipe 4	Pump to Recuperator	2″	783	**Pipe 4**	Suction Line to Expansion Valve	2″	630
Pipe 5	Recuperator to Economizer	2″	788	**Pipe 5**	Expansion Valve to Chiller	2″	530
Pipe 6	Economizer to Boiler	2″	806	**Pipe 6**	Chiller to Suction Line	4″	1031
Pipe 7	Boiler to Turbine	3″	678	**Pipe 7**	Suction Line to Compressor	4″	1186

3.6. Performance Modeling

After optimizing heat exchangers and pipes, the sizing model was converted to a performance model. A select number of previously fixed heat exchanger effectiveness values were replaced by setting the number of plates for each heat exchanger constant. To avoid under constraining the model, the condenser subcooling amount, boiler subcooled region effectiveness,

and evaporator superheated region effectiveness must remain fixed. A summary of methods used to calculate each heat exchanger sections' performance is provided in Table 3-11. Floating values are those that do not have fixed performance and are influenced by other parameters such as seawater temperature rise and waste heat temperatures and flow rates. Pipe lengths and diameters were also fixed in the performance model.

The performance model was used for two different use cases: power density improvement and fuel savings mode. Power density improvement mode is when the electricity offset from using the TCCS to provide cooling is used for other purposes. In this mode of operation, the engine load and waste heat remain unchanged when the TCCS is operating. Alternatively, in fuel saving mode, the electricity that is freed up from using the TCCS is not used for other purposes, and the benefits are reduced fuel consumption. In this mode, the engine load and waste heat availability are reduced from using the TCCS. The following two sections provide the necessary equations and methodology used for both use cases.

Table 3-11: Summary of methods used to calculate heat exchanger performance

Heat Exchanger	**Heat Exchanger Section**		
	Subcooled	**Two-Phase**	**Superheat**
Waste Heat Boiler	Fixed Effectiveness	Floating	Heat Exchanger Model
PC Condenser	Fixed Subcooling	Heat Exchanger Model	Floating
Evaporator	-	Heat Exchanger Model	Fixed Effectiveness
CC Condenser	Fixed Subcooling	Heat Exchanger Model	Floating
Recuperative Heat Exchangers	Heat Exchanger Model		

3.6.1. Power Density Improvement Methodology

To calculate the power density improvement from using the TCCS, the fixed geometry performance model is run over the range of seawater and engine conditions introduced in Section 3.1. The engine load is held constant as was done during thermodynamic model. The primary metric used to determine the power density improvement is given in Equation (3.56):

$$\text{Power Density Improvement} = \frac{\dot{W}_{VCC} - \dot{W}_{TCCS}}{\dot{W}_{gen}} \tag{3.56}$$

where $\dot{W}_{VCC}$ is the electricity consumption of the legacy systems, $\dot{W}_{TCCS}$ is the electricity consumption of the TCCS power cycle pump and electric compressor, and $\dot{W}_{gen}$ is the electricity output of the generator set at the current loading condition. For example, at 50% engine load the electric output of the generator set is 1300 kW_e. If the TCCS reduces power consumption for cooling by 130 kW_e, the power density improvement would be 10%.

A weighted average process was performed to determine the average annual power density improvement of the system. First, the power reduction and power density improvement were determined on a per engine load basis by assigning a weighted factor to each seawater temperature. The weighted factor is simply the percent of the operational time that occurs at that seawater temperature and must sum to one. To determine the weighted performance, the power reduction at every seawater temperature was multiplied by its weighted factor and the values were summed to find the total weighted power reduction at that engine load. Then, the power density improvements were multiplied by the engine load weighted factors and summed to determine the overall yearly average power density improvement. The modeling results were then compared to the fixed effectiveness method used in Section 3.4 to determine the accuracy of past work methodology.

3.6.2. Fuel Savings Improvement Methodology

A fuel saving model was required to perform economic calculations. In fuel saving mode, the electricity offset by the TCCS is not used elsewhere and the engine load decreases, reducing fuel consumption. A consequence of this operational mode is that waste heat availability also decreases, as was seen in Figure 3-2. Therefore, an iterative engine model was required. The baseline vapor compression chiller model was used to determine the original electricity draw for cooling at each seawater temperature, which allows for the power reduction to be calculated. The power reduction was then subtracted from the engine output and a new engine load was determine. As this occurs, the amount of waste heat available was reduced, and the model iterates.

The engine model starts with the generator set electricity output, which was divided by the generator efficiency, η_{gen}, to determine the engine power, $\dot{W}_{engine}$.

$$\dot{W}_{engine} = \frac{\dot{W}_{gen}}{\eta_{gen}} \tag{3.57}$$

The generator efficiency was assumed to be 95% at all loading conditions. The engine load was then divided by the thermal efficiency, $\eta_{thermal}$, to calculate the heat input of the fuel, $\dot{Q}_{fuel}$.

$$\dot{Q}_{fuel} = \frac{\dot{W}_{engine}}{\eta_{thermal}} \tag{3.58}$$

The thermal efficiency of the engine varies with engine load, and is 39.1%, 39.3%, 39.5%, and 40.3% at 25%, 50%, 75%, and 85% engine loads, respectively. It was assumed that during each loading condition, the engine thermal efficiency remained constant. For example, if the TCCS reduced the engine load from 85% to 80%, the engine thermal efficiency remained at 40.3%. Next, the heat input of the engine was divided by the lower heating value of the fuel, LHV_{fuel}, to find the mass flow of the fuel, $\dot{m}_{fuel}$.

$$\dot{m}_{fuel} = \frac{\dot{Q}_{fuel}}{LHV_{fuel}} \tag{3.59}$$

The lower heating value was assumed to be 42,780 kJ kg^{-1}. The mass flow rate, which was calculated in kg s^{-1}, was converted to mt yr^{-1} and multiplied by the percent of time per year that the engine operates at that loading condition. The sum of percentages for the engine loads was approximately 45%, not 100%, because the engine did not operate for the full year. This process determines the actual fuel consumed per year at each engine load. Values were summed to determine the annual fuel consumed over all engine loads. The original fuel consumption profile was compared to the new load profile to determine the annual fuel savings from the TCCS. This allows for economic calculations, such as payback period, to be performed.

3.7. Economic Modeling

An economic model was created to determine the cost and financial savings of the designed TCCS. First, individual component costs were estimated through a combination of correlations and known costs. Refrigerant charge was estimated based on average fluid conditions in the piping and heat exchangers and added to the component costs. After including installation costs, economic metrics, such as payback period and net present value, were calculated. Since the TCCS can be used in place of a commercial electrically driven centrifugal chiller, economic calculations were performed for retrofits and new installations, in which the cost of commercial equipment were subtracted from the TCCS cost. Lastly, the TCCS cost, performance, and size were compared with a SOA absorption chiller.

3.7.1. Component Cost Models

Heat exchangers account for a large percentage of the total cost of the system. Their costs were predicted using a correlation from Brown [103]:

$$\text{Cost}_{\text{HX}} = 475 * \text{A}_{\text{sf,total}}^{0.54} * \text{F}_{\text{material}} * \text{F}_{\text{pressure}} * \text{F}_{\text{custom}} * \frac{\text{CEPCI}_{2018}}{\text{CEPCI}_{2005}} \tag{3.60}$$

where $A_{sf,total}$ is the total heat transfer surface area in feet, $F_{material}$ is a material cost factor, $F_{pressure}$ is a pressure cost factor, F_{custom} is a custom cost factor based on quotes, and CEPCI is the Chemical Engineering Plant Cost Index. $F_{material}$ is 1 for stainless steel heat exchangers and 1.6 for titanium heat exchanger plates used for the condensers. $F_{pressure}$ is 1 for pressures below 235 psig, 1.23 for pressures between 235 psig and 370 psig, and 1.35 for pressures above 370 psig. F_{custom} was included as it was found that this correlation consistently overpredicted heat exchanger costs compared to quoted values. The custom factor used was 0.9 for two-phase heat exchangers and 0.8 for recuperative heat exchangers. Justification for this factor is provided in Appendix A.4. The CEPCI is used to update the model to modern day prices. $CEPCI_{2005}$ is equal to 468.2 and $CEPCI_{2018}$ is 603.1.

The cost of piping and fittings were also predicted from Brown [103], given in Equation (3.61):

$$\text{Cost}_{\text{pipe}} = 10 * \left(0.1 * \text{N}_{\text{fittings}} + 0.924\right) * L_{pipe} * \text{D}_{\text{pipe}}^{0.83} * \frac{\text{CEPCI}_{2018}}{\text{CEPCI}_{2005}} \tag{3.61}$$

where $N_{fittings}$ is the number of fittings per 100 feet of pipe, L_{pipe} is the length of the pipe in feet, and D_{pipe} is the diameter of the pipe in inches. It was assumed that 20 fittings were required per 100 feet of pipe, or about 1 fitting every 5 feet.

The cost of the turbo-compressor was based on a curve fit using price points from previous applications of the TCCS and is a function of the turbine power.

$$\text{Cost}_{\text{TC}} = \text{Cost}_{6\text{kW}} * \left(\frac{\dot{\text{W}}_{\text{turbine}}}{6\ \text{kW}}\right)^{\frac{\log\left(\frac{\text{Cost}_{10\text{kW}}}{\text{Cost}_{6\text{kW}}}\right)}{\log\left(\frac{10\ \text{kW}}{6\ \text{kW}}\right)}} \tag{3.62}$$

The cost of the 6 kW turbo-compressor was $2620, and the cost of the 10 kW turbo-compressor was $3140. These cost predictions were based on high volume production of 1,000 turbo-compressors per year. The cost of the turbo-compressor represents the highest uncertainty because it is not a commercial product and the cost is not well understood. Future development of this component will influence the predicted cost of the turbo-compressor. It is expected that at initial low production volumes, the costs should be significantly higher.

The remaining components were based on design considerations and product quotes. The electric compressor was chosen to be a Danfoss Turbocor TTS700, which is rated at 130 to 200 tons of cooling with R134a. Turbocor centrifugal compressors are oil-free and have magnetic bearings and an integrated variable speed drive, making it an optimal solution to operate with the turbo-compressor. The list price of the TTS700 is $46,696 [104].

The power cycle pump was chosen to be a Sero SRZS 446 side channel pump [105] with a Yaskawa P1000 variable frequency drive (VFD) [106]. These components are used as a part of the current TCCS test facility. The design pump power in this study was 17.7 kW_e, and the design power of the Sero pump is 18.6 kW_e, making it a suitable choice for this system. The cost of the pump is $15,208 and the cost of the VFD is $2,502, for a total of $17,710.

The system requires instrumentation to monitor and control system functions during operation. It was assumed that thermocouples were used on the inlet and outlets of major components, including phase change heat exchangers and turbomachinery, for a total of 16 thermocouples. The thermocouples used in the current test facility are $39 per unit, for a total of $624. Pressure transducers were assumed to be placed at the inlets of all phase change heat exchangers and turbomachinery for a total of 8 units. At $276 per unit, the cost of pressure transducers was $2,208. Lastly, differential pressure transducers are used to monitor

turbomachinery components, including the turbine, pump, and both compressors. At $1,079 per unit, the differential pressure transducers cost $4,316. In total, instrumentation cost $7,148.

A variety of valves are also necessary for system operation, and their costs are estimated based on equipment in the current test facility. The expansion valve is a Sporlan electronic expansion valve (EEV) and costs $1,566 including the valve, controller, and temperature and pressure sensors. Ten different ball valves are required, including: at the inlet and outlets of the turbine and compressor, at the outlets of the turbo-compressor coolant lines, and for pressure safety vents for both cycles. These valves cost a total of $3,351. Remaining valves include gate/needle valves for the turbo-compressor coolant lines, and a globe valve for a turbine bypass for system start-up. In total, valves account for $5,528 of the system cost.

Refrigerant costs were also considered. To calculate these costs, it was necessary to predict the fluid charge in the system. First, the mass in each piping route, m_{pipe}, was estimated using Equation (3.63):

$$m_{pipe} = \rho_{pipe} * \frac{\pi * D_{pipe}^2}{4} * L_{pipe} \tag{3.63}$$

where the density, ρ_{pipe} is the average density of the fluid at the inlet and outlet of the pipe. An equivalent density was used for the pipe connecting the expansion valve to the evaporator, as provided in Equation (3.47). For the heat exchangers, it was assumed that 25% of the heat exchanger core volume contained refrigerant, and the density used was the average of the saturated liquid and saturated vapor densities. For the recuperative heat exchangers, the density was simply the average of the inlet and outlet densities.

$$m_{HX} = 0.25 * Volume_{total} * \rho_{HX} \tag{3.64}$$

The refrigerant mass in the pipes and the heat exchangers were summed to obtain the total refrigerant charge. This charge was then multiplied by a specific cost of R134a, which was \$11.68 kg^{-1}.

3.7.2. Economic Performance Metrics

Financial savings were calculated based on the annual fuel savings for the designed system and the total component costs. Construction and installation costs were calculated by assuming an installation factor, $F_{install}$. The installation factor is the cost of installation divided by the system component cost. Commercial centrifugal chillers have installation factors <0.2 [40], while absorption chillers can have installation factors >1.5 due to their large volumes and need for waste heat recovery equipment [41]. For the TCCS, an installation factor of 0.5 was assumed because it was designed to be the same volume as commercial centrifugal chillers but has added complexity and waste heat recovery. The total installed cost of the system is given in Equation (3.65):

$$\text{Installed Cost} = \text{Cost}_{\text{TCCS}} + \text{Cost}_{\text{Install}} = \text{Cost}_{\text{TCCS}} * (1 + F_{\text{install}}) \quad (3.65)$$

The shipboard diesel engine used in this engine can be run using marine gas oil (MGO) or marine diesel oil (MDO). These fuels are both distillate fuels and are commonly used in in larger engines and gensets and are generally cleaner and less polluting than alternative fuel types. The DOD has standard prices of fuel to insulate military services from the volatility of fuel prices on the market. The standard price of MGO for 2021 was \$2.47 per gallon, or \$778 per mt [107]. A 2% annual cost inflation on fuel was assumed. Using this information, a payback period was calculated which is the amount of time required for an investment to break even. In other words, it is the amount of time for the annual savings to equal the initial capital expense of the project. Payback period should consider the difference in maintenance costs between the proposed project

and the baseline case, but it was assumed that these maintenance costs were equivalent for this study. Therefore, the payback period is estimated using Equation (3.66).

$$\text{Payback Period} = \frac{\text{Installed Cost}}{\dot{m}_{\text{fuel}} * \text{Cost}_{\text{fuel}}} \tag{3.66}$$

As previously noted, a 2% annual cost inflation on fuel was assumed, and therefore the actual payback period will be lower than that calculated in Equation (3.66) due to rising fuel costs.

Two other economic metrics were considered: net present value (NPV) and internal rate of return (IRR). The NPV is the difference between the value of expected cash flow and the value of invested cash over a period of time. The NPV is given in Equation (3.67):

$$\text{NPV} = \sum_{t=1}^{n} \frac{R_t}{(1+y)^t} \tag{3.67}$$

where R_t is the net cash flow during the single time period, y is the discount rate, and t is the number of time periods. The discount rate is a metric used to estimate the possible return that could be earned from an alternative investment and is typically assumed to be 10% for higher-risk technologies such as the TCCS. The net cash flow takes into consideration fuel savings and maintenance costs compared to the baseline case. The lifetime of the TCCS is unknown because it is currently only operated in a lab environment, but the project evaluation period was assumed to be 15 years. The NPV of a project should be greater than zero to indicate that the discounted present value of future cash flows will be positive. In general, a project with a higher NPV is a more attractive investment than one with a lower NPV. The IRR is a similar metric to NPV and is the discount rate required to achieve a NPV of zero and may be more appropriate to compare projects of different scales or lifetimes. To calculate the IRR, Equation (3.67) is set to zero and the discount rate, y, is calculated, also shown in Equation (3.68).

$$0 = \text{NPV} = \sum_{t=1}^{n} \frac{R_t}{(1 + \text{IRR})^t} \tag{3.68}$$

This calculation is an iterative process and is best done using a computer program such as Microsoft Excel.

Since the TCCS designed can completely replace an electric chiller, two case scenarios were considered: new installations and retrofits. In a retrofit project, the payback period, NPV, and IRR were calculated using the true installed cost of the TCCS. However, in a new installation the cost to install a vapor compression chiller was subtracted from the investment cost. Regardless of the proposed project, a vapor compression chiller would need to be purchased to provide cooling. Therefore, the differential cost of the TCCS to the vapor compression chiller is a better representation of the investment required for the project. The payback period, NPV, and IRR were then be calculated using the differential cost as the initial capital cost required.

Table 3-12: Summary of economic assumptions

Fixed Economic Inputs	Value
TCCS Installation Factor	0.5
Fuel (MGO) Cost	\$2.47 gal^{-1}
Annual Fuel Cost Inflation	2%
Project Evaluation Years	15 Years
Discount Rate	10%

3.7.3. SOA System Costs and Performance

The cost, performance, and size of the TCCS was compared to SOA electric centrifugal chillers and absorption chillers, which are summarized in Table 3-13. The size and performance of a comparative 200-ton electrical centrifugal chiller has been discussed in detail in Sections 3.4 and 3.5. The cost of an electrical chiller was estimated from the US Energy Information

Administration (EIA) updated buildings sector appliance and equipment costs and efficiencies report [40]. As of 2017, a typical 400-ton commercial water-cooled centrifugal chiller cost $425 ton^{-1} in equipment. It was assumed that this was the same specific cost for a 200-ton chiller. However, unique to shipboard applications is the required use of titanium or copper-nickel condensers. It was found that using titanium condensers in the TCCS increased the total equipment cost by 13.7%. This percent increase was applied to the equipment costs of the SOA options. With an installation factor of 0.18, the baseline vapor compression chilled had an installed cost of $113,700.

Table 3-13: Summary of SOA chiller costs

Heat Exchanger	Centrifugal Chiller	Absorption Chiller
Design Cooling Duty	200 tons	144 tons
DOE Equipment Costs	$425 ton^{-1}	$1751 ton^{-1}
	$85,000	$251,399
Percent Increase from Titanium	13.7%	13.7%
New Equipment Costs	$483 ton^{-1}	$1991 ton^{-1}
	$96,645	$285,841
Installation Factor	0.18	1.21
Installation Costs	$85 ton^{-1}	$2403 ton^{-1}
	$17,055	$345,083
Total Install Cost	$568 ton^{-1}	$4394 ton^{-1}
	$113,700	$630,924

A commercially available Thermax Cogenie LT 16C hot water driven absorption chiller rated at 160-tons of cooling was used for size and performance comparisons [24]. The Thermax chiller has a design COP of 0.676 at 29°C condenser water temperatures. This chiller was selected based on the design case of 747 kW_{th} of waste heat at 85% engine load. With a COP of 0.676, the resulting cooling duty would be 144 tons, which was used for costing purposes. Absorption

equipment costs were linearly interpolated from the Department of Energy (DOE) absorption chillers factsheet [41] and were \$1,991 ton^{-1} after accounting for the 13.7% increase in costs from using titanium condensers. Installation costs were assumed to be based on the volume of the system, given in Equation (3.69):

$$F_{\text{abs}} = F_{\text{TCCS}} \frac{\text{V}_{\text{abs}}}{\text{V}_{\text{TCCS}}} \tag{3.69}$$

where V_{TCCS} and V_{abs} are the volumes of the TCCS and absorption chiller, respectively. The absorption chiller was 100" tall, 59.1" wide, and 188.6" long, with a volume of 645 ft^3. This is approximately 2.4 times larger than the TCCS and Daikin chiller. Therefore, the installation factor was assumed to be 1.21. A detailed performance model for the absorption chiller was not developed during this study. Instead, the COP of the absorption chiller was assumed to be a function of the seawater temperature, and a linear curve fit was used based on data from Wang et. al. [108]. The cooling duty was calculated by multiplying the COP by the waste heat available. The absorption chiller model was run over the range of engine and seawater conditions described in Section 3.1 and fuel savings were calculated using the methodology presented in Section 3.6.2. The absorption chiller model provided less than 200-tons of cooling over the range of conditions, indicating the need for a secondary electrical chiller to provide the remaining cooling. However, the secondary chiller was not included in economic calculations.

The multiple modeling steps used in this study were presented in this Chapter. Modeling began with in introduction of the case study, followed by thermodynamic modeling, heat exchanger modeling, and economic modeling. Five different working fluids and three system configurations were modeled for performance over a range of conditions. A single system was

designed using R134a and the cost and financial savings were calculated. The following Chapter presents the results from each modeling step in detail.

CHAPTER 4 Results

The design and modeling approach outlined in Chapter 3 aimed to solve the major issues with using thermally driven technologies on ships. Existing technologies are simply too large and thermally driven chillers cannot be used to replace electric chillers on ships because the engine and diesel generator set loads are highly variable, and thus the waste heat loads are not steady. The system modeled and designed in this study addresses these issues while providing economic performance metrics for comparison with existing technologies.

4.1. Thermodynamic Modeling

Three system configuration options and five fluids were thermodynamically modeled over a range of conditions. Weighted average results were obtained based on the percent of time that the system operated at each condition. The first system configuration, Option 1, was to use the waste heat driven cooling system to provide supplemental chilled water and reduce the electric cooling load on baseline equipment. The weighted results of all five fluids in Option 1 are shown in Table 4-1.

The TCCS operating with R245fa had the highest power cycle performance with a thermal efficiency of 8.61%, which was expected as this fluid is typically used in commercial ORC systems. This was mostly due to the low pumping power requirements of the cycle and despite the high efficiency, the system had the lowest turbine power output. Contributing to the low pumping power was that R245fa has a higher enthalpy of vaporization at the boiler saturation conditions. At design conditions (29°C, 85% engine load), the system operating with R245fa had an enthalpy of vaporization of 155.3 kJ kg^{-1}, compared to 112.2 kJ kg^{-1} when operating with R134a. The increased enthalpy of vaporization resulted in a lower power cycle mass flow rate being calculated

for R245fa (3.70 kg s^{-1} vs. 4.24 kg s^{-1}). However, R245fa had the lowest cooling cycle COP and cooling duty and the evaporator operated under vacuum conditions, making it not an ideal fluid for this application. The system operating with R1234yf had the highest turbine output and chiller duty, but consequently had the largest power cycle pump electricity draw and therefore did not have the largest power reduction. Systems operating with R134a, R1234ze(E), and R515a all had similar performance across both cycles, including power reduction savings between 71.4 and 72 kW_{th}.

Table 4-1: Option 1 weighted thermodynamic results

Fluid	**η_{PC}**	**COP_{CC}**	**COP_{TCCS}**	**W_{pump} [kW]**	**$W_{turbine}$ [kW]**	**$Q_{chiller}$ [kW]**	**Power Reduction [kW]**
R134a	7.66%	6.95	0.663	10.9	50.3	347	71.9
R1234ze(E)	7.75%	7.00	0.647	8.72	48.7	338	72.0
R1234yf	7.25%	6.95	0.668	13.8	51.2	353	70.4
R245fa	8.61%	6.42	0.581	2.80	47.4	302	69.3
R515a	7.76%	6.94	0.641	8.60	48.6	335	71.4

Figure 4-1 displays the cooling duty of the five fluids over a range of seawater temperatures when the engine was at 50% load. At very low temperatures the TCCS provided the maximum amount of cooling set in this case study, 200-tons or 703 kW_{th}. For R134a and R1234yf, this occurs at 14°C, while for R515a, and R1234ze(E) this occurs at 13°C. R245fa was a clear outlier and provided less cooling over the entire range and didn't meet the maximum cooling amount until the seawater reached 10°C. The temperature at which the fluids reach their peak cooling amount was dependent on the engine load due to the reduction of waste heat availability. For example, R134a reached maximum cooling at 18°C when at 85% engine load and reached it at 10°C when at 25% engine load.

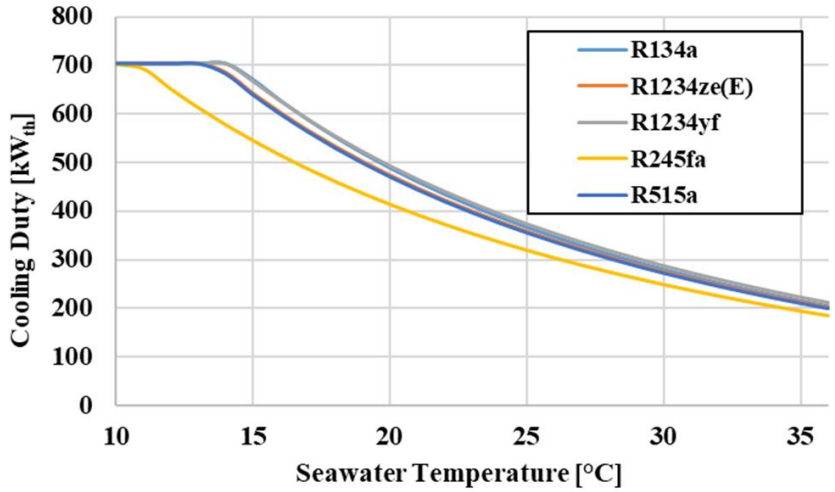

Figure 4-1: Option 1 fluid cooling duty comparison at 50% engine load and varying seawater conditions

The second TCCS system configuration studied, Option 2, was to use the TCCS to pre-cool seawater that was used in the condenser of the baseline shipboard 200-ton vapor compression chiller. The TCCS and VCC models were carefully integrated so that seawater was first cooled in the evaporator of the TCCS before entering the condenser of the VCC. Reducing the condenser water temperature of the VCC improves performance by reducing the pressure ratio across the electric compressor. For example, the system operating with R134a at design conditions cooled 37.24 kg s^{-1} of seawater from 29°C to 23.5°C in the evaporator. With an inlet condenser water temperature of 23.5°C, the electric compressor had a pressure ratio of 3.25 and consumed 159 kW_e to provide 200-tons of cooling. Without pre-cooling the seawater, the electric compressor would have had a pressure ratio of 3.79 and consumed 191 kW_e to provide 200-tons of cooling. In this example, the TCCS reduced power of the VCC by 32 kW_e, but also consumed 15.5 kW_e in the power cycle pump, for a net savings of 16.5 kW_e.

Table 4-2: Option 2 weighted thermodynamic results

Fluid	η_{PC}	COP_{CC}	W_{pump} [kW]	$W_{turbine}$ [kW]	Temperature Reduction (°C)	New VCC COP	Power Reduction [kW]
R134a	7.48%	14.2	10.5	49.3	4.44	4.95	14.5
R1234ze(E)	7.44%	14.5	8.25	46.8	4.30	4.93	16.0
R1234yf	6.96%	14.3	13.0	49.1	4.44	4.95	12.0
R245fa	8.19%	13.6	2.61	45.1	3.89	4.84	19.4
R515a	7.48%	14.4	8.19	47.0	4.28	4.92	15.9

Option 2 greatly underperformed compared to directly providing chilled water in Option 1. As seen in Table 4-2, R245fa had the largest power reduction of 19.4 kW_e despite cooling the seawater the least. Due to the small power reduction compared to Option 1, the pump power significantly impacted which fluid performed best. Even though R245fa had the lowest performing cooling cycle and cooled the seawater the least, it had the lowest power draw of only 2.61 kW_e. In contrast, R1234yf required on average 13 kW_e of electricity but only reduced the electric load of the baseline chiller by a weighted average of 25 kW_e. Thus, over 50% of the potential electrical savings were consumed by the power cycle pump. In summary, pre-cooling seawater improved VCC COP from 4.19 to approximately 4.9, but overall energy savings lagged those possible by off-setting the cooling demand of the vapor compression chillers in Option 1.

The third configuration studied, Option 3, was to boost the compressor power of the TCCS cooling cycle by using an electric compressor in series with the turbo-compressor. This strategy enabled the TCCS to provide the full 200-tons of cooling over the entire range of conditions. As seen in Table 4-3, the power boosted TCCS operating with R1234ze(E) had the highest power reduction of 103.9 kW_e out of all the configurations and fluids in this study, closely followed by R515a and R134a. The use of highly efficient turbomachinery, compact heat exchangers, and heat recuperation strategies resulted in a higher cooling cycle COP compared to the baseline chiller. As

seen in Table 4-1 and Table 4-3, the TCCS cooling cycle COP averaged between 6.4 and 7.0, compared to the baseline VCC COP of 4.19. This means that using additional compressor work in the TCCS cooling cycle is a more efficient use of energy than using a separate electrically driven chiller.

Table 4-3: Option 3 weighted thermodynamic results

Fluid	η_{PC}	COP_{CC}	COP_{Elec}	W_{pump} [kW]	$W_{turbine}$ [kW]	$W_{elec,comp}$ [kW]	**Power Reduction [kW]**
R134a	8.17%	6.95	14.3	12.0	54.0	52.7	103.1
R1234ze(E)	8.09%	7.01	14.7	9.29	50.9	54.7	103.9
R1234yf	7.50%	6.96	13.1	14.5	53.1	53.6	99.7
R245fa	9.06%	6.42	14.8	3.01	49.9	64.1	100.7
R515a	8.16%	6.95	14.6	9.25	51.2	55.3	103.3

Another metric used to compare the hybrid, electrically and thermally driven system to the baseline chiller system is the electrical COP. The electrical COP is the ratio of cooling to the electrical input to the system. The comparison of electrical COPs from seawater temperatures of 15°C to 36°C at 50% engine load is seen in Figure 4-2. As expected, the power boosted TCCS had a significant advantage over the electrical only system due to the higher cooling cycle COP and thermally driven compressor. Figure 4-2 is also a good indication of the performance of the different fluids. R134a, R1234ze(E), and R515a all had almost identical performance, as expected. R1234ze(E) was created as a replacement for R134a, and R515a is a blend consisting of R1234ze(E) and a fire suppressant. R1234yf underperformed slightly due to its less efficient power cycle, and R245fa was clearly the lowest performing fluid due to its poor cooling cycle performance. Overall, the TCCS operating with any of the studied fluids had an electric COP

greater than 10 below the design point, which is a significant improvement over the state-of-the-art.

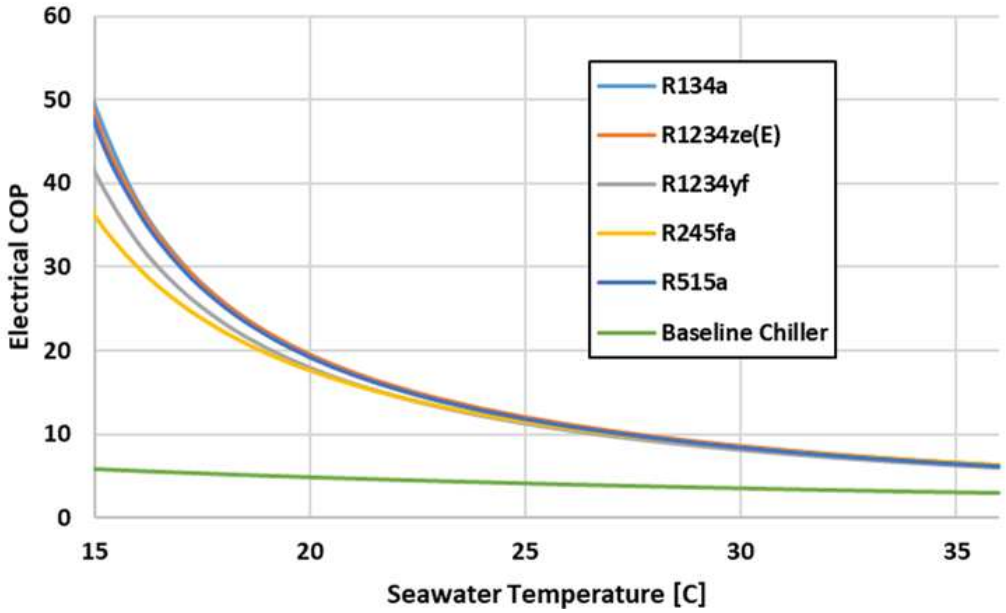

Figure 4-2: Option 3 electric COP comparison at 50% engine load and varying seawater conditions

This study presented two major improvements over previous ORVC and TCCS systems: the addition of an electric compressor in series with a thermally driven compressor and an improved heat recuperation strategy. The former is discussed in the Option 3 results above and significantly increases the operational flexibility of the system. The importance of the heat recuperation strategy is highlighted by the effect of the cross-cycle economizer heat duty on the power cycle performance. No modifications were made to the power cycle between configurations, yet as is shown in Table 4-1, Table 4-2, and Table 4-3, the power cycle efficiency and turbine work fluctuated. Figure 4-3 presents the economizer heat duty and turbine work of each system option using R134a at 50% engine load over the range of seawater temperatures. When the seawater was hotter than 15°C, Option 1 could not provide the maximum amount of cooling and the waste heat amount was constant. The heat duty of the economizer in Option 1 leveled out due to a reduced

cooling cycle mass flow rate, and performance was reduced as the condenser saturation pressure increased. In Option 3, the mass flow rate of the cooling cycle refrigerant remained high across all seawater temperatures because the cooling duty was always set, and the electrical compressor provides the additional work required to maintain the mass flow rate. The TCCS condenser saturation pressure increased with increasing seawater temperature, so the compressor discharge temperature increased as well. The hot discharge and high mass flow rate increased the heat transfer in the economizer and improved power cycle performance in Option 3. Option 2 performance was lower because of the increased saturation pressure in the cooling cycle evaporator and reduced pressure rise in the compressor compared to the other two options. This occurred because the system cooled relatively hot seawater instead of chilled water. As a result, the compressor discharge temperature was lower for Option 2 and less heat was transferred in the economizer. Overall, the increased economizer heat duty when using R134a resulted in Option 3 having an average turbine power improvement of 7.4% and 9.5% over Options 1 and 2, respectively. At 36°C and 50% engine load, the power output of Option 3 was 20% higher than in Option 2.

In summary, it was seen through thermodynamic modeling that Option 3, electrically boosting the compressor power in the TCCS cooling cycle, was the best option to replace baseline equipment and provide constant cooling loads independent of engine load and waste heat availability. This option reduced the weighted average power consumption for 200-tons of cooling by up to 104 kW_e, compared to 74 kW_e and 20 kW_e for Options 1 and 2, respectively. The TCCS operating with R1234ze(E) had the highest performance and has favorable environmental properties, but it is slightly flammable which may make shipboard implementation challenging. R515a may be a reasonable long-term shipboard replacement for R134a because it has similar

performance to R1234ze(E) and is blended with R227ea, which is a flame suppressant. Despite these advantages, the following design was conducted using the Option 3 configuration with R134a, which is most commonly used in state-of-the-art chillers. In addition, past TCCS work has been conducted on heat exchanger sizing for R134a, and there is an abundance of heat transfer correlations available for this fluid.

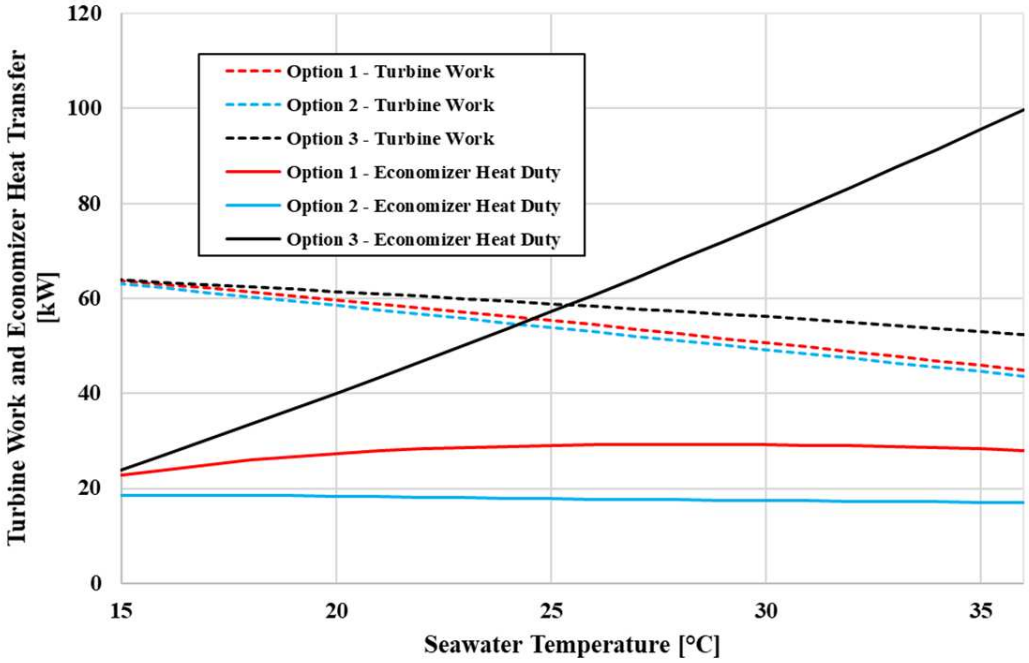

Figure 4-3: Economizer heat transfer and turbine work of the three TCCS options using R134a at 50% engine load

4.2. Heat Exchanger and Component Design

Heat exchangers and other components were selected for the power boosted TCCS, Option 3, using R134a as the working fluid. The objective was to design a system that fits within the footprint and volume of a commercial electrical chiller of the same cooling capacity. To meet this goal, plate frame heat exchangers were used in place of traditional shell and tube heat exchangers. Heat exchanger models were selected from commercially available Alfa-Laval options to obtain reasonable pressure drops and performance for each heat exchanger. Based on prior design work,

it was estimated that the plate frame heat exchanger cores would account for approximately 32% of the system volume. A parametric table was constructed to determine the combination of heat exchanger sizes with the highest electrical COP while remaining below 32% of the allowed volume. A summary of results is shown in Table 4-4. The allowed system volume was 7.57 m^3 and was based on a Daikin WMC dual compressor chiller. The starting effectiveness values for the table were based on the maximum number of plates for the chosen heat exchanger model. All calculations were done at the design conditions shown in Table 3-8.

Table 4-4: Optimized heat exchanger sizes

Heat Exchanger	**Boiler**	**PC Condenser**	**Evaporator**	**CC Condenser**	**Recuperator**	**Economizer**	**Suction Line**	**Volume %**	**Electric COP**
Fluid Region	Super-heat	Two-Phase	Two-Phase	Two-Phase	Single-Phase	Single-Phase	Single-Phase		
Maximum ε Value	0.75	0.82	0.82	0.80	0.75	0.78	0.77	46.9%	10.8
Final ε Value	0.60	0.67	0.82	0.75	0.65	0.73	0.77	31.8%	9.84
Resulting Number of Plates	196	178	530	314	118	162	258	-	-
Resulting Core Volume [m^3]	0.286	0.483	0.387	0.857	0.085	0.117	0.187	-	-

Due to the computational complexity and time requirements for conducting a parametric sweep of 7 variables, only two passes were conducted. The first parametric sweep only varied the effectiveness values of the four phase-change heat exchangers, which are generally significantly larger than the recuperative heat exchangers. The recuperative heat exchanger sizes were held constant at their maximum values. The optimized result was the combination of effectiveness values that had the highest electrical COP while remaining below 32% of the total system volume. A summary of the first parametric sweep results are shown in Table 4-5.

Table 4-5: Summary of the first heat exchanger sizing parametric sweep

Heat Exchanger	Boiler	PC Condenser	Evaporator	CC Condenser	Recuperator	Economizer	Suction Line	Volume %	Electric COP
Fluid Region	Super-heat	Two-Phase	Two-Phase	Two-Phase	Single-Phase	Single-Phase	Single-Phase	-	-
Maximum ε Value	0.75	0.82	0.82	0.80	0.75	0.78	0.77	46.9%	10.8
ε Range Included	0.55 to 0.65	0.62 to 0.72	0.72 to 0.82	0.65 to 0.75	0.75	0.78	0.77	-	-
Resulting ε Values	0.60	0.67	0.82	0.70	0.75*	0.78*	0.77*	31.9%	9.72

*** Value was held constant**

To meet the size constraint, the power cycle boiler and condenser effectiveness values were reduced by 0.15, while the cooling cycle condenser value was reduced by 0.10. The size of the cooling cycle evaporator did not change, indicating that its size had a strong impact on system performance. By reducing the size of the boiler and condensers, the electrical COP was reduced from 10.8 to 9.72. A second parametric sweep was used to include the recuperative heat exchangers and ensure that the two-phase heat exchangers were appropriately sized. Since the evaporator two-phase heat exchanger effectiveness value remained at its maximum value after the first sweep, it was left as constant to significantly reduce computational time. A summary of the second is shown in Table 4-6.

Table 4-6: Summary of the second heat exchanger sizing parametric sweep

Heat Exchanger	Boiler	PC Condenser	Evaporator	CC Condenser	Recuperator	Economizer	Suction Line	Volume %	Electric COP
Fluid Region	Super-heat	Two-Phase	Two-Phase	Two-Phase	Single-Phase	Single-Phase	Single-Phase	-	-
Starting ε Value	0.60	0.67	0.82	0.70	0.75	0.78	0.77	31.9%	9.72
ε Range Included	0.55 to 0.65	0.62 to 0.72	0.82	0.65 to 0.75	0.65 to 0.75	0.68 to 0.78	0.67 to 0.77	-	-
Resulting ε Values	0.60	0.67	0.82*	0.75	0.65	0.73	0.77	31.8%	9.84

*** Value was held constant**

It was again found that the performance of the power cycle could be reduced at the expense of greater cooling cycle performance. The recuperator and economizer sizes were reduced, and the cooling cycle condenser size was increased. The boiler and power cycle condenser effectiveness values remained unchanged. The second parametric sweep resulted in the electrical COP increasing from 9.72 to 9.84, a 1.2% improvement. Figure 4-4 displays the heat exchanger core volumes and system electrical COP for the maximum effectiveness system, first parametric sweep, and second parametric sweep.

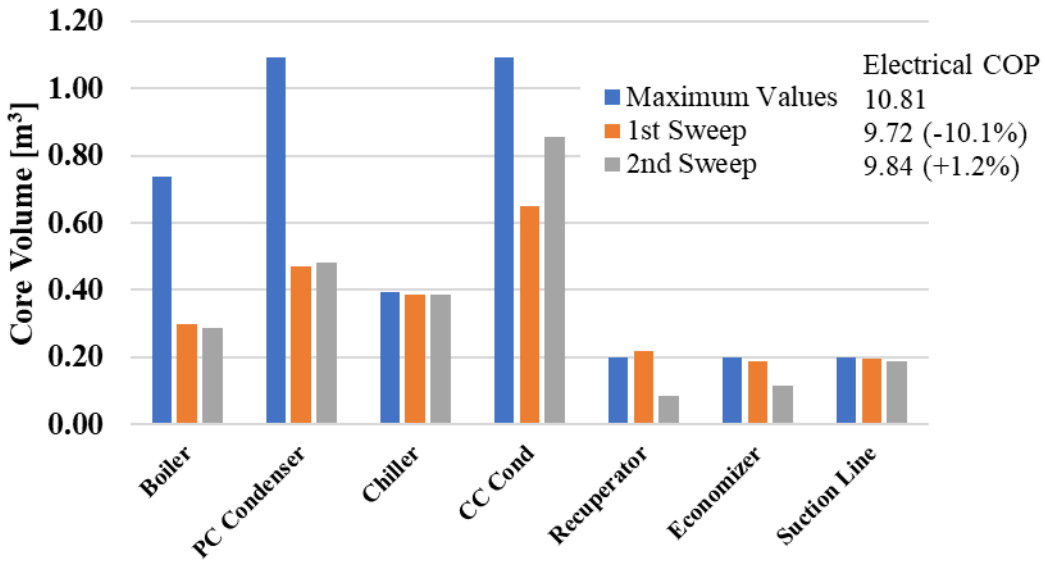

Figure 4-4: Heat exchanger core volumes and electrical COP

The resulting values from the second parametric sweep were used as the final heat exchanger sizes. Additional parametric passes could be conducted but marginal improvements would be expected. Also, any additional adjustments to the size of the heat exchangers could be made after solid modeling the complete system. The optimized system produced 72.4 kW of mechanical turbine work, while consuming 17.7 kW_e in the power cycle pump and 53.7 kW_e in the electric compressor. The resulting power cycle efficiency and cooling cycle COP were 7.31% and 5.64, respectively.

The unique hybrid operational mode of the power boosted TCCS requires the selection of a COTS electric compressor capable of operating in series with the turbo-compressor and must be capable of operating over a range of saturation pressures and flow rates. The Danfoss Turbocor TTS700, rated at 130 to 200 tons of cooling, was selected because it is oil-free and has an integrated variable speed drive for turn-down. The compressor is expected to operate over a range of inlet and outlet pressures which are dependent on seawater temperature and waste heat availability. Figure 4-5 shows the operational envelope of the Danfoss compressor.

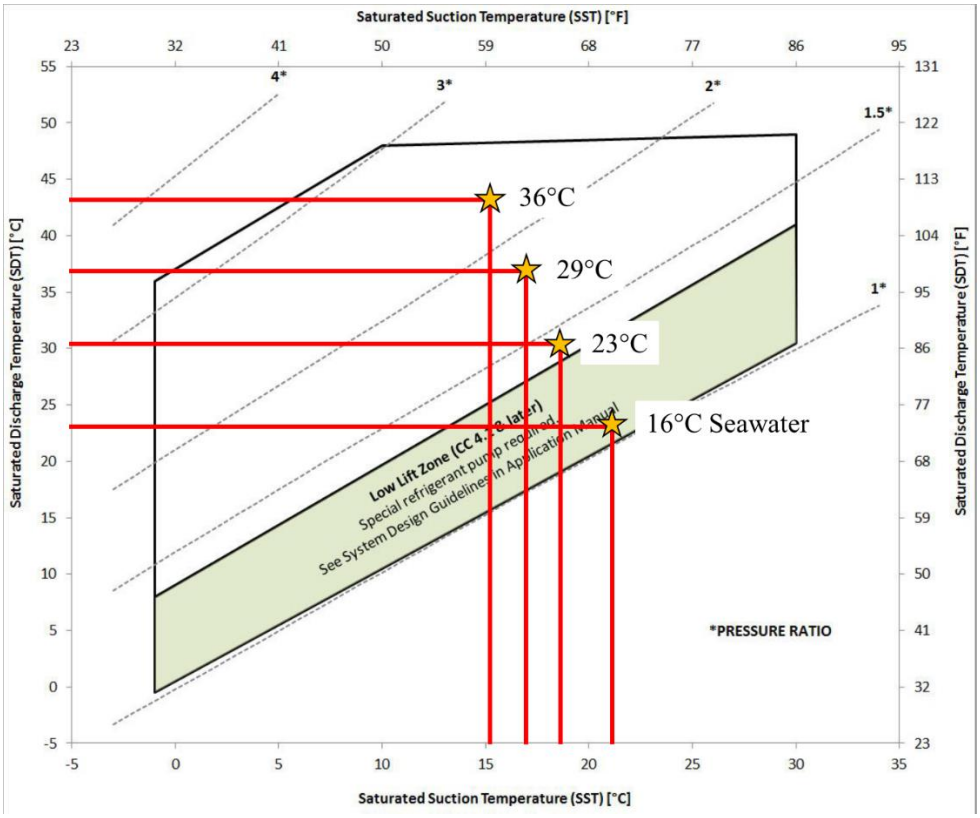

Figure 4-5: Operating envelope of a Danfoss TTS700 and state points of the optimized system at 50% engine load

Operation within the black outlined box represents safe operation, and within the green shaded region is the low-life operating zone. When functioning in the low-lift zone, subcooled refrigerant must be supplied at a flow-rate of 0.06 kg s^{-1} to cool the compressor. Table 4-7 lists the electric compressor operating conditions over the entire range of seawater and engine load

conditions using the optimized heat exchanger sizes found above. At low seawater temperatures and high engine loads, the compressor operated in the low-lift zone, indicated by yellow cells. When the turbo-compressor can provide the entire required compression for 200-tons of cooling, the electric compressor was turned off, indicated by the red cells. Overall, the compressor can be safely operated over the range of studied conditions.

Table 4-7: Danfoss compressor operation

Seawater Condenser Temperature		36°C	29°C	23°C	16°C	10°C
85%	Compressor Work [kW_e]	92.1	53.6	23.1	0.0	0.0
	Sat. Suction T [°C]	18.3	21.2	23.7	23.6	17.7
	Sat. Discharge T [°C]	43.5	36.5	30.6	23.6	17.7
	Suction Pressure [kPa]	543	594	640	639	533
	Discharge Pressure [kPa]	1116	925	783	639	533
75%	Compressor Work [kW_e]	95.5	57.7	27.7	0.0	0.0
	Sat. Suction T [°C]	17.5	20.1	22.4	23.6	17.7
	Sat. Discharge T [°C]	43.5	36.5	30.6	23.6	17.7
	Suction Pressure [kPa]	529	574	616	639	533
	Discharge Pressure [kPa]	1116	925	783	639	533
50%	Compressor Work [kW_e]	104.3	68.1	39.4	8.2	0.0
	Sat. Suction T [°C]	15.3	17.3	19.1	21.1	17.7
	Sat. Discharge T [°C]	43.5	36.5	30.6	23.6	17.7
	Suction Pressure [kPa]	493	526	555	592	533
	Discharge Pressure [kPa]	1115	925	783	639	533
25%	Compressor Work [kW_e]	113.8	79.2	51.8	22.0	0.0
	Sat. Suction T [°C]	12.9	14.4	15.6	17.1	17.7
	Sat. Discharge T [°C]	43.5	36.5	30.6	23.6	17.7
	Suction Pressure [kPa]	457	479	498	522	533
	Discharge Pressure [kPa]	1115	925	783	639	533

Normal Operation
Low-Lift Zone
Not Operating

After the heat exchangers and pipes were sized and the turbomachinery components were selected, a 3D solid model of the system was created using SolidWorks to provide a visual representation of the system and ensure that the equipment fits within the dimensions of a commercial chiller. Figure 4-6 displays two isometric views of the solid model with all major components labeled. Grey pipes connect internal components, while red, blue, and green pipes circulate hot water, chilled water, and seawater, respectively. It is important to note that this is a preliminary design and does not include valves, electronics, cooling lines, or other auxiliary equipment. The system was modeled to fit within a 3.4 meter long, 1.1 meter wide, and 2.0 meter tall container. The three gasketed plate and frame heat exchangers are bolted to the ground because

they are the largest and heaviest equipment in the system. The heat exchangers were piped so that refrigerant flows downwards in the condensers and upwards in the evaporator. The power cycle refrigerant pump was also bolted to the ground to ensure that it has sufficient suction head to avoid cavitation issues. The recuperative heat exchanger was placed directly above the pump to minimize the piping route between the two components. The two evaporator cores and the suction line heat exchanger were placed on a platform above the boiler and recuperator. The economizer, turbo-compressor, and electric compressor were located in the middle of the system to allow for simple piping route to components in both sub cycles.

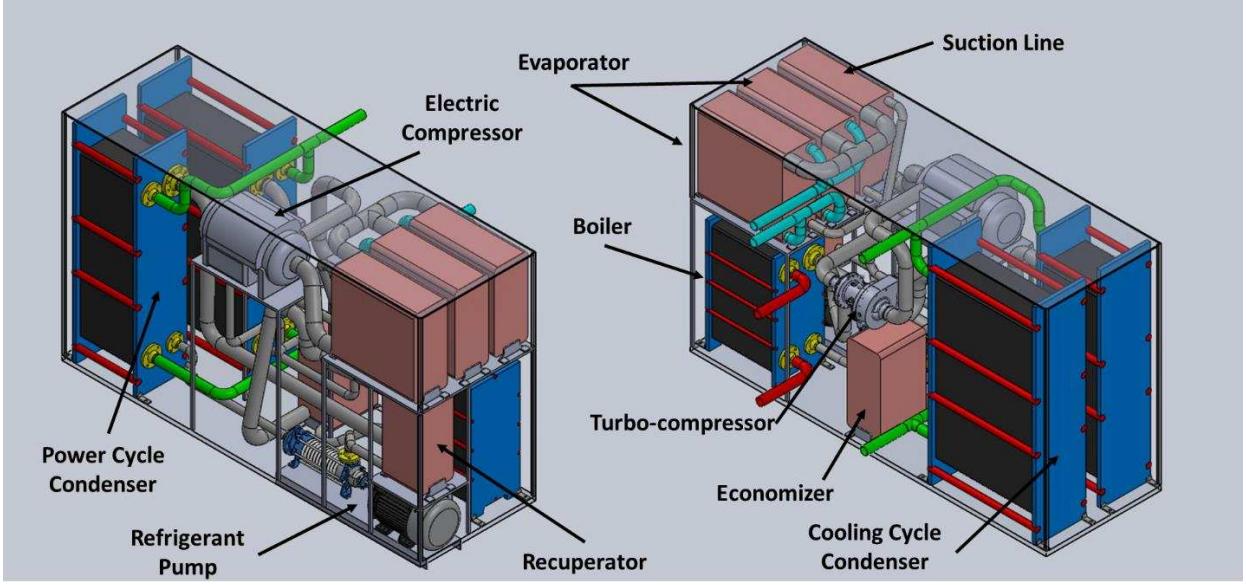

Figure 4-6: Solid model of the volume-optimized TCCS

4.3. Performance Modeling

Two modes of operation were studied for the power boosted TCCS (Option 3): power density improvement (fixed generator set electricity output) and fuel savings (engine load reduced by the TCCS). For the final performance modeling, heat exchanger and pipe geometries were fixed based on the optimization results. This removed seven previously fixed effectiveness values from the thermodynamic model. Power density improvement was defined as the power reduction

divided by the engine load and weighted seawater temperature results per engine load are shown in Table 4-8. The power density improvement ranged from 5.2% at 85% engine load to 14.6% at 25% engine load. The power density improvement increases at lower engine loads because the cooling electricity accounts for a larger portion of the engine's electricity output. The power density improvement at each engine load was then multiplied by a weighted factor and summed to determine an annual average improvement of 11.0%. This value represents the average amount of electricity that was offset by the TCCS which can be used for other purposes.

Table 4-8: Power density improvement results per engine load

Engine Load [%]	**85%**	**75%**	**50%**	**25%**
Engine Load [kW_e]	2210	1950	1300	650
VCC Electricity [kW_e]	167.8	167.8	167.8	167.8
TCCS Electricity [kW_e]	53.3	56.2	64.1	73.0
Power Reduction [kW_e]	114.5	111.6	103.8	94.9
Power Density Improvement [%]	5.2%	5.7%	8.0%	14.6%

The fixed geometry model was compared to the fixed-effectiveness thermodynamic model previously discussed. The thermodynamic model was updated to use the effectiveness values found during the heat exchanger sizing optimization, shown in Table 4-9, and both models were run over the entire seawater and engine load profile.

Table 4-9: Fixed heat exchanger effectiveness values for performance model comparison

Heat Exchanger	Heat Exchanger Section		
	Subcooled	Two-Phase	Superheat
Waste Heat Boiler	0.70		0.60
PC Condenser	1°C Subcool	0.67	
Evaporator	-	0.75	0.1
CC Condenser	1°C Subcool	0.82	
Recuperator	0.65		
Economizer	0.73		
Suction Line	0.77		

Heat Exchanger Model Calculated Values
Assumed Fixed Values
Non-Fixed Values (Floating)

As seen in Figure 4-7 (a), the sub cycle performances of both methods were very similar over the range of seawater conditions when at 85% engine load. However, at low seawater temperatures the fixed geometry model had a slightly higher ORC efficiency than the fixed effectiveness model. At 10°C, the fixed geometry model calculated an ORC efficiency of 10.34%, compared to 9.75% with the fixed effectiveness model. This was because the heat exchangers were designed for operation at 29°C seawater conditions. As the seawater temperature was reduced, the performance of the sub cycle improved, and the mass flow rate decreased. The reduction in mass flow rate resulted in the fixed geometry heat exchangers being oversized at low-temperature conditions. This can be seen in Figure 4-7 (b), which shows the effectiveness values of the heat exchangers over the same range of seawater temperatures. The cooling cycle heat exchanger effectiveness values remained constant because the electric compressor held heat duties and flow rates steady. The power cycle heat exchanger effectiveness values fall below design values when the temperature increases above the design point (29°C) but increase at low seawater temperature conditions.

The change in effectiveness values in the power cycle was largely because of a change in power cycle flow rate. The power cycle mass flow rate was 5.06 kg s^{-1} at 36°C, 4.52 kg s^{-1} at 29°C, 3.84 kg s^{-1} at 18°C, and was 2.15 kg s^{-1} at 10°C for the fixed geometry model. The rate in which the power cycle flow rate changed was higher at seawater temperatures below 18°C because the system provided the entire cooling load from the thermally driven turbo-compressor and the jacket water heat duty was decreased to maintain 200-tons of cooling. The power cycle boiler superheat region experienced the largest change in heat exchanger effectiveness and ranged from 0.43 at 36°C to 0.91 at 10°C. This was the only phase change heat exchanger in which the superheat region was optimized instead of the two-phase region. It was found during modeling that fixing the power cycle boiler two-phase effectiveness in addition to the hot water flow and inlet/outlet temperatures caused drastic swings in superheat or subcooled effectiveness values. At certain conditions the fluid entered or exited the heat exchanger as a two-phase fluid. To avoid this issue, it was desirable to set a fixed value for both the subcooled and superheat regions and maintain the hot water conditions. Increasing the amount of superheat at the boiler outlet increases the enthalpy of the refrigerant and thus more power is produced in the turbine. However, this benefit was counteracted by the large reduction in mass flow rate at lower seawater temperatures. In the fixed effectiveness model, the boiler superheat effectiveness was set at 0.6 but the mass flow rate was slightly higher which resulted in the two models producing similar results.

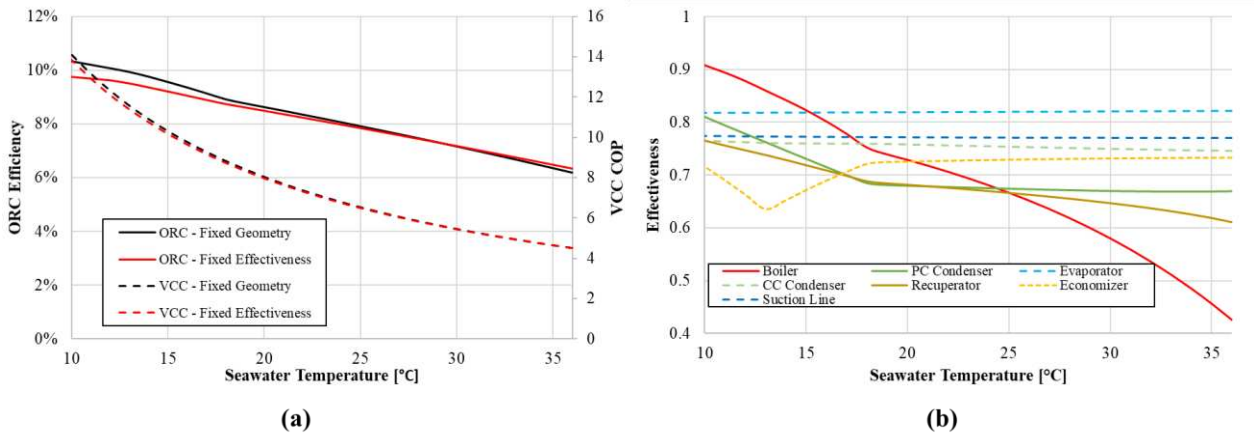

Figure 4-7: (a) Sub cycle performance method comparison vs. seawater temperature (b) Fixed geometry method heat exchanger effectiveness vs. seawater temperature

The overall impact of the variability of heat exchanger effectiveness values is shown in Table 4-10. The weighted average power density improvement of the fixed geometry and fixed effectiveness methods were 11.0% and 10.9%, respectively. Since the majority of the time was spent at seawater temperatures and engine load conditions below design point, the fixed effectiveness method slightly underpredicted performance. However, this difference is minor and gives confidence that fixing effectiveness values was an appropriate method in comparing configurations and fluids over the range of conditions. It is expected that the differences between the two methods would be enlarged if the electric compressor was not used to stabilize the cooling cycle. In general, it is suggested that the fixed effectiveness method is used to quickly compare options at similar conditions, but that the fixed heat exchanger model method is used for increased accuracy at off-design conditions.

Table 4-10: Weighted average power density improvement for fixed geometry and fixed effectiveness modeling methods

Method	η_{PC}	COP_{CC}	COP_{Elec}	W_{pump} [kW]	$W_{turbine}$ [kW]	$W_{elec,comp}$ [kW]	Power Reduction [kW]	Power Density Improvement
Fixed Geometry	8.43%	6.71	13.76	12.2	55.4	55.0	100.6	11.0%
Fixed Effectiveness	8.17%	6.68	13.01	12.6	54.5	56.1	99.1	10.9%

If the cooling electricity offset by the TCCS is not used elsewhere, then the engine load must decrease to accommodate the reduced demand. The decreased engine load results in fuel savings and diminished heat availability. Table 4-11 displays the operational profile and fuel consumption of a singular generator set when using an electric chiller to provide 200-tons of cooling and when using the power boosted TCCS. The fuel consumption at each engine loading condition is summed to find the total annual fuel consumption for the engine. The use of the TCCS reduced fuel consumption by 92.1 mt yr^{-1}, from 962.3 mt yr^{-1} to 870.2 mt yr^{-1}, which was a 9.6% reduction in annual fuel use.

Table 4-11: Annual fuel consumption reduction

Cooling System:	**Legacy Electrically Driven Chiller**				
Engine Load [%]	**85%**	**75%**	**50%**	**25%**	**Total**
Engine Load [kW_e]	2210	1950	1300	650	
Fuel Mass Flow Rate [kg s^{-1}]	0.135	0.121	0.081	0.041	
Annual Operating Hours	302	313	1283	2056	3954
Fuel Consumption [mt yr^{-1}]	146.7	136.9	375.9	302.8	**962.3**
Cooling System:	**Power-Boosted TCCS**				
Engine Load [%]	**80.5%**	**70.6%**	**45.9%**	**21.2%**	**Total**
Engine Load [kW_e]	2093	1836	1193	552	
Fuel Mass Flow Rate [kg s^{-1}]	0.128	0.114	0.075	0.035	
Annual Operating Hours	302	313	1283	2056	3954
Fuel Consumption [mt yr^{-1}]	138.9	128.8	345.1	257.3	**870.2**

4.4. Economic Modeling

Individual component costs were estimated using a combination of quoted values and correlations. The total system was estimated to cost $295,036 in equipment ($419 kW_{th}^{-1}, $1474 ton^{-1}), and $147,518 for construction and installation, for a total installed cost of $442,554 ($629 kW_{th}^{-1}, $2,212 ton^{-1}). The breakdown of costs is shown in Figure 4-8. The cooling cycle condenser was the most expensive component, $53,799, because it was the largest heat exchanger and required titanium plates. It was found that using titanium plates in the condensers increased the total system equipment costs by 13.7%. The second most expensive component was the electric compressor at $46,696. In some land-based applications, such as exhaust gas heat recovery in CCHP, there may be sufficient heat to provide the total amount of required cooling using only the turbo-compressor. However, for shipboard applications the electric compressor is a necessary component to provide a consistent amount of cooling with highly transient engine operation. Even with the added electric compressor cost, the heat exchangers accounted for 67% of the total equipment cost while turbomachinery, including the turbo-compressor, electric compressor, and pump, accounted for 24%. Remaining equipment, such as piping and instrumentation, only accounted for 9% of system costs.

State-of-the-art system costs were estimated for comparison. To predict these systems costs, equipment costs were increased by 13.7% to account for titanium condensers. This value is very conservative for centrifugal and absorption chillers because the condenser accounts for a larger percentage of total costs than with the TCCS, which has several additional components. The installed cost of a 200-ton shipboard centrifugal chiller was estimated to be $113,700 ($568 ton^{-1}) while a 144-ton shipboard single stage absorption chiller was estimated to cost $630,924 ($4,394 ton^{-1}). It was also estimated that the absorption chiller would save 75.8 mt yr^{-1} of fuel annually by

providing supplemental cooling to offset the electric compressor load of a centrifugal chiller. Since the absorption chiller would be unable to provide a constant 200-tons of cooling, it would need to operate in parallel with an electric centrifugal chiller, similar to the Option 1 TCCS discussed previously. In addition, the absorption chiller had a volume of 645 ft^3 compared to the allowed space of 267 ft^3, making it impossible to be implemented in a space constrained ship.

Component	Cost
Electric Compressor	$46,696
Turbo-Compressor	$6,336
PC Pump	$17,710
PC Boiler	$24,861
PC Condenser	$39,597
CC Evaporator	$34,229
CC Condenser	$53,799
Recuperator	$13,268
Economizer	$15,745
Suction Line	$14,995
Piping/Fittings	$6,037
Refrigerant	$4,588
Valves	$5,528
Instrumentation	$7,148
Chassis	$4,500
Equipment Total	**$295,036**
	$419 kW_{th}^{-1}
Installation Factor	0.5
Installation	$147,518
	$210 kW_{th}^{-1}
Total Installed Cost	**$442,554**
	$629 kW_{th}^{-1}

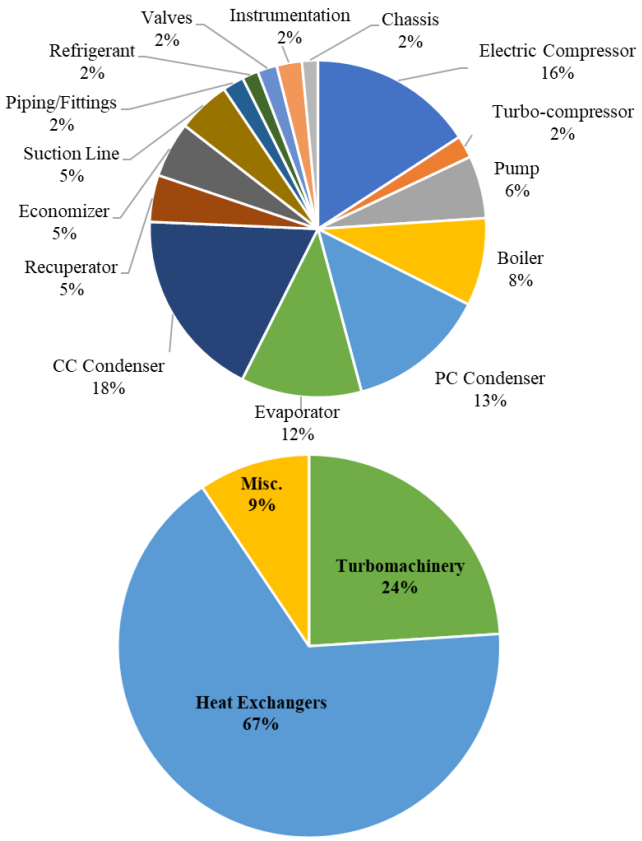

Figure 4-8: TCCS equipment and installation cost breakdown

Two scenarios were investigated using the economic model: retrofit projects and required installations. For a retrofit project, the TCCS was directly compared to the performance and cost of an absorption chiller. Payback period, net present value (NPV), and the internal rate of return (IRR) for the two systems are shown in Table 4-12. The TCCS had greater economic benefits because it had a lower initial investment cost while also saving more fuel per year than absorption.

The TCCS payback period was 5.77 years, compared to 9.61 years for absorption chillers. Further, the TCCS has a significantly higher IRR of 16% vs. 6.6% over the 15-year project period.

Table 4-12: Retrofit project economic results

System	Initial Costs	Annual Fuel Savings [mt yr^{-1}]	Payback Period [years]	NPV 15 Years	IRR 15 Years
Boosted TCCS	$442,554	92.1	5.77	$176,734	16%
Absorption	$630,924	75.8	9.61	$79,370	6.6%

For required installations, the cost of the baseline electric vapor compression chiller was subtracted from the cost of the TCCS, thus reducing the project costs by $113,700. This differential metric is appropriate for required installations because the baseline chiller represents the minimum investment cost for a cooling system on a ship. Therefore, the differential installation cost can be used to determine the economic viability of the TCCS as a new investment, shown in Table 4-13. The differential payback period is reduced to 4.4 years when considering the minimum investment costs, while the 15-year NPV and IRR increase to $287,926 and 23%, respectively. Absorption chillers do not have the ability to replace the electric chillers and would still require an additional chiller to meet peek cooling demands while at lower engine loads.

Table 4-13: New installation economic results vs. a retrofit project

System	Initial Costs	Annual Fuel Savings [mt yr^{-1}]	Payback Period [years]	NPV 15 Years	IRR 15 Years
Retrofit TCCS	$442,554	92.1	5.77	$176,734	16%
New Install TCCS	$328,854	92.1	4.37	$287,926	23%

Figure 4-9 displays the simple cumulative cash flows over a 15-year period for the retrofit TCCS, retrofit absorption chiller, and new installation TCCS. The respective lines start as negative values in year 0 which represents the initial installation costs of the project. The cumulative cash flow in subsequent years increases from the annual fuel savings of the systems. The horizontal red

line is the break-even point where the financial savings of the system equals the initial investment costs. The operational time it takes for the cumulative cash flow line to cross the break-even point is the payback period. The two TCCS curves have the same slope because the annual fuel savings and thus annual cash flow are the same. However, since the investment cost of the new installation was less, it reaches the break-even point first. The absorption chiller cash flow line is slightly less steep because the annual fuel savings are less. Overall, all projects result in positive cash flow at the end of the 15-year period, and are $821,470, $409,316, and $930,052 for the retrofit TCCS, absorption chiller, and new installation TCCS, respectively.

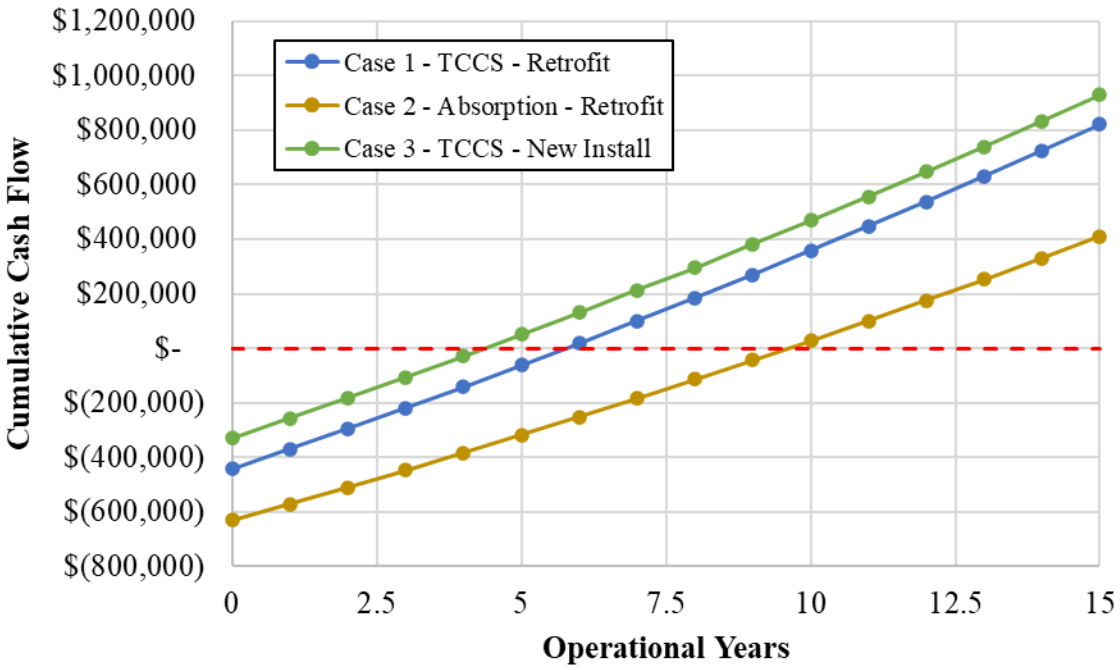

Figure 4-9: Simple cumulative cash flow diagram for the TCCS and absorption chiller

4.5. Sensitivity Analysis

A sensitivity analysis was performed on the economic model to determine what variables and assumptions had the highest impact on payback period. This was done by increasing or decreasing key variables by +/- 10% and observing the changes to payback period for the TCCS.

Results are displayed in a tornado plot in Figure 4-10. The key variables studied were diesel cost, annual fuel inflation percentage, installation factor, cost of the heat exchangers, cost of the turbomachinery, cost of miscellaneous equipment, and fuel savings per year.

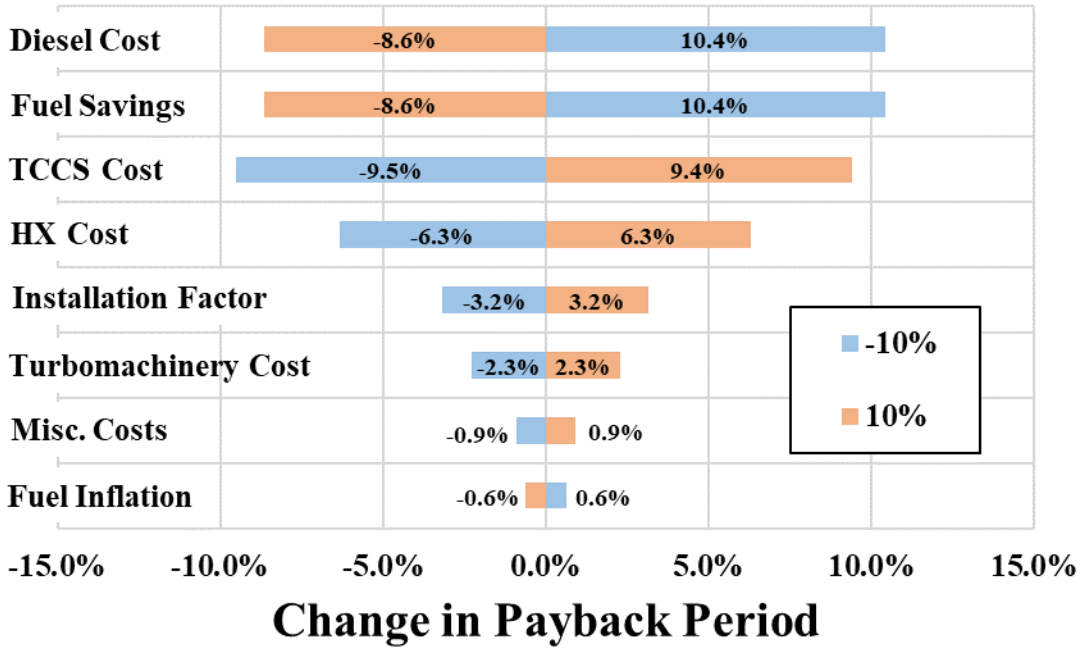

Figure 4-10: Sensitivity analysis on the payback period from the economic model

It was found that the payback period was most sensitive to reducing the cost of diesel fuel or annual fuel savings, which both increased the payback period by 10.4%. Decreasing or increasing the cost of the diesel fuel did not have equal impact in absolute percentage because of the annual fuel inflation factor built into the model. The second largest impact was increasing or decreasing the equipment cost of the TCCS. This was further broken down into the impact of adjusting heat exchanger, turbomachinery, or miscellaneous equipment costs. Since heat exchangers account for 67% of the total TCCS equipment cost, it had the largest impact on payback period of the three cost categories at +/- 6.3%. It was also seen that changing the installation factor was more impactful than the turbomachinery or miscellaneous costs. Annual fuel inflation

percentage and miscellaneous costs were least impactful and changed payback period by +/- 0.6% and 0.9%, respectively.

A sensitivity analysis was also performed on the heat exchanger sizing model to determine which effectiveness values had the highest impact on the electrical COP and heat exchanger core volume. For this analysis, the maximum plate count for each heat exchanger was not considered. The effectiveness value of each optimized heat exchanger was increased or decreased by 0.1 one at a time while the remaining 6 heat exchanger sizes were fixed by defining the number of plates. Figure 4-11 displays the impact of all seven heat exchangers on these two metrics. The orange bars represent the increase or decrease in total heat exchanger core volume, which is the sum of the core volumes of all seven heat exchangers, and the green bars represent the change in electrical COP. Changing the cooling cycle condenser two-phase effectiveness, which is the largest heat exchanger in the optimized system, had the greatest impact on the total heat exchanger volume at +27% or -14%, as expected. However, varying the evaporator two-phase heat exchanger effectiveness had a greater impact on the electrical COP of the system at +9% or -11%. The suction line heat exchanger had the second largest impact on performance when decreasing the size at -9% despite the small change in system volume. This emphasizes the need for a highly effect suction line heat exchanger. As the effectiveness of the suction line heat exchanger decreased, the heat transfer decreased and the pressure drop increased, which reduced both the evaporator and compressor performance. In general, it was seen that increasing the heat exchanger effectiveness values had a greater impact on total system volume compared to decreasing the effectiveness, while the opposite was true of the electrical COP. The recuperator, economizer, and superheated boiler region effectiveness values had the smallest impact on both system performance and sizing. These results are consistent with the outcomes of the heat exchanger optimization study in which

the sizes of the power cycle equipment were reduced to maintain high cooling cycle heat exchanger performance while fitting within the volume constraints. In addition, it was expected that heat exchangers with higher starting effectiveness values would experience larger swings in performance or volumes as the effectiveness values were changed. When a heat exchanger effectiveness approaches 1, dramatic increases to heat exchanger sizes are required. Therefore, reasonable heat exchanger sizes are typically experienced between effectiveness values of 0.6 to 0.8.

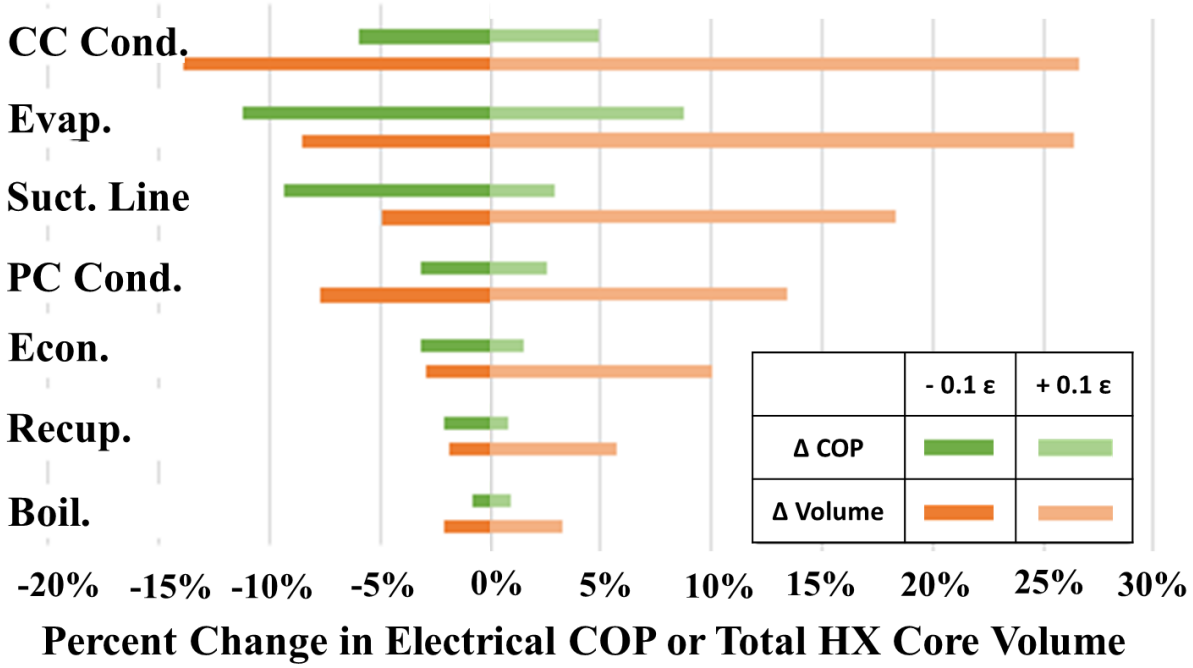

Figure 4-11: Sensitivity analysis on the heat exchanger core volume and electrical COP from the heat exchanger sizing model

CHAPTER 5 Conclusions

The present work evaluated and designed a thermally driven cooling system that was suitable for shipboard applications. Waste heat recovery technologies can save on fuel costs and address increased electricity and cooling demands on ships. Main propulsion engines and shipboard service diesel generator sets are typically less than 50% efficient and are highly variable with potential turndown below 25% of the engines rated power. The state-of-the-art thermally driven cooling systems require the use of an electric chiller for peak cooling at low waste heat availability conditions and are too large to be used on a ship due to the extremely limited space in the engine and mechanical rooms. This study focused on modeling the performance and size of a thermally driven cooling system that could fit within the volume of a commercially available electrical chiller and operate using low-grade waste heat from the diesel generator set's jacket water and lubrication oil.

A case study of a marine diesel generator set co-located with an electric chiller was presented in this study. The ship's auxiliary electricity is produced by a 2.6 MW shipboard diesel generator set and cooling was provided by a 200-ton seawater cooled electric centrifugal chiller. The engine loading profile was provided by the US Navy for a singular engine on a T-AKE Lewis and Clark class dry cargo chip which operated from 25% to 85% load for 3,954 hours a year. It was assumed that the ship required at least 200-tons of cooling over the entire 3,954 hours of operation. A representative annual seawater temperature profile for T-AKE class ships was also provided and utilized to complete the operational profile.

The thermally driven cooling system used in this study is the turbo-compression cooling system. The TCCS combines the use of a waste heat driven organic Rankine cycle (ORC) with a

vapor compression cooling cycle (VCC). The turbine in the ORC shares a common shaft with the compressor in the VCC to transfer power and deliver cooling in an evaporator. Included in the TCCS used in this study was three heat recuperation heat exchangers: a power cycle recuperator, a cross cycle economizer, and a cooling cycle suction line heat exchanger. The use of recuperative heat exchangers increases system performance and reliability, but also increases the number of components and complexity.

A multi-step modeling process was used to evaluate and design the TCCS for the case study ship. First, a thermodynamic model was developed to evaluate the performance of three TCCS configuration options operating with five different fluids: R134a, R1234ze(E), R1234yf, R245fa, and R515a. Option 1 was to provide supplemental chilled water to offset the load on the baseline chiller, Option 2 was to cool seawater used in the condenser of the baseline chiller to increase performance, and Option 3 was to add an electric compressor to the TCCS to provide the entire 200-tons of cooling. Heat exchangers were divided into sections based on the fluid's phase, and heat exchanger effectiveness values and turbomachinery efficiencies were assumed to be constant.

The power boosted TCCS, Option 3, operating with R134a was further designed using plate and frame heat exchanger models. The goal of the heat exchanger sizing process was to design a system that would be no larger than a commercial water-cooled centrifugal chiller of the same cooling capacity. Heat exchanger sizes were found by assuming that the heat exchanger core volume could be no larger than 32% of the total system volume. The combination of heat exchanger effectiveness values which resulted in the highest performing system while remaining within the allowed volume was chosen and pipes were sized. Heat exchanger and pipe geometries were then set constant to replace heat exchanger effectiveness values and the model was run over

the range of seawater and engine loading conditions to determine the yearly average power density improvement and fuel savings. An economic model was used to estimate the system equipment cost using correlations from literature and quoted values, and included heat exchangers, turbomachinery, and miscellaneous components. Based on the fuel savings results, the project payback period, net present value, and internal rate of return were calculated for a retrofit project and new installation and compared to a state-of-the-art absorption chiller.

Results from the initial thermodynamic model were that Option 1 reduced power consumption for 200-tons of cooling by up to 72 kW_e, Option 2 reduced power by up to 20 kW_e, and Option 3 reduced power consumption by up to 104 kW_e. Results were based on weighted averages over the entire range of engine loads and seawater temperatures. The highest performing fluids for Options 1 and 3 were R1234ze(E), R515a, and R134a which all had very similar power reduction. R1234ze(E) may be favorable for a land-based system because of its low GWP, but it is slightly flammability which may be a concern on ships. However, the system was designed using R134a due to its high performance, existing use in SOA chillers, and the abundance of heat transfer correlations available.

The volume optimized power boosted TCCS operating with R134a had an electric COP of 9.84 at the design conditions and saved 92.1 mt yr^{-1} of fuel, resulting in financial savings greater than $72,000 per year. The system was solid modeled to demonstrate the ability of the major components and piping to fit within the volume of a commercial chiller. The designed system was estimated to cost $295,036 in equipment and $147,518 for construction and installation, for a total installed cost of $442,554. Based on the fuel savings calculated, 2% annual fuel inflation, and a 10% discount rate for NPV calculations, the project payback period was 5.77 years and the 15-year NPV and IRR were $176,734 and 16.2%, respectively. For comparison purposes, a

commercial absorption chiller was also modeled and was estimated to have an installed cost of $630,924, payback period of 9.61 years, and have 15-year NPV and IRRs of $79,370 and 6.6%, respectively. For new installation projects, the required cost of an electric chiller, $113,700, was subtracted from the initial capital cost because the TCCS would completely replace the need for an electric chiller. The resulting differential payback period, NPV, and IRR were 4.37 years, $287,926, and 23%, respectively.

In summary, this study presented a design methodology which included evaluating different system configurations and fluids over range of operational conditions, sizing heat exchangers based on volume constrains, and estimating performance of the designed system using a fixed geometry model to determine the annual fuel savings of the system. The outcome of the study was a solid model, performance model, and economic model of a 200-ton power boosted TCCS which can be a drop-in replacement of shipboard centrifugal chillers and provide fuel savings of 92 mt yr^{-1} with favorable economic benefits.

5.1. Recommendations for Further Work

The present study introduced a preliminary design approach for evaluating system configurations and fluids for performance and optimizing heat exchanger sizes to meet volume constraints of shipboard cooling systems. The following items are recommendations for future work to lead the technology to commercialization and implementation in the field:

- Further development of the duel compressor configuration is necessary. This includes the development of a controls strategy for turning on and off compressors, controlling turndown, and providing steady cooling output. Different compressor configurations should also be investigated. It may be more desirable to operate the compressors in parallel

during some operational conditions, or it may be appropriate to place the electric compressor before the turbo-compressor. These configurations should be tested in an experimental lab setup.

- Experimental heat exchanger model validation should be conducted over the range of conditions. It may be found that the heat transfer correlations are more appropriate at design conditions but are less accurate at lower flow rates or temperatures. In addition, more heat exchanger types should be investigated, and models developed. For some applications it may be more appropriate to use traditional shell and tube heat exchangers or custom bar-plate heat exchangers.
- Technoeconomic analysis should be performed on the different components. Specifically, the tradeoff between added cost and complexity from recuperative heat exchangers to the increased sub cycle performance should be investigated. In addition, some applications may be less sized constraint and the electric compressor may not be necessary for retrofit projects. The potential markets for the different configurations should be quantified to help inform initial commercialization efforts.
- Prediction of off-design turbo-compressor performance within the model would help better inform the controls strategy for the duel compressor configuration. This was outside the scope of this study because turbomachinery modeling requires knowledge of the turbine and compressor maps for a specific machine. A turbo-compressor for the 200-ton system presented in this study has not been development.

REFERENCES

[1] United Nations, "World population projected to reach 9.8 billion in 2050, and 11.2 billion in 2100," 21 June 2017. [Online]. Available: https://www.un.org/development/desa/en/news/population/world-population-prospects-2017.html.

[2] U.S. Energy Information Administration, "EIA projects nearly 50% increase in world energy usage by 2050, led by growth in Asia," 24 September 2019. [Online]. Available: https://www.eia.gov/todayinenergy/detail.php?id=41433.

[3] NASA, "The Effects of Climate Change," [Online]. Available: https://climate.nasa.gov/effects/#:~:text=The%20Intergovernmental%20Panel%20on%20Climate,Fahrenheit%20over%20the%20next%20century.

[4] Lawrence Livermore National Laboratory, "Energy Flow Charts," 2019. [Online]. Available: https://flowcharts.llnl.gov/.

[5] International Maritime Organization (IMO), "Third IMO Greenhouse Gas Study 2014," 2014.

[6] DNV GL, "Maritime Energy Management Study 2015," 2015.

[7] S. Wang, S. Gao, T. Tan and W. Yang, "Bunker fuel cost and freight revenue optimization for a single liner shipping service," *Computers & Operations Research,* vol. 111, pp. 67-83, 2019.

[8] T. E. Notteboom, "The Time Factor in Liner Shipping Services," *Maritime Economics & Logistics,* vol. 8, pp. 19-39, 2006.

[9] M. M. Golias, G. K. Saharidis, M. Boile, S. Theofanis and M. G. Leperpetritou, "The berth allocation problem: optimizing vessel arrival time," *Maritime Economics & Logistics,* vol. 11, no. 4, pp. 358-377, 2009.

[10] D. Ronen, "The effect of oil price on containership speed and fleet size," *Journal of the Operational Research Society,* vol. 62, no. 1, pp. 211-216, 2011.

[11] R. Adland, C. P, H. Jia and F. Walff, "The energy efficiency effects of periodic ship hull cleaning," *Journal of Cleaner Production,* vol. 178, pp. 1-13, 2018.

[12] CE Delft, The ICCT, and Mikis Tsimplis, "Regulated Slow Steaming in Maritime Transport: An Assesment of Options, Costs and Benefits," Seas At Risk and T&E, 2012.

[13] L. H. Liang, "The economics of slow steaming," 07 October 2014. [Online]. Available: https://www.seatrade-maritime.com/americas/economics-slow-steaming.

[14] S. L. Nadaf and P. B. Gangavati, "A review on waste heat recovery and utilization from diesel engines," *International Journal of Advanced Engineering Technology,* vol. 5, no. 4, pp. 31-39, 2014.

[15] K. Senary, A. Tawfik, E. Hegazy and A. Ali, "Development of a waste heat recovery system onboard LNG carrier to meet IMO regulations," *Alexandria Engineering Journal,* vol. 55, no. 3, pp. 1951-1960, 2016.

[16] *C280-8 Auxiliary and Diesel Electric Propulsion Specifications and Performance Data.*

[17] Q. Xin, "Durability and reliability in diesel engine system design," Woodhead Publishing, 2013.

[18] B. Sunden, "High Temperature Heat Exchangers (HTHE)," in *Fifth International Conference on Ehanced, Compact and Ultra-Compact Heat Exchangers: Science, Engineering and Technology*, Hoboken, 2005.

[19] J. K. Min, J. H. Jeong, M. Y. Ha and K. S. Kim, "High temperature heat exchanger studies for applications to gas turbines," *Heat and Mass Transfer,* vol. 46, pp. 175-186, 2009.

[20] C. Michos, S. Lion, I. Vlaskos and R. Taccani, "Analysis of the backpressure effect of an Organic Rankine Cycle (ORC) evaporator on the exhaust line of a turbocharged heavy duty diesel power generator for marine applications," *Energy Conversion and Management,* vol. 132, pp. 347-360, 2017.

[21] H. Sapra, M. Godjevac, K. Visser, D. Stapersma and C. and Dijkstra, "Experimental and simulation-based investigations of marine diesel engine performance against static back pressure," *Applied Energy,* vol. 204, pp. 79-92, 2017.

[22] T. Cao, H. Lee, Y. Hwang, R. Radermacher and H. Chun, "Modeling of waste heat powered energy system for container ships," *Energy,* vol. 106, pp. 408-421, 2016.

[23] R. Wang, L. Jiang, Z. Ma, A. Gonzalez-Diaz and Y. Wang, "Comparative Analysis of Small-Scale Organic Rankine Cycle Systems for Solar Energy Utilisation," *Energies,* vol. 12, no. 5, p. 829, 2019.

[24] Trane Technologies, "Absorption Liquid Chillers," [Online]. Available: https://www.trane.com/commercial/asia-pacific/ph/en/products-systems/equipment/chillers/absorption-liquid-chillers.html.

[25] Carrier, "Absorption Chillers," [Online]. Available: https://www.carrier.com/commercial/en/eu/products/air-conditioning/absorption-chillers/.

[26] York, "Absorption Chillers," [Online]. Available: https://www.york.com/commercial-equipment/chilled-water-systems/absorption-chillers.

[27] A. Gonzalez-Gil, M. Izquierdo, J. D. Marcos and E. Palacios, "Experimental evaluation of direct air-cooled lithium bromide-water absorption prototype for solar air conditioning," *Applied Thermal Engineering,* vol. 31, pp. 3358-3368, 2011.

[28] S. C. Kaushik and A. Arora, "Energy and exergy analysis of single effect and series flow double effect water-lithium bromide absorption refrigeration systems," *International Journal of Refrigeration,* vol. 32, no. 6, pp. 1247-1258, 2009.

[29] A. Hamed, S. A. Kaseb and A. S. Hanafi, "Prediction of energetic and exergetic performance of double-effect absorption system," *International Journal of Hydrogen Energy,* vol. 40, pp. 15320-15327, 2015.

[30] M. B. Arun, M. P. Mauya and S. S. Murthy, "Performance comparision of double-effect parallel-flow and series flow water-lithium bromide absorption systems," *Applied Thermal Engineering,* vol. 21, pp. 1273-1279, 2001.

[31] P. Srikhirin, S. Aphornratana and S. Chungpaibulpatana, "A review of absorption technologies," *Renewable and Sustainable Energy Reviews,* vol. 5, pp. 343-372, 2001.

[32] A. Shirazi, R. A. Taylor, S. D. White and G. L. Morrison, "A systematic parametric study and feasibility assessment of solar-assisted single-effect, double-effect, and triple-effect absorption chillers for heating and cooling applications," *Energy Conversion and Management,* vol. 114, pp. 258-277, 2016.

[33] G. A. Florides, S. A. Kalogirou, S. A. Tassou and L. C. Wrobel, "Design and construction of a LiBr-water absorption machine," *Energy Conversion and Management,* vol. 44, pp. 2483-2508, 2003.

[34] A. Brotzu, F. Felli, S. Natali and D. Pilone, "Pipeline corrosion failure in an absorption chiller," *Procedia Engineering,* vol. 109, pp. 43-54, 2015.

[35] U.S. Department of Health and Human Services, "Toxicological Profile for Ammonia," 2004.

[36] M. Khamooshi, K. Parham and U. Atikol, "Overview of Ionic Liquids Used as Working Fluids in Absorption Cycles".

[37] G. Foley, R. DeVault and R. Sweetser, "The Future of Absorption Technology in America: A Critical Look at the Impact of BCHP and Innovation," in *Advanced Building Systems*, 2000.

[38] Frost & Sullivan, "North American Absorption Chillers Market," 2008.

[39] Frost & Sullivan, "Analysis of the Global HVAC Equipment Market," 2014.

[40] U.S. Energy Information Administration, "Updated Building Sector Appliance and Equipment Costs and Efficiencies," 2018.

[41] U.S. Department of Energy (DOE), "Combined Heat and Power Fact Sheet, Absorption Chillers for CHP Systems," 2017.

[42] AIDA, "Innovative technology," 2017. [Online]. Available: https://www.aida.de/en/aida-cruises/responsibility/aida-cares-2017/environment/innovative-technology.34564.html.

[43] Heinen & Hopman, 2017. [Online]. Available: https://heinenhopman.com/heinen-and-hopman/pdfs-gecomprimeerd/hh-maritime-absorption-chiller.pdf.

[44] Gadcooler, 2016. [Online]. Available: http://www.gadlab.fi/wp-content/uploads/2016/09/Gadcooler_BROCHURE_2016.pdf.

[45] A. Hafner, C. H. Cabrielii and K. Widell, "Refrigeration Units in Marine Vessels: Alternatives to HCFCs and High GWP HFCs," Nordic Council of Ministers, 2018.

[46] A. Ouadha and Y. El-Gotni, "Integration of an ammonia-water absorption system with a marine Diesel engine: A thermodynamic study," *Procedia Computer Science,* vol. 19, pp. 754-761, 2013.

[47] N. R. Ammar and I. S. Seddiek, "Thermodynamic, environmental and economic analysis of absorption air conditioning unit for emissions reduction onboard passenger ships," *Transportation Research Part D,* vol. 62, pp. 726-738, 2018.

[48] T. Cao, H. Lee, Y. Hwang, R. Radermacher and H. Chun, "Performance investigation of engine waste heat powererd absorption cycle cooling system for shipboard applicatins," *Applied Thermal Engineering,* vol. 90, pp. 820-830, 2015.

[49] Y. Liang, G. Shu, H. Tian, H. Wei, X. Liang, L. Liu and X. Wang, "Theoretical analysis of a novel electricity-cooling cogeneration system (ECCS) based on cascade use of waste heat of marine engine," *Energy Conversion and Management,* vol. 85, pp. 888-894, 2014.

[50] Y. Liang, G. Shu, H. Tian and Z. Sun, "Investigation of a cascade waste heat recovery system based on coupling of steam Rankine cycle and NH3-H2O absorption refrigeration cycle," *Energy Conversion and Management,* vol. 166, pp. 697-703, 2018.

[51] W. Salmi, J. Vanttola, M. Elg, M. Kuosa and R. Lahdelma, "Using waste heat of ship as energy source for an absorption refrigeration system," *Applied Thermal Engineering,* vol. 115, pp. 501-516, 2017.

[52] Bry-Air, "Adsorption Chiller," [Online]. Available: https://www.bryair.com/products-solutions/adsorption-chillers/adsorption-chiller/.

[53] M. B. Elsheniti, O. A. Elsamni, R. K. Al-dadah, S. Mahmoud, E. Elsayed and K. Saleh, "Adsorption Refrigeration Technologies," in *Sustainable Air Conditioning Systems*, IntechOpen, 2018, pp. 71-95.

[54] Q. Pan, J. Peng and R. Wang, "Experimental study of an adsorption chiller for extra low temperature waste heat utilization," *Applied Thermal Engineering,* vol. 163, p. 114341, 2019.

[55] H. T. Chua, K. C. Ng, A. Malek, T. Kashiwagi, A. Akisawa and B. B. Saha, "Multi-bed regenerative adsorption chiller - improving the utilization of waste heat and reducing the chilled water outlet temperature fluctuation," *International Journal of Refrigeration,* vol. 24, pp. 124-136, 2001.

[56] M. Kubota, T. Ueda, R. Fujisawa, J. Kobayashi, F. Watanabe, N. Kobayashi and M. Hasatani, "Cooling output performance of a prototype adsorption heat pump with fin-type silica gel tube module," *Applied Thermal Engineering,* vol. 28, pp. 87-93, 2008.

[57] H. T. Chua, K. C. Ng, W. Wang, C. Yap and X. L. Wang, "Transient modeling of a two-bed silica gel-water adsorption chiller," *International Journal of Heat and Mass Transfer,* vol. 47, pp. 659-669, 2004.

[58] H. Demir, M. Mobedi and S. Ulku, "A review on adsorption heat pump: Problems and solutions," *Renewable and Sustainable Energy Reviews,* vol. 12, no. 9, pp. 2381-2403, 2008.

[59] K. Wang and E. A. Vineyard, "Adsorption Refrigeration," *ASHRAE Journal,* pp. 14-24, 2011.

[60] X. Bu, Z. Lu and L. Wang, "Preperation of compsoite adsorbent with high performance of heat and mass transfer," *Chinese Science Bulletin,* vol. 58, no. 30, pp. 3709-3714, 2013.

[61] S. K. Henninger, K. T. Witte, T. Fuldner, T. Nunez and P. Schossig, "Technical and Economical Review of Thermally Driven Heat Pumps," in *10th IEA Heat Pump Conference*, Tokyo, 2011.

[62] Southern Research Institute, "Demonstration of a Solart Thermal Combined Heating, Cooling and Hot Water System Utilizing an Adsorption Chiller for DoD Installations," U.S. Department of Defense Environmental Security Technology Certification Program , 2014.

[63] A. Alahmer, X. Wang and K. C. Amanul Alam, "Dynamic and Economic Investigation of a Solar Thermal-Driven Two-Bed Adsorption Chiller under Perth Climatic Conditions," *Energies,* vol. 13, p. 1005, 2020.

[64] L. W. Wang, R. Z. Wang, J. Y. Wu, Z. Z. Xia and K. Wang, "A new type of adsorber for adsorption ice maker on fishing boats," *Energy Conversion and Management,* vol. 46, pp. 2301-2316, 2004.

[65] K. Wang, J. Y. Wu, Z. Z. Xia, S. L. Li and R. Z. Wang, "Design and performance prediction of a novel double heat pipes type adsorption chiller for fishing boats," *Renewable Energy,* vol. 33, pp. 780-790, 2008.

[66] L. Zisheng and W. Ruzhu, "Experimental performance study of sorption refrigerators driven by waste gases from fishing vessels diesel engine," *Applied Energy,* vol. 174, pp. 224-231, 2016.

[67] V. Palomba, M. Aprile, M. Motta and S. Vasta, "Study of sorption systems for application on low-emission fishing vessels," *Energy,* vol. 134, pp. 554-565, 2017.

[68] H. Wang, R. Peterson, K. Harada, E. Miller, R. Ingram-Goble, L. Fisher, J. Yih and C. Ward, "Performance of a combine organic Rankine cycle and vapor compression cycle for heat activated cooling," *Energy,* vol. 36, pp. 447-458, 2011.

[69] B. Saleh, A. A. Aly, A. F. Alogla, A. M. Aljuaid, M. M. Altharthi, K. I. E. Ahmed and Y. S. Hamed, "Performance investigation of organic Rankine-vapor compression refrigeration integrated system activated by renewable energy," *Mechanics & Industry,* vol. 20, p. 206, 2019.

[70] A. B. Little and S. Garimella, "Comparitive assessment of alternative cycles for waste heat recovery and upgrade," *Energy,* vol. 36, pp. 4492-4504, 2011.

[71] I. K. Smith, N. Stosic, A. Kovacevic and R. Langson, "Cost effective small scale ORC systems for power recovery from low enthalpy geothermal resources," *Transactions - Geothermal Resources Council,* vol. 31, 2007.

[72] TIAX LLC, "Review of Thermally Activated Technologies," U.S. Department of Energy, 2004.

[73] X. Ma, W. Zhang, S. A. Omer and S. B. Riffat, "Experimental investigation of a novel steam ejector refrigerator suitable for solar energy applications," *Applied Thermal Engineering,* vol. 30, pp. 1320-1325, 2010.

[74] S. S. Murthy, R. Balasubramanian and M. V. K. Murthy, "Experiments on vapour jet refrigeration system suitable for solar energy applications," *Renewable Energy,* vol. 1, pp. 757-768, 1991.

[75] C. J. Korres, A. T. Papaioannou, V. Lygerou and N. G. Koumoutsos, "Solar cooling by thermal compression: The dependence of the jet thermal compressor efficiency on the compression ratio," *Energy,* vol. 27, pp. 795-805, 2002.

[76] O. Bounefour and A. Ouadha, "Thermodynamic analysis and working fluid optimization of a combined ORC-VCC system using waste heat from a marine diesel engine," in *ASME International Mechanical Engineering Congress and Exposition*, Montreal, 2014.

[77] O. Bounefour and A. Ouadha, "Performance improvement of combined organic Rankine-vapor compression cycle using serial cascade evaporation in the organic cycle," *Energy Procedia,* vol. 139, pp. 248-253, 2017.

[78] O. Bounefour, A. Ouadha and Y. Addad, "An exergy analysis of various layouts of ORC-VCC systems for usage in waste heat recovery onboard ships," *Marine Systems and Ocean Technology,* vol. 15, pp. 26-44, 2020.

[79] X. Bu, L. Wang and H. Li, "Working fluids selection for fishing boards waste heat powered organic Rankine-vapor compression ice maker," *Heat Mass Transfer,* vol. 50, pp. 1479-1485, 2014.

[80] C. Ezgi and I. Girgin, "Design and Thermodynamic Analysis of a Steam Ejector Refrigeration/Heat Pump System for Naval Surface Ship Applications," *Entropy,* vol. 17, pp. 8152-8173, 2015.

[81] T. M. Bandhauer and S. D. Garland, "Dry Air Turbo-Compression Cooling," in *ASME Power Conference*, Charlotte, 2016.

[82] S. D. Garland, T. M. Bandhauer and J. Noall, "Performance Model of a Waste Heat Driven Turbo-Compression Chiller," in *2nd Thermal and Fluid Engineering Conference*, Las Vegas, 2017.

[83] S. D. Garland, T. M. Bandhauer, A. Grauberger, J. Simon, D. Young, K. Eisemann, R. Fuller, J. Noall, J. Shull, R. V. Sami, M. J. Reinke and L. W. Gabbery, "Experimental Investigation of a Waste Heat Driven Turbo-Compression Chiller," in *3rd Thermal and Fluids Engineering Conference*, Fort Lauderdale, 2018.

[84] S. D. Garland, J. Noall and T. M. Bandhauer, "Experimentally validated modeling of a turbo-compression cooling system for power plant waste heat recovery," *Energy,* vol. 156, pp. 32-44, 2018.

[85] S. C. Gibson, D. Young and T. M. Bandhauer, "Technoeconomic Optimization of Turbocompression Cooling Systems," in *25th International Mechanical Engineering Congress & Exposition*, Tampa, 2017.

[86] D. Young, S. C. Gibson and T. M. Bandhauer, "Working Fluid Selection and Technoeconomic Optimization of a Turbocompression Cooling System," *Journal of Thermal Science and Engineering Applications,* vol. 10, no. 6, p. 061017, 2018.

[87] ASHRAE, "ASHRAE Refrigerant Designations," [Online]. Available: https://www.ashrae.org/technical-resources/standards-and-guidelines/ashrae-refrigerant-designations.

[88] Environmental Protection Agency, "Protection of Stratospheric Ozone: New Listings of Substitutes; Changes of Listing Status; and Reinterpretation of Unacceptability for Closed Cell Foam Products Under the Significant New Alternatives Policy Program; and Revision of Clean Air Act Section..," 01 12 2016. [Online]. Available: https://www.federalregister.gov/documents/2016/12/01/2016-25167/protection-of-stratospheric-ozone-new-listings-of-substitutes-changes-of-listing-status-and.

[89] M. Petersen, G. Pottker, A. Sethi and S. F. Yana Motta, "Refrigerants with low environmental impact for refrigeration systems," in *17th International Refrigeration and Air Conditioning Congress*, Purdue, 2018.

[90] SERO Pump Systems, "Side Channel Pump Product Information".

[91] Airedale, "TurboChill Water Cooled," [Online]. Available: https://www.airedale.com/wp-content/uploads/2020/01/modine.comuserdataLEEDGBDesktopshardyDesktopTTWC-v4.6.pdf.

[92] Alfa Laval, "Gasketed plate-and-frame heat exchangers AlfaQ," [Online]. Available: https://www.alfalaval.us/products/heat-transfer/plate-heat-exchangers/gasketed-plate-and-frame-heat-exchangers/alfaq/.

[93] J. R. Simon III, "Plate Frame and Bar Plate Evaporator Model Validation and Volume Minimization," M.S. Thesis, 2019.

[94] D. N. Young, "Technoeconomic Optimization and Working Fluid Selection for an Engine Coolant Driven Turbo-Compression Cooling System," M.S. Thesis, 2018.

[95] Y. Y. Hsieh and T. F. Lin, "Evaporation Heat Transfer and Pressure Drop of Refrigerant R-410A Flow in a Vertical Plate Heat Exchanger," *Journal of Heat Transfer,* vol. 125, pp. 852-857, 2003.

[96] T. L. Bergman, A. S. Lavine, F. P. Incropera and D. P. Dewitt, Fundamentals of Heat Transfer, John Wiley & Sons, 2011.

[97] M. G. Cooper, "Saturation Nucleate Pool Boiling: A Simple Correlation," in *1st U.K. National Conference on the Heat Transfer*, 1984.

[98] B. Thonon, R. Vidil and C. Marvillet, "Recent Research and Developments in Plate Heat Exchangers," *Journal of Enhanced Heat Transfer,* vol. 2, pp. 149-155, 1995.

[99] A. Muley, "Heat Transfer and Pressure Drop in Plate Heat Exchangers," Ph. D. Thesis, University of Cincinnati, 1997.

[100] Y. Y, H. Lio and T. Lin, "Condensation heat transfer and pressure drop of refrigerant R134a in a plate heat exchanger," *International Journal of Heat and Mass Transfer,* vol. 42, pp. 993-1006, 1999.

[101] Daikin Applied, "Megnitude Magnetic Bearing Centrifugal Chiller," [Online]. Available: https://www.daikinapplied.com/products/chiller-products/magnitude.

[102] J. W. Mitchell and J. E. Braun, Principles of Heating, Ventilation, and Air Conditioning in Buildings, John Wiley & Sons, Inc., 2013.

[103] T. Brown, Engineering Economics and Economic Design for Process Engineers, Boca Raton, FL: CRC Press, 2007.

[104] Danfoss, "Turbocor," 2021. [Online]. Available: https://www.danfoss.com/en/products/dcs/compressors/turbocor/#tab-overview.

[105] Sero, "Sero Model SRZS," [Online]. Available: https://seropumps.com/srzs/.

[106] Yaskawa, "P1000 Drive," [Online]. Available: https://www.yaskawa.com/products/drives/industrial-ac-drives/fan-pump-drives/p1000-drive.

[107] Department Logistics Agency, "Standard Prices," 2021. [Online]. Available: https://www.dla.mil/Energy/Business/StandardPrices/.

[108] J. Wang, S. Shang, X. Li, B. Wang, W. Wu and W. Shi, "Dynamic Performance Analysis for an Absorption Chiller under Different Working Conditions," *Applied Sciences,* vol. 7, p. 797, 2017.

APPENDIX A. Representative Calculations for the TCCS

The following appendix will provide hand calculations for the volume optimized power boosted TCCS to verify the accuracy of the thermodynamic and heat exchanger model results which were calculated using Engineering Equation Solver (EES). The system process flow diagram and state points are shown in Figure A-1. The effectiveness values for each heat exchanger section in the optimized system are provided in Table A-1. The EES calculated state points and flow rates are listed in Table A-2. Note that fluid properties used in the hand calculations were still calculated using EES.

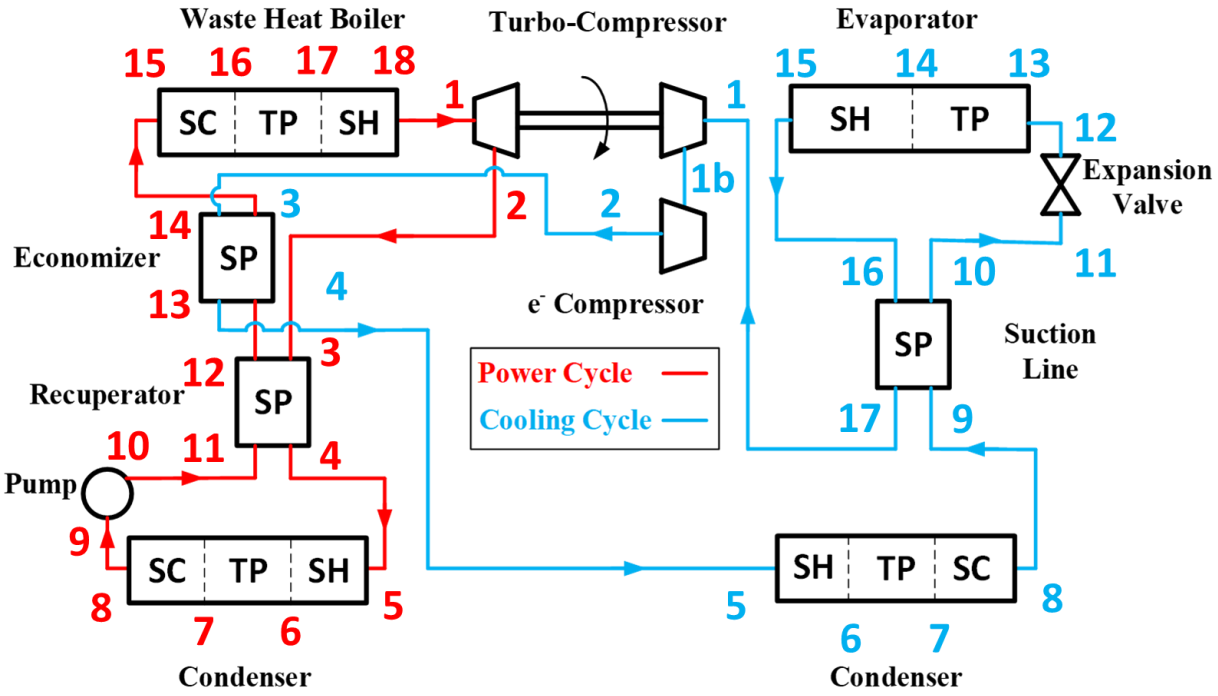

Figure A-1: Power boosted TCCS process flow diagram and state point locations

Table A-1: Design point optimized heat exchanger effectiveness values

Heat Exchanger	Subcooled	Two-Phase	Superheat
Boiler	0.7**	0.432	0.6*
PC Condenser	0.115	0.67*	0.612
Evaporator	-	0.82*	0.1**
CC Condenser	0.136	0.75*	0.856
Recuperator	0.65*		
Economizer	0.73*		
Suction Line	0.77*		

* Optimized Value

** Fixed Value

Table A-2: EES calculated design state points

	Power Cycle (4.52 kg s^{-1})	P [kPa]	T [C]	h [kJ kg^{-1}]	s [kJ kg^{-1} K^{-1}]
1	Turbine Inlet	2531	88.1	297.3	0.9380
2	Turbine Outlet	963	47.9	281.3	0.9506
3	Recuperator Inlet (Hot)	962	47.9	281.3	0.9506
4	Recuperator Outlet (Hot)	956	42.4	275.4	0.9326
5	Condenser Inlet	955	42.3	275.4	0.9326
6	Condenser Sat. Vap.	955	37.7	270.2	0.9162
7	Condenser Sat. Liq.	955	37.7	104.8	0.3840
8	Condenser Outlet	956	36.7	103.3	0.3792
9	Pump Inlet	955	36.7	103.3	0.3792
10	Pump Outlet	2554	39.5	107.2	0.3874
11	Recuperator Inlet (Cold)	2553	39.5	107.2	0.3874
12	Recuperator Outlet (Cold)	2545	43.4	113.1	0.4060
13	Economizer Inlet (Cold)	2545	43.4	113.1	0.4060
14	Economizer Outlet (Cold)	2537	55.7	131.9	0.4642
15	Boiler Inlet	2537	55.7	131.9	0.4642
16	Boiler Sat. Liq.	2533	78.2	170.8	0.5785
17	Boiler Sat. Vap.	2532	78.1	280.8	0.8915
18	Boiler Outlet	2531	88.1	297.3	0.9380
	Cooling Cycle (4.05 kg s^{-1})	P [kPa]	T [C]	h [kJ kg^{-1}]	s [kJ kg^{-1} K^{-1}]
1	Compressor Inlet	325	28.3	275.0	1.009
1b	Compressor Mid-Point	593	52.2	292.5	1.020
2	Compressor Outlet	925	70.8	305.8	1.027
3	Economizer Inlet (Hot)	925	70.7	305.8	1.027
4	Economizer Outlet (Hot)	921	50.5	284.8	0.965
5	Condenser Inlet	921	50.5	284.8	0.965
6	Condenser Sat. Vap.	921	36.3	269.6	0.917
7	Condenser Sat. Liq.	921	36.4	102.8	0.378
8	Condenser Outlet	921	35.4	101.4	0.373
9	Suction Line Inlet (Hot)	921	35.4	101.4	0.373
10	Suction Line Outlet (Hot)	913	20.0	79.4	0.300
11	Expansion Valve Inlet	913	20.0	79.4	0.300
12	Expansion Valve Outlet	344	4.5	79.4	0.304
13	Evaporator Inlet	344	4.5	79.4	0.304
14	Evaporator Sat. Vap.	331	3.4	252.4	0.930
15	Evaporator Outlet	331	4.1	253.0	0.932
16	Suction Line Inlet (Cold)	330	4.0	253.0	0.932
17	Suction Line Outlet (Cold)	327	28.3	275.0	1.009

A.1 Thermodynamic Model Calculations

Hand calculations were performed to verify the thermodynamic model used in this study. EES was used to iteratively and simultaneously solve the Equations provided in Chapter 3. Direct inputs to the model are listed in Table A-3. Some of the effectiveness values listed as inputs were the optimized values found using the heat exchanger sizing model and can be treated as fixed inputs for the thermodynamic model. In addition, the pressure drop in the piping routes were previously listed in Table 3-10. The pressure drops in the heat exchangers were calculated using the heat exchanger model and will be discussed in the following section. Table A-4 walks through example hand calculations and compares the evaluated value with the EES calculated value for the thermodynamic model.

Table A-3: Thermodynamic model hand calculation inputs

Parameter	Value	Unit
Evaporator Cooling Duty ($\dot{Q}_{chill}$)	703.4	kW_{th}
Turbine efficiency (η_{turb})	80	%
Compressor efficiency (η_{comp})	80	%
Mechanical shaft efficiency (η_{mech})	98	%
Pump efficiency (η_{pump})	35	%
Engine load (EL)	85	%
Intermediate loop heat exchanger effectiveness (ε_{int})	90	%
Seawater temperature inlet ($T_{cond,i}$)	29	°C
Seawater temperature rise (ΔT_{cond})	6	°C
Jacket water engine inlet temperature ($T_{JW,i}$)	90	°C
Jacket water engine outlet temperature ($T_{JW,o}$)	95	°C
Lubrication oil engine inlet temperature ($T_{oil,i}$)	85	°C
Lubrication oil engine outlet temperature ($T_{oil,o}$)	90	°C
Chilled water inlet temperature ($T_{chill,i}$)	10.39	°C
Chilled water outlet temperature ($T_{chill,o}$)	5.56	°C
Degrees of subcooling at the PC condenser outlet ($\Delta T_{pc,cond,sc}$)	1	°C

Parameter	Value	Unit
Degrees of subcooling at the CC condenser outlet ($\Delta T_{cc,cond,sc}$)	1	°C
Boiler subcooled pressure drop ($\Delta P_{boil,sc}$)	3.294	kPa
Boiler two-phase pressure drop ($\Delta P_{boil,tp}$)	1.477	kPa
Boiler superheated pressure drop ($\Delta P_{boil,sh}$)	0.4739	kPa
PC condenser superheated pressure drop ($\Delta P_{pc,cond,sh}$)	0.875	kPa
PC condenser two-phase pressure drop ($\Delta P_{pc,cond,tp}$)	-0.3657	kPa
PC condenser subcooled pressure drop ($\Delta P_{pc,cond,sc}$)	-0.2697	kPa
Evaporator two-phase pressure drop ($\Delta P_{evap,tp}$)	13.39	kPa
Evaporator superheated pressure drop ($\Delta P_{evap,sh}$)	0.0208	kPa
CC condenser superheated pressure drop ($\Delta P_{cc,cond,sh}$)	0.094	kPa
CC condenser two-phase pressure drop ($\Delta P_{cc,cond,tp}$)	-0.6362	kPa
CC condenser subcooled pressure drop ($\Delta P_{cc,cond,sc}$)	-0.2491	kPa
Recuperator hot side pressure drop ($\Delta P_{recup,h}$)	5.656	kPa
Recuperator cold side pressure drop ($\Delta P_{recup,c}$)	7.497	kPa
Economizer hot side pressure drop ($\Delta P_{econ,h}$)	3.174	kPa
Economizer cold side pressure drop ($\Delta P_{econ,c}$)	7.253	kPa
Suction line HX hot side pressure drop ($\Delta P_{slhx,h}$)	7.271	kPa
Suction line HX cold side pressure drop ($\Delta P_{slhx,c}$)	2.917	kPa

Table A-4: Thermodynamic model hand calculations

Parameter	Equation	Evaluated	EES Calc. Valve	Hand Calc. Value	Units
Boiler - Subcooled					
Minimum Specific Heat Rate ($C_{min,b,sc}$)	$C_{min,b,sc} = \min(\dot{m}_{pc} * c_{p,b,sc}, \dot{m}_{int} * c_{p,int})$	$C_{min,b,sc} = \min(4.52 * 1.788, 18.78 * 4.029)$	8.083	8.082	kW K^{-1}
Heat Duty ($\dot{Q}_{b,sc}$)	$\dot{Q}_{b,sc} = \dot{m}_{int} * c_{p,int} * (T_{int,l} - T_{int,o})$	$\dot{Q}_{b,sc} = 18.78 * 4.029 * (86.77 - 84.44)$	175.8	176.3	kW
Heat Duty ($\dot{Q}_{b,sc}$)	$\dot{Q}_{b,sc} = \dot{m}_{pc} * (i_{pc,16} - i_{pc,15})$	$\dot{Q}_{b,sc} = 4.52 * (170.8 - 131.9)$	175.8	175.8	kW
Heat Duty ($\dot{Q}_{b,sc}$)	$\dot{Q}_{b,sc} = \varepsilon_{b,sc} * C_{min,b,sc} * (T_{int,l} - T_{pc,15})$	$\dot{Q}_{b,sc} = 0.7 * 8.083 * (86.77 - 55.7)$	175.8	175.8	kW
Boiler - Two-Phase					
Minimum Specific Heat Rate ($C_{min,b,tp}$)	$C_{min,b,tp} = \dot{m}_{int} * c_{p,int}$	$C_{min,b,tp} = 18.78 * 4.044$	75.97	75.95	kW K^{-1}
Heat Duty ($\dot{Q}_{b,tp}$)	$\dot{Q}_{b,tp} = \dot{m}_{int} * c_{p,int} * (T_{int,v} - T_{int,l})$	$\dot{Q}_{b,tp} = 18.78 * 4.044 * (93.31 - 86.77)$	497.2	496.7	kW
Heat Duty ($\dot{Q}_{b,tp}$)	$\dot{Q}_{b,tp} = \dot{m}_{pc} * (i_{pc,17} - i_{pc,16})$	$\dot{Q}_{b,tp} = 4.52 * (280.8 - 170.8)$	497.2	497.2	kW
Heat Duty ($\dot{Q}_{b,tp}$)	$\dot{Q}_{b,tp} = \varepsilon_{b,tp} * C_{min,b,tp} * (T_{int,v} - T_{pc,16})$	$\dot{Q}_{b,tp} = 0.4318 * 75.97 * (93.31 - 78.16)$	497.2	497.0	kW
Boiler - Superheat					

Parameter	Equation	Evaluated	EES Calc. Valve	Hand Calc. Value	Units
Minimum Specific Heat Rate ($C_{min,b,sh}$)	$C_{min,b,sh} = \min(\dot{m}_{pc} * c_{p,b,sh}, \dot{m}_{int} * c_{p,int})$	$C_{min,b,sh} = \min(4.52 * 1.704, 18.78 * 4.046)$	7.704	7.702	kW K^{-1}
Heat Duty ($\dot{Q}_{b,sh}$)	$\dot{Q}_{b,sh} = \dot{m}_{int} * c_{p,int} * (T_{int,i} - T_{int,v})$	$\dot{Q}_{b,sh} = 18.78 * 4.046 * (94.3 - 93.31)$	74.73	75.22	kW
Heat Duty ($\dot{Q}_{b,sh}$)	$\dot{Q}_{b,sh} = \dot{m}_{pc} * (i_{pc,18} - i_{pc,17})$	$\dot{Q}_{b,sh} = 4.52 * (297.3 - 280.8)$	74.73	74.58	kW
Heat Duty ($\dot{Q}_{b,sh}$)	$\dot{Q}_{b,sh} = \varepsilon_{b,sh} * C_{min,b,sh} * (T_{int,i} - T_{pc,17})$	$\dot{Q}_{b,sh} = 0.6 * 7.704 * (94.3 - 78.13)$	74.73	74.74	kW
Boiler - Total					
Total Boiler Heat Duty ($\dot{Q}_{boil}$)	$\dot{Q}_{b,total} = \dot{m}_{pc} * (i_{pc,18} - i_{pc,15})$	$\dot{Q}_{b,total} = 4.52 * (297.3 - 131.9)$	747.7	747.6	kW
Total Boiler Heat Duty ($\dot{Q}_{boil}$)	$\dot{Q}_{b,total} = \dot{Q}_{b,sc} + \dot{Q}_{b,tp} + \dot{Q}_{b,sh}$	$\dot{Q}_{b,total} = 175.8 + 497.2 + 74.73$	747.7	747.7	kW
Turbine					
Turbine Outlet Enthalpy ($i_{pc,2}$)	$\eta_{turb} = \frac{i_{pc,1} - i_{pc,2}}{i_{pc,1} - i_{pc,2,s}}$	$0.8 = \frac{297.3 - i_{pc,2}}{297.3 - 277.3}$	281.3	281.3	kJ kg^{-1}
Turbine Work ($\dot{W}_{turb}$)	$\dot{W}_{turb} = \dot{m}_{r} * (i_{r,i} - i_{r,o})$	$\dot{W}_{turb} = 4.52 * (297.3 - 281.3)$	72.43	72.32	kW

Parameter	Equation	Evaluated	EES Calc. Valve	Hand Calc. Value	Units
PC Condenser - Superheat					
Minimum Specific Heat Rate ($C_{min,pcc,sh}$)	$C_{min,pcc,sh} = \min(\dot{m}_{pc} * c_{p,pcc,sh}, \dot{m}_{cond} * c_{p,cond})$	$C_{min,pcc,sh} = \min(4.52 * 1.125, 32.37 * 4.009)$	5.084	5.085	kW K^{-1}
Heat Duty ($\dot{Q}_{pcc,sh}$)	$\dot{Q}_{pcc,sh} = \dot{m}_{cond} * c_{p,cond} * (T_{cond,o} - T_{cond,v})$	$\dot{Q}_{pcc,sh} = 32.37 * 4.009 * (35 - 34.82)$	23.34	23.36	kW
Heat Duty ($\dot{Q}_{pcc,sh}$)	$\dot{Q}_{pcc,sh} = \dot{m}_{pc} * (i_{pc,5} - i_{pc,6})$	$\dot{Q}_{pcc,sh} = 4.52 * (275.4\text{-}270.2)$	23.34	23.50	kW
Heat Duty ($\dot{Q}_{pcc,sh}$)	$\dot{Q}_{pcc,sh} = \varepsilon_{pcc,sh} * C_{min,pcc,sh} * (T_{pc,5} - T_{cond,v})$	$\dot{Q}_{pcc,sh} = 0.6115 * 5.084 * (42.33 - 34.82)$	23.34	23.35	kW
PC Condenser - Two-Phase					
Minimum Specific Heat Rate ($C_{min,pcc,tp}$)	$C_{min,pcc,tp} = \dot{m}_{cond} * c_{p,cond}$	$C_{min,pcc,tp} = 32.37 * 4.004$	129.6	129.6	kW K^{-1}
Heat Duty ($\dot{Q}_{pcc,tp}$)	$\dot{Q}_{pcc,tp} = \dot{m}_{cond} * c_{p,cond} * (T_{cond,v} - T_{cond,l})$	$\dot{Q}_{pcc,tp} = 32.37 * 4.004 * (34.82 - 29.05)$	747.8	747.8	kW
Heat Duty ($\dot{Q}_{pcc,tp}$)	$\dot{Q}_{pcc,tp} = \dot{m}_{pc} * (i_{pc,6} - i_{pc,7})$	$\dot{Q}_{pcc,tp} = 4.52 * (270.2 - 104.8)$	747.8	747.6	kW
Heat Duty ($\dot{Q}_{pcc,tp}$)	$\dot{Q}_{pcc,tp} = \varepsilon_{pcc,tp} * C_{min,pcc,tp} * (T_{pc,6} - T_{cond,l})$	$\dot{Q}_{pcc,tp} = 0.67 * 129.6 * (37.66 - 29.05)$	747.8	747.6	kW

Parameter	Equation	Evaluated	EES Calc. Valve	Hand Calc. Value	Units
PC Condenser - Subcool					
Minimum Specific Heat Rate ($C_{min,pcc,sc}$)	$C_{min,pcc,sc} = \min(\dot{m}_{pc} * c_{p,pcc,sc}, \dot{m}_{cond} * c_{p,cond})$	$C_{min,pcc,sc} = \min(4.52 * 1.485, 32.37 * 4.004$	6.713	6.712	kW K^{-1}
Heat Duty ($\dot{Q}_{pcc,sc}$)	$\dot{Q}_{pcc,sc} = \dot{m}_{cond} * c_{p,cond} * (T_{cond,l} - T_{cond,i})$	$\dot{Q}_{pcc,sc} = 32.37 * 4.004 * (29.05 - 29)$	6.7	6.5	kW
Heat Duty ($\dot{Q}_{pcc,sc}$)	$\dot{Q}_{pcc,sc} = \dot{m}_{pc} * (i_{pc,7} - i_{pc,8})$	$\dot{Q}_{pcc,sc} = 4.52 * (104.8 - 103.3)$	6.7	6.8	kW
Heat Duty ($\dot{Q}_{pcc,sc}$)	$\dot{Q}_{pcc,sc} = \varepsilon_{pcc,sc} * C_{min,pcc,sc} * (T_{pc,7} - T_{cond,i})$	$\dot{Q}_{pcc,sc} = 0.115 * 6.713 * (37.68 - 29)$	6.7	6.7	kW
PC Condenser - Total					
Total Condenser Heat Duty ($\dot{Q}_{pc,cond}$)	$\dot{Q}_{pcc,total} = \dot{m}_{pc} * (i_{pc,5} - i_{pc,8})$	$\dot{Q}_{b,total} = 4.52 * (275.4 - 103.3)$	777.8	777.9	kW
Total Condenser Heat Duty ($\dot{Q}_{pc,cond}$)	$\dot{Q}_{pcc,total} = \dot{Q}_{pcc,sc} + \dot{Q}_{pcc,tp} + \dot{Q}_{pcc,sh}$	$\dot{Q}_{b,total} = 6.7 + 747.8 + 23.34$	777.8	777.8	kW
Power Cycle Pump					

Parameter	Equation	Evaluated	EES Calc. Valve	Hand Calc. Value	Units
Pump Outlet Enthalpy ($i_{pc,10}$)	$\eta_{pump} = \frac{i_{pc,10,s} - i_{pc,9}}{i_{pc,10} - i_{pc,9}}$	$0.35 = \frac{104.7 - 103.3}{i_{pc,10} - 103.3}$	107.2	107.3	kJ kg^{-1}
Pump Work ($\dot{W}_{pump}$)	$\dot{W}_{pump} = \dot{m}_{pc} * (i_{pc,10} - i_{pc,9})$	$\dot{W}_{pump} = 4.52 * (107.2\text{-}103.3)$	17.73	17.63	kW
Recuperator					
Minimum Specific Heat Rate ($C_{min,recup}$)	$C_{min,recup} = \min(\dot{m}_{pc} * c_{p,recup,h}, \dot{m}_{pc} * c_{p,recup,c})$	$C_{min,recup} = \min(4.52 * 1.072, 4.52 * 1.467)$	4.846	4.845	kW K^{-1}
Heat Duty ($\dot{Q}_{recup}$)	$\dot{Q}_{recup} = \dot{m}_{pc} * (i_{pc,3} - i_{pc,4})$	$\dot{Q}_{recup} = 4.52 * (281.3 - 275.4)$	26.52	26.67	kW
Heat Duty ($\dot{Q}_{recup}$)	$\dot{Q}_{recup} = \dot{m}_{pc} * (i_{pc,12} - i_{pc,11})$	$\dot{Q}_{recup} = 4.52 * (113.1 - 107.2)$	26.52	26.67	kW
Heat Duty ($\dot{Q}_{recup}$)	$\dot{Q}_{recup} = \varepsilon_{recup} * C_{min,recup} * (T_{pc,3} - T_{pc,11})$	$\dot{Q}_{recup} = 0.65 * 4.846 * (47.88 - 39.46)$	26.52	26.57	kW
Compressors					
Compressor Outlet Enthalpy ($i_{cc,2}$)	$\eta_{comp} = \frac{i_{cc,2,s} - i_{cc,1}}{i_{cc,2} - i_{cc,1}}$	$0.8 = \frac{299.6 - 275}{i_{cc,2} - 275}$	305.8	305.8	kJ kg^{-1}
Compressor Work ($\dot{W}_{comp}$)	$\dot{W}_{comp} = \dot{m}_{cc} * (i_{cc,2} - i_{cc,1})$	$\dot{W}_{comp} = 4.051 * (305.8 - 275)$	124.7	124.8	kW

Parameter	Equation	Evaluated	EES Calc. Valve	Hand Calc. Value	Units
Turbo-Compressor Work ($\dot{W}_{comp,mech}$)	$\dot{W}_{comp,mech} = \dot{W}_{turb} * \eta_{mech}$	$\dot{W}_{comp,mech} = 72.43 * 0.98$	70.98	70.98	kW
Compressor Midpoint Enthalpy ($i_{comp,mid}$)	$\eta_{comp} = \frac{i_{,comp,mid,s} - i_{cc,1}}{i_{comp,mid} - i_{cc,1}}$	$0.8 = \frac{289 - 275}{i_{comp,mid} - 275}$	292.5	292.5	kJ kg^{-1}
Electric compressor work ($\dot{W}_{comp,elec}$)	$\dot{W}_{comp,elec} = \dot{m}_{cc} * (i_{cc,2} - i_{comp,mid})$	$\dot{W}_{comp,elec} = 4.051 * (305.8 - 292.5)$	53.69	53.88	kW
Electric compressor work ($\dot{W}_{comp,elec}$)	$\dot{W}_{comp,elec} = \dot{W}_{comp} - \dot{W}_{comp,mech}$	$\dot{W}_{comp,elec} = 124.7 - 70.98$	53.69	53.72	kW
Economizer					
Minimum Specific Heat Rate ($C_{min,econ}$)	$C_{min,econ} = \min(\dot{m}_{pc} * c_{p,econ,c}, \dot{m}_{cc} * c_{p,econ,h})$	$C_{min,econ} = \min(4.52 * 1.489, 4.051 * 1.05)$	4.255	4.254	kW K^{-1}
Heat Duty ($\dot{Q}_{econ}$)	$\dot{Q}_{econ} = \dot{m}_{pc} * (i_{pc,14} - i_{pc,13})$	$\dot{Q}_{econ} = 4.52 * (131.9 - 113.1)$	84.81	84.98	kW

Parameter	Equation	Evaluated	EES Calc. Valve	Hand Calc. Value	Units
Heat Duty ($\dot{Q}_{econ}$)	$\dot{Q}_{econ} = \dot{m}_{cc} * (i_{cc,3} - i_{pc,4})$	$\dot{Q}_{econ} = 4.051 * (305.8 - 284.8)$	84.81	85.07	kW
Heat Duty ($\dot{Q}_{econ}$)	$\dot{Q}_{econ} = \varepsilon_{econ} * C_{min,econ} * (T_{cc,3} - T_{pc,13})$	$\dot{Q}_{econ} = 0.73 * 4.255 * (70.74 - 43.43)$	84.81	83.90	kW
CC Condenser - Superheat					
Minimum Specific Heat Rate ($C_{min,ccc,sh}$)	$C_{min,ccc,sh} = \min(\dot{m}_{cc} * c_{p,ccc,sh}, \dot{m}_{cond,cc} * c_{p,cond,cc})$	$C_{min,ccc,sh} = \min(4.051 * 1.114, 30.93 * 4.009)$	4.511	4.513	kW K^{-1}
Heat Duty ($\dot{Q}_{ccc,sh}$)	$\dot{Q}_{ccc,sh} = \dot{m}_{cond,cc} * c_{p,cond,cc} * (T_{cond,cc,o} - T_{cond,cc,v})$	$\dot{Q}_{ccc,sh} = 30.93 * 4.009 * (35 - 34.5)$	61.6	62.0	kW
Heat Duty ($\dot{Q}_{ccc,sh}$)	$\dot{Q}_{ccc,sh} = \dot{m}_{cc} * (i_{cc,5} - i_{cc,6})$	$\dot{Q}_{ccc,sh} = 4.051 * (284.8 - 269.6)$	61.6	61.6	kW
Heat Duty ($\dot{Q}_{ccc,sh}$)	$\dot{Q}_{ccc,sh} = \varepsilon_{ccc,sh} * C_{min,ccc,sh} * (T_{cc,5} - T_{cond,cc,v})$	$\dot{Q}_{ccc,sh} = 0.8559 * 4.511 * (50.46 - 34.5)$	61.6	61.6	kW
CC Condenser - Two-Phase					
Minimum Specific Heat Rate ($C_{min,ccc,tp}$)	$C_{min,ccc,tp} = \dot{m}_{cond,cc} * c_{p,cond,cc}$	$C_{min,ccc,tp} = 30.93 * 4.004$	123.9	123.8	kW K^{-1}
Heat Duty ($\dot{Q}_{ccc,tp}$)	$\dot{Q}_{ccc,tp} = \dot{m}_{cond,cc} * c_{p,cond,cc} * (T_{cond,cc,v} - T_{cond,cc,l})$	$\dot{Q}_{ccc,tp} = 30.93 * 4.004 * (34.5 - 29.05)$	675.6	674.9	kW

Parameter	Equation	Evaluated	EES Calc. Valve	Hand Calc. Value	Units
Heat Duty ($\dot{Q}_{ccc,tp}$)	$\dot{Q}_{ccc,tp} = \dot{m}_{cc} * (i_{cc,6} - i_{cc,7})$	$\dot{Q}_{ccc,tp} = 4.051 * (269.6 - 102.8)$	675.6	675.7	kW
Heat Duty ($\dot{Q}_{ccc,tp}$)	$\dot{Q}_{ccc,tp} = \varepsilon_{ccc,tp} * C_{min,ccc,tp} * (T_{cc,6} - T_{cond,cc,l})$	$\dot{Q}_{ccc,tp} = 0.75 * 123.9 * (36.32 - 29.05)$	675.6	675.6	kW
CC Condenser - Subcool					
Minimum Specific Heat Rate ($C_{min,ccc,sc}$)	$C_{min,ccc,sc} = \min(\dot{m}_{cc} * c_{p,ccc,sc}, \dot{m}_{cond,cc} * c_{p,cond,cc})$	$C_{min,ccc,sc} = \min(4.051 * 1.478, 30.93 * 4.004)$	5.987	5.987	kW K^{-1}
Heat Duty ($\dot{Q}_{ccc,sc}$)	$\dot{Q}_{ccc,sc} = \dot{m}_{cond,cc} * c_{p,cond,cc} * (T_{cond,cc,l} - T_{cond,cc,i})$	$\dot{Q}_{ccc,sc} = 30.93 * 4.004 * (29.05 - 29)$	5.975	6.192	kW
Heat Duty ($\dot{Q}_{ccc,sc}$)	$\dot{Q}_{ccc,sc} = \dot{m}_{cc} * (i_{cc,7} - i_{cc,8})$	$\dot{Q}_{ccc,sc} = 4.051 * (102.8 - 101.4)$	5.975	5.671	kW
Heat Duty ($\dot{Q}_{ccc,sc}$)	$\dot{Q}_{ccc,sc} = \varepsilon_{ccc,sc} * C_{min,ccc,sc} * (T_{cc,7} - T_{cond,cc,i})$	$\dot{Q}_{ccc,sc} = 0.1359 * 5.987 * (36.35 - 29)$	5.975	5.980	kW
CC Condenser - Total					
Total Condenser Heat Duty ($\dot{Q}_{cc,cond}$)	$\dot{Q}_{ccc,total} = \dot{m}_{cc} * (i_{cc,5} - i_{cc,8})$	$\dot{Q}_{ccc,total} = 4.051 * (284.8 - 101.4)$	743.2	743.0	kW
Total Condenser	$\dot{Q}_{ccc,total} = \dot{Q}_{ccc,sc} + \dot{Q}_{ccc,tp} + \dot{Q}_{ccc,sh}$	$\dot{Q}_{ccc,total} = 5.975 + 675.6 + 61.6$	743.2	743.2	kW

Parameter	Equation	Evaluated	EES Calc. Valve	Hand Calc. Value	Units
Heat Duty ($\dot{Q}_{cc,cond}$)					
Evaporator - Two-Phase					
Minimum Specific Heat Rate ($C_{min,chill,tp}$)	$C_{min,chill,tp} = \dot{m}_{chill} * c_{p,chill}$	$C_{min,chill,tp} = 34.67 * 4.2$	145.6	145.6	kW K^{-1}
Heat Duty ($\dot{Q}_{chill,tp}$)	$\dot{Q}_{chill,tp} = \dot{m}_{chill} * c_{p,chill} * (T_{chill,v} - T_{chill,o})$	$\dot{Q}_{chill,tp} = 34.67 * 4.2 * (10.37 - 5.56)$	700.8	700.4	kW
Heat Duty ($\dot{Q}_{chill,tp}$)	$\dot{Q}_{chill,tp} = \dot{m}_{cc} * (i_{cc,14} - i_{cc,13})$	$\dot{Q}_{chill,tp} = 4.051 * (252.4 - 79.41)$	700.8	700.8	kW
Heat Duty ($\dot{Q}_{chill,tp}$)	$\dot{Q}_{chill,tp} = \varepsilon_{chill,tp} * C_{min,chill,tp} * (T_{chill,v} - T_{cc,13})$	$\dot{Q}_{chill,tp} = 0.82 * 145.6 * (10.37 - 4.504)$	700.8	700.4	kW
Evaporator - Superheat					
Minimum Specific Heat Rate ($C_{min,chill,sh}$)	$C_{min,chill,sh} = \min(\dot{m}_{cc} * c_{p,evap,sh}, \dot{m}_{chill} * c_{p,chill})$	$C_{min,chill,sh} = \min(4.051 * 0.913, 34.67 * 4.197)$	3.698	3.699	kW K^{-1}
Heat Duty ($\dot{Q}_{chill,sh}$)	$\dot{Q}_{chill,sh} = \dot{m}_{chill} * c_{p,chill} * (T_{chill,i} - T_{chill,v})$	$\dot{Q}_{chill,sh} = 34.67 * 4.197 * (10.39 - 10.37)$	2.596	2.910	kW
Heat Duty ($\dot{Q}_{chill,sh}$)	$\dot{Q}_{chill,sh} = \dot{m}_{cc} * (i_{cc,15} - i_{cc,14})$	$\dot{Q}_{chill,sh} = 4.051 * (253 - 252.4)$	2.596	2.431	kW

Parameter	Equation	Evaluated	EES Calc. Valve	Hand Calc. Value	Units
Heat Duty ($\dot{Q}_{evap,sh}$)	$\dot{Q}_{chill,sh} = \varepsilon_{chill,sh} * C_{min,chill,sh} * (T_{chill,i} - T_{cc,14})$	$\dot{Q}_{chill,sh} = 0.1 * 3.698 * (10.39 - 3.371)$	2.596	2.596	kW
Evaporator - Total					
Total Condenser Heat Duty ($\dot{Q}_{chill}$)	$\dot{Q}_{chill,total} = \dot{m}_{cc} * (i_{cc,15} - i_{cc,13})$	$\dot{Q}_{chill,total} = 4.051 * (253 - 79.41)$	703.4	703.2	kW
Total Condenser Heat Duty ($\dot{Q}_{chill}$)	$\dot{Q}_{chill,total} = \dot{Q}_{chill,tp} + \dot{Q}_{chill,sh}$	$\dot{Q}_{chill,total} = 700.8 + 2.596$	703.4	703.4	kW
Suction Line					
Minimum Specific Heat Rate ($C_{min,slhx}$)	$C_{min,slhx} = \min(\dot{m}_{cc} * c_{p,slhx,c}, \dot{m}_{cc} * c_{p,slhx,h})$	$C_{min,slhx} = \min(4.051 * 0.9109, 4.051 * 1.472)$	3.69	3.69	kW K^{-1}
Heat Duty ($\dot{Q}_{slhx}$)	$\dot{Q}_{slhx} = \dot{m}_{cc} * (i_{cc,17} - i_{pc,16})$	$\dot{Q}_{slhx} = 4.051 * (275 - 253)$	88.95	89.12	kW
Heat Duty ($\dot{Q}_{slhx}$)	$\dot{Q}_{slhx} = \dot{m}_{cc} * (i_{cc,9} - i_{pc,10})$	$\dot{Q}_{slhx} = 4.051 * (101.4 - 79.41)$	88.95	89.08	kW
Heat Duty ($\dot{Q}_{slhx}$)	$\dot{Q}_{slhx} = \varepsilon_{slhx} * C_{min,slhx} * (T_{cc,9} - T_{cc,16})$	$\dot{Q}_{slhx} = 0.77 * 3.69 * (35.35 - 4.041)$	88.95	88.96	kW
System Performance					

Parameter	Equation	Evaluated	EES Calc. Valve	Hand Calc. Value	Units
Power Cycle Efficiency (η_{pc})	$\eta_{pc} = \frac{\dot{W}_{turb} - \dot{W}_{pump}}{\dot{Q}_{boiler}}$	$\eta_{pc} = \frac{72.43 - 17.73}{747.7}$	0.07315	0.07316	-
Cooling Cycle COP (COP_{cc})	$COP_{cc} = \frac{\dot{Q}_{chill}}{\dot{W}_{comp,total}}$	$COP_{cc} = \frac{703.4}{124.7}$	5.642	5.641	-
Overall COP (COP_{TCCS})	$COP_{TCCS} = \frac{\dot{Q}_{chill}}{\dot{W}_{comp,elec} + \dot{W}_{pump} + \dot{Q}_{boiler}}$	$COP_{TCCS} = \frac{703.4}{53.69 + 17.73 + 747.7}$	0.8587	0.8587	-
Thermal COP ($COP_{thermal}$)	$COP_{thermal} = \frac{\dot{Q}_{chill}}{\dot{Q}_{boiler}}$	$COP_{thermal} = \frac{703.4}{747.7}$	0.9407	0.9408	-
Electrical COP (COP_{elec})	$COP_{elec} = \frac{\dot{Q}_{chill}}{\dot{W}_{comp,elec} + \dot{W}_{pump}}$	$COP_{elec} = \frac{703.4}{53.69 + 17.73}$	9.848	9.849	-

A.2 Heat Exchanger Sizing Calculations

Heat exchangers were sized using fixed plate geometry and thermodynamic state points as inputs. A UA-LMTD approach was used to calculate the overall conductance of each heat exchanger, and correlations from literature were used to calculate the heat transfer coefficient, allowing for the heat transfer area to be solved. The geometries of each heat exchanger are shown in Table A-5. The two-phase regions have a predefined two-phase region length, $L_{tp,fixed}$, to assist with heat flux calculations. Also, the number of plates for each heat exchanger may not a whole number. This was to keep the model as simple as possible and to reduce computational time. When solid modeling, the number of plates were rounded up to be a whole number and a multiple of 2. The evaporator was solid modeled as two cores in parallel, but the heat exchanger model treated the two units as one core. Hand calculations were performed for each heat exchanger region, and are shown in Table A-6 through A-12.

Table A-5: Heat exchanger geometries and results

Heat Exchanger:	Boiler	PC Condenser	Evaporator	CC Condenser	Recuperator	Economizer	Suction Line
Model	M10 (semi-welded)	AQ4L (gasketed)	AC500DQ (brazed, 2 cores)	AQ4L (gasketed)	AC500DQ (brazed)	AC500DQ (brazed)	AC500DQ (brazed)
Plate Material	AISI304	Titanium	AISI304	Titanium	AISI304	AISI304	AISI304
L_{port}	0.719 m	1.338 m	0.632 m	1.338 m	0.632 m	0.632 m	0.632 m
L_{total}	1.084 m	1.981 m	0.739 m	1.981 m	0.739 m	0.739 m	0.739 m
$L_{tp,fixed}$	0.3595 m	0.669 m	0.5056 m	0.669 m	-	-	-
W_{plate}	0.438 m	0.448 m	0.322 m	0.448 m	0.322 m	0.322 m	0.322 m
Pt	0.5 mm						
Ps	2.574 mm						
N_{plates}	195.8	177	528.7	314	116.8	160.4	256.3
Depth	0.602 m	0.5441 m	1.625 m	0.9653 m	0.3591 m	0.4931 m	0.7877 m
Volume	0.286 m^3	0.4832 m^3	0.3867 m^3	0.8572 m^3	0.08545 m^3	0.1173 m^3	0.1874 m^3
Subcooled ε	0.7	0.6115	-	0.8559	0.65	0.73	0.77
Two-Phase ε	0.4319	0.67	0.82	0.75			
Superheat ε	0.6	0.115	0.1	0.1359			

Table A-6: Boiler heat exchanger sizing model hand calculations

Parameter	Equation	Evaluated	EES Calc. Valve	Hand Calc. Value	Units
Wetted Perimeter (P_b)	$P_b = 2 * (Ps + W_{plate,b})$	$P_b = 2 * (0.002574 + 0.4383)$	0.8816	0.8817	m
Cross-Sectional Area ($A_{cs,b}$)	$A_{cs,b} = Ps * W_{plate,b}$	$A_{cs,b} = 0.002574 * 0.4383$	0.001128	0.001128	m^2
Hydraulic Diameter ($D_{h,b}$)	$D_{h,b} = \frac{4 * A_{cs,b}}{P_b}$	$D_{h,b} = \frac{4 * 0.001128}{0.8816}$	0.005118	0.00518	m
Refrigerant Channel Mass Flow Rate ($\dot{m}_{r,b}$)	$\dot{m}_{r,b} = \frac{2 * \dot{m}_{pc}}{N_{plates,b}}$	$\dot{m}_{r,b} = \frac{2 * 4.52}{195.8}$	0.04616	0.04617	kg s^{-1}
Water Channel Mass Flow Rate ($\dot{m}_{w,b}$)	$\dot{m}_{w,b} = \frac{2 * \dot{m}_{int}}{N_{plates,b}}$	$\dot{m}_{w,b} = \frac{2 * 18.78}{195.8}$	0.1918	0.1918	kg s^{-1}
Subcooled Region					
Channel Heat Transfer ($\dot{Q}_{b,sc}$)	$\dot{Q}_{b,sc} = \dot{m}_{r,b} * (i_{pc,16} - i_{pc,15})$	$\dot{Q}_{b,sc} = 0.04616 * (170.8 - 131.9)$	1.795	1.796	kW

Parameter	Equation	Evaluated	EES Calc. Valve	Hand Calc. Value	Units
Temperature Difference 1 ($\Delta T_{1,b}$)	$\Delta T_{1,b} = T_{int,o} - T_{pc,15}$	$\Delta T_{1,b} = 84.44 - 55.7$	28.74	28.74	K
Temperature Difference 2 ($\Delta T_{2,b}$)	$\Delta T_{2,b} = T_{int,l} - T_{pc,16}$	$\Delta T_{2,b} = 86.77 - 78.16$	8.61	8.61	K
Log-Mean Temperature Difference ($LMTD_{b,sc}$)	$LMTD_{b,sc} = \frac{\Delta T_{2,b} - \Delta T_{1,b}}{\ln\left(\frac{\Delta T_{2,b}}{\Delta T_{1,b}}\right)}$	$LMTD_{b,sc} = \frac{8.61 - 28.74}{\ln\left(\frac{8.61}{28.74}\right)}$	16.7	16.7	K
Overall Conductance ($UA_{b,sc}$)	$\dot{Q}_{b,sc} = UA_{b,sc} * LMTD_{b,sc}$	$1.795 = UA_{b,sc} * 16.7$	0.1075	0.1075	kW K^{-1}
Water-Side Reynolds Number ($Re_{w,b,sc}$)	$Re_{w,b,sc} = \frac{4 * \dot{m}_{w,b}}{P_b * \mu_{w,b}}$	$Re_{w,b,sc} = \frac{4 * 0.1918}{0.8816 * 0.0006539}$	1331	1331	-
Water-Side Heat Transfer Coefficient ($h_{w,b,sc}$)	$h_{w,b,sc} = 0.44 * \left(\frac{6\beta}{\pi}\right)^{0.38} * Re_{w,b,sc}^{0.5} * Pr_{w,b}^{1/3} * \frac{k_{w,b}}{D_{h,b}}$	$h_{w,b,sc} = 0.44 * \left(\frac{6 * 1.047}{\pi}\right)^{0.38} * 1331^{0.5} * 5.309^{1/3} * \frac{0.0004955}{0.005118}$	3.528	3.528	kW K^{-1} m^{-2}

Parameter	Equation	Evaluated	EES Calc. Valve	Hand Calc. Value	Units
Water-Side Thermal Resistance ($R_{w,b,sc}$)	$R_{w,b,sc} = \left(h_{w,b,sc} * L_{b,sc} * W_{plate,b}\right)^{-1}$	$R_{w,b,sc} = (3.528 * 0.3066 * 0.4383)^{-1}$	2.11	2.11	K kW^{-1}
Refrigerant Reynolds Number ($Re_{r,b,sc}$)	$Re_{r,b,sc} = \frac{4 * \dot{m}_{r,b}}{P_b * \mu_{r,l,b}}$	$Re_{r,b,sc} = \frac{4 * 0.04616}{0.8816 * 0.0001356}$	1545	1545	-
Refrigerant Heat Transfer Coefficient ($h_{r,b,sc}$)	$h_{r,b,sc} = 0.2267 * Re_{r,b,sc}^{0.631} * Pr_{r,b}^{1/3} * \frac{k_{r,b}}{D_{h,b}}$	$h_{r,b,sc} = 0.2267 * 1545^{0.631} * 3.099^{1/3} * \frac{0.00006897}{0.005118}$	0.458	0.458	kW K^{-1} m^{-2}
Refrigerant Thermal Resistance ($R_{r,b,sc}$)	$R_{r,b,sc} = \left(h_{r,b,sc} * L_{b,sc} * W_{plate,b}\right)^{-1}$	$R_{r,b,sc} = (0.458 * 0.3066 * 0.4383)^{-1}$	16.25	16.25	K kW^{-1}
Wall Thermal Resistance ($R_{plate,b,sc}$)	$R_{plate,b,sc} = \frac{Pt}{K_{plate} * L_{b,sc} * W_{plate,b}}$	$R_{plate,b,sc} = \frac{0.0005}{0.01512 * 0.3066 * 0.4383}$	0.2461	0.2461	K kW^{-1}
Overall Conductance ($UA_{b,sc}$)	$UA_{b,sc} = \left[\left(R_{r,b,sc} + R_{plate,b,sc} + R_{w,b,sc}\right)/2\right]^{-1}$	$UA_{b,sc} = [(16.25 + 0.2461 + 2.11)/2]^{-1}$	0.1075	0.1075	kW K^{-1}

Parameter	Equation	Evaluated	EES Calc. Valve	Hand Calc. Value	Units
Gravitational Pressure Drop ($\Delta P_{g,b,sc}$)	$\Delta P_{g,b,sc} = \rho_{r,b,sc} * g * L_{b,sc}$	$\Delta P_{g,b,sc} = 1087 * 9.78 * 0.3066$	3260	3259	Pa
Velocity ($u_{b,sc}$)	$u_{b,sc} = \frac{\dot{m}_{r,b}}{\rho_{r,b,sc} * A_{cs,b}}$	$u_{b,sc} = \frac{0.04616}{1087 * 0.001128}$	0.03764	0.03765	m s^{-1}
Friction Factor ($f_{b,sc}$)	$f_{b,sc} = 0.6857 * Re_{r,b,sc}^{-0.172}$	$f_{b,sc} = 0.6857 * 1545^{-0.172}$	0.1939	0.1939	-
Frictional Pressure Drop ($\Delta P_{f,b,sc}$)	$\Delta P_{f,b,sc} = \frac{2 * f_{b,sc} * \rho_{r,b,sc} * u_{b,sc}^2 * L_{b,sc}}{D_{h,b}}$	$\Delta P_{f,b,sc} = 2 * 0.1939 * 1087 * 0.03764^2 * 0.3066/0.005118$	35.79	35.78	Pa
Total Pressure Drop ($\Delta P_{b,sc}$)	$\Delta P_{b,sc} = \Delta P_{f,b,sc} + \Delta P_{g,b,sc}$	$\Delta P_{b,sc} = 3260 + 35.79$	3295	3296	Pa
Two-Phase Region					
Channel Heat Transfer ($\dot{Q}_{b,tp}$)	$\dot{Q}_{b,tp} = \dot{m}_{r,b} * (i_{pc,17} - i_{pc,16})$	$\dot{Q}_{b,tp} = 0.04616 * (280.8 - 170.8)$	5.078	5.078	kW
Temperature Difference 3 ($\Delta T_{3,b}$)	$\Delta T_{3,b} = T_{int,v} - T_{pc,17}$	$\Delta T_{3,b} = 93.31 - 78.13$	15.18	15.18	K
Log-Mean Temperature Difference ($LMTD_{b,tp}$)	$LMTD_{b,tp} = \frac{\Delta T_{3,b} - \Delta T_{2,b}}{\ln\left(\frac{\Delta T_{3,b}}{\Delta T_{2,b}}\right)}$	$LMTD_{b,tp} = \frac{15.18 - 8.61}{\ln\left(\frac{15.18}{8.61}\right)}$	11.59	11.59	K

Parameter	Equation	Evaluated	EES Calc. Valve	Hand Calc. Value	Units
Overall Conductance ($UA_{b,tp}$)	$\dot{Q}_{b,tp} = UA_{b,tp} * LMTD_{b,tp}$	$5.078 = UA_{b,tp} * 11.59$	0.4382	0.4381	kW K^{-1}
Water-Side Reynolds Number ($Re_{w,b,tp}$)	$Re_{w,b,tp} = \frac{4 * \dot{m}_{w,b}}{P_b * \mu_{w,b}}$	$Re_{w,b,tp} = \frac{4 * 0.1918}{0.8817 * 0.0006001}$	1450	1450	-
Water-Side Heat Transfer Coefficient ($h_{w,b,tp}$)	$h_{w,b,tp} = 0.44 * \left(\frac{6\beta}{\pi}\right)^{0.38} * Re_{w,b,tp}^{0.5} * Pr_{w,b}^{1/3} * \frac{k_{w,b}}{D_{h,b}}$	$h_{w,b,tp} = 0.44 * \left(\frac{6 * 1.047}{\pi}\right)^{0.38} * 1450^{0.5} * 4.847^{1/3} * \frac{0.0004997}{0.005118}$	3.606	3.602	kW K^{-1} m^{-2}
Water-Side Thermal Resistance ($R_{w,b,tp}$)	$R_{w,b,tp} = \left(h_{w,b,tp} * L_{b,tp} * W_{plate,b}\right)^{-1}$	$R_{w,b,tp} = (3.606 * 0.1792 * 0.4383)^{-1}$	3.533	3.531	K kW^{-1}
Refrigerant Reynolds Number ($Re_{r,b,tp}$)	$Re_{r,b,tp} = \frac{4 * \dot{m}_{r,b}}{P_b * \mu_{r,l,b}}$	$Re_{r,b,tp} = \frac{4 * 0.04616}{0.8817 * 0.00009299}$	2252	2252	-
Refrigerant Mass Flux ($G_{r,b,tp}$)	$G_{r,b,tp} = \frac{\dot{m}_{r,b}}{A_{cs,b}}$	$G_{r,b,tp} = \frac{0.04616}{0.001128}$	40.92	40.92	kg s^{-1} m^{-2}

Parameter	Equation	Evaluated	EES Calc. Valve	Hand Calc. Value	Units
Refrigerant Heat Flux ($q_{r,b,tp}$)	$q_{r,b,tp} = \frac{\dot{Q}_{b,tp}}{L_{b,tp,fixed} * W_{plate,b}}$	$q_{r,b,tp} = \frac{5.078}{0.3595 * 0.4383}$	32.23	32.23	kW m^{-2}
Martinelli Parameter ($X_{tt,b}$)	$X_{tt,b} = \left(\frac{1 - x_m}{x_m}\right)^{0.9} * \left(\frac{\rho_{r,v,b}}{\rho_{r,l,b}}\right)^{0.5} * \left(\frac{\mu_{l,b}}{\mu_{v,b}}\right)^{0.1}$	$X_{tt,b} = \left(\frac{1 - 0.5}{0.5}\right)^{0.9} * \left(\frac{146.9}{942}\right)^{0.5} * \left(\frac{0.00009299}{0.00001574}\right)^{0.1}$	0.4716	0.4717	-
Boiling Number (Bo_b)	$Bo_b = \frac{q_{r,b,tp}}{G_{r,b,tp} * i_{fg,b}}$	$Bo_b = \frac{32.23}{40.92 * 110}$	0.00716	0.00718	-
Liquid Heat Transfer Coefficient ($h_{l,b,tp}$)	$h_{l,b,tp} = 0.023 * Re_{l,b,tp}^{0.8} * Pr_{r,b}^{0.4} * \frac{k_{r,b}}{D_{h,b}}$	$h_{l,b,tp} = 0.023 * 2252^{0.8} * 3.486^{0.4} * \frac{0.00005337}{0.005118}$	0.1901	0.1901	kW K^{-1} m^{-2}
Pool Boiling Heat Transfer Coefficient ($h_{pool,b}$)	$h_{pool,b} = \left(55 * P_{r,b}^{0.12} * M_b^{-0.5} * \left(q_{r,b,tp} * 1000\right)^{0.67}\right) /1000$	$h_{pool,b} = (55 * 0.6241^{0.12} * 102^{-0.5} * (32.23 * 1000)^{0.67}) /1000$	5.394	5.395	kW K^{-1} m^{-2}
Enhancement Factor (E_b)	$E_b = 1 + 24000 * Bo_b^{1.16} + 1.37 * \left(X_{tt,b}\right)^{-0.86}$	$E_b = 1 + 24000 * 0.00716^{1.16} + 1.37 * (0.4716)^{-0.86}$	81.58	81.58	-
Suppression Factor (S_b)	$S_b = \left(1 + 1.15 * 10^{-6} * E_b^2 * Re_{r,b,tp}^{1.17}\right)^{-1}$	$S_b = (1 + 1.15 * 10^{-6} * 81.58^2 * 2252^{1.17})^{-1}$	0.9905	0.9905	-

Parameter	Equation	Evaluated	EES Calc. Valve	Hand Calc. Value	Units
Refrigerant Heat Transfer Coefficient ($h_{r,b,tp}$)	$h_{r,b,tp} = E_b * h_{l,b,tp} + S_b * h_{pool,b}$	$h_{r,b,tp} = 81.58 * 0.1901 + 0.9905 * 5.394$	20.85	20.85	kW K^{-1} m^{-2}
Refrigerant Thermal Resistance ($R_{r,b,tp}$)	$R_{r,b,tp} = \left(h_{r,b,tp} * L_{b,tp} * W_{plate,b}\right)^{-1}$	$R_{r,b,tp} = (20.85 * 0.1792 * 0.4383)^{-1}$	0.6105	0.6106	K kW^{-1}
Wall Thermal Resistance ($R_{plate,b,tp}$)	$R_{plate,b,tp} = \frac{Pt}{K_{plate} * L_{b,tp} * W_{plate,b}}$	$R_{plate,b,tp} = \frac{0.0005}{0.01512 * 0.1792 * 0.4383}$	0.4209	0.4210	K kW^{-1}
Overall Conductance ($UA_{b,tp}$)	$UA_{b,tp} = \left[\left(R_{r,b,tp} + R_{plate,b,tp} + R_{w,b,tp}\right)/2\right]^{-1}$	$UA_{b,tp} = [(0.6105 + 0.4209 + 3.533)/2]^{-1}$	0.4382	0.4382	kW K^{-1}
Equivalent Mass Flux ($G_{eq,b}$)	$G_{eq,b} = G_{r,b,tp} * \left[1 - x_m + x_m * \left(\frac{\rho_{l,b}}{\rho_{v,b}}\right)^{0.5}\right]$	$G_{eq,b} = 40.92 * \left[1 - 0.5 + 0.5 * \left(\frac{942}{146.9}\right)^{0.5}\right]$	72.28	72.27	kg s^{-1} m^{-2}
Equivalent Reynolds Number ($Re_{eq,b}$)	$Re_{eq,b} = \frac{G_{eq,b} * D_{h,b}}{\mu_{l,b}}$	$Re_{eq,b} = \frac{72.28 * 0.005118}{0.00009299}$	3978	3978	-

Parameter	Equation	Evaluated	EES Calc. Valve	Hand Calc. Value	Units
Equivalent Specific Density ($\rho_{eq,b}$)	$\rho_{eq,b} = \left(x_m * \left(\frac{1}{\rho_{v,b}} - \frac{1}{\rho_{l,b}}\right) + \frac{1}{\rho_{l,b}}\right)^{-1}$	$\rho_{eq,b} = \left(0.5 * \left(\frac{1}{146.9} - \frac{1}{942}\right) + \frac{1}{942}\right)^{-1}$	254.1	254.2	kg m^{-3}
Friction Factor ($f_{b,tp}$)	$f_{b,tp} = 23820 * \left(Re_{eq,b}\right)^{-1.12}$	$f_{b,tp} = 23820 * (3978)^{-1.12}$	2.215	2.215	-
Frictional Pressure Drop ($\Delta P_{f,b,tp}$)	$\Delta P_{f,b,tp} = \frac{2 * f_{b,tp} * G_{r,b,tp}^2 * L_{b,tp}}{\rho_{eq,b} * D_{h,b}}$	$\Delta P_{f,b,tp} = \frac{2 * 2.215 * 40.92^2 * 0.1792}{254.1 * 0.005118}$	1022	1022	Pa
Acceleration Pressure Drop ($\Delta P_{a,b,tp}$)	$\Delta P_{a,b,tp} = G_{r,b,tp}^2 * \left(\rho_{v,b}^{-1} - \rho_{l,b}^{-1}\right) * \Delta x$	$\Delta P_{a,b,tp} = 40.92^2 * (146.9^{-1} - 942^{-1}) * 1$	9.625	9.621	Pa
Gravitational Pressure Drop ($\Delta P_{g,b,tp}$)	$\Delta P_{g,b,tp} = \rho_{eq,b} * g * L_{b,tp}$	$\Delta P_{g,b,tp} = 254.1 * 9.78 * 0.1792$	445.5	445.3	Pa
Total Pressure Drop Total Pressure Drop ($\Delta P_{b,tp}$)	$\Delta P_{b,tp} = \Delta P_{f,b,tp} + \Delta P_{g,b,tp} + \Delta P_{a,b,tp}$	$\Delta P_{b,tp} = 1022 + 445.5 + 9.625$	1477	1477	Pa
Superheat Region					
Channel Heat Transfer ($\dot{Q}_{b,sh}$)	$\dot{Q}_{b,sh} = \dot{m}_{r,b} * (i_{pc,18} - i_{pc,17})$	$\dot{Q}_{b,sh} = 0.04616 * (297.3 - 280.8)$	0.7632	0.7616	kW

Parameter	Equation	Evaluated	EES Calc. Valve	Hand Calc. Value	Units
Temperature Difference 4 ($\Delta T_{4,b}$)	$\Delta T_{4,b} = T_{int,i} - T_{pc,18}$	$\Delta T_{4,b} = 94.3 - 88.09$	6.207	6.21	K
Log-Mean Temperature Difference ($LMTD_{b,sh}$)	$LMTD_{b,sh} = \frac{\Delta T_{4,b} - \Delta T_{3,b}}{\ln\left(\frac{\Delta T_{4,b}}{\Delta T_{3,b}}\right)}$	$LMTD_{b,sh} = \frac{6.207 - 15.18}{\ln\left(\frac{6.207}{15.18}\right)}$	10.03	10.03	K
Overall Conductance ($UA_{b,sh}$)	$\dot{Q}_{b,sh} = UA_{b,sh} * LMTD_{b,sh}$	$0.7632 = UA_{b,sh} * 10.03$	0.07605	0.07609	kW K^{-1}
Water-Side Reynolds Number ($Re_{w,b,sh}$)	$Re_{w,b,sh} = \frac{4 * \dot{m}_{w,b}}{P_b * \mu_{w,b}}$	$Re_{w,b,sh} = \frac{4 * 0.1918}{0.8816 * 0.0005625}$	1547	1547	-
Water-Side Heat Transfer Coefficient ($h_{w,b,sh}$)	$h_{w,b,sc} = 0.44 * \left(\frac{6\beta}{\pi}\right)^{0.38} * Re_{w,b,sh}^{0.5} * Pr_{w,b}^{1/3} * \frac{k_{w,b}}{D_{h,b}}$	$h_{w,b,sc} = 0.44 * \left(\frac{6 * 1.047}{\pi}\right)^{0.38} * 1547^{0.5} * 4.526^{1/3} * \frac{0.0005029}{0.005118}$	3.661	3.660	kW K^{-1} m^{-2}
Water-Side Thermal Resistance ($R_{w,b,sh}$)	$R_{w,b,sh} = \left(h_{w,b,sh} * L_{b,sh} * W_{plate,b}\right)^{-1}$	$R_{w,b,sh} = (3.661 * 0.2332 * 0.4383)^{-1}$	2.673	2.672	K kW^{-1}

Parameter	Equation	Evaluated	EES Calc. Valve	Hand Calc. Value	Units
Refrigerant Reynolds Number ($Re_{r,b,sh}$)	$\mathrm{Re_{r,b,sh}} = \frac{4 * \dot{m}_{r,b}}{P_b * \mu_{r,l,b}}$	$\mathrm{Re_{r,b,sh}} = \frac{4 * 0.04616}{0.8816 * 0.00001574}$	13310	13306	-
Refrigerant Heat Transfer Coefficient ($h_{r,b,sh}$)	$\mathrm{h_{r,b,sh}} = 0.2267 * Re_{r,b,sh}^{0.631} * Pr_{r,b}^{1/3} * \frac{k_{r,b}}{D_{h,b}}$	$\mathrm{h_{r,b,sh}} = 0.2267 * 13310^{0.631} * 1.435^{1/3} * \frac{0.000021}{0.005118}$	0.42	0.42	kW K^{-1} m^{-2}
Refrigerant Thermal Resistance ($R_{r,b,sh}$)	$\mathrm{R_{r,b,sh}} = \left(h_{r,b,sh} * L_{b,sh} * W_{plate,b}\right)^{-1}$	$\mathrm{R_{r,b,sh}} = (0.42 * 0.2332 * 0.4383)^{-1}$	23.3	23.3	K kW^{-1}
Wall Thermal Resistance ($R_{plate,b,sh}$)	$\mathrm{R_{plate,b,sh}} = \frac{Pt}{K_{plate} * L_{b,sh} * W_{plate,b}}$	$\mathrm{R_{plate,b,sh}} = \frac{0.0005}{0.01512 * 0.2332 * 0.4383}$	0.3235	0.3235	K kW^{-1}
Overall Conductance ($UA_{b,sh}$)	$UA_{b,sh} = \left[\left(\mathrm{R_{r,b,sh}} + \mathrm{R_{plate,b,sh}} + \mathrm{R_{w,b,sh}}\right)/2\right]^{-1}$	$UA_{b,sh} = [(23.3 + 0.3235 + 2.673)/2]^{-1}$	0.07605	0.07606	kW K^{-1}
Gravitational Pressure Drop ($\Delta P_{g,b,sh}$)	$\Delta \mathrm{P_{g,b,sh}} = \rho_{r,b,sh} * g * \mathrm{L_{b,sh}}$	$\Delta \mathrm{P_{g,b,sh}} = 146.7 * 9.78 * 0.2332$	334.7	334.6	Pa
Velocity ($u_{b,sh}$)	$u_{b,sh} = \frac{\dot{m}_{r,b}}{\rho_{r,b,sh} * A_{cs,b}}$	$u_{b,sh} = \frac{0.04616}{146.7 * 0.001128}$	0.2789	0.2790	m s^{-1}

Parameter	Equation	Evaluated	EES Calc. Valve	Hand Calc. Value	Units
Friction Factor ($f_{b,sh}$)	$f_{b,sh} = 0.6857 * Re_{r,b,sh}^{-0.172}$	$f_{b,sh} = 0.6857 * 13310^{-0.172}$	0.1339	0.1339	-
Frictional Pressure Drop ($\Delta P_{f,b,sh}$)	$\Delta P_{f,b,sh} = \frac{2 * f_{b,sh} * \rho_{r,b,sh} * u_{b,sh}^2 * L_{b,sh}}{D_{h,b}}$	$\Delta P_{f,b,sh} = \frac{2 * 0.1339 * 146.7 * 0.2789^2 * 0.233}{0.005118}$	139.3	139.1	Pa
Total Pressure Drop ($\Delta P_{b,sh}$)	$\Delta P_{b,sh} = \Delta P_{f,b,sh} + \Delta P_{g,b,sh}$	$\Delta P_{b,sh} = 139.3 + 334.7$	473.9	474	Pa

Table A-7: Power cycle condenser heat exchanger sizing model hand calculations

Parameter	Equation	Evaluated	EES Calc. Valve	Hand Calc. Value	Units
Wetted Perimeter (P_{pcc})	$P_{pcc} = 2 * (Ps + W_{plate,pcc})$	$P_{pcc} = 2 * (0.002574 + 0.4483)$	0.9016	0.9017	m
Cross-Sectional Area ($A_{cs,pcc}$)	$A_{cs,pcc} = Ps * W_{plate,pcc}$	$A_{cs,pcc} = 0.002574 * 0.4483$	0.001154	0.001154	m^2
Hydraulic Diameter ($D_{h,pcc}$)	$D_{h,pcc} = \frac{4 * A_{cs,pcc}}{P_{pcc}}$	$D_{h,pcc} = \frac{4 * 0.001154}{0.9016}$	0.005119	0.005120	m

Parameter	Equation	Evaluated	EES Calc. Valve	Hand Calc. Value	Units
Refrigerant Channel Mass Flow Rate ($\dot{m}_{r,pcc}$)	$\dot{m}_{r,pcc} = \frac{2 * \dot{m}_{pc}}{N_{plates,pcc}}$	$\dot{m}_{r,pcc} = \frac{2 * 4.52}{177}$	0.05108	0.05107	kg s^{-1}
Water Channel Mass Flow Rate ($\dot{m}_{w,pcc}$)	$\dot{m}_{w,pcc} = \frac{2 * \dot{m}_{cond}}{N_{plates,pcc}}$	$\dot{m}_{w,pcc} = \frac{2 * 32.38}{177}$	0.3658	0.3659	kg s^{-1}
Superheated Region					
Channel Heat Transfer ($\dot{Q}_{pcc,sh}$)	$\dot{Q}_{pcc,sh} = \dot{m}_{r,pcc} * (i_{pc,5} - i_{pc,6})$	$\dot{Q}_{b,sh} = 0.05108 * (275.4 - 270.2)$	0.2637	0.2656	kW
Temperature Difference 1 ($\Delta T_{1,pcc}$)	$\Delta T_{1,pcc} = T_{pc,5} - T_{cond,o}$	$\Delta T_{1,pcc} = 42.33 - 35$	7.328	7.330	K
Temperature Difference 2 ($\Delta T_{2,b}$)	$\Delta T_{2,pcc} = T_{pc,6} - T_{cond,v}$	$\Delta T_{4,pcc} = 37.66 - 34.82$	2.841	2.840	K
Log-Mean Temperature Difference ($LMTD_{pcc,sh}$)	$LMTD_{pcc,sh} = \frac{\Delta T_{2,pcc} - \Delta T_{1,pcc}}{\ln\left(\frac{\Delta T_{2,pcc}}{\Delta T_{1,pcc}}\right)}$	$LMTD_{pcc,sh} = \frac{2.841 - 7.328}{\ln\left(\frac{2.841}{7.328}\right)}$	4.736	4.735	K

Parameter	Equation	Evaluated	EES Calc. Valve	Hand Calc. Value	Units
Overall Conductance ($UA_{pcc,sh}$)	$\dot{Q}_{pcc,sh} = UA_{pcc,sh} * LMTD_{pcc,sh}$	$0.2637 = UA_{pcc,sh} * 4.736$	0.05569	0.05568	kW K^{-1}
Water-Side Reynolds Number ($Re_{w,pcc,sh}$)	$Re_{w,pcc,sh} = \frac{4 * \dot{m}_{w,pcc}}{P_{pcc} * \mu_{w,pcc}}$	$Re_{w,pcc,sh} = \frac{4 * 0.3658}{0.9016 * 0.0007666}$	2117	2117	-
Water-Side Heat Transfer Coefficient ($h_{w,pcc,sh}$)	$h_{w,pcc,sc} = 0.44 * \left(\frac{6\beta}{\pi}\right)^{0.38} * Re_{w,pcc,sh}^{0.5} * Pr_{w,pcc}^{1/3} * \frac{k_{w,pcc}}{D_{h,pcc}}$	$h_{w,pcc,sc} = 0.44 * \left(\frac{6 * 1.047}{\pi}\right)^{0.38} * 2117^{0.5} * 4.964^{1/3} * \frac{0.0006191}{0.005119}$	5.436	5.435	kW K^{-1} m^{-2}
Water-Side Thermal Resistance ($R_{w,pcc,sh}$)	$R_{w,pcc,sh} = (h_{w,pcc,sh} * L_{pcc,sh} * W_{plate,pcc})^{-1}$	$R_{w,pcc,sh} = (5.436 * 0.2025 * 0.4483)^{-1}$	2.027	2.026	K kW^{-1}
Refrigerant Reynolds Number ($Re_{r,pcc,sh}$)	$Re_{r,pcc,sh} = \frac{4 * \dot{m}_{r,pcc}}{P_{pcc} * \mu_{r,l,pcc}}$	$Re_{r,pcc,sh} = \frac{4 * 0.05108}{0.9016 * 0.00001273}$	17797	17802	-
Refrigerant Heat Transfer Coefficient ($h_{r,pcc,sh}$)	$h_{r,pcc,sh} = 0.2267 * Re_{r,pcc,sh}^{0.631} * Pr_{r,pcc}^{1/3} * \frac{k_{r,pcc}}{D_{h,pcc}}$	$h_{r,pcc,sh} = 0.2267 * 17797^{0.631} * 0.8614^{1/3} * \frac{0.00001617}{0.005119}$	0.3276	0.3276	kW K^{-1} m^{-2}

Parameter	Equation	Evaluated	EES Calc. Valve	Hand Calc. Value	Units
Refrigerant Thermal Resistance ($R_{r,pcc,sh}$)	$R_{r,pcc,sh} = \left(h_{r,pcc,sh} * L_{pcc,sh} * W_{plate,pcc}\right)^{-1}$	$R_{r,pcc,sh} = (0.3276 * 0.2025 * 0.4483)^{-1}$	33.63	33.63	K kW^{-1}
Wall Thermal Resistance ($R_{plate,pcc,sh}$)	$R_{plate,pcc,sh} = \frac{Pt}{K_{plate} * L_{pcc,sh} * W_{plate,pcc}}$	$R_{plate,pcc,sh} = \frac{0.0005}{0.02185 * 0.2025 * 0.4483}$	0.2521	0.2521	K kW^{-1}
Overall Conductance ($UA_{pcc,sh}$)	$UA_{pcc,sh} = \left[\left(R_{r,pcc,sh} + R_{plate,pcc,sh} + R_{w,pcc,sh}\right)/2\right]^{-1}$	$UA_{pcc,sh} = [(33.63 + 0.2521 + 2.027)/2]^{-1}$	0.05569	0.05570	kW K^{-1}
Gravitational Pressure Drop ($\Delta P_{g,pcc,sh}$)	$\Delta P_{g,pcc,sh} = \rho_{r,pcc,sh} * g * L_{pcc,sh}$	$\Delta P_{g,pcc,sh} = 45.44 * 9.78 * 0.2025$	89.99	89.99	Pa
Velocity ($u_{pcc,sh}$)	$u_{pcc,sh} = \frac{\dot{m}_{r,pcc}}{\rho_{r,pcc,sh} * A_{cs,pcc}}$	$u_{pcc,sh} = \frac{0.05108}{45.44 * 0.001154}$	0.9741	0.9741	m s^{-1}
Friction Factor ($f_{pcc,sh}$)	$f_{pcc,sh} = 0.6857 * Re_{r,pcc,sh}^{-0.172}$	$f_{pcc,sh} = 0.6857 * 17797^{-0.172}$	0.1274	0.1274	-
Frictional Pressure Drop ($\Delta P_{f,pcc,sh}$)	$\Delta P_{f,pcc,sh} = \frac{2 * f_{pcc,sh} * \rho_{r,pcc,sh} * u_{pcc,sh}^2 * L_{pcc,sh}}{D_{h,pcc}}$	$\Delta P_{f,pcc,sh} = 2 * 0.1274 * 45.44 * 0.9741^2 * 0.2025/0.005119$	434.6	434.6	Pa
Total Pressure Drop ($\Delta P_{pcc,sh}$)	$\Delta P_{pcc,sh} = \Delta P_{f,pcc,sh} - \Delta P_{g,pcc,sh}$	$\Delta P_{pcc,sh} = 434.6 - 89.99$	344.6	344.6	Pa
Two-Phase Region					

Parameter	Equation	Evaluated	EES Calc. Valve	Hand Calc. Value	Units
Channel Heat Transfer ($\dot{Q}_{pcc,tp}$)	$\dot{Q}_{pcc,tp} = \dot{m}_{r,pcc} * (i_{pc,6} - i_{pc,7})$	$\dot{Q}_{pcc,tp} = 0.05108 * (270.2 - 104.8)$	8.45	8.45	kW
Temperature Difference 3 ($\Delta T_{3,pcc}$)	$\Delta T_{3,pcc} = T_{cond,l} - T_{pc,7}$	$\Delta T_{3,pcc} = 37.68 - 29.05$	8.624	8.63	K
Log-Mean Temperature Difference ($LMTD_{pcc,tp}$)	$LMTD_{pcc,tp} = \frac{\Delta T_{3,pcc} - \Delta T_{2,pcc}}{\ln\left(\frac{\Delta T_{3,pcc}}{\Delta T_{2,pcc}}\right)}$	$LMTD_{pcc,tp} = \frac{8.624 - 2.841}{\ln\left(\frac{8.624}{2.841}\right)}$	5.208	5.208	K
Overall Conductance ($UA_{pcc,tp}$)	$\dot{Q}_{pcc,tp} = UA_{pcc,tp} * LMTD_{pcc,tp}$	$8.45 = UA_{pcc,tp} * 5.208$	1.622	1.623	kW K^{-1}
Water-Side Reynolds Number ($Re_{w,pcc,tp}$)	$Re_{w,pcc,tp} = \frac{4 * \dot{m}_{w,pcc}}{P_{pcc} * \mu_{w,pcc}}$	$Re_{w,pcc,tp} = \frac{4 * 0.3658}{0.9016 * 0.0008127}$	1997	1997	-
Water-Side Heat Transfer Coefficient ($h_{w,pcc,tp}$)	$h_{w,pcc,tp} = 0.44 * \left(\frac{6\beta}{\pi}\right)^{0.38} * Re_{w,pcc,tp}^{0.5} * Pr_{w,pcc}^{1/3} * \frac{k_{w,pcc}}{D_{h,pcc}}$	$h_{w,pcc,tp} = 0.44 * \left(\frac{6 * 1.047}{\pi}\right)^{0.38} * 1997^{0.5} * 5.299^{1/3} * \frac{0.0006144}{0.005119}$	5.355	5.354	kW K^{-1} m^{-2}

Parameter	Equation	Evaluated	EES Calc. Valve	Hand Calc. Value	Units
Water-Side Thermal Resistance ($R_{w,pcc,tp}$)	$R_{w,pcc,tp} = \left(h_{w,pcc,tp} * L_{pcc,tp} * W_{plate,pcc}\right)^{-1}$	$R_{w,pcc,tp} = (5.355 * 1.111 * 0.4483)^{-1}$	0.3748	0.3749	K kW^{-1}
Refrigerant Mass Flux ($G_{r,pcc,tp}$)	$G_{r,pcc,tp} = \frac{\dot{m}_{r,pcc}}{A_{cs,pcc}}$	$G_{r,pcc,tp} = \frac{0.05108}{0.001154}$	44.27	44.26	kg s^{-1} m^{-2}
Equivalent Mass Flux ($G_{eq,pcc}$)	$G_{eq,pcc} = G_{r,pcc,tp} * \left[1 - x_m + x_m * \left(\frac{\rho_{l,pcc}}{\rho_{v,pcc}}\right)^{0.5}\right]$	$G_{eq,pcc} = 44.27 * \left[1 - 0.5 + 0.5 * \left(\frac{1157}{46.89}\right)^{0.5}\right]$	132.1	132.1	kg s^{-1} m^{-2}
Equivalent Reynolds Number ($Re_{eq,pcc}$)	$Re_{eq,pcc} = \frac{G_{eq,pcc} * D_{h,pcc}}{\mu_{l,pcc}}$	$Re_{eq,pcc} = \frac{132.1 * 0.005119}{0.000166}$	4072	4074	-
Refrigerant Heat Transfer Coefficient ($h_{r,pcc,tp}$)	$h_{r,pcc,tp} = 4.118 * Re_{eq,pcc}^{0.4} * Pr_{w,pcc}^{1/3} * \frac{k_{r,pcc}}{D_{h,pcc}}$	$h_{r,pcc,tp} = 4.118 * 4072^{0.4} * 3.205^{1/3} * \frac{0.00007692}{0.005119}$	2.536	2.536	kW K^{-1} m^{-2}
Refrigerant Thermal	$R_{r,pcc,tp} = \left(h_{r,pcc,tp} * L_{pcc,tp} * W_{plate,pcc}\right)^{-1}$	$R_{r,pcc,tp} = (2.536 * 1.111 * 0.4483)^{-1}$	0.7915	0.7917	K kW^{-1}

Parameter	Equation	Evaluated	EES Calc. Valve	Hand Calc. Value	Units
Resistance ($R_{r,pcc,tp}$)					
Wall Thermal Resistance ($R_{plate,pcc,tp}$)	$R_{plate,pcc,tp} = \frac{Pt}{K_{plate} * L_{pcc,tp} * W_{plate,pcc}}$	$R_{plate,pcc,tp} = \frac{0.0005}{0.01512 * 1.111 * 0.4483}$	0.06636	0.0640	K kW^{-1}
Overall Conductance ($UA_{pcc,tp}$)	$UA_{pcc,tp} = [(R_{r,pcc,tp} + R_{plate,pcc,tp} + R_{w,pcc,tp})/2]^{-1}$	$UA_{pcc,tp} = [(0.7915 + 0.06636 + 0.3748)/2]^{-1}$	1.622	1.623	kW K^{-1}
Refrigerant Reynolds Number ($Re_{r,pcc,tp}$)	$Re_{r,pcc,tp} = \frac{4 * \dot{m}_{r,pcc}}{P_{pcc} * \mu_{r,l,pcc}}$	$Re_{r,pcc,tp} = \frac{4 * 0.05108}{0.9016 * 0.000166}$	1365	1365	-
Refrigerant Heat Flux ($q_{r,pcc,tp}$)	$q_{r,pcc,tp} = \frac{\dot{Q}_{pcc,tp}}{L_{pcc,tp,fixed} * W_{plate,pcc}}$	$q_{r,pcc,tp} = \frac{8.45}{0.669 * 0.4483}$	28.18	28.17	kW m^{-2}
Boiling Number (Bo_{pcc})	$Bo_{pcc} = \frac{q_{r,pcc,tp}}{G_{r,pcc,tp} * i_{fg,pcc}}$	$Bo_{pcc} = \frac{28.18}{44.27 * 165.5}$	0.003847	0.003846	-
Equivalent Specific Density ($\rho_{eq,pcc}$)	$\rho_{eq,pcc} = \left(x_m * \left(\frac{1}{\rho_{v,pcc}} - \frac{1}{\rho_{l,pcc}}\right) + \frac{1}{\rho_{l,pcc}}\right)^{-1}$	$\rho_{eq,pcc} = \left(0.5 * \left(\frac{1}{46.89} - \frac{1}{1157}\right) + \frac{1}{1157}\right)^{-1}$	90.13	90.13	kg m^{-3}

Parameter	Equation	Evaluated	EES Calc. Valve	Hand Calc. Value	Units
Friction Factor ($f_{pcc,tp}$)	$f_{pcc,tp} = 94.75 * \left(Re_{eq,pcc}\right)^{-0.0467} * Re_{pcc,tp}^{-0.4} * Bo_{pcc}^{0.5} * P_{r,pcc}{}^{0.8}$	$f_{pcc,tp} = 94.75 * (4072)^{-0.0467} * 1365^{-0.4} * 0.003847^{0.5} * 0.2352^{0.8}$	0.06978	0.6977	-
Frictional Pressure Drop ($\Delta P_{f,pcc,tp}$)	$\Delta P_{f,pcc,tp} = \frac{2 * f_{pcc,tp} * G_{r,pcc,tp}^2 * L_{pcc,tp}}{\rho_{eq,pcc} * D_{h,pcc}}$	$\Delta P_{f,pcc,tp} = \frac{2 * 0.06978 * 44.27^2 * 1.111}{90.13 * 0.005119}$	658.8	658.6	Pa
Acceleration Pressure Drop ($\Delta P_{a,pcc,tp}$)	$\Delta P_{a,pcc,tp} = G_{r,pcc,tp}^2 * \left(\rho_{v,pcc}^{-1} - \rho_{l,pcc}^{-1}\right) * \Delta x$	$\Delta P_{a,pcc,tp} = 44.27^2 * (46.89^{-1} - 1157^{-1}) * 1$	40.09	40.10	Pa
Gravitational Pressure Drop ($\Delta P_{g,pcc,tp}$)	$\Delta P_{g,pcc,tp} = \rho_{eq,pcc} * g * L_{pcc,tp}$	$\Delta P_{g,pcc,tp} = 90.13 * 9.78 * 1.111$	979.8	979.3	Pa
Total Pressure Drop Total Pressure Drop ($\Delta P_{pcc,tp}$)	$\Delta P_{pcc,tp} = \Delta P_{f,pcc,tp} - \Delta P_{g,pcc,tp} - \Delta P_{a,pcc,tp}$	$\Delta P_{pcc,tp} = 658.8 - 40.09 - 979.8$	-361.1	-361.1	Pa
Subcooled Region					
Channel Heat Transfer ($\dot{Q}_{pcc,sc}$)	$\dot{Q}_{pcc,sc} = \dot{m}_{r,pcc} * (i_{pc,7} - i_{pc,8})$	$\dot{Q}_{pcc,sc} = 0.05108 * (104.8 - 103.3)$	0.07571	0.07662	kW

Parameter	Equation	Evaluated	EES Calc. Valve	Hand Calc. Value	Units
Temperature Difference 4 ($\Delta T_{4,pcc}$)	$\Delta T_{4,pcc} = T_{pc,8} - T_{cond,i}$	$\Delta T_{4,pcc} = 36.68 - 29$	7.675	7.680	K
Log-Mean Temperature Difference ($LMTD_{pcc,sc}$)	$LMTD_{pcc,sc} = \frac{\Delta T_{4,pcc} - \Delta T_{3,pcc}}{\ln\left(\frac{\Delta T_{4,pcc}}{\Delta T_{3,pcc}}\right)}$	$LMTD_{pcc,sc} = \frac{7.675 - 8.624}{\ln\left(\frac{7.675}{8.624}\right)}$	8.14	8.14	K
Overall Conductance ($UA_{pcc,sc}$)	$\dot{Q}_{pcc,sc} = UA_{pcc,sc} * LMTD_{pcc,sc}$	$0.07571 = UA_{pcc,sc} * 8.14$	0.0093	0.0093	kW K^{-1}
Water-Side Reynolds Number ($Re_{w,pcc,sc}$)	$Re_{w,pcc,sc} = \frac{4 * \dot{m}_{w,pcc}}{P_{pcc} * \mu_{w,pcc}}$	$Re_{w,pcc,sc} = \frac{4 * 0.3658}{0.9016 * 0.0008624}$	1882	1882	-
Water-Side Heat Transfer Coefficient ($h_{w,pcc,sc}$)	$h_{w,pcc,sc} = 0.44 * \left(\frac{6\beta}{\pi}\right)^{0.38} * Re_{w,pcc,sc}^{0.5} * Pr_{w,pcc}^{1/3} * \frac{k_{w,pcc}}{D_{h,pcc}}$	$h_{w,pcc,sc} = 0.44 * \left(\frac{6 * 1.047}{\pi}\right)^{0.38} * 1882^{0.5} * 5.663^{1/3} * \frac{0.0006098}{0.005119}$	5.275	5.274	kW K^{-1} m^{-2}
Water-Side Thermal Resistance ($R_{w,pcc,sc}$)	$R_{w,pcc,sc} = \left(h_{w,pcc,sc} * L_{pcc,sc} * W_{plate,pcc}\right)^{-1}$	$R_{w,pcc,sc} = (5.275 * 0.02403 * 0.4483)^{-1}$	17.6	17.6	K kW^{-1}

Parameter	Equation	Evaluated	EES Calc. Valve	Hand Calc. Value	Units
Refrigerant Reynolds Number ($Re_{r,pcc,sc}$)	$Re_{r,pcc,sc} = \frac{4 * \dot{m}_{r,pcc}}{P_{pcc} * \mu_{r,l,pcc}}$	$Re_{r,pcc,sc} = \frac{4 * 0.05108}{0.9016 * 0.0001682}$	1347	1347	-
Refrigerant Heat Transfer Coefficient ($h_{r,pcc,sc}$)	$h_{r,pcc,sc} = 0.2267 * Re_{r,pcc,sc}^{0.631} * Pr_{r,pcc}^{1/3} * \frac{k_{r,pcc}}{D_{h,pcc}}$	$h_{r,pcc,sc} = 0.2267 * 1347^{0.631} * 3.212^{1/3} * \frac{0.00007746}{0.005119}$	0.4775	0.4774	kW K^{-1} m^{-2}
Refrigerant Thermal Resistance ($R_{r,pcc,sc}$)	$R_{r,pcc,sc} = (h_{r,pcc,sc} * L_{pcc,sc} * W_{plate,pcc})^{-1}$	$R_{r,pcc,sc} = (0.4775 * 0.02403 * 0.4483)^{-1}$	194.4	194.4	K kW^{-1}
Wall Thermal Resistance ($R_{plate,pcc,sc}$)	$R_{plate,pcc,sc} = \frac{Pt}{K_{plate} * L_{pcc,sc} * W_{plate,pcc}}$	$R_{plate,pcc,sc} = \frac{0.0005}{0.01512 * 0.02403 * 0.4483}$	3.069	3.070	K kW^{-1}
Overall Conductance ($UA_{pcc,sc}$)	$UA_{pcc,sc} = [(R_{r,pcc,sc} + R_{plate,pcc,sc} + R_{w,pcc,sc})/2]^{-1}$	$UA_{pcc,sc} = [(194.4 + 3.069 + 17.6)/2]^{-1}$	0.0093	0.0093	kW K^{-1}
Gravitational Pressure Drop ($\Delta P_{g,pcc,sc}$)	$\Delta P_{g,pcc,sc} = \rho_{r,pcc,sc} * g * L_{pcc,sc}$	$\Delta P_{g,pcc,sc} = 1161 * 9.78 * 0.02403$	272.9	272.9	Pa
Velocity ($u_{pcc,sc}$)	$u_{pcc,sc} = \frac{\dot{m}_{r,pcc}}{\rho_{r,pcc,sc} * A_{cs,pcc}}$	$u_{pcc,sc} = \frac{0.05108}{1161 * 0.001154}$	0.03813	0.03813	m s^{-1}

Parameter	Equation	Evaluated	EES Calc. Valve	Hand Calc. Value	Units
Friction Factor ($f_{pcc,sc}$)	$f_{pcc,sc} = 0.6857 * Re_{r,pcc,sc}^{-0.172}$	$f_{pcc,sc} = 0.6857 * 1347^{-0.172}$	0.1985	0.1986	-
Frictional Pressure Drop ($\Delta P_{f,pcc,sc}$)	$\Delta P_{f,pcc,sc} = \frac{2 * f_{pcc,sc} * \rho_{r,pcc,sc} * u_{pcc,sc}^2 * L_{pcc,sc}}{D_{h,pcc}}$	$\Delta P_{f,pcc,sc} = 2 * 0.1985 * 1161 * 0.03813^2 * 0.02403/0.005119$	3.148	3.146	Pa
Total Pressure Drop ($\Delta P_{pcc,sc}$)	$\Delta P_{pcc,sc} = \Delta P_{f,pcc,sc} - \Delta P_{g,pcc,sc}$	$\Delta P_{pcc,sc} = 3.148 - 272.9$	-269.7	-269.8	Pa

Table A-8: Evaporator heat exchanger sizing model hand calculations

Parameter	Equation	Evaluated	EES Calc. Valve	Hand Calc. Value	Units
Wetted Perimeter (P_{ch})	$P_{ch} = 2 * (Ps + W_{plate,ch})$	$P_{ch} = 2 * (0.002574 + 0.322)$	0.6491	0.6491	m
Cross-Sectional Area ($A_{cs,ch}$)	$A_{cs,ch} = Ps * W_{plate,ch}$	$A_{cs,ch} = 0.002574 * 0.322$	0.0008288	0.0008288	m^2
Hydraulic Diameter ($D_{h,ch}$)	$D_{h,ch} = \frac{4 * A_{cs,ch}}{P_{ch}}$	$D_{h,ch} = \frac{4 * 0.0008288}{0.6491}$	0.5107	0.5107	m

Parameter	Equation	Evaluated	EES Calc. Valve	Hand Calc. Value	Units
Refrigerant Channel Mass Flow Rate ($\dot{m}_{r,ch}$)	$\dot{m}_{r,ch} = \frac{2 * \dot{m}_{cc}}{N_{plates,ch}}$	$\dot{m}_{r,ch} = \frac{2 * 4.051}{528.7}$	0.01532	0.01532	kg s^{-1}
Water Channel Mass Flow Rate ($\dot{m}_{w,ch}$)	$\dot{m}_{w,ch} = \frac{2 * \dot{m}_{chill}}{N_{plates,ch}}$	$\dot{m}_{w,ch} = \frac{2 * 34.67}{528.7}$	0.1312	0.1312	kg s^{-1}
Two-Phase Region					
Channel Heat Transfer ($\dot{Q}_{ch,tp}$)	$\dot{Q}_{ch,tp} = \dot{m}_{r,ch} * (i_{cc,14} - i_{pc,13})$	$\dot{Q}_{ch,sh} = 0.01532 * (252.4 - 79.41)$	2.651	2.650	kW
Temperature Difference 1 ($\Delta T_{1,ch}$)	$\Delta T_{1,ch} = T_{ch,o} - T_{cc,13}$	$\Delta T_{1,ch} = 5.56 - 4.504$	1.056	1.056	K
Temperature Difference 2 ($\Delta T_{2,ch}$)	$\Delta T_{2,ch} = T_{ch,v} - T_{pc,14}$	$\Delta T_{2,ch} = 10.37 - 3.369$	7.004	7.001	K
Log-Mean Temperature Difference ($LMTD_{ch,tp}$)	$LMTD_{ch,tp} = \frac{\Delta T_{2,ch} - \Delta T_{1,ch}}{\ln\left(\frac{\Delta T_{2,ch}}{\Delta T_{1,ch}}\right)}$	$LMTD_{ch,tp} = \frac{7.004 - 1.056}{\ln\left(\frac{7.004}{1.056}\right)}$	3.144	3.144	K

Parameter	Equation	Evaluated	EES Calc. Valve	Hand Calc. Value	Units
Overall Conductance ($UA_{ch,tp}$)	$\dot{Q}_{ch,tp} = UA_{ch,tp} * LMTD_{ch,tp}$	$2.651 = UA_{ch,tp} * 3.144$	0.8432	0.8432	kW K^{-1}
Water-Side Reynolds Number ($Re_{w,ch,tp}$)	$Re_{w,ch,tp} = \frac{4 * \dot{m}_{w,ch}}{P_{ch} * \mu_{w,ch}}$	$Re_{w,ch,tp} = \frac{4 * 0.1312}{0.6491 * 0.001403}$	576.1	576.3	-
Water-Side Heat Transfer Coefficient ($h_{w,ch,tp}$)	$h_{w,ch,tp} = 0.44 * \left(\frac{6\beta}{\pi}\right)^{0.38} * Re_{w,ch,tp}^{0.5} * Pr_{w,ch}^{1/3} * \frac{k_{w,ch}}{D_{h,ch}}$	$h_{w,ch,tp} = 0.44 * \left(\frac{6 * 1.047}{\pi}\right)^{0.38} * 576.1^{0.5} * 10.21^{1/3} * \frac{0.0005771}{0.005107}$	3.369	3.369	kW K^{-1} m^{-2}
Water-Side Thermal Resistance ($R_{w,ch,tp}$)	$R_{w,ch,tp} = \left(h_{w,ch,tp} * L_{ch,tp} * W_{plate,ch}\right)^{-1}$	$R_{w,ch,tp} = (3.369 * 0.6165 * 0.322)^{-1}$	1.495	1.495	K kW^{-1}
Refrigerant Reynolds Number ($Re_{r,ch,tp}$)	$Re_{r,ch,tp} = \frac{4 * \dot{m}_{r,ch}}{P_{ch} * \mu_{r,l,ch}}$	$Re_{r,ch,tp} = \frac{4 * 0.01532}{0.6491 * 0.0002508}$	376.5	376.4	-
Refrigerant Mass Flux ($G_{r,ch,tp}$)	$G_{r,ch,tp} = \frac{\dot{m}_{r,ch}}{A_{cs,ch}}$	$G_{r,ch,tp} = \frac{0.01532}{0.0008288}$	18.49	18.48	kg s^{-1} m^{-2}

Parameter	Equation	Evaluated	EES Calc. Valve	Hand Calc. Value	Units
Refrigerant Heat Flux ($q_{r,ch,tp}$)	$q_{r,ch,tp} = \frac{\dot{Q}_{ch,tp}}{L_{ch,tp,fixed} * W_{plate,ch}}$	$q_{r,ch,tp} = \frac{2.651}{0.5056 * 0.322}$	16.28	16.28	kW m^{-2}
Martinelli Parameter ($X_{tt,ch}$)	$X_{tt,ch} = \left(\frac{1 - x_m}{x_m}\right)^{0.9} * \left(\frac{\rho_{r,v,ch}}{\rho_{r,l,ch}}\right)^{0.5} * \left(\frac{\mu_{l,ch}}{\mu_{v,ch}}\right)^{0.1}$	$X_{tt,ch} = \left(\frac{1 - 0.555}{0.555}\right)^{0.9} * \left(\frac{16.86}{1280}\right)^{0.5} * \left(\frac{0.0002508}{0.0000111}\right)^{0.1}$	0.1285	0.1285	-
Boiling Number (Bo_{ch})	$Bo_{ch} = \frac{q_{r,ch,tp}}{G_{r,ch,tp} * i_{fg,ch}}$	$Bo_{ch} = \frac{16.28}{18.49 * 195.1}$	0.004541	0.004513	-
Liquid Heat Transfer Coefficient ($h_{l,ch,tp}$)	$h_{l,ch,tp} = 0.023 * Re_{l,ch,tp}^{0.8} * Pr_{r,ch}^{0.4} * \frac{k_{r,ch}}{D_{h,ch}}$	$h_{l,ch,tp} = 0.023 * 376.5^{0.8} * 3.663^{0.4} * \frac{0.00009267}{0.005107}$	0.08066	0.08066	kW K^{-1} m^{-2}
Pool Boiling Heat Transfer Coefficient ($h_{pool,ch}$)	$h_{pool,ch} = \left(55 * P_{r,ch}^{0.12} * M_{ch}{}^{-0.5} * \left(q_{r,ch,tp} * 1000\right)^{0.67}\right) /1000$	$h_{pool,ch} = (55 * 0.08473^{0.12} * 102^{-0.5} * (16.28 * 1000)^{0.67}) /1000$	2.687	2.687	kW K^{-1} m^{-2}
Enhancement Factor (E_{ch})	$E_{ch} = 1 + 24000 * Bo_{ch}^{1.16} + 1.37 * \left(X_{tt,ch}\right)^{-0.86}$	$E_{ch} = 1 + 24000 * 0.004541^{1.16} + 1.37 * (0.1285)^{-0.86}$	54.65	54.97	-
Suppression Factor (S_{ch})	$S_{ch} = \left(1 + 1.15 * 10^{-6} * E_{ch}^2 * Re_{r,ch,tp}^{1.17}\right)^{-1}$	$S_{ch} = (1 + 1.15 * 10^{-6} * 54.65^2 * 376.5^{1.17})^{-1}$	0.9988	0.9988	-

Parameter	Equation	Evaluated	EES Calc. Valve	Hand Calc. Value	Units
Refrigerant Heat Transfer Coefficient ($h_{r,ch,tp}$)	$h_{r,ch,tp} = E_{ch} * h_{l,ch,tp} + S_{ch} * h_{pool,ch}$	$h_{r,ch,tp} = 54.65 * 0.08066 + 0.9988 * 2.687$	7.092	7.092	kW K^{-1} m^{-2}
Refrigerant Thermal Resistance ($R_{r,ch,tp}$)	$R_{r,ch,tp} = \left(h_{r,ch,tp} * L_{ch,tp} * W_{plate,ch}\right)^{-1}$	$R_{r,ch,tp} = (7.092 * 0.6165 * 0.322)^{-1}$	0.7103	0.7103	K kW^{-1}
Wall Thermal Resistance ($R_{plate,ch,tp}$)	$R_{plate,ch,tp} = \frac{Pt}{K_{plate} * L_{ch,tp} * W_{plate,ch}}$	$R_{plate,ch,tp} = \frac{0.0005}{0.01512 * 0.6165 * 0.322}$	0.1665	0.1666	K kW^{-1}
Overall Conductance ($UA_{ch,tp}$)	$UA_{ch,tp} = \left[\left(R_{r,ch,tp} + R_{plate,ch,tp} + R_{w,ch,tp}\right)/2\right]^{-1}$	$UA_{ch,tp} = [(0.7103 + 0.1665 + 1.495)/2]^{-1}$	0.8432	0.8432	kW K^{-1}
Equivalent Mass Flux ($G_{eq,ch}$)	$G_{eq,ch} = G_{r,ch,tp} * \left[1 - x_m + x_m * \left(\frac{\rho_{l,ch}}{\rho_{v,ch}}\right)^{0.5}\right]$	$G_{eq,ch} = 18.49 * \left[1 - 0.5 + 0.5 * \left(\frac{1280}{16.86}\right)^{0.5}\right]$	97.63	97.64	kg s^{-1} m^{-2}
Equivalent Reynolds Number ($Re_{eq,ch}$)	$Re_{eq,ch} = \frac{G_{eq,ch} * D_{h,ch}}{\mu_{l,ch}}$	$Re_{eq,ch} = \frac{97.63 * 0.005107}{0.0002508}$	1988	1988	-

Parameter	Equation	Evaluated	EES Calc. Valve	Hand Calc. Value	Units
Equivalent Specific Density ($\rho_{eq,ch}$)	$\rho_{eq,ch} = \left(x_m * \left(\frac{1}{\rho_{v,ch}} - \frac{1}{\rho_{l,ch}}\right) + \frac{1}{\rho_{l,ch}}\right)^{-1}$	$\rho_{eq,ch} = \left(0.5 * \left(\frac{1}{16.86} - \frac{1}{1280}\right) + \frac{1}{1280}\right)^{-1}$	30.06	30.06	kg m^{-3}
Friction Factor ($f_{ch,tp}$)	$f_{ch,tp} = 23820 * \left(Re_{eq,ch}\right)^{-1.12}$	$f_{ch,tp} = 23820 * (1988)^{-1.12}$	4.815	4.816	-
Frictional Pressure Drop ($\Delta P_{f,ch,tp}$)	$\Delta P_{f,ch,tp} = \frac{2 * f_{ch,tp} * G_{r,ch,tp}^2 * L_{ch,tp}}{\rho_{eq,ch} * D_{h,ch}}$	$\Delta P_{f,ch,tp} = \frac{2 * 4.815 * 18.49^2 * 0.6165}{30.06 * 0.005107}$	13221	13221	Pa
Acceleration Pressure Drop ($\Delta P_{a,ch,tp}$)	$\Delta P_{a,ch,tp} = G_{r,ch,tp}^2 * \left(\rho_{v,ch}^{-1} - \rho_{l,ch}^{-1}\right) * \Delta x$	$\Delta P_{a,ch,tp} = 18.49^2 * (16.86^{-1} - 1280^{-1}) * 0.8899$	17.81	17.81	Pa
Gravitational Pressure Drop ($\Delta P_{g,ch,tp}$)	$\Delta P_{g,ch,tp} = \rho_{eq,ch} * g * L_{ch,tp}$	$\Delta P_{g,ch,tp} = 30.06 * 9.78 * 0.6165$	181.2	181.2	Pa
Total Pressure Drop Total Pressure Drop ($\Delta P_{ch,tp}$)	$\Delta P_{ch,tp} = \Delta P_{f,ch,tp} + \Delta P_{g,ch,tp} + \Delta P_{a,ch,tp}$	$\Delta P_{ch,tp} = 13221 + 181.2 + 17.81$	13420	13420	Pa
Superheat Region					
Channel Heat Transfer ($\dot{Q}_{ch,sh}$)	$\dot{Q}_{ch,sh} = \dot{m}_{r,ch} * (i_{cc,15} - i_{pc,14})$	$\dot{Q}_{ch,sh} = 0.01532 * (253 - 252.4)$	0.009823	0.009192	kW

Parameter	Equation	Evaluated	EES Calc. Valve	Hand Calc. Value	Units
Temperature Difference 3 ($\Delta T_{3,ch}$)	$\Delta T_{3,ch} = T_{chill,i} - T_{cc,15}$	$\Delta T_{3,ch} = 10.39 - 4.071$	6.319	6.319	K
Log-Mean Temperature Difference ($LMTD_{ch,sh}$)	$LMTD_{b,sh} = \frac{\Delta T_{3,ch} - \Delta T_{2,ch}}{\ln\left(\frac{\Delta T_{3,ch}}{\Delta T_{2,ch}}\right)}$	$LMTD_{ch,sh} = \frac{6.319 - 7.004}{\ln\left(\frac{6.319}{7.004}\right)}$	6.656	6.656	K
Overall Conductance ($UA_{ch,sh}$)	$\dot{Q}_{ch,sh} = UA_{ch,sh} * LMTD_{ch,sh}$	$0.009823 = UA_{ch,sh} * 6.656$	0.001476		kW K^{-1}
Water-Side Reynolds Number ($Re_{w,ch,sh}$)	$Re_{w,ch,sh} = \frac{4 * \dot{m}_{w,ch}}{P_{ch} * \mu_{w,ch}}$	$Re_{w,ch,sh} = \frac{4 * 0.1312}{0.6491 * 0.001306}$	618.7	619.1	-
Water-Side Heat Transfer Coefficient ($h_{w,ch,sh}$)	$h_{w,ch,sc} = 0.44 * \left(\frac{6\beta}{\pi}\right)^{0.38} * Re_{w,ch,sh}^{0.5} * Pr_{w,ch}^{1/3} * \frac{k_{w,ch}}{D_{h,ch}}$	$h_{w,ch,sc} = 0.44 * \left(\frac{6 * 1.047}{\pi}\right)^{0.38} * 618.7^{0.5} * 9.423^{1/3} * \frac{0.0005817}{0.005107}$	3.427	3.426	kW K^{-1} m^{-2}
Water-Side Thermal Resistance ($R_{w,ch,sh}$)	$R_{w,ch,sh} = \left(h_{w,ch,sh} * L_{ch,sh} * W_{plate,ch}\right)^{-1}$	$R_{w,ch,sh} = (3.427 * 0.01546 * 0.322)^{-1}$	58.62	58.62	K kW^{-1}

Parameter	Equation	Evaluated	EES Calc. Valve	Hand Calc. Value	Units
Refrigerant Reynolds Number ($Re_{r,ch,sh}$)	$Re_{r,ch,sh} = \frac{4 * \dot{m}_{r,ch}}{P_{ch} * \mu_{r,l,ch}}$	$Re_{r,ch,sh} = \frac{4 * 0.01532}{0.6491 * 0.00001105}$	8544	8543	-
Refrigerant Heat Transfer Coefficient ($h_{r,ch,sh}$)	$h_{r,ch,sh} = 0.2267 * Re_{r,ch,sh}^{0.631} * Pr_{r,ch}^{1/3} * \frac{k_{r,ch}}{D_{h,ch}}$	$h_{r,ch,sh} = 0.2267 * 8544^{0.631} * 0.8118^{1/3} * \frac{0.00001243}{0.005107}$	0.1557	0.1558	kW K^{-1} m^{-2}
Refrigerant Thermal Resistance ($R_{r,ch,sh}$)	$R_{r,ch,sh} = \left(h_{r,ch,sh} * L_{ch,sh} * W_{plate,ch}\right)^{-1}$	$R_{r,ch,sh} = (0.1557 * 0.01546 * 0.322)^{-1}$	1290	1290	K kW^{-1}
Wall Thermal Resistance ($R_{plate,ch,sh}$)	$R_{plate,ch,sh} = \frac{Pt}{K_{plate} * L_{ch,sh} * W_{plate,ch}}$	$R_{plate,ch,sh} = \frac{0.0005}{0.01512 * 0.01546 * 0.322}$	6.641	6.643	K kW^{-1}
Overall Conductance ($UA_{ch,sh}$)	$UA_{ch,sh} = \left[\left(R_{r,ch,sh} + R_{plate,ch,sh} + R_{w,ch,sh}\right)/2\right]^{-1}$	$UA_{ch,sh} = [(1290 + 6.641 + 58.62)/2]^{-1}$	0.001476	0.001476	kW K^{-1}
Gravitational Pressure Drop ($\Delta P_{g,ch,sh}$)	$\Delta P_{g,ch,sh} = \rho_{r,ch,sh} * g * L_{ch,sh}$	$\Delta P_{g,ch,sh} = 16.22 * 9.78 * 0.01546$	2.453	2.452	Pa
Velocity ($u_{ch,sh}$)	$u_{ch,sh} = \frac{\dot{m}_{r,ch}}{\rho_{r,ch,sh} * A_{cs,ch}}$	$u_{ch,sh} = \frac{0.01532}{16.22 * 0.0008288}$	1.14	1.14	m s^{-1}

Parameter	Equation	Evaluated	EES Calc. Valve	Hand Calc. Value	Units
Friction Factor ($f_{ch,sh}$)	$f_{ch,sh} = 0.6857 * Re_{r,ch,sh}^{-0.172}$	$f_{ch,sh} = 0.6857 * 8544^{-0.172}$	0.1445	0.1445	-
Frictional Pressure Drop ($\Delta P_{f,ch,sh}$)	$\Delta P_{f,ch,sh} = \frac{2 * f_{ch,sh} * \rho_{r,ch,sh} * u_{ch,sh}^2 * L_{ch,sh}}{D_{h,ch}}$	$\Delta P_{f,ch,sh} = 2 * 0.1445 * 16.22 * 1.14^2 * 0.01546/0.005107$	18.44	18.44	Pa
Total Pressure Drop ($\Delta P_{ch,sh}$)	$\Delta P_{ch,sh} = \Delta P_{f,ch,sh} + \Delta P_{g,ch,sh}$	$\Delta P_{ch,sh} = 18.44 + 2.453$	20.89	20.89	Pa

Table A-9: Cooling cycle condenser heat exchanger sizing model hand calculations

Parameter	Equation	Evaluated	EES Calc. Valve	Hand Calc. Value	Units
Wetted Perimeter (P_{ccc})	$P_{ccc} = 2 * (Ps + W_{plate,pcc})$	$P_{ccc} = 2 * (0.002574 + 0.4483)$	0.9016	0.9017	m
Cross-Sectional Area ($A_{cs,ccc}$)	$A_{cs,ccc} = Ps * W_{plate,ccc}$	$A_{cs,ccc} = 0.002574 * 0.4483$	0.001154	0.001154	m^2
Hydraulic Diameter ($D_{h,ccc}$)	$D_{h,ccc} = \frac{4 * A_{cs,ccc}}{P_{ccc}}$	$D_{h,ccc} = \frac{4 * 0.001154}{0.9016}$	0.005119	0.005120	m

Parameter	Equation	Evaluated	EES Calc. Valve	Hand Calc. Value	Units
Refrigerant Channel Mass Flow Rate ($\dot{m}_{r,ccc}$)	$\dot{m}_{r,ccc} = \frac{2 * \dot{m}_{cc}}{N_{plates,ccc}}$	$\dot{m}_{r,ccc} = \frac{2 * 4.051}{314}$	0.0258	0.0258	kg s^{-1}
Water Channel Mass Flow Rate ($\dot{m}_{w,ccc}$)	$\dot{m}_{w,ccc} = \frac{2 * \dot{m}_{cond,cc}}{N_{plates,ccc}}$	$\dot{m}_{w,ccc} = \frac{2 * 30.93}{314}$	0.197	0.197	kg s^{-1}
Superheated Region					
Channel Heat Transfer ($\dot{Q}_{ccc,sh}$)	$\dot{Q}_{ccc,sh} = \dot{m}_{r,ccc} * (i_{cc,5} - i_{cc,6})$	$\dot{Q}_{ccc,sh} = 0.0258 * (284.8 - 269.6)$	0.3924	0.3922	kW
Temperature Difference 1 ($\Delta T_{1,ccc}$)	$\Delta T_{1,pcc} = T_{cc,5} - T_{cond,o}$	$\Delta T_{1,ccc} = 50.46 - 35$	15.46	15.46	K
Temperature Difference 2 ($\Delta T_{2,ccc}$)	$\Delta T_{2,ccc} = T_{cc,6} - T_{cond,cc,v}$	$\Delta T_{2,ccc} = 36.32 - 34.5$	1.816	1.820	K
Log-Mean Temperature Difference ($LMTD_{ccc,sh}$)	$LMTD_{ccc,sh} = \frac{\Delta T_{2,ccc} - \Delta T_{1,ccc}}{\ln\left(\frac{\Delta T_{2,ccc}}{\Delta T_{1,ccc}}\right)}$	$LMTD_{ccc,sh} = \frac{1.816 - 15.46}{\ln\left(\frac{1.816}{15.46}\right)}$	6.373	6.371	K

Parameter	Equation	Evaluated	EES Calc. Valve	Hand Calc. Value	Units
Overall Conductance ($UA_{ccc,sh}$)	$\dot{Q}_{ccc,sh} = UA_{ccc,sh} * LMTD_{ccc,sh}$	$0.3924 = UA_{ccc,sh} * 6.373$	0.06157	0.06157	kW K^{-1}
Water-Side Reynolds Number ($Re_{w,ccc,sh}$)	$Re_{w,ccc,sh} = \frac{4 * \dot{m}_{w,ccc}}{P_{ccc} * \mu_{w,ccc}}$	$Re_{w,ccc,sh} = \frac{4 * 0.197}{0.9016 * 0.0007666}$	1140	1141	-
Water-Side Heat Transfer Coefficient ($h_{w,ccc,sh}$)	$h_{w,ccc,sc} = 0.44 * \left(\frac{6\beta}{\pi}\right)^{0.38} * Re_{w,ccc,sh}^{0.5} * Pr_{w,ccc}^{1/3} * \frac{k_{w,ccc}}{D_{h,ccc}}$	$h_{w,ccc,sc} = 0.44 * \left(\frac{6 * 1.047}{\pi}\right)^{0.38} * 1140^{0.5} * 4.964^{1/3} * \frac{0.0006191}{0.005119}$	3.989	3.988	kW K^{-1} m^{-2}
Water-Side Thermal Resistance ($R_{w,ccc,sh}$)	$R_{w,ccc,sh} = (h_{w,ccc,sh} * L_{ccc,sh} * W_{plate,ccc})^{-1}$	$R_{w,ccc,sh} = (3.989 * 0.3414 * 0.4483)^{-1}$	1.638	1.638	K kW^{-1}
Refrigerant Reynolds Number ($Re_{r,ccc,sh}$)	$Re_{r,ccc,sh} = \frac{4 * \dot{m}_{r,ccc}}{P_{ccc} * \mu_{r,l,ccc}}$	$Re_{r,ccc,sh} = \frac{4 * 0.0258}{0.9016 * 0.00001301}$	8796	8798	-
Refrigerant Heat Transfer Coefficient ($h_{r,ccc,sh}$)	$h_{r,ccc,sh} = 0.2267 * Re_{r,ccc,sh}^{0.631} * Pr_{r,ccc}^{1/3} * \frac{k_{r,ccc}}{D_{h,ccc}}$	$h_{r,ccc,sh} = 0.2267 * 8796^{0.631} * 0.8205^{1/3} * \frac{0.00001665}{0.005119}$	0.2128	0.2128	kW K^{-1} m^{-2}

Parameter	Equation	Evaluated	EES Calc. Valve	Hand Calc. Value	Units
Refrigerant Thermal Resistance ($R_{r,ccc,sh}$)	$R_{r,ccc,sh} = \left(h_{r,ccc,sh} * L_{ccc,sh} * W_{plate,ccc}\right)^{-1}$	$R_{r,ccc,sh} = (0.2128 * 0.3414 * 0.4483)^{-1}$	30.7	30.7	K kW^{-1}
Wall Thermal Resistance ($R_{plate,ccc,sh}$)	$R_{plate,ccc,sh} = \frac{Pt}{K_{plate} * L_{ccc,sh} * W_{plate,ccc}}$	$R_{plate,ccc,sh} = \frac{0.0005}{0.02185 * 0.3414 * 0.4483}$	0.1495	0.1495	K kW^{-1}
Overall Conductance ($UA_{ccc,sh}$)	$UA_{ccc,sh} = \left[\left(R_{r,ccc,sh} + R_{plate,ccc,sh} + R_{w,ccc,sh}\right)/2\right]^{-1}$	$UA_{ccc,sh} = [(30.7 + 0.1495 + 1.638)/2]^{-1}$	0.06157	0.06156	kW K^{-1}
Gravitational Pressure Drop ($\Delta P_{g,ccc,sh}$)	$\Delta P_{g,ccc,sh} = \rho_{r,ccc,sh} * g * L_{ccc,sh}$	$\Delta P_{g,ccc,sh} = 41.32 * 9.78 * 0.3414$	138	138	Pa
Velocity ($u_{ccc,sh}$)	$u_{ccc,sh} = \frac{\dot{m}_{r,ccc}}{\rho_{r,ccc,sh} * A_{cs,ccc}}$	$u_{ccc,sh} = \frac{0.0258}{41.32 * 0.001154}$	0.5412	0.5411	m s^{-1}
Friction Factor ($f_{ccc,sh}$)	$f_{ccc,sh} = 0.6857 * Re_{r,ccc,sh}^{-0.172}$	$f_{ccc,sh} = 0.6857 * 8796^{-0.172}$	0.1438	0.1438	-
Frictional Pressure Drop ($\Delta P_{f,ccc,sh}$)	$\Delta P_{f,ccc,sh} = \frac{2 * f_{ccc,sh} * \rho_{r,ccc,sh} * u_{ccc,sh}^2 * L_{ccc,sh}}{D_{h,ccc}}$	$\Delta P_{f,ccc,sh} = 2 * 0.1438 * 41.32 * 0.5412^2 * 0.3414/0.005119$	232.1	232.1	Pa
Total Pressure Drop ($\Delta P_{ccc,sh}$)	$\Delta P_{ccc,sh} = \Delta P_{f,ccc,sh} - \Delta P_{g,ccc,sh}$	$\Delta P_{ccc,sh} = 232.1 - 138$	94.15	94.1	Pa
Two-Phase Region					

Parameter	Equation	Evaluated	EES Calc. Valve	Hand Calc. Value	Units
Channel Heat Transfer ($\dot{Q}_{ccc,tp}$)	$\dot{Q}_{ccc,tp} = \dot{m}_{r,ccc} * (i_{cc,6} - i_{cc,7})$	$\dot{Q}_{ccc,tp} = 0.0258 * (269.6 - 102.8)$	4.303	4.303	kW
Temperature Difference 3 ($\Delta T_{3,ccc}$)	$\Delta T_{3,ccc} = T_{cc,7} - T_{cond,cc,l}$	$\Delta T_{3,ccc} = 36.35 - 29.05$	7.298	7.3	K
Log-Mean Temperature Difference ($LMTD_{ccc,tp}$)	$LMTD_{ccc,tp} = \frac{\Delta T_{3,ccc} - \Delta T_{2,ccc}}{\ln\left(\frac{\Delta T_{3,ccc}}{\Delta T_{2,ccc}}\right)}$	$LMTD_{ccc,tp} = \frac{7.298 - 1.818}{\ln\left(\frac{7.298}{1.818}\right)}$	3.943	3.943	K
Overall Conductance ($UA_{ccc,tp}$)	$\dot{Q}_{ccc,tp} = UA_{ccc,tp} * LMTD_{ccc,tp}$	$4.303 = UA_{ccc,tp} * 3.943$	0.1091	1.091	kW K^{-1}
Water-Side Reynolds Number ($Re_{w,ccc,tp}$)	$Re_{w,ccc,tp} = \frac{4 * \dot{m}_{w,ccc}}{P_{ccc} * \mu_{w,ccc}}$	$Re_{w,ccc,tp} = \frac{4 * 0.197}{0.9016 * 0.0008153}$	1072	1072	-
Water-Side Heat Transfer Coefficient ($h_{w,ccc,tp}$)	$h_{w,ccc,tp} = 0.44 * \left(\frac{6\beta}{\pi}\right)^{0.38} * Re_{w,ccc,tp}^{0.5} * Pr_{w,ccc}^{1/3} * \frac{k_{w,ccc}}{D_{h,ccc}}$	$h_{w,ccc,tp} = 0.44 * \left(\frac{6 * 1.047}{\pi}\right)^{0.38} * 1072^{0.5} * 5.318^{1/3} * \frac{0.0006142}{0.005119}$	3.927	3.926	kW K^{-1} m^{-2}

Parameter	Equation	Evaluated	EES Calc. Valve	Hand Calc. Value	Units
Water-Side Thermal Resistance ($R_{w,ccc,tp}$)	$R_{w,ccc,tp} = \left(h_{w,ccc,tp} * L_{ccc,tp} * W_{plate,ccc}\right)^{-1}$	$R_{w,ccc,tp} = (3.927 * 0.9746 * 0.4483)^{-1}$	0.5829	0.5828	K kW^{-1}
Refrigerant Mass Flux ($G_{r,ccc,tp}$)	$G_{r,ccc,tp} = \frac{\dot{m}_{r,ccc}}{A_{cs,ccc}}$	$G_{r,ccc,tp} = \frac{0.0258}{0.001154}$	22.36	22.36	kg s^{-1} m^{-2}
Equivalent Mass Flux ($G_{eq,ccc}$)	$G_{eq,ccc} = G_{r,ccc,tp} * \left[1 - x_m + x_m * \left(\frac{\rho_{l,ccc}}{\rho_{v,ccc}}\right)^{0.5}\right]$	$G_{eq,ccc} = 22.36 * \left[1 - 0.5 + 0.5 * \left(\frac{1162}{45.13}\right)^{0.5}\right]$	67.91	67.91	kg s^{-1} m^{-2}
Equivalent Reynolds Number ($Re_{eq,ccc}$)	$Re_{eq,ccc} = \frac{G_{eq,ccc} * D_{h,ccc}}{\mu_{l,ccc}}$	$Re_{eq,ccc} = \frac{67.91 * 0.005119}{0.0001688}$	2060	2059	-
Refrigerant Heat Transfer Coefficient ($h_{r,ccc,tp}$)	$h_{r,ccc,tp} = 4.118 * Re_{eq,ccc}^{0.4} * Pr_{w,ccc}^{1/3} * \frac{k_{r,ccc}}{D_{h,ccc}}$	$h_{r,ccc,tp} = 4.118 * 2060^{0.4} * 3.215^{1/3} * \frac{0.0000776}{0.005119}$	1.95	1.95	kW K^{-1} m^{-2}
Refrigerant Thermal	$R_{r,ccc,tp} = \left(h_{r,ccc,tp} * L_{ccc,tp} * W_{plate,ccc}\right)^{-1}$	$R_{r,ccc,tp} = (1.95 * 0.9746 * 0.4483)^{-1}$	1.174	1.174	K kW^{-1}

Parameter	Equation	Evaluated	EES Calc. Valve	Hand Calc. Value	Units
Resistance ($R_{r,ccc,tp}$)					
Wall Thermal Resistance ($R_{plate,ccc,tp}$)	$R_{plate,ccc,tp} = \frac{Pt}{K_{plate} * L_{ccc,tp} * W_{plate,ccc}}$	$R_{plate,ccc,tp} = \frac{0.0005}{0.01512 * 0.9746 * 0.4483}$	0.07568	0.07569	K kW^{-1}
Overall Conductance ($UA_{ccc,tp}$)	$UA_{ccc,tp} = \left[\left(R_{r,ccc,tp} + R_{plate,ccc,tp} + R_{w,ccc,tp}\right)/2\right]^{-1}$	$UA_{ccc,tp} = [(1.174 + 0.07568 + 0.5829)/2]^{-1}$	1.091	1.091	kW K^{-1}
Refrigerant Reynolds Number ($Re_{r,ccc,tp}$)	$Re_{r,ccc,tp} = \frac{4 * \dot{m}_{r,ccc}}{P_{ccc} * \mu_{r,l,ccc}}$	$Re_{r,ccc,tp} = \frac{4 * 0.0258}{0.9016 * 0.0001688}$	678.1	678.1	-
Refrigerant Heat Flux ($q_{r,ccc,tp}$)	$q_{r,ccc,tp} = \frac{\dot{Q}_{ccc,tp}}{L_{ccc,tp,fixed} * W_{plate,ccc}}$	$q_{r,ccc,tp} = \frac{4.303}{0.669 * 0.4483}$	14.35	14.35	kW m^{-2}
Boiling Number (Bo_{ccc})	$Bo_{ccc} = \frac{q_{r,ccc,tp}}{G_{r,ccc,tp} * i_{fg,ccc}}$	$Bo_{ccc} = \frac{14.35}{22.36 * 166.8}$	0.003847	0.003848	-
Equivalent Specific Density ($\rho_{eq,ccc}$)	$\rho_{eq,ccc} = \left(x_m * \left(\frac{1}{\rho_{v,ccc}} - \frac{1}{\rho_{l,ccc}}\right) + \frac{1}{\rho_{l,ccc}}\right)^{-1}$	$\rho_{eq,ccc} = \left(0.5 * \left(\frac{1}{45.13} - \frac{1}{1162}\right) + \frac{1}{1162}\right)^{-1}$	86.89	86.89	kg m^{-3}

Parameter	Equation	Evaluated	EES Calc. Valve	Hand Calc. Value	Units
Friction Factor ($f_{ccc,tp}$)	$f_{ccc,tp} = 94.75 * \left(Re_{eq,ccc}\right)^{-0.0467} * Re_{ccc,tp}^{-0.4} * Bo_{ccc}^{0.5} * P_{r,ccc}{}^{0.8}$	$f_{ccc,tp} = 94.75 * (2060)^{-0.0467} * 678.1^{-0.4} * 0.003847^{0.5} * 0.2268^{0.8}$	0.09254	0.09241	-
Frictional Pressure Drop ($\Delta P_{f,ccc,tp}$)	$\Delta P_{f,ccc,tp} = \frac{2 * f_{ccc,tp} * G_{r,ccc,tp}^2 * L_{ccc,tp}}{\rho_{eq,ccc} * D_{h,ccc}}$	$\Delta P_{f,ccc,tp} = \frac{2 * 0.09254 * 22.36^2 * 0.9746}{86.89 * 0.005119}$	202.8	202.8	Pa
Acceleration Pressure Drop ($\Delta P_{a,ccc,tp}$)	$\Delta P_{a,ccc,tp} = G_{r,ccc,tp}^2 * \left(\rho_{v,ccc}^{-1} - \rho_{l,ccc}^{-1}\right) * \Delta x$	$\Delta P_{a,ccc,tp} = 22.36^2 * (45.13^{-1} - 1162^{-1}) * 1$	10.65	10.65	Pa
Gravitational Pressure Drop ($\Delta P_{g,ccc,tp}$)	$\Delta P_{g,ccc,tp} = \rho_{eq,ccc} * g * L_{ccc,tp}$	$\Delta P_{g,ccc,tp} = 86.89 * 9.78 * 0.9746$	828.2	828.2	Pa
Total Pressure Drop Total Pressure Drop ($\Delta P_{ccc,tp}$)	$\Delta P_{ccc,tp} = \Delta P_{f,ccc,tp} + \Delta P_{g,ccc,tp} + \Delta P_{a,ccc,tp}$	$\Delta P_{ccc,tp} = 202.8 - 828.2 - 10.65$	-636.1	-636.1	Pa
Subcooled Region					
Channel Heat Transfer ($\dot{Q}_{ccc,sc}$)	$\dot{Q}_{ccc,sc} = \dot{m}_{r,ccc} * (i_{cc,7} - i_{cc,8})$	$\dot{Q}_{ccc,sc} = 0.0258 * (102.8 - 101.4)$	0.03806	0.03612	kW

Parameter	Equation	Evaluated	EES Calc. Valve	Hand Calc. Value	Units
Temperature Difference 4 ($\Delta T_{4,ccc}$)	$\Delta T_{4,ccc} = T_{cc,8} - T_{cond,cc,i}$	$\Delta T_{4,ccc} = 35.35 - 29$	6.347	6.35	K
Log-Mean Temperature Difference ($LMTD_{ccc,sc}$)	$LMTD_{ccc,sc} = \frac{\Delta T_{4,ccc} - \Delta T_{4,ccc}}{\ln\left(\frac{\Delta T_{4,ccc}}{\Delta T_{4,ccc}}\right)}$	$LMTD_{ccc,sc} = \frac{6.347 - 7.298}{\ln\left(\frac{6.347}{7.298}\right)}$	6.811	6.811	K
Overall Conductance ($UA_{ccc,sc}$)	$\dot{Q}_{ccc,sc} = UA_{ccc,sc} * LMTD_{ccc,sc}$	$0.03806 = UA_{ccc,sc} * 6.811$	0.005587	0.005588	kW K^{-1}
Water-Side Reynolds Number ($Re_{w,ccc,sc}$)	$Re_{w,ccc,sc} = \frac{4 * \dot{m}_{w,ccc}}{P_{ccc} * \mu_{w,ccc}}$	$Re_{w,ccc,sc} = \frac{4 * 0.197}{0.9016 * 0.0008624}$	1013	1013	-
Water-Side Heat Transfer Coefficient ($h_{w,ccc,sc}$)	$h_{w,ccc,sc} = 0.44 * \left(\frac{6\beta}{\pi}\right)^{0.38} * Re_{w,ccc,sc}^{0.5} * Pr_{w,ccc}^{1/3} * \frac{k_{w,ccc}}{D_{h,ccc}}$	$h_{w,ccc,sc} = 0.44 * \left(\frac{6 * 1.047}{\pi}\right)^{0.38} * 1013^{0.5} * 5.663^{1/3} * \frac{0.0006098}{0.005119}$	3.871	3.869	kW K^{-1} m^{-2}
Water-Side Thermal Resistance ($R_{w,ccc,sc}$)	$R_{w,ccc,sc} = (h_{w,ccc,sc} * L_{ccc,sc} * W_{plate,ccc})^{-1}$	$R_{w,ccc,sc} = (3.871 * 0.02191 * 0.4483)^{-1}$	26.3	26.3	K kW^{-1}

Parameter	Equation	Evaluated	EES Calc. Valve	Hand Calc. Value	Units
Refrigerant Reynolds Number ($Re_{r,ccc,sc}$)	$Re_{r,ccc,sc} = \frac{4 * \dot{m}_{r,ccc}}{P_{ccc} * \mu_{r,l,ccc}}$	$Re_{r,ccc,sc} = \frac{4 * 0.0258}{0.9016 * 0.000171}$	669.3	669.4	-
Refrigerant Heat Transfer Coefficient ($h_{r,ccc,sc}$)	$h_{r,ccc,sc} = 0.2267 * Re_{r,ccc,sc}^{0.631} * Pr_{r,ccc}^{1/3} * \frac{k_{r,ccc}}{D_{h,ccc}}$	$h_{r,ccc,sc} = 0.2267 * 669.3^{0.631} * 3.222^{1/3} * \frac{0.00007814}{0.005119}$	0.3101	0.3101	kW K^{-1} m^{-2}
Refrigerant Thermal Resistance ($R_{r,ccc,sc}$)	$R_{r,ccc,sc} = (h_{r,ccc,sc} * L_{ccc,sc} * W_{plate,ccc})^{-1}$	$R_{r,ccc,sc} = (0.3101 * 0.02191 * 0.4483)^{-1}$	328.3	328.3	K kW^{-1}
Wall Thermal Resistance ($R_{plate,ccc,sc}$)	$R_{plate,ccc,sc} = \frac{Pt}{K_{plate} * L_{pcc,sc} * W_{plate,pcc}}$	$R_{plate,ccc,sc} = \frac{0.0005}{0.01512 * 0.02191 * 0.4483}$	3.366	3.367	K kW^{-1}
Overall Conductance ($UA_{ccc,sc}$)	$UA_{ccc,sc} = [(R_{r,ccc,sc} + R_{plate,ccc,sc} + R_{w,ccc,sc})/2]^{-1}$	$UA_{ccc,sc} = [(328.3 + 3.366 + 26.3)/2]^{-1}$	0.005587	0.005587	kW K^{-1}
Gravitational Pressure Drop ($\Delta P_{g,ccc,sc}$)	$\Delta P_{g,ccc,sc} = \rho_{r,ccc,sc} * g * L_{ccc,sc}$	$\Delta P_{g,ccc,sc} = 1166 * 9.78 * 0.02191$	250	250	Pa
Velocity ($u_{ccc,sc}$)	$u_{ccc,sc} = \frac{\dot{m}_{r,ccc}}{\rho_{r,ccc,sc} * A_{cs,ccc}}$	$u_{ccc,sc} = \frac{0.0258}{1166 * 0.001154}$	0.01917	0.01917	m s^{-1}

Parameter	Equation	Evaluated	EES Calc. Valve	Hand Calc. Value	Units
Friction Factor ($f_{ccc,sc}$)	$f_{ccc,sc} = 0.6857 * Re_{r,ccc,sc}^{-0.172}$	$f_{ccc,sc} = 0.6857 * 669.3^{-0.172}$	0.2239	0.2239	-
Frictional Pressure Drop ($\Delta P_{f,ccc,sc}$)	$\Delta P_{f,ccc,sc} = \frac{2 * f_{ccc,sc} * \rho_{r,ccc,sc} * u_{ccc,sc}^2 * L_{ccc,sc}}{D_{h,ccc}}$	$\Delta P_{f,ccc,sc} = 2 * 0.2239 * 1166 * 0.01917^2 * 0.02191/0.005119$	0.8221	0.8213	Pa
Total Pressure Drop ($\Delta P_{ccc,sc}$)	$\Delta P_{ccc,sc} = \Delta P_{f,ccc,sc} + \Delta P_{g,ccc,sc}$	$\Delta P_{ccc,sc} = 0.8221 - 250$	-249.1	-249.2	Pa

Table A-10: Recuperator heat exchanger sizing model hand calculations

Parameter	Equation	Evaluated	EES Calc. Valve	Hand Calc. Value	Units
Wetted Perimeter (P_{re})	$P_{re} = 2 * (Ps + W_{plate,re})$	$P_{re} = 2 * (0.002574 + 0.322)$	0.6491	0.6491	m
Cross-Sectional Area ($A_{cs,re}$)	$A_{cs,re} = Ps * W_{plate,re}$	$A_{cs,re} = 0.002574 * 0.322$	0.0008288	0.0008288	m^2
Hydraulic Diameter ($D_{h,re}$)	$D_{h,re} = \frac{4 * A_{cs,re}}{P_{re}}$	$D_{h,re} = \frac{4 * 0.0008288}{0.6491}$	0.005107	0.005107	m

Parameter	Equation	Evaluated	EES Calc. Valve	Hand Calc. Value	Units
Hot Side Channel Mass Flow Rate ($\dot{m}_{re,h}$)	$\dot{m}_{re,h} = \frac{2 * \dot{m}_{pc}}{N_{plates,re}}$	$\dot{m}_{re,h} = \frac{2 * 4.52}{116.8}$	0.07739	0.0740	kg s^{-1}
Cold Side Channel Mass Flow Rate ($\dot{m}_{re,c}$)	$\dot{m}_{re,c} = \frac{2 * \dot{m}_{pc}}{N_{plates,re}}$	$\dot{m}_{re,c} = \frac{2 * 4.52}{116.8}$	0.07739	0.0740	kg s^{-1}
Channel Heat Transfer ($\dot{Q}_{re}$)	$\dot{Q}_{re} = \dot{m}_{re,h} * (i_{pc,3} - i_{pc,4})$	$\dot{Q}_{re,h} = 0.07739 * (281.3 - 275.4)$	0.4546	0.4566	kW
Temperature Difference 1 ($\Delta T_{1,re}$)	$\Delta T_{1,re} = T_{pc,3} - T_{pc.12}$	$\Delta T_{1,re} = 47.9 - 43.44$	4.456	4.46	K
Temperature Difference 2 ($\Delta T_{2,re}$)	$\Delta T_{2,re} = T_{pc,4} - T_{pc,11}$	$\Delta T_{2,re} = 42.35 - 39.47$	2.884	2.88	K
Log-Mean Temperature Difference ($LMTD_{re}$)	$LMTD_{re} = \frac{\Delta T_{2,re} - \Delta T_{1,re}}{\ln\left(\frac{\Delta T_{2,re}}{\Delta T_{1,re}}\right)}$	$LMTD_{re} = \frac{4.456 - 2.884}{\ln\left(\frac{4.456}{2.884}\right)}$	3.613	3.613	K
Overall Conductance (UA_{re})	$\dot{Q}_{re} = UA_{re} * LMTD_{re}$	$0.4546 = UA_{re} * 3.613$	0.1258	0.1258	kW K^{-1}

Parameter	Equation	Evaluated	EES Calc. Valve	Hand Calc. Value	Units
Hot-Side					
Hot Side Reynolds Number ($Re_{re,h}$)	$\mathrm{Re_{re,h}} = \frac{4 * \dot{m}_{re,h}}{P_{re} * \mu_{re,l,h}}$	$\mathrm{Re_{re,h}} = \frac{4 * 0.07739}{0.6491 * 0.00001294}$	36861	36855	-
Refrigerant Heat Transfer Coefficient ($h_{re,h}$)	$\mathrm{h_{re,h}} = 0.2267 * Re_{re,h}^{0.631} * Pr_{re,h}^{1/3} * \frac{k_{re,h}}{D_{h,re}}$	$\mathrm{h_{re,h}} = 0.2267 * 36861^{0.631} * 0.8385^{1/3} * \frac{0.00001654}{0.005107}$	0.527	0.527	kW K^{-1} m^{-2}
Refrigerant Thermal Resistance ($R_{re,h}$)	$\mathrm{R_{re,h}} = \left(h_{re,h} * L_{re} * W_{plate,re}\right)^{-1}$	$\mathrm{R_{re,h}} = (0.527 * 0.632 * 0.322)^{-1}$	9.324	9.324	K kW^{-1}
Gravitational Pressure Drop ($\Delta P_{g,re,h}$)	$\Delta \mathrm{P_{g,re,h}} = \rho_{re,h} * g * \mathrm{L_{re}}$	$\Delta \mathrm{P_{g,re,h}} = 44.27 * 9.78 * 0.632$	273.6	273.6	Pa
Velocity ($u_{re,h}$)	$u_{re,h} = \frac{\dot{m}_{re,h}}{\rho_{re,h} * A_{cs,re}}$	$u_{re,h} = \frac{0.07739}{44.27 * 0.0008288}$	2.109	2.109	m s^{-1}
Friction Factor ($f_{re,h}$)	$\mathrm{f_{re,h}} = 0.6857 * Re_{re,h}^{-0.172}$	$\mathrm{f_{re,h}} = 0.6857 * 36861^{-0.172}$	0.1124	0.1124	-
Frictional Pressure Drop ($\Delta P_{f,re,h}$)	$\Delta \mathrm{P_{f,re,h}} = \frac{2 * \mathrm{f_{re,h}} * \rho_{re,h} * \mathrm{u_{re,h}^2} * \mathrm{L_{re}}}{\mathrm{D_{h,re}}}$	$\Delta \mathrm{P_{f,re,h}} = 2 * 0.1124 * 44.27 * 2.109^2 * 0.632/0.005107$	5477	5478	Pa

Parameter	Equation	Evaluated	EES Calc. Valve	Hand Calc. Value	Units
Total Pressure Drop ($\Delta P_{re,h}$)	$\Delta P_{re,h} = \Delta P_{f,re,h} + \Delta P_{g,re,h}$	$\Delta P_{re,h} = 5477 + 273.6$	5751	5751	Pa
Cold Side					
Hot Side Reynolds Number ($Re_{re,c}$)	$Re_{re,c} = \frac{4 * \dot{m}_{re,c}}{P_{re} * \mu_{re,l,c}}$	$Re_{re,c} = \frac{4 * 0.07739}{0.6491 * 0.0001681}$	2837	2837	-
Refrigerant Heat Transfer Coefficient ($h_{re,c}$)	$h_{re,c} = 0.2267 * Re_{re,c}^{0.631} * Pr_{re,c}^{1/3} * \frac{k_{re,c}}{D_{h,re}}$	$h_{re,c} = 0.2267 * 2837^{0.631} * 3.163^{1/3} * \frac{0.00007796}{0.005107}$	0.7667	0.7667	kW K^{-1} m^{-2}
Refrigerant Thermal Resistance ($R_{re,c}$)	$R_{re,c} = \left(h_{re,c} * L_{re} * W_{plate,re}\right)^{-1}$	$R_{re,c} = (0.7667 * 0.632 * 0.322)^{-1}$	6.409	6.409	K kW^{-1}
Gravitational Pressure Drop ($\Delta P_{g,re,c}$)	$\Delta P_{g,re,c} = \rho_{re,c} * g * L_{re}$	$\Delta P_{g,re,c} = 1161 * 9.78 * 0.632$	7178	7176	Pa
Velocity ($u_{re,c}$)	$u_{re,c} = \frac{\dot{m}_{re,c}}{\rho_{re,c} * A_{cs,re}}$	$u_{re,c} = \frac{0.07739}{1161 * 0.0008288}$	0.08041	0.08043	m s^{-1}
Friction Factor ($f_{re,c}$)	$f_{re,c} = 0.6857 * Re_{re,c}^{-0.172}$	$f_{re,c} = 0.6857 * 2837^{-0.172}$	0.1747	0.1747	-

Parameter	Equation	Evaluated	EES Calc. Valve	Hand Calc. Value	Units
Frictional Pressure Drop ($\Delta P_{f,re,c}$)	$\Delta P_{f,re,c} = \frac{2 * f_{re,c} * \rho_{re,c} * u_{re,c}^2 * L_{re}}{D_{h,re}}$	$\Delta P_{f,re,c} = 2 * 0.1747 * 1161 * 0.08041^2 * 0.632/0.005107$	324.6	324.6	Pa
Total Pressure Drop ($\Delta P_{re,c}$)	$\Delta P_{re,c} = \Delta P_{f,re,c} + \Delta P_{g,re,c}$	$\Delta P_{re,c} = 7178 + 324.6$	7502	7503	Pa
Total					
Wall Thermal Resistance ($R_{plate,re}$)	$R_{plate,re} = \frac{Pt}{K_{plate} * L_{re} * W_{plate,re}}$	$R_{plate,re} = \frac{0.0005}{0.01512 * 0.632 * 0.322}$	0.1625	0.1625	K kW^{-1}
Overall Conductance (UA_{re})	$UA_{re} = \left[\left(R_{re,h} + R_{plate,re} + R_{w,re,c}\right)/2\right]^{-1}$	$UA_{re} = [(9.324 + 0.1625 + 6.409)/2]^{-1}$	0.1258	0.1258	kW K^{-1}

Table A-11: Economizer heat exchanger sizing model hand calculations

Parameter	Equation	Evaluated	EES Calc. Valve	Hand Calc. Value	Units
Wetted Perimeter (P_{ec})	$P_{ec} = 2 * (Ps + W_{plate,ec})$	$P_{re} = 2 * (0.002574 + 0.322)$	0.6491	0.6491	m

Parameter	Equation	Evaluated	EES Calc. Valve	Hand Calc. Value	Units
Cross-Sectional Area ($A_{cs,ec}$)	$A_{cs,ec} = Ps * W_{plate,ec}$	$A_{cs,re} = 0.002574 * 0.322$	0.0008288	0.0008288	m^2
Hydraulic Diameter ($D_{h,ec}$)	$D_{h,re} = \frac{4 * A_{cs,ec}}{P_{ec}}$	$D_{h,ec} = \frac{4 * 0.0008288}{0.6491}$	0.005107	0.005107	m
Hot Side Channel Mass Flow Rate ($\dot{m}_{ec,h}$)	$\dot{m}_{ec,h} = \frac{2 * \dot{m}_{cc}}{N_{plates,ec}}$	$\dot{m}_{ec,h} = \frac{2 * 4.051}{160.4}$	0.0505	0.0505	kg s^{-1}
Cold Side Channel Mass Flow Rate ($\dot{m}_{ec,c}$)	$\dot{m}_{ec,c} = \frac{2 * \dot{m}_{pc}}{N_{plates,ec}}$	$\dot{m}_{ec,c} = \frac{2 * 4.52}{160.4}$	0.05636	0.05636	kg s^{-1}
Channel Heat Transfer ($\dot{Q}_{ec}$)	$\dot{Q}_{ec} = \dot{m}_{ec,h} * (i_{cc,3} - i_{cc,4})$	$\dot{Q}_{ec,h} = 0.0505 * (305.8 - 284.8)$	1.057	1.061	kW
Temperature Difference 1 ($\Delta T_{1,ec}$)	$\Delta T_{1,ec} = T_{cc,3} - T_{pc.14}$	$\Delta T_{1,ec} = 70.74 - 55.7$	15.04	15.04	K
Temperature Difference 2 ($\Delta T_{2,ec}$)	$\Delta T_{2,ec} = T_{cc,4} - T_{pc,13}$	$\Delta T_{2,ec} = 50.48 - 43.44$	7.037	7.04	K

Parameter	Equation	Evaluated	EES Calc. Valve	Hand Calc. Value	Units
Log-Mean Temperature Difference ($LMTD_{ec}$)	$\mathrm{LMTD}_{ec} = \frac{\Delta \mathrm{T}_{2,\mathrm{ec}} - \Delta \mathrm{T}_{1,\mathrm{ec}}}{\ln\left(\frac{\Delta \mathrm{T}_{2,\mathrm{ec}}}{\Delta \mathrm{T}_{1,\mathrm{ec}}}\right)}$	$\mathrm{LMTD}_{ec} = \frac{7.037 - 15.04}{\ln\left(\frac{7.037}{15.04}\right)}$	10.54	10.54	K
Overall Conductance (UA_{ec})	$\dot{\mathrm{Q}}_{\mathrm{ec}} = \mathrm{UA}_{ec} * LMTD_{ec}$	$1.057 = \mathrm{UA}_{ec} * 10.54$	0.1004	0.1003	kW K^{-1}
Hot-Side					
Hot Side Reynolds Number ($Re_{ec,h}$)	$\mathrm{Re}_{\mathrm{ec,h}} = \frac{4 * \dot{\mathrm{m}}_{\mathrm{ec,h}}}{\mathrm{P}_{ec} * \mu_{\mathrm{ec,l,h}}}$	$\mathrm{Re}_{\mathrm{ec,h}} = \frac{4 * 0.0505}{0.6491 * 0.00001376}$	22610	22616	-
Refrigerant Heat Transfer Coefficient ($h_{ec,h}$)	$\mathrm{h}_{\mathrm{ec,h}} = 0.2267 * Re_{ec,h}^{0.631} * Pr_{ec,h}^{1/3} * \frac{\mathrm{k}_{ec,h}}{\mathrm{D}_{\mathrm{h,ec}}}$	$\mathrm{h}_{\mathrm{ec,h}} = 0.2267 * 22610^{0.631} * 0.7896^{1/3} * \frac{0.00001792}{0.005107}$	0.4112	0.4111	kW K^{-1} m^{-2}
Refrigerant Thermal Resistance ($R_{ec,h}$)	$\mathrm{R}_{\mathrm{ec,h}} = \left(\mathrm{h}_{ec,h} * L_{ec} * W_{plate,ec}\right)^{-1}$	$\mathrm{R}_{\mathrm{ec,h}} = (0.4112 * 0.632 * 0.322)^{-1}$	11.95	11.95	K kW^{-1}
Gravitational Pressure Drop ($\Delta P_{g,ec,h}$)	$\Delta \mathrm{P}_{\mathrm{g,ec,h}} = \rho_{ec,h} * \mathrm{g} * \mathrm{L}_{\mathrm{ec}}$	$\Delta \mathrm{P}_{\mathrm{g,ec,h}} = 37.51 * 9.78 * 0.632$	231.9	231.8	Pa

Parameter	Equation	Evaluated	EES Calc. Valve	Hand Calc. Value	Units
Velocity ($u_{ec,h}$)	$u_{ec,h} = \frac{\dot{m}_{ec,h}}{\rho_{ec,h} * A_{cs,ec}}$	$u_{ec,h} = \frac{0.0505}{37.51 * 0.0008288}$	1.624	1.624	m s^{-1}
Friction Factor ($f_{ec,h}$)	$f_{ec,h} = 0.6857 * Re_{ec,h}^{-0.172}$	$f_{ec,h} = 0.6857 * 22610^{-0.172}$	0.1222	0.1222	-
Frictional Pressure Drop ($\Delta P_{f,ec,h}$)	$\Delta P_{f,ec,h} = \frac{2 * f_{ec,h} * \rho_{ec,h} * u_{ec,h}^2 * L_{ec}}{D_{h,ec}}$	$\Delta P_{f,ec,h} = 2 * 0.1222 * 37.51 * 1.624^2 * 0.632/0.005107$	2995	2292	Pa
Total Pressure Drop ($\Delta P_{ec,h}$)	$\Delta P_{ec,h} = \Delta P_{f,ec,h} + \Delta P_{g,ec,h}$	$\Delta P_{ec,h} = 2995 + 231.9$	3226	3227	Pa
Cold Side					
Hot Side Reynolds Number ($Re_{ec,c}$)	$Re_{ec,c} = \frac{4 * \dot{m}_{ec,c}}{P_{ec} * \mu_{ec,l,c}}$	$Re_{ec,c} = \frac{4 * 0.05636}{0.6491 * 0.0001598}$	2174	2173	-
Refrigerant Heat Transfer Coefficient ($h_{ec,c}$)	$h_{ec,c} = 0.2267 * Re_{ec,c}^{0.631} * Pr_{ec,c}^{1/3} * \frac{k_{ec,c}}{D_{h,ec}}$	$h_{ec,c} = 0.2267 * 2174^{0.631} * 3.136^{1/3} * \frac{0.00007586}{0.005107}$	0.6288	0.6289	kW K^{-1} m^{-2}
Refrigerant Thermal Resistance ($R_{ec,c}$)	$R_{ec,c} = \left(h_{ec,c} * L_{ec} * W_{plate,ec}\right)^{-1}$	$R_{ec,c} = (0.6288 * 0.632 * 0.322)^{-1}$	7.815	7.815	K kW^{-1}

Parameter	Equation	Evaluated	EES Calc. Valve	Hand Calc. Value	Units
Gravitational Pressure Drop ($\Delta P_{g,ec,c}$)	$\Delta P_{g,ec,c} = \rho_{ec,c} * g * L_{ec}$	$\Delta P_{g,ec,c} = 1144 * 9.78 * 0.632$	7073	7071	Pa
Velocity ($u_{ec,c}$)	$u_{ec,c} = \frac{\dot{m}_{ec,c}}{\rho_{ec,c} * A_{cs,ec}}$	$u_{ec,c} = \frac{0.05636}{1144 * 0.0008288}$	0.05952	0.05944	m s^{-1}
Friction Factor ($f_{ec,c}$)	$f_{ec,c} = 0.6857 * Re_{ec,c}^{-0.172}$	$f_{ec,c} = 0.6857 * 2174^{-0.172}$	0.1829	0.1829	-
Frictional Pressure Drop ($\Delta P_{f,ec,c}$)	$\Delta P_{f,ec,c} = \frac{2 * f_{ec,c} * \rho_{ec,c} * u_{ec,c}^2 * L_{ec}}{D_{h,ec}}$	$\Delta P_{f,ec,c} = 2 * 0.1829 * 1144 * 0.05952^2 * 0.632/0.005107$	182.9	183.5	Pa
Total Pressure Drop ($\Delta P_{ec,c}$)	$\Delta P_{ec,c} = \Delta P_{f,ec,c} + \Delta P_{g,ec,c}$	$\Delta P_{ec,c} = 182.9 + 7073$	7256	7256	Pa
Total					
Wall Thermal Resistance ($R_{plate,ec}$)	$R_{plate,ec} = \frac{Pt}{K_{plate} * L_{ec} * W_{plate,ec}}$	$R_{plate,ec} = \frac{0.0005}{0.01512 * 0.632 * 0.322}$	0.1625	0.1625	K kW^{-1}
Overall Conductance (UA_{ec})	$UA_{ec} = \left[\left(R_{ec,h} + R_{plate,ec} + R_{w,ec,c}\right)/2\right]^{-1}$	$UA_{ec} = [(11.95 + 0.1625 + 7.815)/2]^{-1}$	0.1004	0.1004	kW K^{-1}

Table A-12: Suction line heat exchanger sizing model hand calculations

Parameter	Equation	Evaluated	EES Calc. Valve	Hand Calc. Value	Units
Wetted Perimeter (P_{sl})	$P_{sl} = 2 * (Ps + W_{plate,sl})$	$P_{sl} = 2 * (0.002574 + 0.322)$	0.6491	0.6491	m
Cross-Sectional Area ($A_{cs,sl}$)	$A_{cs,sl} = Ps * W_{plate,sl}$	$A_{cs,sl} = 0.002574 * 0.322$	0.0008288	0.0008288	m^2
Hydraulic Diameter ($D_{h,sl}$)	$D_{h,sl} = \frac{4 * A_{cs,sl}}{P_{sl}}$	$D_{h,sl} = \frac{4 * 0.0008288}{0.6491}$	0.005107	0.005107	m
Hot Side Channel Mass Flow Rate ($\dot{m}_{sl,h}$)	$\dot{m}_{sl,h} = \frac{2 * \dot{m}_{cc}}{N_{plates,sl}}$	$\dot{m}_{sl,h} = \frac{2 * 4.051}{256.3}$	0.03162	0.03161	kg s^{-1}
Cold Side Channel Mass Flow Rate ($\dot{m}_{sl,c}$)	$\dot{m}_{sl,c} = \frac{2 * \dot{m}_{cc}}{N_{plates,sl}}$	$\dot{m}_{sl,c} = \frac{2 * 4.051}{256.3}$	0.03162	0.03161	kg s^{-1}
Channel Heat Transfer ($\dot{Q}_{sl}$)	$\dot{Q}_{sl} = \dot{m}_{sl,h} * (i_{cc,9} - i_{cc,10})$	$\dot{Q}_{sl,h} = 0.03162 * (101.4 - 79.41)$	0.6942	0.6953	kW
Temperature Difference 1 ($\Delta T_{1,sl}$)	$\Delta T_{1,sl} = T_{cc,9} - T_{pc.17}$	$\Delta T_{1,sl} = 35.35 - 28.32$	7.026	7.03	K

Parameter	Equation	Evaluated	EES Calc. Valve	Hand Calc. Value	Units
Temperature Difference 2 ($\Delta T_{2,sl}$)	$\Delta T_{2,sl} = T_{cc,10} - T_{pc,16}$	$\Delta T_{2,sl} = 20.04 - 4.039$	16	16	K
Log-Mean Temperature Difference ($LMTD_{sl}$)	$LMTD_{sl} = \frac{\Delta T_{2,sl} - \Delta T_{1,sl}}{\ln\left(\frac{\Delta T_{2,sl}}{\Delta T_{1,sl}}\right)}$	$LMTD_{sl} = \frac{16 - 7.026}{\ln\left(\frac{16}{7.026}\right)}$	10.9	10.9	K
Overall Conductance (UA_{sl})	$\dot{Q}_{ec} = UA_{ec} * LMTD_{ec}$	$0.6942 = UA_{ec} * 10.9$	0.06366	0.06369	kW K^{-1}
Hot-Side					
Hot Side Reynolds Number ($Re_{sl,h}$)	$Re_{sl,h} = \frac{4 * \dot{m}_{sl,h}}{P_{sl} * \mu_{sl,l,h}}$	$Re_{sl,h} = \frac{4 * 0.03162}{0.6491 * 0.000171}$	1139	1139	-
Refrigerant Heat Transfer Coefficient ($h_{sl,h}$)	$h_{sl,h} = 0.2267 * Re_{sl,h}^{0.631} * Pr_{sl,h}^{1/3} * \frac{k_{sl,h}}{D_{h,sl}}$	$h_{sl,h} = 0.2267 * 1139^{0.631} * 3.222^{1/3} * \frac{0.00007814}{0.005107}$	0.4347	0.4347	kW K^{-1} m^{-2}
Refrigerant Thermal Resistance ($R_{sl,h}$)	$R_{sl,h} = \left(h_{sl,h} * L_{sl} * W_{plate,sl}\right)^{-1}$	$R_{sl,h} = (0.4347 * 0.632 * 0.322)^{-1}$	11.3	11.3	K kW^{-1}

Parameter	Equation	Evaluated	EES Calc. Valve	Hand Calc. Value	Units
Gravitational Pressure Drop ($\Delta P_{g,sl,h}$)	$\Delta P_{g,sl,h} = \rho_{sl,h} * g * L_{sl}$	$\Delta P_{g,sl,h} = 1166 * 9.78 * 0.632$	7209	7207	Pa
Velocity ($u_{sl,h}$)	$u_{sl,h} = \frac{\dot{m}_{sl,h}}{\rho_{sl,h} * A_{cs,sl}}$	$u_{sl,h} = \frac{0.03162}{1166 * 0.0008288}$	0.03271	0.03272	m s^{-1}
Friction Factor ($f_{sl,h}$)	$f_{sl,h} = 0.6857 * Re_{sl,h}^{-0.172}$	$f_{sl,h} = 0.6857 * 1139^{-0.172}$	0.2044	0.2044	-
Frictional Pressure Drop ($\Delta P_{f,sl,h}$)	$\Delta P_{f,sl,h} = \frac{2 * f_{sl,h} * \rho_{sl,h} * u_{sl,h}^2 * L_{sl}}{D_{h,sl}}$	$\Delta P_{f,ec,h} = 2 * 0.2044 * 1166 * 0.03271^2 * 0.632/0.005107$	63.1	63.1	Pa
Total Pressure Drop ($\Delta P_{sl,h}$)	$\Delta P_{sl,h} = \Delta P_{f,sl,h} + \Delta P_{g,sl,h}$	$\Delta P_{sl,h} = 63.1 + 7209$	7272	7272	Pa
Cold Side					
Hot Side Reynolds Number ($Re_{sl,c}$)	$Re_{sl,c} = \frac{4 * \dot{m}_{sl,c}}{P_{sl} * \mu_{sl,l,c}}$	$Re_{sl,c} = \frac{4 * 0.03162}{0.6491 * 0.00001108}$	17587	17586	-
Refrigerant Heat Transfer Coefficient ($h_{sl,c}$)	$h_{sl,c} = 0.2267 * Re_{sl,c}^{0.631} * Pr_{sl,c}^{1/3} * \frac{k_{sl,c}}{D_{h,sl}}$	$h_{sl,c} = 0.2267 * 17587^{0.631} * 0.8083^{1/3} * \frac{0.00001248}{0.005107}$	0.2463	0.2463	kW K^{-1} m^{-2}
Refrigerant Thermal	$R_{sl,c} = \left(h_{sl,c} * L_{sl} * W_{plate,sl}\right)^{-1}$	$R_{sl,c} = (0.2463 * 0.632 * 0.322)^{-1}$	19.95	19.95	K kW^{-1}

Parameter	Equation	Evaluated	EES Calc. Valve	Hand Calc. Value	Units
Resistance ($R_{sl,c}$)					
Gravitational Pressure Drop ($\Delta P_{g,sl,c}$)	$\Delta P_{g,sl,c} = \rho_{sl,c} * g * L_{sl}$	$\Delta P_{g,sl,c} = 16.11 * 9.78 * 0.632$	99.56	99.58	Pa
Velocity ($u_{sl,c}$)	$u_{sl,c} = \frac{\dot{m}_{sl,c}}{\rho_{sl,c} * A_{cs,sl}}$	$u_{sl,c} = \frac{0.03162}{16.11 * 0.0008288}$	2.368	2.368	m s^{-1}
Friction Factor ($f_{sl,c}$)	$f_{sl,c} = 0.6857 * Re_{ec,c}^{-0.172}$	$f_{sl,c} = 0.6857 * 17587^{-0.172}$	0.1276	0.1276	-
Frictional Pressure Drop ($\Delta P_{f,sl,c}$)	$\Delta P_{f,sl,c} = \frac{2 * f_{sl,c} * \rho_{sl,c} * u_{sl,c}^2 * L_{sl}}{D_{h,sl}}$	$\Delta P_{f,sl,c} = 2 * 0.1276 * 16.11 * 2.368^2 * 0.632/0.005107$	2853	2853	Pa
Total Pressure Drop ($\Delta P_{sl,c}$)	$\Delta P_{sl,c} = \Delta P_{f,sl,c} + \Delta P_{g,sl,c}$	$\Delta P_{sl,c} = 2853 + 99.56$	2953	2853	Pa
Total					
Wall Thermal Resistance ($R_{plate,sl}$)	$R_{plate,sl} = \frac{Pt}{K_{plate} * L_{sl} * W_{plate,sl}}$	$R_{plate,sl} = \frac{0.0005}{0.01512 * 0.632 * 0.322}$	0.1625	0.1625	K kW^{-1}
Overall Conductance (UA_{sl})	$UA_{sl} = \left[\left(R_{sl,h} + R_{plate,sl} + R_{w,sl,c}\right)/2\right]^{-1}$	$UA_{sl} = [(11.3 + 0.1625 + 19.95)/2]^{-1}$	0.06366	0.06367	kW K^{-1}

A.3. Pipe Sizing Calculations

Piping routes between major components were assumed to be 1.5-meters as a conservative estimate. Pipe sizes were selected in half inch increments to achieve pressure drops that were approximately 1 kPa or less. Table A-13 displays a description of each pipe including connected components and geometries. Table A-14 and Table A-15 provide hand calculations used to calculate the pressure drop in each pipe.

Table A-13: Pipe geometries for hand calculations

Power Cycle				Cooling Cycle			
Pipe Number	**Description**	**Diameter**	**Length**	**Pipe Number**	**Description**	**Diameter**	**Length**
Pipe 1	Turbine to Recuperator (2-3)	3.5″ (0.0889 m)	1.5 m	**Pipe 1**	Compressor to Economizer (2-3)	3.5″ (0.0889 m)	1.5 m
Pipe 2	Recuperator to Condenser (4-5)	3.5″ (0.0889 m)	1.5 m	**Pipe 2**	Economizer to Condenser (4-5)	3.5″ (0.0889 m)	1.5 m
Pipe 3	Condenser to Pump (8-9)	2″ (0.0508 m)	1.5 m	**Pipe 3**	Condenser to Suction Line (8-9)	2″ (0.0508 m)	1.5 m
Pipe 4	Pump to Recuperator (10-11)	2″ (0.0508 m)	1.5 m	**Pipe 4**	Suction Line to Expansion Valve (10-11)	2″ (0.0508 m)	1.5 m
Pipe 5	Recuperator to Economizer (12-13)	2″ (0.0508 m)	1.5 m	**Pipe 5**	Expansion Valve to Chiller (12-13)	2″ (0.0508 m)	1.5 m
Pipe 6	Economizer to Boiler (14-15)	2″ (0.0508 m)	1.5 m	**Pipe 6**	Chiller to Suction Line (15-16)	4″ (0.1016 m)	1.5 m
Pipe 7	Boiler to Turbine (18-1)	3″ (0.0762 m)	1.5 m	**Pipe 7**	Suction Line to Compressor (17-1)	4″ (0.1016 m)	1.5 m

Table A-14: Power cycle pipes hand calculations

Parameter	Equation	Evaluated	EES Calc. Valve	Hand Calc. Value	Units
Pipe 1					
Cross-Sectional Area ($A_{pc,pipe,1}$)	$A_{pc,pipe,1} = \frac{\pi * D_{pc,pipe,1}^2}{4}$	$A_{pc,pipe,1} = \frac{\pi * 0.0889^2}{4}$	0.006207	0.006207	m^2
Reynolds Number ($Re_{pc,pipe,1}$)	$Re_{pc,pipe,1} = \frac{4 * \dot{m}_{pc}}{\pi * D_{pc,pipe,1} * \mu_{pc,pipe,1}}$	$Re_{pc,pipe,1} = \frac{4 * 4.521}{\pi * 0.0889 * 0.00001294}$	5.005 E6	5.004 E6	-
Velocity ($u_{pc,pipe,1}$)	$u_{pc,pipe,1} = \frac{\dot{m}_{pc}}{\rho_{pc,pipe,1} * A_{pc,pipe,1}}$	$u_{pc,pipe,1} = \frac{4.521}{44.27 * 0.006207}$	16.45	16.45	$m\ s^{-1}$
Friction Factor ($f_{pc,pipe,1}$)	$f_{pc,pipe,1} = 0.0032 + \frac{0.221}{Re_{pc,pipe,1}^{0.237}}$	$f_{pc,pipe,1} = 0.0032 + \frac{0.221}{(5.005 * 10^6)^{0.237}}$	0.00891	0.00891	-
Frictional Pressure Drop ($\Delta P_{pc,pipe,1}$)	$\Delta P_{pc,pipe,1} = f_{pc,pipe,1} * \frac{L_{pc,pipe,1}}{D_{pc,pipe,1}} * \frac{\rho_{pc,pipe,1} * u_{pc,pipe,1}^2}{2}$	$\Delta P_{pc,pipe,1} = 0.00891 * \frac{1.5}{0.0889} * \frac{44.27 * 16.45^2}{2}$	900.8	900.5	Pa
Pipe 2					
Cross-Sectional Area ($A_{pc,pipe,2}$)	$A_{pc,pipe,2} = \frac{\pi * D_{pc,pipe,2}^2}{4}$	$A_{pc,pipe,2} = \frac{\pi * 0.0889^2}{4}$	0.006207	0.006207	m^2

Parameter	Equation	Evaluated	EES Calc. Valve	Hand Calc. Value	Units
Reynolds Number ($Re_{pc,pipe,2}$)	$Re_{pc,pipe,2} = \frac{4 * \dot{m}_{pc}}{\pi * D_{pc,pipe,2} * \mu_{pc,pipe,2}}$	$Re_{pc,pipe,2} = \frac{4 * 4.521}{\pi * 0.0889 * 0.00001273}$	5.086 E6	5.086 E6	-
Velocity ($u_{pc,pipe,2}$)	$u_{pc,pipe,2} = \frac{\dot{m}_{pc}}{\rho_{pc,pipe,2} * A_{pc,pipe,2}}$	$u_{pc,pipe,2} = \frac{4.521}{45.45 * 0.006207}$	16.02	16.03	m s^{-1}
Friction Factor ($f_{pc,pipe,2}$)	$f_{pc,pipe,2} = 0.0032 + \frac{0.221}{Re_{pc,pipe,2}^{0.237}}$	$f_{pc,pipe,2} = 0.0032 + \frac{0.221}{(5.086 * 10^6)^{0.237}}$	0.008888	0.008888	-
Frictional Pressure Drop ($\Delta P_{pc,pipe,2}$)	$\Delta P_{pc,pipe,2} = f_{pc,pipe,2} * \frac{L_{pc,pipe,2}}{D_{pc,pipe,2}} * \frac{\rho_{pc,pipe,2} * u_{pc,pipe,2}^2}{2}$	$\Delta P_{pc,pipe,2} = 0.008888 * \frac{1.5}{0.0889} * \frac{45.45 * 16.02^2}{2}$	875.2	874.6	Pa
Pipe 3					
Cross-Sectional Area ($A_{pc,pipe,3}$)	$A_{pc,pipe,3} = \frac{\pi * D_{pc,pipe,3}^2}{4}$	$A_{pc,pipe,3} = \frac{\pi * 0.0508^2}{4}$	0.002027	0.002023	m^2
Reynolds Number ($Re_{pc,pipe,3}$)	$Re_{pc,pipe,3} = \frac{4 * \dot{m}_{pc}}{\pi * D_{pc,pipe,3} * \mu_{pc,pipe,3}}$	$Re_{pc,pipe,3} = \frac{4 * 4.521}{\pi * 0.0508 * 0.0001682}$	673612	673682	-
Velocity ($u_{pc,pipe,3}$)	$u_{pc,pipe,3} = \frac{\dot{m}_{pc}}{\rho_{pc,pipe,3} * A_{pc,pipe,3}}$	$u_{pc,pipe,3} = \frac{4.521}{1161 * 0.002027}$	1.921	1.921	m s^{-1}

Parameter	Equation	Evaluated	EES Calc. Valve	Hand Calc. Value	Units
Friction Factor ($f_{pc,pipe,3}$)	$f_{pc,pipe,3} = 0.0032 + \frac{0.221}{Re_{pc,pipe,3}^{0.237}}$	$f_{pc,pipe,3} = 0.0032 + \frac{0.221}{(673612)^{0.237}}$	0.01238	0.01238	-
Frictional Pressure Drop ($\Delta P_{pc,pipe,3}$)	$\Delta P_{pc,pipe,3} = f_{pc,pipe,3} * \frac{L_{pc,pipe,3}}{D_{pc,pipe,3}} * \frac{\rho_{pc,pipe,3} * u_{pc,pipe,3}^2}{2}$	$\Delta P_{pc,pipe,3} = 0.01238 * \frac{1.5}{0.0508} * \frac{1161 * 1.921^2}{2}$	783.6	783.1	Pa
Pipe 4					
Cross-Sectional Area ($A_{pc,pipe,4}$)	$A_{pc,pipe,4} = \frac{\pi * D_{pc,pipe,4}^2}{4}$	$A_{pc,pipe,4} = \frac{\pi * 0.0508^2}{4}$	0.002027	0.002023	m^2
Reynolds Number ($Re_{pc,pipe,4}$)	$Re_{pc,pipe,4} = \frac{4 * \dot{m}_{pc}}{\pi * D_{pc,pipe,4} * \mu_{pc,pipe,4}}$	$Re_{pc,pipe,4} = \frac{4 * 4.521}{\pi * 0.0508 * 0.0001681}$	673957	674083	-
Velocity ($u_{pc,pipe,4}$)	$u_{pc,pipe,4} = \frac{\dot{m}_{pc}}{\rho_{pc,pipe,4} * A_{pc,pipe,4}}$	$u_{pc,pipe,4} = \frac{4.521}{1161 * 0.002027}$	1.921	1.921	$m\ s^{-1}$
Friction Factor ($f_{pc,pipe,4}$)	$f_{pc,pipe,4} = 0.0032 + \frac{0.221}{Re_{pc,pipe,4}^{0.237}}$	$f_{pc,pipe,4} = 0.0032 + \frac{0.221}{(673957)^{0.237}}$	0.01238	0.01238	-

Parameter	Equation	Evaluated	EES Calc. Valve	Hand Calc. Value	Units
Frictional Pressure Drop ($\Delta P_{pc,pipe,4}$)	$\Delta P_{pc,pipe,4} = f_{pc,pipe,4} * \frac{L_{pc,pipe,4}}{D_{pc,pipe,4}} * \frac{\rho_{pc,pipe,4} * u_{pc,pipe,4}^2}{2}$	$\Delta P_{pc,pipe,4} = 0.01238 * \frac{1.5}{0.0508} * \frac{1161 * 1.921^2}{2}$	783.3	783.1	Pa
Pipe 5					
Cross-Sectional Area ($A_{pc,pipe,5}$)	$A_{pc,pipe,5} = \frac{\pi * D_{pc,pipe,5}^2}{4}$	$A_{pc,pipe,5} = \frac{\pi * 0.0508^2}{4}$	0.002027	0.002023	m^2
Reynolds Number ($Re_{pc,pipe,5}$)	$Re_{pc,pipe,5} = \frac{4 * \dot{m}_{pc}}{\pi * D_{pc,pipe,5} * \mu_{pc,pipe,5}}$	$Re_{pc,pipe,5} = \frac{4 * 4.521}{\pi * 0.0508 * 0.0001598}$	709086	709095	-
Velocity ($u_{pc,pipe,5}$)	$u_{pc,pipe,5} = \frac{\dot{m}_{pc}}{\rho_{pc,pipe,5} * A_{pc,pipe,5}}$	$u_{pc,pipe,5} = \frac{4.521}{1144 * 0.002027}$	1.949	1.950	$m\ s^{-1}$
Friction Factor ($f_{pc,pipe,5}$)	$f_{pc,pipe,5} = 0.0032 + \frac{0.221}{Re_{pc,pipe,5}^{0.237}}$	$f_{pc,pipe,5} = 0.0032 + \frac{0.221}{(709086)^{0.237}}$	0.01227	0.01227	-
Frictional Pressure Drop ($\Delta P_{pc,pipe,5}$)	$\Delta P_{pc,pipe,5} = f_{pc,pipe,5} * \frac{L_{pc,pipe,5}}{D_{pc,pipe,5}} * \frac{\rho_{pc,pipe,5} * u_{pc,pipe,5}^2}{2}$	$\Delta P_{pc,pipe,5} = 0.01227 * \frac{1.5}{0.0508} * \frac{1144 * 1.949^2}{2}$	787.8	787.2	Pa
Pipe 6					

Parameter	Equation	Evaluated	EES Calc. Valve	Hand Calc. Value	Units
Cross-Sectional Area ($A_{pc,pipe,6}$)	$A_{pc,pipe,6} = \frac{\pi * D_{pc,pipe,6}^2}{4}$	$A_{pc,pipe,6} = \frac{\pi * 0.0508^2}{4}$	0.002027	0.002023	m^2
Reynolds Number ($Re_{pc,pipe,6}$)	$Re_{pc,pipe,6} = \frac{4 * \dot{m}_{pc}}{\pi * D_{pc,pipe,6} * \mu_{pc,pipe,6}}$	$Re_{pc,pipe,6} = \frac{4 * 4.521}{\pi * 0.0508 * 0.0001356}$	835755	835644	-
Velocity ($u_{pc,pipe,6}$)	$u_{pc,pipe,6} = \frac{\dot{m}_{pc}}{\rho_{pc,pipe,6} * A_{pc,pipe,6}}$	$u_{pc,pipe,6} = \frac{4.521}{1087 * 0.002027}$	2.052	2.052	$m\ s^{-1}$
Friction Factor ($f_{pc,pipe,6}$)	$f_{pc,pipe,6} = 0.0032 + \frac{0.221}{Re_{pc,pipe,3}^{0.237}}$	$f_{pc,pipe,6} = 0.0032 + \frac{0.221}{(835755)^{0.237}}$	0.01193	0.01193	-
Frictional Pressure Drop ($\Delta P_{pc,pipe,6}$)	$\Delta P_{pc,pipe,6} = f_{pc,pipe,6} * \frac{L_{pc,pipe,6}}{D_{pc,pipe,6}} * \frac{\rho_{pc,pipe,6} * u_{pc,pipe,6}^2}{2}$	$\Delta P_{pc,pipe,6} = 0.01193 * \frac{1.5}{0.0508} * \frac{1087 * 2.052^2}{2}$	805.9	806.2	Pa
Pipe 7					
Cross-Sectional Area ($A_{pc,pipe,7}$)	$A_{pc,pipe,7} = \frac{\pi * D_{pc,pipe,7}^2}{4}$	$A_{pc,pipe,7} = \frac{\pi * 0.0762^2}{4}$	0.00456	0.00456	m^2

Parameter	Equation	Evaluated	EES Calc. Valve	Hand Calc. Value	Units
Reynolds Number ($Re_{pc,pipe,7}$)	$\mathrm{Re}_{\mathrm{pc,pipe,7}} = \frac{4 * \dot{m}_{pc}}{\pi * D_{pc,pipe,7} * \mu_{pc,pipe,7}}$	$\mathrm{Re}_{\mathrm{pc,pipe,7}} = \frac{4 * 4.521}{\pi * 0.0762 * 0.0000157}$	4.810 E6	4.812 E6	-
Velocity ($u_{pc,pipe,7}$)	$u_{pc,pipe,7} = \frac{\dot{m}_{pc}}{\rho_{pc,pipe,7} * A_{pc,pipe,7}}$	$u_{pc,pipe,7} = \frac{4.521}{127.9 * 0.00456}$	7.752	7.752	m s^{-1}
Friction Factor ($f_{pc,pipe,7}$)	$\mathrm{f}_{\mathrm{pc,pipe,7}} = 0.0032 + \frac{0.221}{Re_{pc,pipe,7}^{0.237}}$	$\mathrm{f}_{\mathrm{pc,pipe,7}} = 0.0032 + \frac{0.221}{(4.810 * 10^6)^{0.237}}$	0.008964	0.008964	-
Frictional Pressure Drop ($\Delta P_{pc,pipe,7}$)	$\Delta \mathrm{P}_{\mathrm{pc,pipe,7}} = \mathrm{f}_{\mathrm{pc,pipe,7}} * \frac{\mathrm{L}_{\mathrm{pc,pipe,7}}}{\mathrm{D}_{\mathrm{pc,pipe,7}}} * \frac{\rho_{pc,pipe,7} * u_{pc,pipe,7}^2}{2}$	$\Delta \mathrm{P}_{\mathrm{pc,pipe,7}} = 0.008964 * \frac{1.5}{0.0762} * \frac{127.9 * 7.752^2}{2}$	678.1	678.1	Pa

Table A-15: Cooling cycle pipes hand calculations

Parameter	Equation	Evaluated	EES Calc. Valve	Hand Calc. Value	Units
Pipe 1					
Cross-Sectional Area ($A_{cc,pipe,1}$)	$A_{cc,pipe,1} = \frac{\pi * D_{cc,pipe,1}^2}{4}$	$A_{cc,pipe,1} = \frac{\pi * 0.0889^2}{4}$	0.006207	0.006207	m^2

Parameter	Equation	Evaluated	EES Calc. Valve	Hand Calc. Value	Units
Reynolds Number ($Re_{cc,pipe,1}$)	$Re_{cc,pipe,1} = \frac{4 * \dot{m}_{cc}}{\pi * D_{cc,pipe,1} * \mu_{cc,pipe,1}}$	$Re_{cc,pipe,1} = \frac{4 * 4.05}{\pi * 0.0889 * 0.00001376}$	4.215 E6	4.215 E6	-
Velocity ($u_{cc,pipe,1}$)	$u_{cc,pipe,1} = \frac{\dot{m}_{cc}}{\rho_{cc,pipe,1} * A_{cc,pipe,1}}$	$u_{cc,pipe,1} = \frac{4.05}{37.51 * 0.006207}$	17.39	17.40	m s^{-1}
Friction Factor ($f_{cc,pipe,1}$)	$f_{cc,pipe,1} = 0.0032 + \frac{0.221}{Re_{cc,pipe,1}^{0.237}}$	$f_{cc,pipe,1} = 0.0032 + \frac{0.221}{(4.215 * 10^6)^{0.237}}$	0.009147	0.009147	-
Frictional Pressure Drop ($\Delta P_{cc,pipe,1}$)	$\Delta P_{cc,pipe,1} = f_{cc,pipe,1} * \frac{L_{cc,pipe,1}}{D_{cc,pipe,1}} * \frac{\rho_{cc,pipe,1} * u_{cc,pipe,1}^2}{2}$	$\Delta P_{cc,pipe,1} = 0.009147 * \frac{1.5}{0.0889} * \frac{37.51 * 17.39^2}{2}$	876	875	Pa
Pipe 2					
Cross-Sectional Area ($A_{cc,pipe,2}$)	$A_{cc,pipe,2} = \frac{\pi * D_{cc,pipe,2}^2}{4}$	$A_{cc,pipe,2} = \frac{\pi * 0.0889^2}{4}$	0.006207	0.006207	m^2
Reynolds Number ($Re_{cc,pipe,2}$)	$Re_{pc,pipe,2} = \frac{4 * \dot{m}_{cc}}{\pi * D_{cc,pipe,2} * \mu_{cc,pipe,2}}$	$Re_{cc,pipe,2} = \frac{4 * 4.05}{\pi * 0.0889 * 0.00001301}$	4.459 E6	4.458 E6	-
Velocity ($u_{cc,pipe,2}$)	$u_{cc,pipe,2} = \frac{\dot{m}_{cc}}{\rho_{cc,pipe,2} * A_{cc,pipe,2}}$	$u_{cc,pipe,2} = \frac{4.05}{41.35 * 0.006207}$	15.78	15.78	m s^{-1}

Parameter	Equation	Evaluated	EES Calc. Valve	Hand Calc. Value	Units
Friction Factor ($f_{cc,pipe,2}$)	$f_{cc,pipe,2} = 0.0032 + \frac{0.221}{Re_{cc,pipe,2}^{0.237}}$	$f_{cc,pipe,2} = 0.0032 + \frac{0.221}{(4.459 * 10^6)^{0.237}}$	0.009069	0.009068	-
Frictional Pressure Drop ($\Delta P_{cc,pipe,2}$)	$\Delta P_{cc,pipe,2} = f_{cc,pipe,2} * \frac{L_{cc,pipe,2}}{D_{cc,pipe,2}} * \frac{\rho_{cc,pipe,2} * u_{cc,pipe,2}^2}{2}$	$\Delta P_{cc,pipe,2} = 0.009069 * \frac{1.5}{0.0889} * \frac{41.35 * 15.78^2}{2}$	787.9	787.8	Pa
Pipe 3					
Cross-Sectional Area ($A_{cc,pipe,3}$)	$A_{cc,pipe,3} = \frac{\pi * D_{cc,pipe,3}^2}{4}$	$A_{cc,pipe,3} = \frac{\pi * 0.0508^2}{4}$	0.002027	0.002023	m^2
Reynolds Number ($Re_{cc,pipe,3}$)	$Re_{cc,pipe,3} = \frac{4 * \dot{m}_{cc}}{\pi * D_{cc,pipe,3} * \mu_{cc,pipe,3}}$	$Re_{cc,pipe,3} = \frac{4 * 4.05}{\pi * 0.0508 * 0.000171}$	593655	593616	-
Velocity ($u_{cc,pipe,3}$)	$u_{cc,pipe,3} = \frac{\dot{m}_{cc}}{\rho_{cc,pipe,3} * A_{cc,pipe,3}}$	$u_{cc,pipe,3} = \frac{4.05}{1166 * 0.002027}$	1.713	1.714	$m\ s^{-1}$
Friction Factor ($f_{cc,pipe,3}$)	$f_{cc,pipe,3} = 0.0032 + \frac{0.221}{Re_{cc,pipe,3}^{0.237}}$	$f_{cc,pipe,3} = 0.0032 + \frac{0.221}{(593655)^{0.237}}$	0.012666	0.012666	-

Parameter	Equation	Evaluated	EES Calc. Valve	Hand Calc. Value	Units
Frictional Pressure Drop ($\Delta P_{cc,pipe,3}$)	$\Delta P_{cc,pipe,3} = f_{cc,pipe,3} * \frac{L_{cc,pipe,3}}{D_{cc,pipe,3}} * \frac{\rho_{cc,pipe,3} * u_{cc,pipe,3}^2}{2}$	$\Delta P_{cc,pipe,3} = 0.01266 * \frac{1.5}{0.0508} * \frac{1166 * 1.713^2}{2}$	640.2	639.5	Pa
Pipe 4					
Cross-Sectional Area ($A_{cc,pipe,4}$)	$A_{cc,pipe,4} = \frac{\pi * D_{cc,pipe,4}^2}{4}$	$A_{cc,pipe,4} = \frac{\pi * 0.0508^2}{4}$	0.002027	0.002023	m^2
Reynolds Number ($Re_{cc,pipe,4}$)	$Re_{cc,pipe,4} = \frac{4 * \dot{m}_{cc}}{\pi * D_{cc,pipe,4} * \mu_{cc,pipe,4}}$	$Re_{cc,pipe,4} = \frac{4 * 4.05}{\pi * 0.0508 * 0.0002079}$	488298	488255	-
Velocity ($u_{cc,pipe,4}$)	$u_{cc,pipe,4} = \frac{\dot{m}_{cc}}{\rho_{cc,pipe,4} * A_{cc,pipe,4}}$	$u_{cc,pipe,4} = \frac{4.05}{1227 * 0.002027}$	1.629	1.628	$m\ s^{-1}$
Friction Factor ($f_{cc,pipe,4}$)	$f_{cc,pipe,4} = 0.0032 + \frac{0.221}{Re_{cc,pipe,4}^{0.237}}$	$f_{cc,pipe,4} = 0.0032 + \frac{0.221}{(488298)^{0.237}}$	0.01311	0.01311	-
Frictional Pressure Drop ($\Delta P_{cc,pipe,4}$)	$\Delta P_{cc,pipe,4} = f_{cc,pipe,4} * \frac{L_{cc,pipe,4}}{D_{cc,pipe,4}} * \frac{\rho_{cc,pipe,4} * u_{cc,pipe,4}^2}{2}$	$\Delta P_{cc,pipe,4} = 0.01311 * \frac{1.5}{0.0508} * \frac{1227 * 1.629^2}{2}$	630	630	Pa
Pipe 5					

Parameter	Equation	Evaluated	EES Calc. Valve	Hand Calc. Value	Units
Cross-Sectional Area ($A_{cc,pipe,5}$)	$A_{cc,pipe,5} = \frac{\pi * D_{cc,pipe,5}^2}{4}$	$A_{cc,pipe,5} = \frac{\pi * 0.0508^2}{4}$	0.002027	0.002027	m^2
Mass Flux ($G_{cc,pipe,5}$)	$G_{cc,pipe,5} = \frac{\dot{m}_{cc}}{A_{cc,pipe,5}}$	$G_{cc,pipe,5} = \frac{4.05}{0.002027}$	1998	1998	kg m^{-2} s^{-1}
Equivalent Mass Flux ($G_{eq,cc,pipe,5}$)	$G_{eq,cc,pipe,5} = G_{cc,pipe,5} * \left(\frac{1}{x_m} + x_m * \left(\frac{\rho_l}{\rho_v}\right)^{1/2}\right)$	$G_{eq,cc,pipe,5} = 1998 * \left(\frac{1}{0.1098} + 0.1098 * \left(\frac{1280}{16.89}\right)^{1/2}\right)$	10094	10053	kg m^{-2} s^{-1}
Reynolds Number ($Re_{cc,pipe,5}$)	$\mathrm{Re}_{cc,pipe,5} = \frac{G_{eq,cc,pipe,5} * D_{cc,pipe,5}}{\mu_{cc,pipe,5}}$	$\mathrm{Re}_{cc,pipe,5} = \frac{10094 * 0.0508}{0.0002506}$	2.046 E6	2.046 E6	-
Equivalent Density ($\rho_{eq,pc,pipe,5}$)	$\rho_{eq,pc,pipe,5} = (1 - x_m) * \rho_l + x_m * \rho_v$	$\rho_{eq,pc,pipe,5} = (1 - 0.1098) * 1280 + 0.1098 * 16.89$	1141	1141	kg m^{-2}
Velocity ($u_{cc,pipe,5}$)	$u_{cc,pipe,5} = \frac{\dot{m}_{cc}}{\rho_{eq,c,pipe,5} * A_{cc,pipe,5}}$	$u_{cc,pipe,5} = \frac{4.05}{1141 * 0.002027}$	1.752	1.751	m s^{-1}
Friction Factor ($f_{cc,pipe,5}$)	$\mathrm{f}_{cc,pipe,5} = 0.0032 + \frac{0.221}{Re_{cc,pipe,5}^{0.237}}$	$\mathrm{f}_{cc,pipe,5} = 0.0032 + \frac{0.221}{(2.046 * 10^6)^{0.237}}$	0.01026	0.01026	-

Parameter	Equation	Evaluated	EES Calc. Valve	Hand Calc. Value	Units
Frictional Pressure Drop ($\Delta P_{cc,pipe,5}$)	$\Delta P_{cc,pipe,5} = f_{cc,pipe,5} * \frac{L_{cc,pipe,5}}{D_{cc,pipe,5}} * \frac{\rho_{eq,cc,pipe,5} * u_{cc,pipe,5}^2}{2}$	$\Delta P_{cc,pipe,5} = 0.01026 * \frac{1.5}{0.0508} * \frac{1141 * 1.752^2}{2}$	530.1	530.5	Pa
Pipe 6					
Cross-Sectional Area ($A_{cc,pipe,6}$)	$A_{cc,pipe,6} = \frac{\pi * D_{cc,pipe,6}^2}{4}$	$A_{cc,pipe,6} = \frac{\pi * 0.1016^2}{4}$	0.008107	0.008107	m^2
Reynolds Number ($Re_{cc,pipe,6}$)	$Re_{cc,pipe,6} = \frac{4 * \dot{m}_{cc}}{\pi * D_{cc,pipe,6} * \mu_{cc,pipe,6}}$	$Re_{cc,pipe,6} = \frac{4 * 4.05}{\pi * 0.1016 * 0.00001108}$	4.582 E6	4.581 E6	-
Velocity ($u_{cc,pipe,6}$)	$u_{cc,pipe,6} = \frac{\dot{m}_{cc}}{\rho_{cc,pipe,6} * A_{cc,pipe,6}}$	$u_{cc,pipe,6} = \frac{4.05}{16.14 * 0.008107}$	30.96	30.95	$m\ s^{-1}$
Friction Factor ($f_{cc,pipe,6}$)	$f_{cc,pipe,6} = 0.0032 + \frac{0.221}{Re_{cc,pipe,3}^{0.237}}$	$f_{cc,pipe,6} = 0.0032 + \frac{0.221}{(4.582 * 10^6)^{0.237}}$	0.009031	0.009031	-
Frictional Pressure Drop ($\Delta P_{cc,pipe,6}$)	$\Delta P_{cc,pipe,6} = f_{cc,pipe,6} * \frac{L_{cc,pipe,6}}{D_{cc,pipe,6}} * \frac{\rho_{cc,pipe,6} * u_{cc,pipe,6}^2}{2}$	$\Delta P_{cc,pipe,6} = 0.009031 * \frac{1.5}{0.1016} * \frac{16.14 * 30.96^2}{2}$	1031	1031	Pa
Pipe 7					

Parameter	Equation	Evaluated	EES Calc. Valve	Hand Calc. Value	Units
Cross-Sectional Area ($A_{cc,pipe,7}$)	$A_{cc,pipe,7} = \frac{\pi * D_{cc,pipe,7}^2}{4}$	$A_{cc,pipe,7} = \frac{\pi * 0.1016^2}{4}$	0.008107	0.008107	m^2
Reynolds Number ($Re_{cc,pipe,7}$)	$Re_{cc,pipe,7} = \frac{4 * \dot{m}_{cc}}{\pi * D_{cc,pipe,7} * \mu_{cc,pipe,7}}$	$Re_{cc,pipe,7} = \frac{4 * 4.05}{\pi * 0.1016 * 0.00001201}$	4.227 E6	4.226 E6	-
Velocity ($u_{cc,pipe,7}$)	$u_{cc,pipe,7} = \frac{\dot{m}_{cc}}{\rho_{cc,pipe,7} * A_{cc,pipe,7}}$	$u_{cc,pipe,7} = \frac{4.05}{14.21 * 0.008107}$	35.17	35.16	$m\ s^{-1}$
Friction Factor ($f_{cc,pipe,7}$)	$f_{cc,pipe,7} = 0.0032 + \frac{0.221}{Re_{cc,pipe,7}^{0.237}}$	$f_{cc,pipe,7} = 0.0032 + \frac{0.221}{(4.227 * 10^6)^{0.237}}$	0.009143	0.009143	-
Frictional Pressure Drop ($\Delta P_{cc,pipe,7}$)	$\Delta P_{cc,pipe,7} = f_{cc,pipe,7} * \frac{L_{cc,pipe,7}}{D_{cc,pipe,7}} * \frac{\rho_{cc,pipe,7} * u_{cc,pipe,7}^2}{2}$	$\Delta P_{cc,pipe,7} = 0.009143 * \frac{1.5}{0.1016} * \frac{14.21 * 35.17^2}{2}$	1186	1186	Pa

A.4. Economic Calculations and Justifications

An economic model was used to calculate the costs of major components to determine a total system equipment and installation costs. Total installed cost was then used to calculate a payback period, net present value (NPV) and internal rate of return (IRR). The cost of the heat exchangers was estimated using a costing correlation which included the heat transfer surface area, material factor, and pressure factor. It was found that using the correlation consistently over predicted costs compared to obtained quotes from past projects. Three examples are provided in Table A-16 below demonstrating the discrepancy between the quotes and correlations. Based on this information, a custom factor of 0.9 was applied to phase-change heat exchanger costs and 0.8 to recuperative heat exchangers.

Table A-16: Quoted heat exchanger costs

Heat Exchanger Type:	**Condenser**	**Evaporator**	**Recuperator**
Heat Duty (kW)	863.1	819.4	44.8
Heat Transfer Area (ft^2)	532.2	1072.9	392.7
Quoted Cost ($)	$14,470	$23,080	$12,054
Correlation Cost ($)	$18,144	$26,494	$15397
Correction Factor	0.798	0.871	0.783

All cost estimates were performed using Microsoft Excel. Heat exchanger and piping sizes were results from the volume optimization study and were used to predict costs. Table A-17 displays calculations and factors used to predict the costs of the heat exchangers. Piping routes were assumed to be 1.5-meters long and required 20 fittings per 100-feet and individual costs are shown in Table A-18. Remaining equipment costs, including turbomachinery, valves, and instrumentations, were discussed in detail in Section 3.7.1. and in Section 4.4. The total equipment cost was $295,036, the installation cost was $147,518, and the total installed cost was $442,554.

Table A-17: Final heat exchanger costs

Heat Exchanger	Plate Area (ft^2)	Number of Plates	Total Area (ft^2)	Material Factor	Pressure Factor	Custom Factor	Cost per Core	Total Cost
PC Boiler	3.392	196	665	1	1.35	0.9	$24,861	$24,861
PC Condenser	6.457	178	1149	1.6	1	0.9	$39,597	$39,597
CC Evaporator	2.191	265	581	1	1	0.9	$17,114	$34,229
CC Condenser	6.457	314	2028	1.6	1	0.9	$53,799	$53,799
Recuperator	2.191	118	259	1	1.35	0.8	$13,268	$13,268
Economizer	2.191	162	355	1	1.35	0.8	$15,745	$15,745
Suction Line	2.191	258	565	1	1	0.8	$14,995	$14,995

Table A-18: Final pipe costs

Pipe	Diameter (in)	Length (ft)	Fittings per 100 ft	Cost	Pipe	Diameter (in)	Length (ft)	Fittings per 100 ft	Cost
PC Pipe 1	3.5	4.92125	20	$524.31	**CC Pipe 1**	3.5	4.92125	20	$524.31
PC Pipe 2	3.5	4.92125	20	$524.31	**CC Pipe 2**	3.5	4.92125	20	$524.31
PC Pipe 3	2	4.92125	20	$329.51	**CC Pipe 3**	2	4.92125	20	$329.51
PC Pipe 4	2	4.92125	20	$329.51	**CC Pipe 4**	2	4.92125	20	$329.51
PC Pipe 5	2	4.92125	20	$329.51	**CC Pipe 5**	2	4.92125	20	$329.51
PC Pipe 6	2	4.92125	20	$329.51	**CC Pipe 6**	4	4.92125	20	$585.76
PC Pipe 7	3	4.92125	20	$461.34	**CC Pipe 7**	4	4.92125	20	$585.76
				$2,828					**$3,209**